TAMPEREEN TEKNILLINEN YLIOPISTO
TAMPERE UNIVERSITY OF TECHNOLOGY

Ville Lehtonen

Modelling Undrained Shear Strength and Pore Pressure Based on an Effective Stress Soil Model in Limit Equilibrium Method

Julkaisu 1337 • Publication 1337

Tampere 2015

Tampereen teknillinen yliopisto. Julkaisu 1337
Tampere University of Technology. Publication 1337

Ville Lehtonen

Modelling Undrained Shear Strength and Pore Pressure Based on an Effective Stress Soil Model in Limit Equilibrium Method

Thesis for the degree of Doctor of Science in Technology to be presented with due permission for public examination and criticism in Rakennustalo Building, Auditorium RG202, at Tampere University of Technology, on the 7th of December 2015, at 12 noon.

Tampereen teknillinen yliopisto - Tampere University of Technology
Tampere 2015

ISBN 978-952-15-3603-8 (printed)
ISBN 978-952-15-3693-9 (PDF)
ISSN 1459-2045

Abstract

This thesis presents the calculation method Hybrid s_u that is used to calculate the undrained shear strength or excess pore pressure in soft clay, based on effective strength parameters, in a limit equilibrium (LEM) framework. The Hybrid s_u method (HSU) can take into account the effects of anisotropy, consolidation state, volumetric hardening, and to some extent, effects of undrained loading rate. The calculation method is intended to be used as a fairly simple design tool with enough complexity to account for the most important properties of undrained soil behavior.

Advanced finite element (FEM) soil models could be used to accurately model and calculate embankment stability. While such models can be very accurate, they are demanding in terms of user expertise, parameter determination and time. On the other hand, basic stability design work is typically carried out with limit equilibrium methods (LEM), where strength input often comes from field vane testing ($\varphi = 0$ analyses). The largest inaccuracy in $\varphi = 0$ analyses is often in strength determination. In the case of undrained effective stress calculations (c'-φ' analyses), the inaccuracy lies in determining excess pore pressure.

The HSU method provides improvements in the determination of s_u and Δu in the context of LEM. It is based on the anisotropic critical state soil model S-CLAY1. The formulation of the original model is simplified with reasonable assumptions to obtain a closed form solution for undrained shear strength, based on effective strength parameters. The method can also be used to derive excess pore pressure at the failure state. As the method relates the calculated pore pressure and effective stresses to the assumed failure state, the known property of overestimating shear strength in traditional undrained effective stress analyses is effectively solved.

The method is validated by fitting it to laboratory data on various soft clays, as well as back-calculations of several failed embankments. HSU is shown to give good results with very reasonable parameter combinations.

The recommended use of the HSU method is determining s_u, which is then used as input in a typical total stress limit equilibrium analysis. The proposed approaches of determining Δu for undrained effective stress analyses work fairly well. However, the Δu approach is mainly presented as a proof of concept due to its complex and redundant nature compared to the s_u approach.

Preface and acknowledgments

This work was done as a part of the research project RASTAPA (2009-2015), which was conducted by Tampere University of Technology and funded by the Finnish Transport Agency. There was recognized need for improvements in stability calculations of embankments on soft soils on the Finnish railway network. This thesis work was started with the aim to improve the usability of undrained effective stress calculations.

My part in the project began in 2009 when I did my Master's thesis on the instrumentation of the Perniö full-scale embankment failure experiment. From there onwards, I was given the task of improving excess pore pressure calculations in undrained effective stress stability analyses. The resulting calculation method has achieved that to a good degree. Over the course of this work I have more and more started to appreciate well conducted total stress analyses over complex undrained effective stress analyses - this is perhaps well in line with many other scholars and practitioners who have tackled the subject.

I wish to thank my supervisor, Professor Tim Länsivaara for his patient commentary and support in this thesis, as well as his understanding of my independent, sometimes overly detail-oriented and deadline-flexible work habits.

My pre-examiners, Prof. Vikas Thakur from NTNU and Prof. Leena Korkiala-Tanttu from Aalto University, have made great efforts in examining this thesis and providing essential feedback on highly important issues. I sincerely thank Professor emeritus Göran Sällfors from Chalmers for his essential role as the main opponent in the dissertation, as well as Prof. Thakur for being the second opponent.

My gratitude goes to the Finnish Transport Agency (FTA) for graciously funding the project, as well as the TUT President's Doctoral Program from where I received most of my personal funding.

Many thanks go also FTA's R&D project manager Erkki Mäkelä for his unwavering support for the whole RASTAPA project, and to Mr. Jaakko Heikkilä from Arcus Oy for providing essential geotechnical guidance and commentary throughout the project.

Special thanks go to my coworkers Dr. Juho Mansikkamäki and M.Sc. Marco D'Ignazio with whom I have spent countless of hours in thought-provoking conversations, as well as all other co-workers at TUT.

I also thank Prof. Christopher Meehan from the University of Delaware for his valuable comments, feedback and sparring in my research and writing work.

And finally, I would like to thank my loving family for their patience with me in these often stressful times. I have been absent and absent-minded more than you ever would deserve.

This work has been at times hugely inspiring, sometimes totally uninspiring, greatly thought-provoking and often frustrating. The end result is here and it matters.

Ville Lehtonen
September 2015

Notation

b	Intermediate principal stress ratio
C	HSU model parameter for setting K_{0NC}
c'	Cohesion [kPa]
D	pore pressure parameter
D	HSU model parameter for setting K_0 (overconsolidated soil)
e	void ratio
F	Factor of safety
f_0	Correction factor in Janbu's simplified method
G	Shear modulus [kPa]
I_p	Plasticity index [%]
J_2	Second deviatoric invariant [kPa]
K_0	Lateral stress coefficient
K_{0NC}	Lateral stress coefficient in the normally consolidated state
M	Inclination of the critical stress line in (p', q) space
m	SHANSEP exponent
p	Total effective stress [kPa]
p'	Mean effective stress, Cambridge definition: $p' = (\sigma'_1 + \sigma'_2 + \sigma'_3) / 3$ [kPa]
p'_0	Initial mean effective stress [kPa]
p'_c	Mean effective stress at preconsolidation pressure [kPa]
p'_m	Yield surface size parameter, HSU & S-CLAY1 model [kPa]
q	Deviatoric stress, Cambridge definition: $q = \sigma'_1 - \sigma'_3$ [kPa]
q_0	Initial deviatoric stress [kPa]
q_c	Mean effective stress at preconsolidation pressure [kPa]
S	SHANSEP strength ratio
s_u	undrained shear strength [kPa]
u	Pore pressure [kPa]

Δu	Excess pore pressure [kPa]
w	Water content [%]
w_L	Liquid limit [%]
w_P	Plastic limit [%]
α	Slope of failure surface against the horizontal direction [°]
α_{rot}	Inclination of the initial yield surface in HSU and S-CLAY1
β	Rotational hardening parameter in the S-CLAY1 model
γ	Unit weight [kN/m^3]
γ	Shear strain
γ	Partial safety factor
ε_a	Axial strain
ε_v	Volumetric strain
η	Stress ratio q/p'
θ	Principal stress rotation [°]
κ	Slope of the unloading-reloading line in (ln p', e) space
λ	Slope of the normal consolidation line in (ln p', e) space
λ/κ	Stress path control parameter in HSU
μ	Reduction factor for s_u
σ'	Effective stress [kPa]
σ'_v	Preconsolidation stress [kPa]
σ'_n	Effective normal stress [kPa]
σ'_v	Effective vertical stress [kPa]
τ	Shear stress [kPa]
τ_f	Shear strength [kPa]
φ'	Friction angle [°]
χ	Rotational hardening parameter in the S-CLAY1 model

Common subscripts:

$_0$	Initial state
$_1$	Major principal stress or strain
$_2$	Intermediate principal stress or strain
$_3$	Minor principal stress or strain
$_c$	Preconsolidation state
$_f$	Failure state

Acronyms:

CAU	Anisotropically consolidated, undrained triaxial test
CK_0UC	K_0-consolidated, undrained triaxial compression test
CK_0UE	K_0-consolidated, undrained triaxial extension test
COV	Coefficient of variation
CSL	Critical state line
DSS	Direct simple shear test
ESA	Effective stress analysis
FEM	Finite Element Method
FTA	Finnish Transport Agency
HSU	Hybrid s_u method
LEM	Limit Equilibrium Method
OCR	Overconsolidation ratio
PSA	Plane strain active (strength or stress state)
PSP	Plane strain passive (strength or stress state)
SHANSEP	Stress History And Normalized Soil Engineering Properties (design procedure)
TC	Triaxial compression
TE	Triaxial extension
TSA	Total stress analysis

TUT	Tampere University of Technology
USA	Undrained strength analysis

Contents

1 Introduction

1.1 Background of the research issue

Calculating slope and embankment stability is a challenging but essential task in any geotechnical design project. The complex behaviour of soft soils adds yet further challenge to stability calculations.

A fairly large proportion of the Finnish railway network is located on soft soil areas (clay or peat), which emphasizes the need for accurate stability calculations. Typical Finnish clays are normally consolidated or slightly overconsolidated, have fairly low shear strength, medium to high plasticity and high sensitivity (Ronkainen 2012).

Further difficulties arise from the desire to increase the design loads of certain track sections, for example due to mining operations. To this end, the Finnish Transport Agency has conducted a study (Ratojen luokittelu; English translation: “Classification of tracks”) to classify all track sections in Finland according to various properties, including embankment stability. Quite often the resulting factor of safety from these stability calculations is unrealistically low. It has been found that there are many existing embankments on the Finnish railway network that have calculated global factors of safety $F < 1$ for undrained loading, without the use of partial safety factors. As these embankments are still standing without critical issues (although often closely monitored), there obviously are problems either with determining the strength parameters or the calculation methods themselves.

Until recently, by far the most dominant design practise in Finland has been to calculate a global factor of safety F against short-term embankment failure by a total stress analysis ($\varphi = 0$) using the limit equilibrium method (LEM). With the introduction of the Eurocodes (EN-1997), stability analyses are increasingly conducted with partial safety factors (especially in projects commissioned by the Finnish Traffic Agency, who require design to be carried out according to Eurocodes). The codes and guidelines used do maintain provision for undrained effective stress stability analyses, but this is only used for a minimal share of all analyses. The use of FEM in design work is slowly increasing, but is typically reserved for large or difficult projects, and is only used by a handful of specialists. The bulk of stability calculations are done using LEM.

In Finland the undrained shear strength of clay is most commonly determined in situ by vane shear testing. The most common vane shear apparatus used is the Nilcon vane that employs a slip coupling above the vane to account for rod friction. The torque is measured from the ground surface. In addition, some soil investigation consultants use field vanes that measure torque from the bottom. CPTU equipment is increasingly used, but still fairly rarely in a national scale.

A recent study (Ukonjärvi 2015) indicates that the commonly used Nilcon vane has many issues that result in unrealistically low measured shear strengths. Especially the slip coupling used to isolate rod friction does not always work as intended, which results in too large measured rod friction. This discussion is however outside the scope of this work, but here it can be argued that the often conservative design strengths will then often lead to overconservative and costly designs.

Total stress analyses (φ = 0) have most of their uncertainty in the actual strength parameter (s_u) due to sometimes unreliable in situ determination. An alternative to total stress analysis is the undrained effective stress analysis (undrained *c'-φ'*). Here the strength parameters *c'* and *φ'* can be determined quite accurately, but now the uncertainty is in the determination of excess pore pressure. Undrained *c'-φ'* analyses also have issues related to the use of the Mohr-Coulomb criterion which leads to an inherent overestimation of *F*. These issues are discussed in Chapter 4.

The research project "RASTAPA" (2009-2015) commissioned and funded by the Finnish Transport Agency and carried out by Tampere University of Technology seeks to improve the commonly used ("state-of-practise") stability calculation methods and to research new calculation methods with emphasis on their usability for everyday design tasks.

One part of the project RASTAPA that is directly linked to this thesis was to improve methods for modelling excess pore pressure (Δu) in LEM, thus facilitating the use of undrained effective stress analyses for design. Special emphasis was put on modelling yield-induced excess pore pressure which is quite difficult – often arbitrary – with traditional parameters used in LEM. The premise was that improving the modelling of Δu can make undrained *c'-φ'* a viable option for stability calculations. The advantage over total stress analyses would then be smaller uncertainty in strength parameters themselves.

1.2 A note on "LEM versus FEM "

Calculating embankment stability with LEM is admittedly constrained by comparison to advanced finite element analyses. A natural question would then be: Does LEM have any relevance in geotechnical design if FEM can be used to calculate stability potentially more accurately (and at the same time give information about deformations)?

Advanced FEM soil models can take into account various physical phenomena affecting soil strength, but this comes at the cost of complex models. Increasing the number of physical parameters a model accounts for is accompanied by more parameters to be determined, as well as increased calculation times. In comparison, LEM analyses require very little input data, and calculation times with modern computers are close to negligible.

There are many recognised issues affecting the accuracy of LEM stability calculations (Section 2.3), but nevertheless LEM remains a widely used and reasonably effective engineering tool. Most of the practical stability design work (e.g. small-medium projects and preliminary studies of more complex projects) is still done with LEM. For example, in large railway or road projects the geotechnical designer needs to be able to quickly calculate the stability of numerous cross-sections. This would often be a laborious and time-consuming task with FEM, especially with variable soil deposits. In this example LEM can be used quickly to identify the most critical cross-sections, and more accurate FEM analyses can then be employed where necessary.

It also has been shown (Cheng et al 2007) that at least for simple, homogenous slopes in drained conditions, both LEM, and FEM analyses using the Strength Reduction Method (SRM), will give essentially the same factor of safety. An SRM analysis has the advantage over LEM in that it implicitly finds the most critical slip surface, while a LEM analysis can potentially fail to converge or find the most critical failure surface. In LEM analyses it is important that the software has reliable and effective search algorithms for the most critical slip surface.

It can be argued that LEM and FEM should not be seen as competing, but rather as mutually complementary geotechnical design tools. At the same time, LEM stability calculations do have room for improvement, especially regarding undrained analyses.

1.3 Aim and premise of the study

There is recognised need for a simple design-oriented calculation tool to better model the shear strength of clay in undrained stability calculations. The calculation tool would need to:

- be easily adaptable for use with LEM (preferably a closed form solution, or at most minor iterations needed)
- analytically take into account the primary factors affecting the undrained strength capacity of clays
- not contain too many model parameters to be determined, so as to preserve the “simple engineering tool” approach

This thesis presents an approach where a constitutive soil model can be applied to:

1. Calculate s_u based on the friction angle and consolidation stress of the clay (total stress $\varphi = 0$)
2. Calculate excess pore pressure at failure (effective stress c'- φ')

It will be shown that the proposed approach satisfies the aforementioned requirements. The approach gives the designer more freedom to analytically model the factors affecting undrained shear strength than has traditionally been possible with LEM. It also can be seen as a solution to the inherent overestimation of the factor of safety in undrained effective stress analyses.

1.4 Defining the problem framework

Under loading, soil is generally considered either drained ($\Delta u = 0$, $\Delta v \neq 0$) or undrained (no pore water dissipation, $\Delta u \neq 0$, $\Delta v = 0$), depending on soil permeability and the time scale of loading. These are the two extremes of the possible drainage conditions. Partial drainage occurs for example during consolidation, where excess pore pressure from loading dissipates during a certain timescale and volume change is occurring.

For a loading problem (e.g. embankment on clay) the lowest factor of safety typically occurs immediately after construction due to excess pore pressure build-up in the undrained state. As consolidation occurs and pore pressures dissipate, the factor of safety increases. The opposite is true for an unloading problem on clay: Removal of soil will decrease pore pressure in clay, increasing the short-term strength. The clay will then swell, pore pressure will equilibrate (increase) and shear strength will decrease. For unloading problems the determining situation is then the long-term drained state.

As this thesis focuses on stability of embankments on clay soils, the focus naturally falls on undrained stability calculations. Specific emphasis is put on railway embankments, both existing (old) and new. While the stability of an old railway embankment might be considered a drained (long-term) problem, this is not the case. The situation used to determine the stability of a railway embankment (both new and old) is a train standing still on the tracks (Ratahallintokeskus 2005). This large traffic load is inherently short-term and thus the loading situation is undrained even for old embankments where consolidation caused by the embankment itself has fully occurred.

A typical soil profile that is relevant for the discussed stability problem includes the embankment and its various structural layers, possible fill layers on the subgrade, possible stiff clay crust, soft soil layers (clay and/or silt), and underlying stiffer layers and/or bedrock.

For sake of simplicity, no attempt is made here to describe partially saturated soil behaviour. The embankment and various fill layers are generally considered dry, a stiff clay crust may be considered dry or saturated depending on the circumstances, and soft clay and any underlying layers are considered fully saturated.

In this thesis ground water conditions are considered static, i.e. the ground water conditions are modelled by a clearly defined water table (which is not necessarily horizontal). No seepage forces are considered.

The new calculation method is mainly intended to be used with soft, normally or slightly overconsolidated clays, solely in undrained conditions. The initial consolidation state is assumed to be cross-anisotropic, with K_0 consolidation.

Due to the nature of the used models and assumptions, the method should not be used with stiff, highly overconsolidated clays or more coarse-grained soils. Various assumptions are made in the derivation of the method (see Section 5.4). In general the results given by the method may not be correct if the conditions differ greatly from these assumptions.

2 About Limit Equilibrium Methods (LEM)

2.1 General characteristics of LEM

In limit equilibrium analyses, as the term implies, the factor of safety is calculated by comparing the available shear strength along a slip surface to a shear stress that is required to achieve equilibrium. Very importantly, the factor of safety is assumed to be constant along the slip surface (Abramson et al 2002 p. 333).

While there are many varieties of limit equilibrium analyses, such as sliding block, infinite slope, planar surface and frictional surface analyses (for brief descriptions see e.g. Abramson et al 2002), arguably the most used Limit Equilibrium Method (LEM) is the method of slices. In the method of slices the soil mass defined by the slip surface is divided into a finite number of vertical slices. From this point onwards this work uses the terms “method of slices” and LEM interchangeably.

Duncan & Wright (1980) give four common characteristics, or implicit assumptions, that are shared by all equilibrium methods (after Duncan & Wright 1980):

1) Factor of safety is given as

$$F = \frac{\tau_f}{\tau} \tag{2.1}$$

where τ_f is shear strength and τ the shear stress that is required for equilibrium.

2) The same value of shear strength can be mobilized over a wide range of shear strains along the slip surface. This is necessary because strains are not considered, and in reality strains can (and will) vary along the slip surface. Problems may arise if the soil exhibits notable post-peak strain softening. In practical design the issue can be mitigated by using design strengths that are lower than the peak strength (Skempton 1977).

3) A set of equilibrium equations is used to calculate the normal stress on the slip surface. This is required because shear strength is calculated using the Mohr-Coulomb failure criterion:

$$\tau_f = c' + \sigma'_n \tan\varphi' \tag{2.2}$$

where c' and φ' are the effective Mohr-Coulomb strength parameters. A total stress analysis (Section 4.2) will substitute these with total stress strength parameters.

4) Since the number of unknowns is higher than the number of available equilibrium equations, a number of assumptions are made to make the problem solvable.

The reason for dividing the soil into several slices in LEM is that this allows complex geometries, variable soil conditions and various external loads to be taken into account

(Abramson et al 2002, Duncan & Wright 1980). Forces acting on a typical slice are slice weight, shear and normal forces acting on the base and sides of the slice, water pressure on the base of the slice and possible external forces. In addition to these unknowns, the locations and directions of the resulting forces also need to be solved or assumed. The overall factor of safety is then typically solved by a process of iteration.

External stresses are not distributed realistically in the soil, but instead they act directly upon the slice where they are located. In effective stress analyses this has an effect on the proper modelling of excess pore pressure (Section 4.3).

Calculating the factor of safety of a given slip surface is only one part of a stability analysis using LEM. The other part is finding the most critical slip surface. For this task different geotechnical software use various search algorithms. A typical calculation process involves calculating tens of thousands of individual slip surfaces to find the most critical one.

2.2 Various limit equilibrium methods

The various limit equilibrium methods differ by the assumptions that they make to reduce the number of unknowns. They correspondingly differ by the equilibrium conditions that they satisfy. For brief descriptions of the various methods the reader is directed to Abramson et al (2002). Some commonly used limit equilibrium methods are Bishop's simplified (Bishop 1955), Janbu's simplified (Janbu 1954, 1973), Spencer's method (Spencer 1967, 1973), Morgenstern-Price method (Morgenstern & Price 1965), the general limit equilibrium (GLE) (Fredlund et al 1981) and Janbu's generalized method (Janbu 1954, 1957).

Bishop's and Janbu's simplified methods are called "simplified" because they do not satisfy all force and moment equilibriums. They also ignore interslice shear forces. Bishop's simplified method does not satisfy the horizontal equilibrium. It should be noted that Bishop's simplified method is limited only to circular slip surfaces, whereas the other mentioned methods can be used for free-form surfaces as well. Janbu's simplified method does not fully satisfy moment equilibrium, but it includes a correction factor to take this into account. (Abramson et al 2002)

The other mentioned methods are often termed "rigorous" because they satisfy both horizontal and vertical force equilibrium and overall moment equilibrium (Janbu's generalized method satisfies moment equilibrium for individual slices). They mainly differ in the assumptions that are made about interslice forces. Spencer's method assumes a constant (but unknown) inclination for the interslice force resultant. Morgenstern-Price assumes a function for the inclination of the interslice force resultant, which makes Spencer's method a special case of Morgenstern-Price. (Abramson et al 2002). The GLE method is quite similar to Morgenstern-Price as it uses similar assumptions of the interslice force function. There are however subtle differences in the location of the normal force resultant acting on the slice bottom.

Janbu's generalized method differs from the aforementioned rigorous methods in that instead of assuming an interslice force function, the locations of the side force resultants are assumed ("line of thrust"). According to Krahn (2003) and Abramson et al (2002), Janbu's generalized method is sensitive to numerical problems, especially with slip surfaces with sharp corners or large stress concentrations. The calculation is sensitive to the assumption of the line of thrust location, which is often assumed to be located at 1/3 of the way from the slice bottom (assuming "hydrostatic" stress distribution where stresses increase linearly with depth).

2.3 Recognised issues in LEM analyses

While LEM has remained a useful and well used tool for stability analyses, there are many recognised issues, discussed e.g. by Tavenas et al (1980), Ladd (1991) and Krahn (2003). One issue (though not limited to LEM only) is the inherent overestimation of the factor of safety in undrained effective stress analyses. This is discussed in detail in Section 4.3.

It has been established that while LEM does often give good results for F that are comparable with corresponding FEM analyses (Cheng et al 2007), the calculated stresses along the slip surface can be very unrealistic (Wright et al 1973, Tavenas et al 1980, Krahn 2003). This is at least partly due to the fact that LEM only considers statics; the calculated forces only need to satisfy force and moment equilibriums instead of taking any mechanical factors into account (Krahn 2003). The global factor of safety can still be very close to reality, or at least correspond to a similarly conducted FEM analysis.

LEM typically assumes a uniform degree of mobilization of strength along the slip surface, representing an "average" shear stress profile. In reality, the degree of mobilization and stress profile will vary along the slip surface. Thus it may be unwise to even expect realistic stress profiles from LEM calculations (Morgenstern and Sangrey 1978). It is debatable if the issue of unrealistic stress distribution is relevant in normal engineering practise. Most often LEM is specifically used to obtain the global factor of safety, and not so much to model stresses. Care should however be taken if there are stress concentrations in the potential sliding mass, as these can affect the calculation result (Krahn 2003).

The assumption of uniform mobilization coupled with no consideration of strains along the slip surface presents problems with shear strength. In reality the shear strength of soil will be different at different strains. Due to anisotropy, the strength and the strain at which peak strength is obtained will also vary along the slip surface (see Section 3.3). The strains themselves will in reality be very different in different parts of the slip surface. Consequently, design should be based on post-peak strengths, as in reality the whole slip surface cannot be at peak strength simultaneously. Certain strain compatibility techniques (e.g. Ladd 1991, Karlsrud & Hernandez-Martinez 2013) may be used to determine realistic design strengths.

One solution for considering the variable degree of mobilization along the slip surface can be found in the proposed method of dual optimization (Cheng et al 2011). An optimization algorithm is used to obtain individual factors of safety for each slice. This approach may to some extent be used to account for the effects of strain softening and progressive failure. However, at least to the author's knowledge this approach is by no means widespread in design work, at least not outside China.

The way external loads act directly on the slice they are located on may lead to inaccuracies in undrained effective stress analyses. Any pore pressure profile measured in situ is a result of the true stress distribution in the soil. It is doubtful if this pore pressure profile should be used as an input in effective stress LEM calculations, because the total stress distribution does not correspond to reality. In other words, combining a realistic pore pressures with inherently unrealistic total stresses will result in unrealistic effective stresses, and consequently unrealistic shear strengths.

2.4 Slip surface optimization

Reliably finding the most critical failure surface can be an issue in LEM, depending on the specifics of the search algorithm and calculation method used. Depending on the software, the search algorithm might entail calculating different circular slip surfaces in a grid pattern, or various trial-and-error search algorithms with different slip surface geometries. Search algorithms of varying levels of sophistication are in use. The main goal is to find the overall most critical slip surface, as well as the actual lowest factor of safety for that given slip surface. The solution may converge to a local minimum of F that is however larger than some other solution (Cheng & Lau 2008).

It is also possible that various limit equilibrium methods are simply unable to converge to a solution with certain slip surfaces. Krahn (2003) points out the possibility that the critical slip surface may be found very close to other slip surfaces that do not converge. This would make it difficult to find the critical surface. In any case, the engineer should also use his/her own judgment to determine if the critical slip surfaces given by the calculation program are correct. Gradually narrowing down the search boundaries may also help in finding the critical slip surface. For more information on slip surface generation, optimization and search algorithms, see e.g. Cheng & Lau (2008).

3 Factors affecting the undrained shear strength of clay

3.1 On critical state shear strength

The shear strength of soil can in general terms be described by the concept of critical states (for extensive textbook descriptions of critical state soil mechanics, see e.g. Schofield & Wroth 1968; Wood 1990; Atkinson 1993).

The critical state concept assumes that when sheared, soil ultimately flows as a "frictional liquid" at constant specific volume v, effective stress p', deviator stress q and pore pressure u. This ultimate state of stress and volume is called the critical state. It is assumed that critical state occurs when any soil structuration has been destroyed. Critical state soil strength is thus often considered purely frictional ($c' = 0$). For a given soil, the critical state can be illustrated by the critical state line in (p', q) and (p', v) coordinate spaces (Figure 3.1).

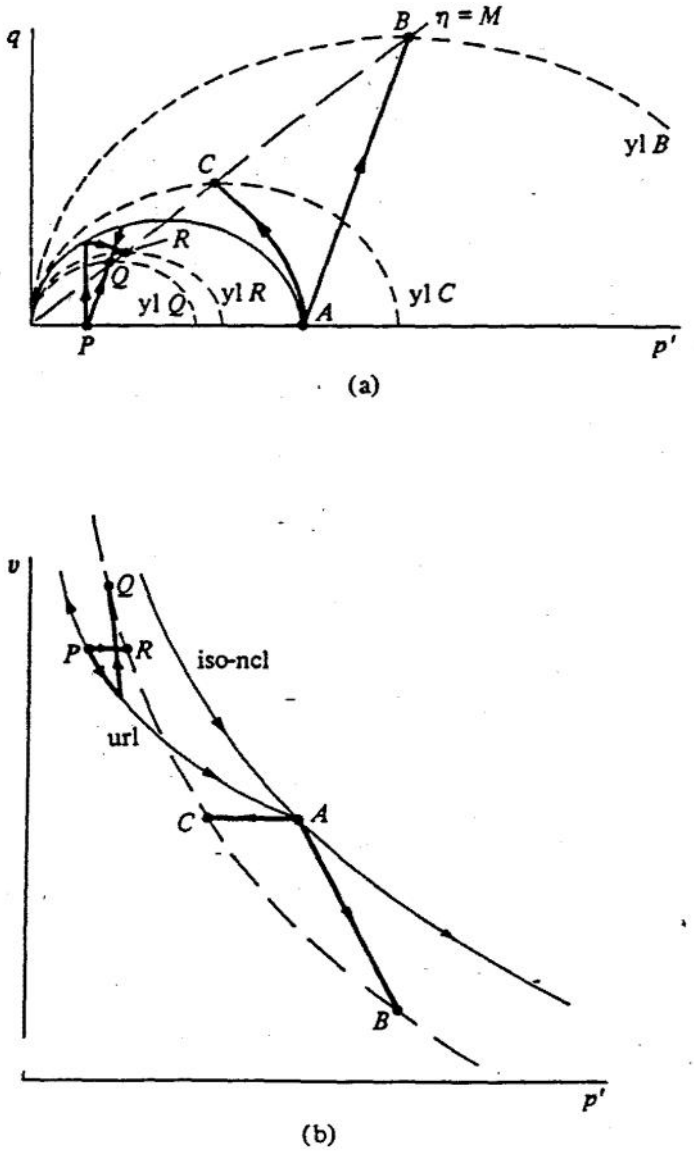

Figure 3.1.Drained (A-B, P-Q) and undrained (A-C, P-R) triaxial compression tests for NC (A-B, A-C) and OC (P-Q, P-R) samples. The critical state lines in both coordinate spaces are represented by the long-dashed lines. Note: "yl" = yield locus = yield surface, "url" = unloading-reloading line, "iso-ncl" = isotropic normal compression line. (Wood 1990 p. 140)

The critical state strength envelope in (p',q) space is the M-line, which is essentially analogous to the Mohr-Coulomb strength envelope used in (σ', τ) space. Defined according to the Mohr-Coulomb failure criterion, the slope of the M-line for triaxial compression is:

$$M = \frac{6 \cdot \sin \varphi'}{3 - \sin \varphi'} \tag{3.1}$$

and for triaxial extension:

$$M = \frac{6 \cdot \sin \varphi'}{3 + \sin \varphi'} \tag{3.2}$$

for triaxial extension, where φ' is the effective critical state friction angle of the soil. Any intermediate stress state between triaxial compression and extension will have a slope for the M-line that is "between" these two boundary values.

In (p', v') space the stress-volume state during shearing moves towards the critical state line as well. The tendency of soil to compress or dilate depends on whether the soil is, respectively, on the "wet" (right side of CSL) or "dry" side (left side of CSL) of the critical state line. If the stress state lies on the wet side of CSL, the soil is loose and has a tendency to contract, i.e. the soil particles tend to rearrange themselves to a smaller volume. The opposite is true for stress states on the dry side, where the initially dense soil particles tend rearrange into a larger volume.

In the case of undrained shearing, the volume will remain constant, which results in a constant v path from the initial state to the CSL. This is illustrated by the cases A-C and P-R in Figure 3.1. The tendency for plastic volumetric straining is counteracted in undrained conditions by equal elastic straining, i.e. pore pressure changes:

$$d\varepsilon_v^p + d\varepsilon_v^e = 0 \tag{3.3}$$

Shear strength can essentially be tied to the internal angle of friction, the initial relative density (void ratio) and the compressive or dilative tendencies of the soil at that relative density. In undrained loading, the stress state of a soil element moves towards the critical state line at a constant volume. The compressive or dilative tendencies are then counteracted by corresponding changes in pore pressure, resulting in changes in effective stress p'. Modelling this pore pressure response in undrained effective stress stability analyses is essential.

For a given initial effective stress and density (p'_0, q_0, v_0) there is then a corresponding critical state stress state (p'_f, q_f, v_f), and thus a corresponding critical state shear strength. The critical state concept describes shear strength in terms of effective stresses. Undrained shear strength can be also described in terms of total stresses. For any effective stress state (p'_f, q_f) in the critical state there is an infinite number of possible total stress states (p_f, q_f). Note that for any of these total stress states, the deviator stress q_f corresponds to the undrained shear strength. In undrained conditions, the failure criterion can be given as

$$\tau_f = \pm s_u \tag{3.4}$$

i.e. the Tresca failure criterion. This simple expression holds true for total stresses even though the shear strength is still governed by effective stresses. It can be described as the result of the interplay between total stress changes, volumetric tendencies and the resulting pore pressure response. For a "given specific volume", "a unique undrained strength" can be given "as a consequence of the principle of effective stresses" (Wood 1990 p. 180). This "unique undrained strength" also implies a certain type of loading regarding anisotropy and rate effects (sections 3.5 and 3.6).

Related to effective stresses, the pore pressure response correlates with OCR (i.e. the relation of the initial consolidation stress to the critical state line). Low OCR clays (in the order of OCR < 2, Atkinson 1993 p. 140)) are initially on the wet side of the CSL, and thus exhibit increasing pore pressure during shearing. The closer the initial stress state is to the CSL, the less pore pressure is generated. Highly overconsolidated clays on the dry side of CSL tend to dilate and thus exhibit negative pore pressure response during

shearing. The higher the OCR and the further away the initial state is from CSL, the more negative pore pressure is generated. Measured examples of the effect of OCR on shear-induced pore pressure response can be found from e.g. Sheahan et al (1996). The pore pressure response affects effective stresses, and consequently, the shear strength.

3.2 Creep and structuration

A matter related to consolidation pressure and undrained shear strength is the general stress-strain-time-behaviour of clays. This is illustrated in Figure 3.2. Descriptions of stress-void ratio-time-related processes can be found from e.g. Bjerrum (1967, 1973) and Leroueil et al (1990).

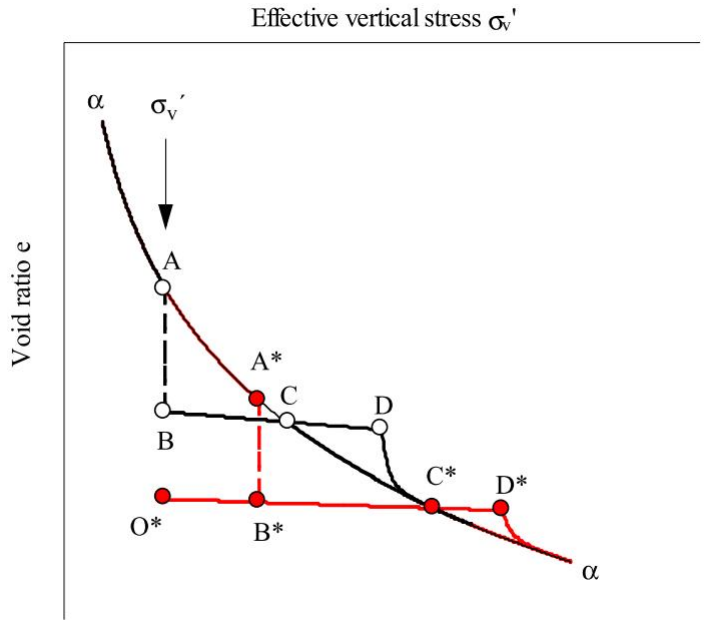

Figure 3.2.Various time and stress-dependent processes in terms of effective stress and void ratio (Länsivaara 1999)

During the sedimentation and primary consolidation process clays tend to follow the virgin compression line α-α, which is a unique stress-volume property for a given soil. If a naturally sedimented clay is then kept a constant effective stress after primary consolidation, it tends to compress further (A-B) due to creep (secondary consolidation) of the soil skeleton. While the initial maximum past pressure A (the maximum vertical pressure the soil has been exposed to) doesn't change during creep, the apparent preconsolidation pressure C is higher.

With time, the soil skeleton may become cemented together due to various chemical processes. This structuration will cause further increase in preconsolidation pressure. If the clay is loaded from point B, it will not start yielding at the virgin compression curve (C) but at a point further out (D). This also will increase the peak strength of the clay. When the clay is compressed or sheared further, the structure will be broken and the clay state will return to the virgin compression curve (C*). At the same time, strains will start to increase quickly as the clay yields.

Creep and structuration processes can thus increase the apparent preconsolidation pressure)and consequently, undrained shear strength) with time even after primary consolidation has ended. Such aged or structured clays may exhibit high peak strengths followed by significant strain softening as the cementation between the soil particles is broken down.

3.3 Typical undrained stress-strain behaviour

An important matter to consider in stability design is the post-peak strain softening behaviour that is often found in structured clays.

Non-structured or remolded clays do not typically exhibit peak strengths and strain softening in undrained conditions. Figure 3.3 shows typical "textbook" stress-strain curves (Craig 2004), where both OC and NC undrained clays exhibit strain-hardening responses, gradually reaching their maximum shear stress levels at high strains. In these cases, the shear strength of the clay would quite unambiguously be interpreted as the level that is asymptotically reached at high strain levels.

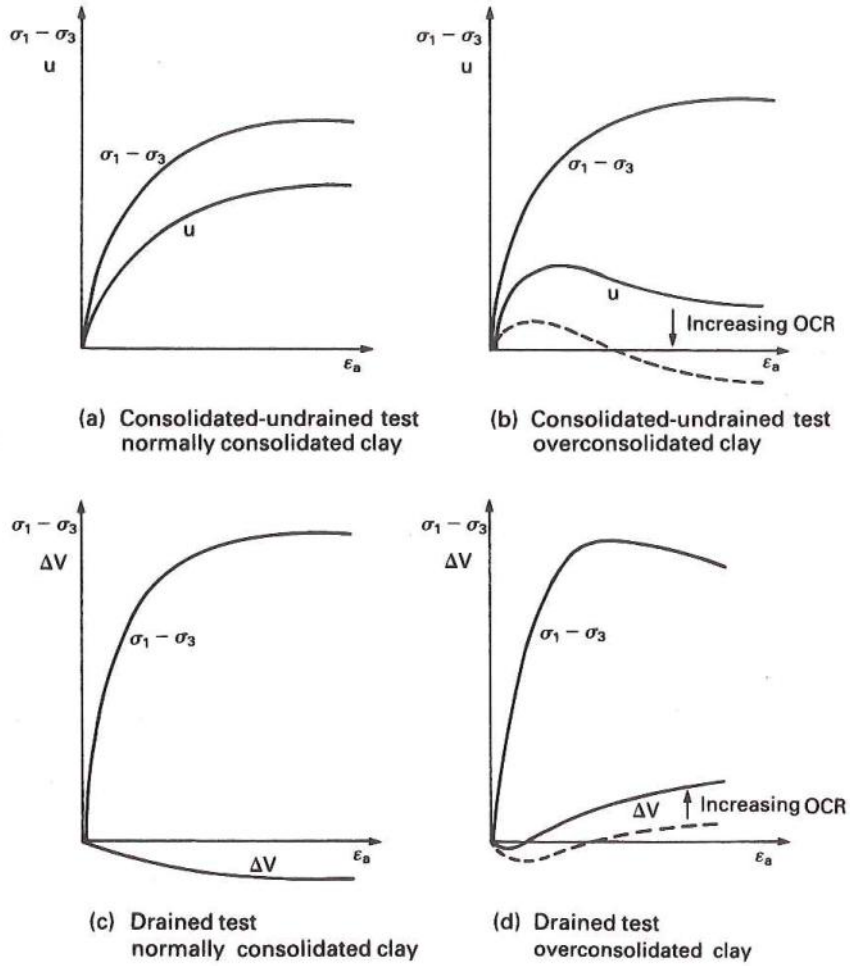

Figure 3.3. Stress-strain curves for clay, different test types and consolidation states (Craig 2004 p. 112)

Structured (cemented), sensitive clays often exhibit high peak strengths (τ_{peak}) at low strains (in the order of 1 % shear strain for good-quality samples), followed by post-peak strain softening (down to roughly 10-20 % shear strains). This strength is often called the fully softened strength (τ_{fs}). During the softening process the clay is being remoulded, shear-induced excess pore pressure increases, and eventually the clay will reach its critical state strength. For very large strains the clay particles may further orient themselves into a laminar orientation (slickenside), resulting in greatly reduced residual shear strength (τ_{res}). These concepts are illustrated in Figure 3.4.

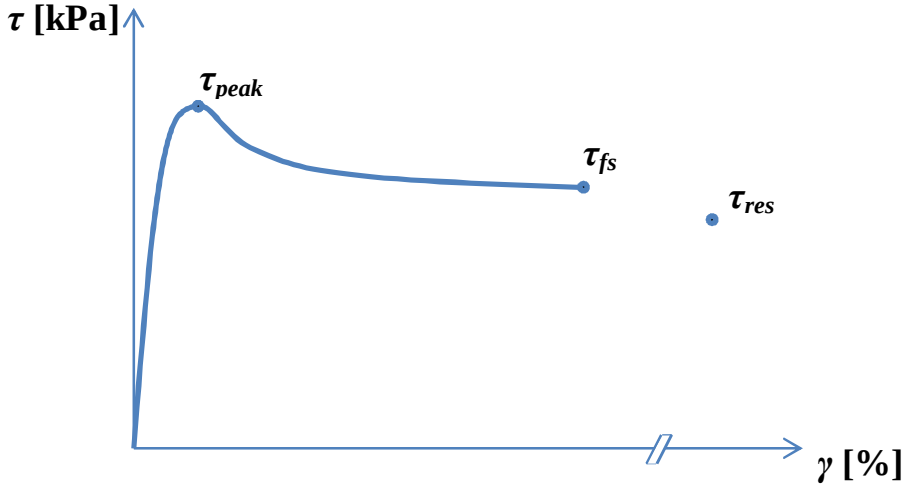

Figure 3.4. A conceptual example of strain softening behavior in undrained shearing.

The post-peak strain softening is often attributed to the initial soil structure and its breakdown (reduction of *c'* and/or *φ'*) during shearing (e.g. Skempton 1964, Burland 1990, Burland et al 1996). Typically it has been observed, especially for stiff OC clays, that cohesion softening due to breakage between soil bonds is the predominant softening mechanism at low strains. Reduction of friction angle may occur at high strains. It should be noted that these findings are mainly based on drained tests.

Thakur et al (2014) however suggest that strain softening of undrained, normally consolidated or slightly overconsolidated Norwegian clays is attributable to shear-induced excess pore pressure, whereas *c'* and *φ'* remain fairly constant up to moderate laboratory strain levels of ca. 20 % (Figure 3.5). Thakur et al (2014) also note that for highly overconsolidated Norwegian clays, cohesion softening (drop in apparent *c'*) in undrained shearing is possible.

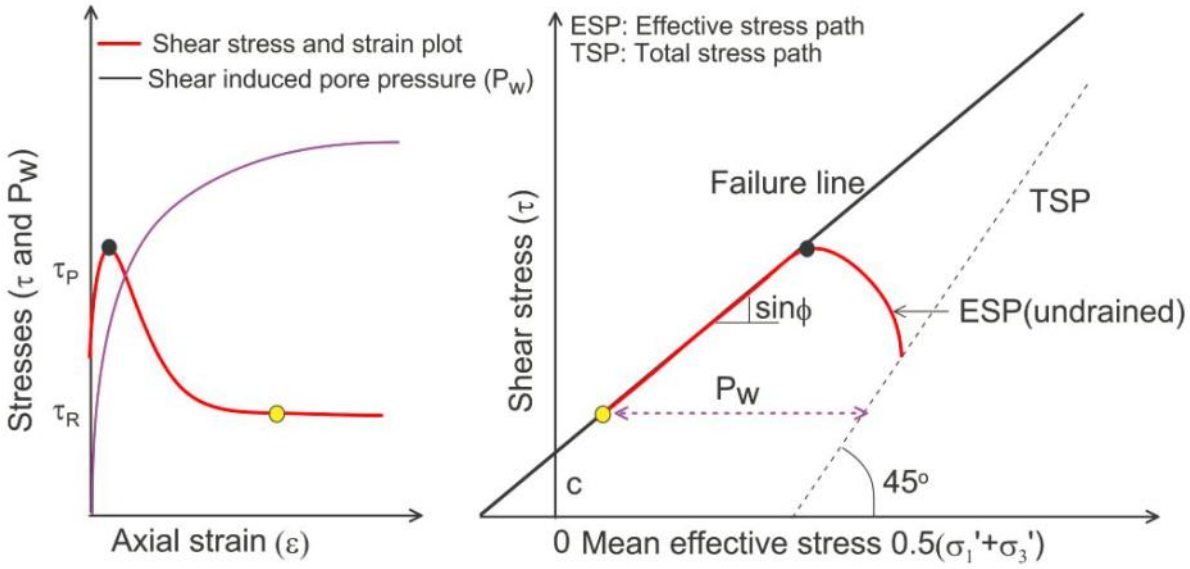

Figure 3.5. Idealised undrained strain softening behaviour in sensitive clays, up to 20 % axial strain. (Thakur et al 2014)

It should be noted that sample quality has a very large effect on measured peak strengths, especially for triaxial compression (e.g. Lunne et al 1997, Karlsrud & Hernandez-Martinez 2013). High quality samples (e.g. large block samples) show much higher triaxial compression strengths than (typically lower quality) piston samples (diameter in the order of 50 mm). Block samples may show 10-50 % higher compression peak strengths compared to 54 mm piston samples whereas in extension the difference may be about 0-10 % (Karlsrud & Hernandez-Martinez 2013). In addition, the peak is attained at higher strains for low quality samples than for block samples (Figure 3.6).

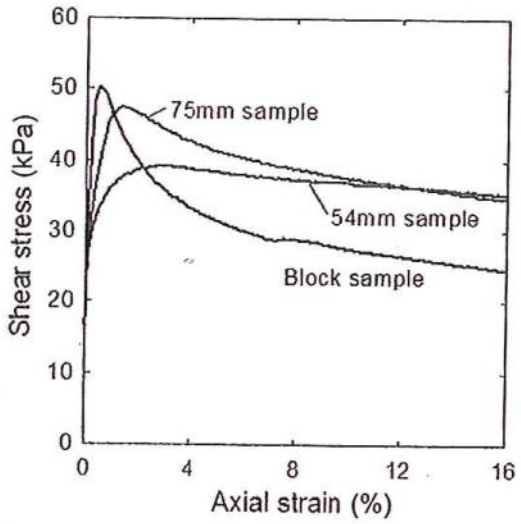

Figure 3.6. Examples of triaxial test results from different size samples, Onsøy clay (Karlsrud & Hernandez-Martinez 2013)

The effects of sample quality have an implication when laboratory results are analysed, as low quality samples often indicate lower peak strengths than good ones. Therefore knowledge of sample quality is essential when comparing test results from different sources.

It is typically inadvisable to use the peak strength as a design parameter unless one can apply a strain-softening soil model. While the peak strength can always be attained locally, it is not attained simultaneously in every part of the slip surface due to the often progressive nature of failure and varying strain levels. When close to failure, some parts of the slip surface may have already surpassed the peak strength while other parts are just approaching peak strength. In addition, peak strength is obtained at different strain levels for different modes of failure (compression-direct shear-extension) (Ladd 1991).

3.4 Undrained shear strength as a function of consolidation pressure

The effect of stress history (i.e. the past and present consolidation stress state) on the strength of clay can constitutively be derived from the critical state concept. Any detailed derivations are omitted here, but examples can be found in e.g. Wood (1990) and Atkinson (1993). In general, higher preconsolidation pressure corresponds to higher relative density, and higher relative density corresponds to higher undrained strength. Undrained shear strength can generally be given as a function of current consolidation pressure and OCR (Jamiolkowski 1985, Larsson et al 2007)

$$s_u = S \cdot \sigma'_{v0} \cdot OCR^{\,m} \tag{3.5}$$

$$\frac{s_u}{\sigma'_{v0}} = S \cdot OCR^{\,m} \tag{3.6}$$

where S is undrained strength ratio, σ'_{v0} is the current effective vertical consolidation stress, OCR is the overconsolidation ratio and m is a material parameter that governs the shape of the $s_u = f(\text{OCR})$ curve.

Equation 3.6 can also be rearranged to give s_u as a function of preconsolidation pressure (i.e. maximum past pressure) σ'_c:

$$s_u = S \cdot \sigma'_c \cdot OCR^{\,(m-1)} \tag{3.7}$$

$$\frac{s_u}{\sigma'_c} = S \cdot OCR^{\,(m-1)} \tag{3.8}$$

The undrained strength ratio S represents the undrained shear strength in *the normally consolidated state,* normalized by vertical consolidation pressure:

$$S = \frac{\tau_f^{\,NC}}{\sigma'_{v0}} \tag{3.9}$$

Typical values of S can vary between ca. 0.08 and 0.35, depending on the mode of shearing and water content/plasticity (Karlsrud & Hernandez-Martinez 2013). Sample quality can have a very large effect on measured strengths, especially for compression strength.

The value of the exponent m depends on the material, but generally its values vary between 0.7 and 0.95 (Karlsrud & Hernandez-Martinez 2013, Larsson et al 2007). Often $m = 0.8$ can be used (Larsson et al 2007).

Parameters S and m can be obtained by fitting a curve to laboratory test results of normalized s_u versus OCR. The curve is fitted for a given mode of shearing, such as triaxial compression or extension test done at various OCR levels. The testing procedures may differ in various design methodologies, such as SHANSEP or Recompression (see Section 4.4). An illustrative example of an s_u/σ'_{v0} versus OCR curve for triaxial compression and extension is shown in Figure 3.7a. The example SHANSEP values are S

= 0.35, m = 0.8 for triaxial compression, and S = 0.15, m = 0.8 for triaxial extension. Figure 3.7b shows the corresponding s_u curves for a case of homogenous, saturated clay where γ' = 5 kN/m^3, and OCR = 1.5.

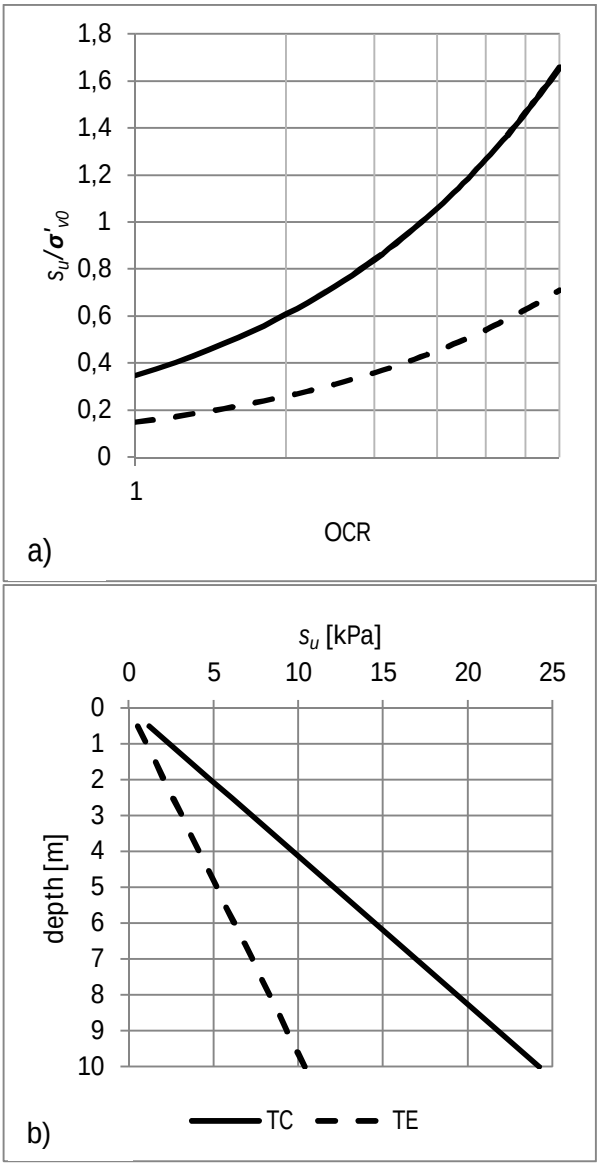

Figure 3.7. a) An example of normalized s_u versus OCR for triaxial compression (TC, S = 0.35, m= 0.8) and extension (TE, S = 0.15, m = 0.8). b) Corresponding s_u versus depth, for γ' = 5 kN/m^3, OCR = 1.5.

If the relevant OCR range is small (e.g. for homogenous lightly overconsolidated or NC clays) it may be enough to give s_u as a simple linear function of preconsolidation pressure where S is now the average normalized shear strength along that OCR range:

$$s_u = S_{avg} \cdot \sigma'_c \tag{3.10}$$

When the relationship between s_u/σ'_{v0} and OCR is known (based on laboratory testing), along with the relevant profile of σ'_{v0} and OCR in the soil, the corresponding s_u profile can be plotted for use in design. However, this assumes that s_u can truly be normalized throughout the entire relevant range of σ'_{v0} and OCR. This assumption may not always apply with structured clays that exhibit cohesion.

3.5 Anisotropy

It is very well known that the strength and stiffness properties of clay are anisotropic. Active (compression) shear strength is higher than field vane strength or DSS strength, which in turn are higher than passive (extension) strength. This is illustrated in Figure 3.8. Shown in Table 3.1 are collected findings from literature regarding the anisotropy of undrained shear strength, friction angle and excess pore pressure response in undrained shearing.

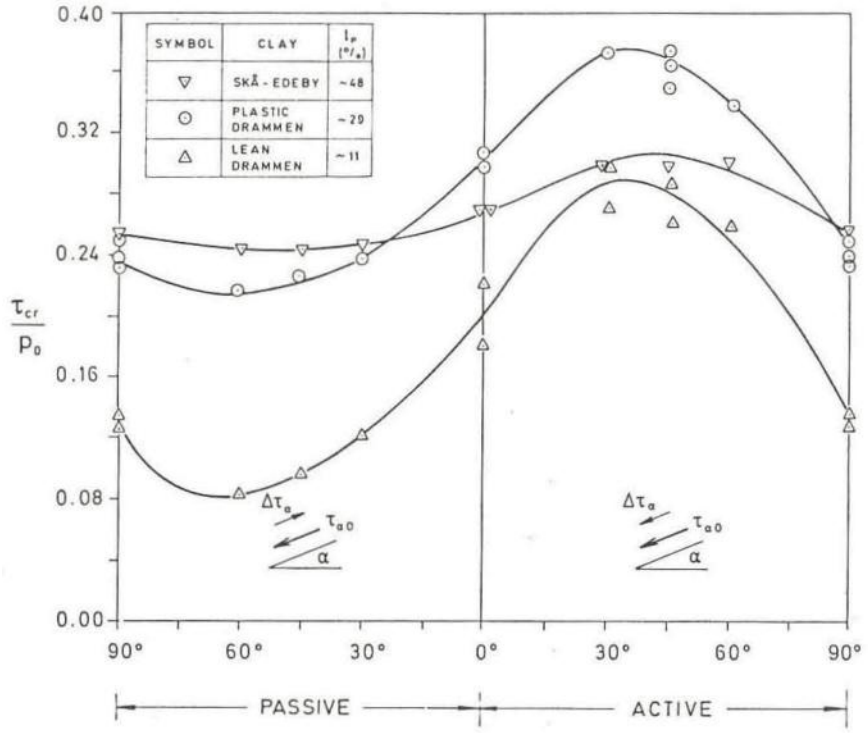

Figure 3.8. Variation in shear strength observed in samples cut in different directions. Active and passive triaxial tests were performed for each direction. (Bjerrum 1973)

Table 3.1 Selected literature on clay anisotropy in undrained tests. The list is not exhaustive; many other studies consider anisotropic effects as well. Focus here is on strength and strength parameters. Most of the given papers discuss strain properties as well, but those discussions are omitted here.

Author(s)	Soil(s) studied	Consolidation and test type	Findings on:		
			Undrained shear strength	Friction angle and failure envelope	Excess pore pressure
Bjerrum 1973	Various clays	TC, TE, DSS, FV	Compression (active) strength higher than extension (passive), anisotropy increases with plasticity		
Vaid & Campanella 1974	Natural Haney clay	K_0 consolidation, triaxial and plane strain compression and extension tests	Compression strength higher than extension; plane strain strength higher than triaxial		Depends on total stress path; effective stress path is independent of total stress path for given mode of shearing
Lade & Musante 1978	Remoulded NC Grundite Clay	Isotropic, true triaxial	Slight decrease with increasing b	Highest φ' values for b = 0.20…0.70, true failure envelope outside of M-C on octahedral plane for b>0	Slight increase with increasing b
Larsson 1980, Ladd 1991	Scandinavian inorganic clays	TC, TE, DSS, FV	Undrained shear strength is distinctly anisotropic, compression strength higher than extension strength. Field vane and DSS fall in between. Shear strengths correlate with plasticity, low plasticity clays most anisotropic		
Mayne 1985	(literature review on effects of stress anisotropy, 42 clays)	CAU, CIU triaxial	Anisotropically consolidated clays have smaller s_u/σ'_{v0} than isotropically consolidated clays. Differences are largest in extension.	φ' is independent of consolidation stress anisotropy	
Kirkgard & Lade 1993	Remoulded NC clay (SFBM)	Isotropic, true triaxial	Generally decreases with increasing b (large scatter however), clearly decreases with larger stress direction angles	Highest φ' values for b = 0.20…0.75, true failure envelope outside of M-C on octahedral plane for b>0	Δu highest for large values of b (differences fairly slight)
Prashant & Penumadu 2004	OC kaolin clay	K_0 consolidation, true triaxial	Deviator stress at failure largest for b = 0…0.25, smaller for $b \geq 0.5$	True failure envelope outside of M-C on octahedral plane for b>0	Δu increases with increasing b, fairly constant for $b > 0.75$
Nishimura et al 2007	Highly OC London Clay	K_0 and isotropic, hollow cylinder apparatus	s_u maximum at θ = 0° or 90°. Minimum shear strengths possibly at b = 0.5, θ = 45°. Large samples indicate s_u minima also at θ = 90°. Influence of b not well defined.	True failure envelope outside of Mohr-Coulomb on octahedral plane for b>0	

Strength anisotropy has two basic components: structural anisotropy and stress anisotropy.

Structural anisotropy is caused by the shape and orientation of the plate-like clay particles. The particles themselves have electrochemical properties that cause them to align in certain preferred orientations. Also more macroscopic structures occur in varved clay where layers of varying particle size have been formed in the sedimentation process. These alignment and layering properties result in a structure with directionally variable shear strength. Generally it appears that the higher the angle between the major principal stress and vertical, the lower the shear strength. Highest strengths are obtained for principal stress rotation of 0°, and lowest for 90°. This is true even for isotropically consolidated samples, which means that the cause is fabric anisotropy. (Jamiolkowski 1985)

Stress anisotropy is a result of the anisotropic stress state that typically occurs in the field. In addition to this initial stress anisotropy, the rotation of principal stresses during loading/consolidation also affects shear strength anisotropy. (Bjerrum 1973, Jamiolkowski 1985)

Due to the stress anisotropy during consolidation, the yield surface of the clay is generally centered around the K_{0NC} –line in (p',q) stress space. It has been established by Länsivaara (1999), that this anisotropic yield surface can be expressed using only the critical state friction angle for a given preconsolidation pressure (see Section 4.3).

The anisotropic properties of soils can be described by shear tests done at different levels of principal stress direction angle θ and intermediate principal stress ratio b. b is used to describe the level of the intermediate principal stress in relation to the major and minor principal stresses (Habib 1953):

$$b = \frac{\sigma'_2 - \sigma'_3}{\sigma'_1 - \sigma'_3} \tag{3.11}$$

The intermediate principal stress can then be given as:

$$\sigma'_2 = \sigma'_3 + b \cdot (\sigma'_1 - \sigma'_3) \tag{3.12}$$

For triaxial compression b = 0 ($\sigma'_2 = \sigma'_3$), and for triaxial extension b = 1 ($\sigma'_2 = \sigma'_1$). Possible values for b range from 0 to 1.

It is evident from literature that at least for NC and lightly OC clays, largest strength and smallest excess pore pressure are obtained at or close to $b = 0$ and $\theta = 0°$, i.e. triaxial compression. The opposite boundary values generally correspond to triaxial extension ($b = 1$ and $\theta = 90°$). Deviations from this trend may occur with heavily overconsolidated clays.

It is also good no notice that the failure envelope itself is anisotropic. The "classical" Mohr-Coulomb criterion results in an anisotropic hexagonal failure surface on the octahedral plane. According to literature, the Mohr-Coulomb failure envelope is typically valid for $b = 0$ (when fitted for triaxial compression). For $b > 0$ (or at least for intermediate values between $b = 0$ and $b = 1$) the Mohr-Coulomb criterion tends so underestimate shear strength (More accurate anisotropic failure criteria have been suggested, such as those by Lade (1977) and Matsuoka & Nakai (1974). Figure 3.9 illustrates the relationships between the total stress Tresca and Mises criteria, as well as the effective stress Mohr-Coulomb and Matsuoka-Nakai criteria.

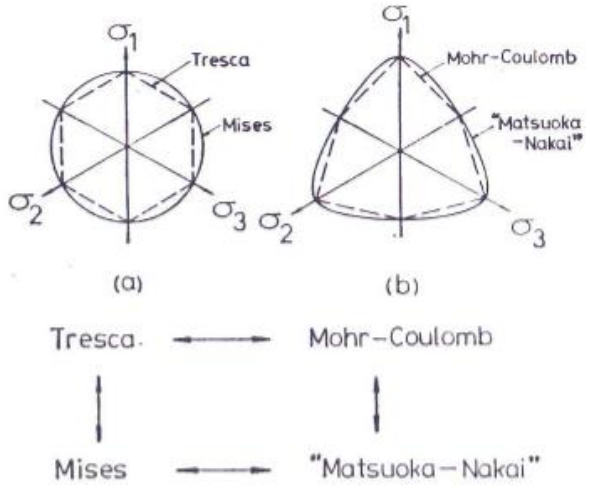

Figure 3.9. Various failure criteria plotted on the octahedral plane (Matsuoka & Nakai 1985)

Sometimes the anisotropic Mohr-Coulomb criterion is approximated using the isotropic Drucker-Prager envelope (Drucker & Prager 1953, Figure 3.10). Drucker-Prager can be mathematically somewhat simpler than Mohr-Coulomb, but it needs to be fitted for a mode of shearing (e.g. triaxial compression or extension), so in some cases it is far less accurate.

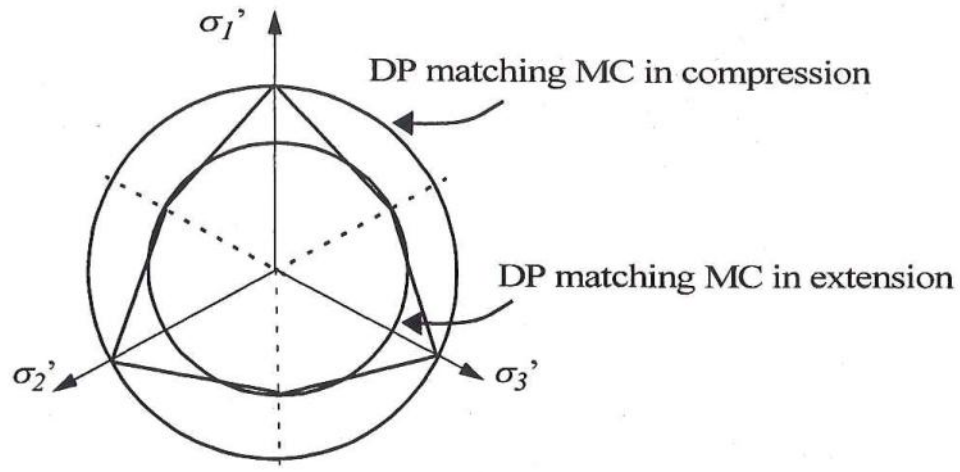

Figure 3.10. Mohr-Coulomb and different fits of Drucker-Prager compared (Nordal 2010)

A general trend can be recognized for typical shearing modes (i.e. triaxial compression, triaxial extension, direct (simple) shear, field vane). Larsson (1980) presents data from several inorganic Scandinavian clays. Larsson compares CAU, CAE and simple shear tests for clays with varying plasticity. For triaxial compression the normalized undrained shear strength averages a fairly constant τ_{fc}/σ'_{v0} = 0.33. For other modes of shearing the normalized shear strength is notably lower and seems to correlate heavily with plasticity (w_L or I_p). (Fig. 3.11).

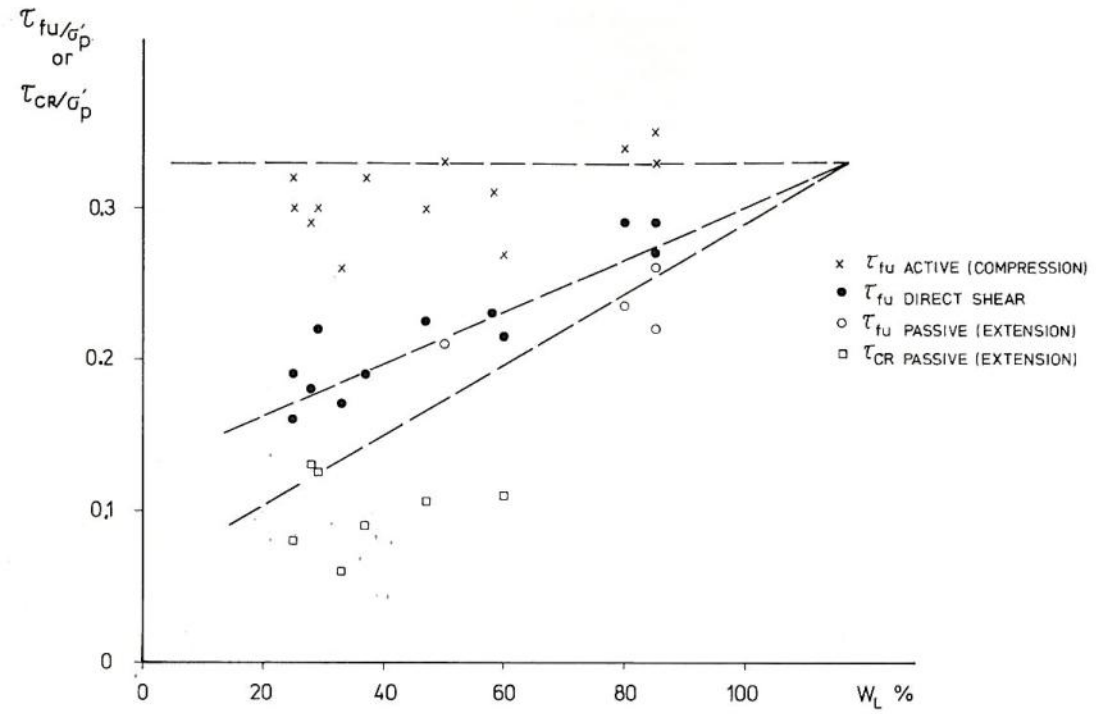

Figure 3.11. Shear strength vs liquid limit for different test types. The strengths represent peak strengths, except τ_{cr}, which is the mobilized shear stress in extension at the strain level where peak compression strength occurs. (Larsson 1980)

It would arguably be desirable to model the anisotropy of undrained shear strength as accurately as possible in stability calculations. This can be done fairly simply by applying measured shear strengths that are obtained by relevant test types to different parts of the slip surface. A common division would be to use triaxial compression strength for the active part of the slip surface, direct simple shear strength for the middle (horizontal) part, and triaxial extension strength for the passive part. (Fig. 3.12) This division is however quite simplified, as the stress system in a given point on the slip surface is in all likelihood closer to plane strain than triaxial conditions. The principal stress direction θ and intermediate principal stress ratio b vary along the slip surface both spatially and temporally.

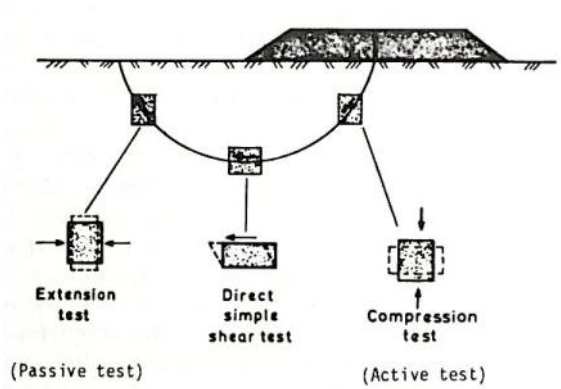

Figure 3.12. Relevance of different laboratory tests to different parts of a slip surface in the field (Larsson 1980 after Bjerrum 1973)

Yet another method of modelling anisotropy would be the use of an anisotropic constitutive soil model. Ideally such a model could predict the available shear strength for any given combination of θ and b. Constitutive soil modelling is strongly associated with the use of FEM. To the knowledge of the author, such models have not yet been applied to LEM, at least not without accompanying FEM calculations that would be used to define a shear strength profile along a slip surface.

In practice, laboratory testing programs including several modes of shearing are feasible only in large projects where there are correspondingly large resources for soil testing. A more common design approach is to use an “average” shear strength for the length of the slip surface. This can be obtained e.g. by field vane or CPTU testing. The shear strength obtained by field testing must then be corrected for various factors such as anisotropy and rate of shearing to better represent the true average available shear strength on the slip surface (Section 3.7).

3.6 Rate and time effects

The time-dependent (viscoplastic) properties of clays present yet another source of variation in undrained shear strength. It is well established by various authors that strain rate and duration of loading have various effects on various properties of clay in undrained loading. Some findings from selected papers are presented in Table 3.2.

Table 3.2. A selection of literature results on rate and time effects on clays.

Author(s)	Soil(s) studied	test type	Measured effect on:				Other notes
			Undrained shear strength	Creep failure	Excess pore pressure	Preconsolidation pressure	
Länsivaara (1999)	Finnish clays	CRS oedometer				apparent σ'_c increases with increasing $d\varepsilon/dt$	
Graham et al (1983)	various clays	various triax. and oedometer	strength increases with increasing $d\varepsilon/dt$			apparent σ'_c increases with increasing $d\varepsilon/dt$	10x decrease in rate -> 10-20% decrease in strength and σ'_c
Leroueil et al (1985)	various clays	CRS and VRS oedometer	strength increases with increasing $d\varepsilon/dt$			apparent σ'_c increases with increasing $d\varepsilon/dt$	σ'_c/σ'_v constant for all values of $d\varepsilon/dt$
Vaid et al (1979)	OC structured clay	CRS consolidation tests; CRS undrained shear tests; triax. undrained creep tests	strength increases with increasing $d\varepsilon/dt$	time to failure decreases with increasing creep stress		apparent σ'_c increases with increasing $d\varepsilon/dt$	
Holzer et al (1973)	SFBM	triax. undrained creep tests		time to failure decreases with increasing creep deviator stress, low enough deviator stress will not cause creep failure	Δu increases with time and deviator stress level		Δu during creep originates partly from deviator stress, partly from arresting of secondary consolidation (dominant)
Arulanandan et al (1971)	SFBM	triax. undrained creep tests		time to failure decreases with increasing creep deviator stress, low enough deviator stress will not cause creep failure	Δu increases with increasing time, deviator stress level and consolidation pressure		
Sheahan et al (1996)	Remoulded BBC	CK_0UC	strength increases with increasing $d\varepsilon/dt$ especially for OCR = 1		Δu decreases with increasing $d\varepsilon/dt$		Peak φ' increases with $d\varepsilon/dt$ for low OCR samples
Lefebvre & Leboeuf (1987)	Structured and remoulded clays	triax.	strength increases with increasing $d\varepsilon/dt$		Structured: no rate-dependency before peak strength Remoulded: Δu decreases with increasing $d\varepsilon/dt$		
Berre & Bjerrum (1973)	Drammen clay	CK_0U	strength increases with increasing $d\varepsilon/dt$				

Based on papers presented in Table 3.2, increasing strain rate results in:

- increased shear strength
- higher measured preconsolidation pressure (and associated with this, larger initial yield surfaces)
- lower shear-induced excess pore pressure for non-structured clay (post-peak response of structured clay is also similarly time-dependent)

It should be noted that the observed increase of undrained shear strength with strain rate can be considered a secondary effect. The rate/time-dependency of s_u seems to be largely caused by the time-dependency of the pore pressure response and the consequent effective stress changes.

The observed effects regarding the rate of loading and undrained creep seem interchangeable. With "low" rates of continuous loading in the NC region, a given deviator stress level is sustained for a "long" time, i.e. *dq/dt* is small. The smaller the value of *dq/dt*, the higher the resulting excess pore pressure response, as a given deviator stress level is sustained for a longer time. In undrained creep tests, a given deviator stress is held constant for a time *t*. Longer creep times lead to higher pore pressure (Figure 3.13a). A similar pore pressure response could then be obtained either by slow constant loading, or a faster loading followed by subsequent undrained creep. This is conceptually illustrated in Fig. 3.13b.

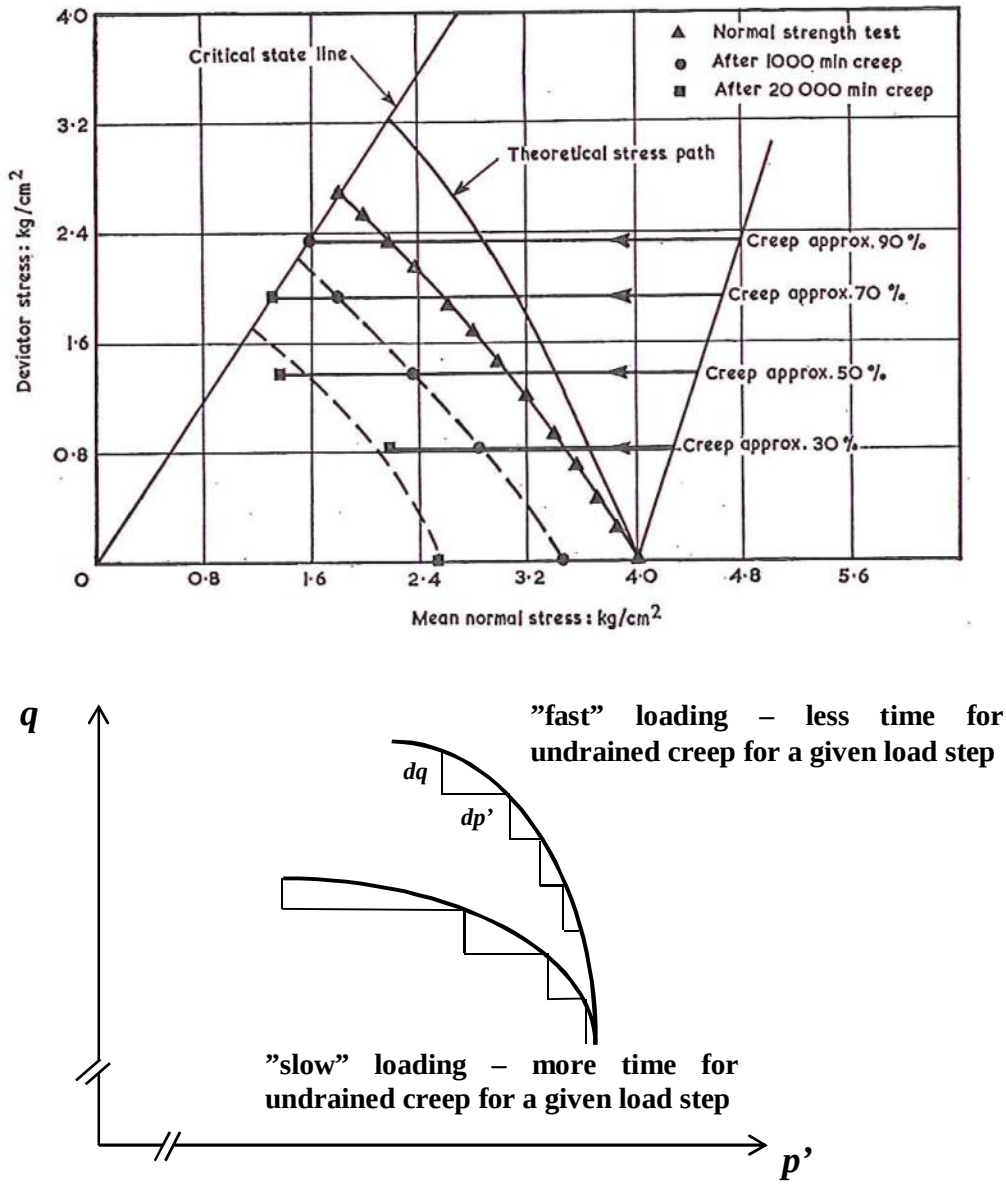

Figure 3.13. a) An example of undrained creep at various deviator stress levels (in percentage of a reference compression test) (Arulanandan et al 1971). b) Illustration of differential "creep steps" in constant rate compression tests at different rates.

Sheahan (1995) presents experimental evidence from several authors that stress paths from triaxial creep tests that do not lead to failure terminate at a "static yield surface" (SYS). The SYS seems to roughly correspond to the effective stress path of a very slow CRS triaxial compression test. Sheahan (1995) and Sheahan and Kaliakin (1999) suggest a "correspondence principle" that states that rate-dependency and undrained creep effects (as well as stress relaxation, which is not covered here) are all governed by same basic mechanisms.

The physical causes of the time-dependent properties of clay in undrained loading are not completely understood. Barden (1969) suggests that creep effects in clay can be caused by jumping of bonds, structural viscosity, and micropore-macropore-fabric. Arulanandan et al (1971) and Holzer et al (1973) suggest the migration of water from a micropore system to a macropore system to be the main cause of clay creep.

3.7 Correction factors for measured s_u

All laboratory and in situ strength tests are conducted at a given rate of strain or stress increase. Typically, the rates at which tests are made are faster than would be involved in true field cases. The measured shear strength needs then be corrected to better match likely field conditions. If design does not explicitly take shear strength anisotropy or the effects of progressive failure into account, the measured shear strength needs to be further corrected.

If vane shear strength is to be used in design, it thus needs to be corrected to match the "true" average strength. To "calibrate" the measured s_u values to represent the average shear strength on the slip surface, various correction factors have been proposed, e.g. by Bjerrum (1972, 1973), Pilot (1972), Dascal & Tournier (1975), Helenelund (1977). Typical correction factors reduce the measured field vane strenght as a function of plasticity (liquid limit or plasticity index). Examples are shown in Figure 3.14.

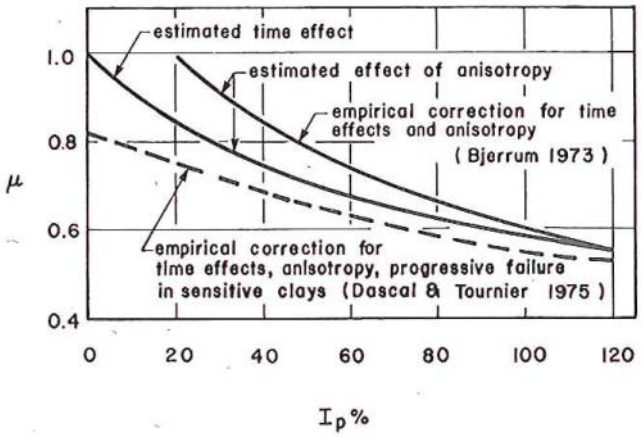

Figure 3.14. Examples of empirical correction coefficients for various factors (Tavenas & Leroueil 1980)

The correction factors are often at least partially obtained by back-analysing sets of slope failures with a given slope stability analysis method (e.g. Bishop's Simplified). While these correction factors often give good results, their validity depends on several issues. Such issues may be how representative the dataset they are based on is; and the accuracy of the stability calculation method used for the back-analyses. Engineering judgment is needed in the proper determination of design strength parameters.

With CPTU testing, undrained shear strength is typically obtained using some semi-empirical function and calibrated against another field or laboratory strength test. The determination of suitable design values becomes, again, largely a matter of engineering judgment.

4 Types of stability analyses

4.1 General

Ladd (1991) distinguishes three types of limit equilibrium stability analyses (Ladd 1991, p. 544):

Effective stress analysis (ESA)
Total stress analysis (TSA)
Undrained strength analysis (USA)

The following sections discuss some of the details and implications of these three types of stability analyses. Special emphasis is given on their suitability and validity for undrained analyses. Note that in this discussion and in subsequent use Ladd's definitions of the analysis types are not accurately followed, but the general division into the three groups can be considered useful.

4.2 Total stress analysis

It is well established that saturated soils exhibit "frictionless" behaviour (i.e. $\varphi = 0$) in terms of total stresses when they are fully undrained. Due to this property it is possible in LEM to simply substitute s_u in place of cohesion (and $\varphi = 0$) in the Mohr-Coulomb failure criterion that is used to define shear strength in limit equilibrium equations. Due to this substitution the failure criterion effectively becomes the Tresca criterion.

The corresponding factor of safety is then simply:

$$F = \frac{s_u}{\tau_m} \tag{4.1}$$

where s_u is the undrained shear strength determined for example by field vane, CPTU or UU laboratory testing. Often such analyses model shear strength as isotropic, or more precisely a "representative average" of the actual shear strength capacity along the slip surface.

With this definition, the shear strength used corresponds to the top of the Mohr's circle, or

$$s_u = \frac{\sigma_1 - \sigma_3}{2}. \tag{4.2}$$

This means that the theoretical failure plane is inclined by $\theta = 45°$ in relation to the principal stresses.

A total stress analysis as defined by e.g. Ladd (1991) corresponds to the "pre-construction", or initial consolidation stress state in the soil. As such it is applicable to the immediate end-of-construction state. If any consolidation occurs and strength increases, e.g. under an embankment, the strength given by pre-construction in situ testing is not applicable. For simple loading problems this is not an issue, because the determining situation where F is smallest is indeed at the end of construction.

Total stress analyses have a distinct theoretical advantage compared to traditional effective stress analyses: The factor of safety is obtained by directly comparing the actual shear capacity at failure to the mobilised shear stress along the slip surface. This of course assumes that the strength profile determined is representative of the average undrained shear strength along the slip surface.

The anisotropy of undrained shear strength (see Section 3.5) can be taken into account for example by dividing the soil into active, direct shear and passive zones, as is done in the Norwegian ADP methodology (see e.g. Bjerrum 1973, Larsson 1980). Ideally, undrained shear strength would be measured with plane strain compression, direct shear and extension tests, which would correspond to strengths found in the active, direct and passive parts of the slip surface (Figure 3.12). As plane strain testing equipment is very rare, triaxial testing can be used instead.

While explicitly modelling the strength anisotropy of clay is possible, in practice this is relatively rare (regional differences in engineering practices notwithstanding). There are however widely used correction factors for field vane strength that implicitly take

anisotropy (among other factors) into account. The various correction factors (Section 3.7) have been obtained by back-analysing various real-life failure cases. The correction factors are generally functions of soil plasticity (I_p or w_L). As they are determined from back-analyses they include the effects of shearing rate, strength anisotropy etc. These physical factors are further discussed in Chapter 3.

4.3 Effective stress analysis

In effective stress limit equilibrium analyses (ESA) the shear strength along the slip surface is calculated using the Mohr-Coulomb effective stress failure criterion:

$$\tau_f = c' + \sigma'_n \tan\varphi' = c' + (\sigma_n - u)\tan\varphi' \qquad (4.3)$$

The factor of safety is expressed as

$$F = \frac{\tau_f}{\tau_m} \qquad (4.4)$$

where τ_m is the mobilized shear stress.

Assuming equal degree of mobilization for both tan φ' and c', the factor of safety can also be expressed as:

$$F = \frac{\tan\varphi'}{\tan\varphi'_m} \qquad (4.5)$$

where φ'_m is the mobilized friction angle

In the equations above, cohesion *c'* and friction angle φ' are the effective strength parameters of the soil, and thus are treated as constants in the calculations. The values of mobilized equilibrium shear stress τ_m and the total normal stress σ_n are products of the specific limit equilibrium method used.

The main applications of ESA are drained stability analyses where there is no excess pore pressure and the effective stresses can be considered known. The usability of ESA for undrained problems has traditionally been questionable due to issues with modelling excess pore pressure, and the inherent overestimation of shear strength due to the use of the Mohr-Coulomb failure criterion with effective stresses.

It is often convenient to describe the undrained pore pressure response of clays in the (*p'*,*q*) stress space, (Cambridge definition, $p' = (\sigma'_1 + \sigma'_2 + \sigma'_3) / 3$). It has been found (see e.g. Wood 1990) that in the overconsolidated (OC) region clay will often exhibit behaviour that is close to linear elasticity, which corresponds to a constant *p'* stress path. This means that for any total stress increment *dp* there will be an equal excess pore pressure increment *du*, resulting in constant mean effective stress (i.e. $dp' = 0$), indicating linearly elastic behaviour.

If the clay is normally consolidated (NC) the undrained effective stress path will depend on the volumetric tendencies of the clay (compression or dilation), and the behaviour will be elasto(visco)plastic (after Wood 1990). The change in effective mean stress *p'* needs to correspond to the tendency for plastic volumetric strains. In the NC region there is also the same effect of counteracting the total stress change as in the OC region. Thus a general incremental form for pore pressure response in (*p'*,*q*) stress space can be written as (Wood 1990 p. 34):

$$\delta u = \delta p - \delta p' \tag{4.6}$$

where δu, δp and $\delta p'$ are increments of pore pressure, total mean stress and effective mean stress.

The expression (4.6) can be derived directly from the principle of effective stress. Here the component $\delta p'$ is an unknown and would need to be determined either by applicable laboratory testing or by means of constitutive modelling.

Modelling other components of pore pressure in soils, such as seepage pressures or static pressure from free ground water is outside the scope of this work. It is however noted that for a geotechnical stability calculation these are just as important as excess pore pressure.

Typical excess pore pressure parameters found in geotechnical design software utilizing LEM (e.g. GeoCalc, Slope/W) offer a way to input desired values of excess pore pressure in a soil layer.

The pore pressure parameter r_u relates pore pressure in soil to vertical total stress:

$$r_u = \frac{u}{\sigma_v} \tag{4.7}$$

where σ_v is the total vertical stress at the bottom of a slice. A value of r_u is often specified for a layer or sometimes for a given point.

Skempton (1954) introduced the parameter $\overline{B}$, which relates loading-induced excess pore pressure to the change of the major principal stress:

$$\overline{B} = \frac{\Delta u}{\Delta \sigma_1} \tag{4.8}$$

For load-induced pore pressure at least the software GeoCalc uses the parameter r_{uq}:

$$r_{uq} = \frac{\Delta u_q}{q_{app}} \tag{4.9}$$

where Δu_q is the load-induced pore pressure and q_{app} is an externally applied vertical load acting on the ground level (loads are fully transferred to the slice bottom in LEM, with no distribution).

The parameter r_{uq} is applied to a layer, but is active only in the bottoms of slices that are externally loaded. Often r_{uq} is utilized so that under loaded slices the resulting shear strength should stay constant regardless of the load level, i.e. the pore pressure increase Δu should be equal to the change of total normal stress $\Delta \sigma_n$. This assumes that the clay behaviour is elastic (which it generally is not). A commonly applied value is r_{uq} = 1, which means that excess pore pressure is equal to the calculated increase in vertical total stress. Experience has however shown that the value of r_{uq} often needs to be less than 1 to avoid unrealistically low shear strength under loads.

Another way of modelling pore pressure is to specify pore pressure iso-lines or points, between which the values are interpolated. This makes inputting quite complex pore pressure profiles possible.

Input values for pore pressure parameters and profiles can be based on in situ measurements and/or laboratory testing, so the current pore pressure state can be modelled quite accurately. It must however be noted that due to the inherent assumptions made in conventional effective stress analyses, using measured pore pressure for undrained calculations will lead to an overestimation of F.

A major limitation of a traditional undrained effective stress analysis is that only the pore pressure response from the initial state to the mobilized state is considered, but further pore pressure generation up to failure is generally ignored. Due to the use of the Mohr-Coulomb strength envelope, this implicit assumption results in an inherent overestimation of shear strength for any factor of safety greater than 1. Correspondingly, the factor of safety will be overestimated. This problem is quite well recognised, e.g. by Ladd (1991), Leroueil et al (1990) and Tavenas et al (1980).

The issue is conceptually illustrated in Figure 4.1. Consider a soil element of compressive ("wet") clay that during construction is loaded from an initial stress state (σ'_0, τ_0) to a mobilized design stress state A (σ'_A, τ_A). The corresponding shear strength is then τ_{fA}. A constant σ' stress path between the design state A and failure is implicitly assumed. It is however very likely that if the soil element is loaded further up to failure, more excess pore pressure will be generated and the effective stress decreases from σ'_A to σ'_B, resulting in an effective stress path that reaches the failure envelope at point (σ'_B, τ_B). When the soil is at failure, the shear stress is then $\tau_B = \tau_{fB} < \tau_{fA}$.

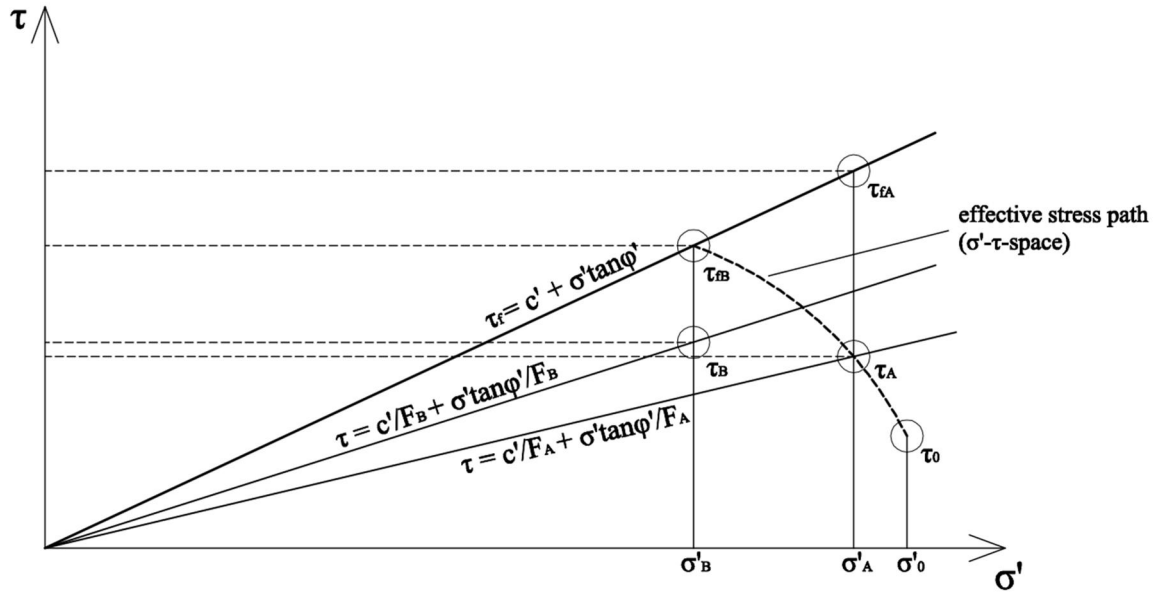

Figure 4.1. Relationship between shear stress and shear strength in undrained effective stress analyses.

It is evident that the available shear strength at failure τ_{fB} is lower than the shear strength τ_{fA} that is implicitly assumed at the "design" stress state A. In fact, the shear strength τ_{fA} that is used in the definition of the factor of safety can never be attained. This means that the resulting factor of safety is obtained by comparing the design state shear stress to an unrealistically high shear strength that does not correspond to failure. This is obviously a very undesirable property in any design task.

Even if the mobilized pore pressure state can be perfectly modelled, the corresponding calculated shear strength is higher than can in most cases be realistically attained. While monitored pore pressures can be used as input values in, the resulting factor of safety will likely not be correct if $F > 1$.

The inherent overestimation of shear strength and F in undrained ESA also means that corresponding total stress analyses cannot, in theory, give same results for any value of $F > 1$. At $F = 1$ the two analysis types will coincide (Figure 4.2).

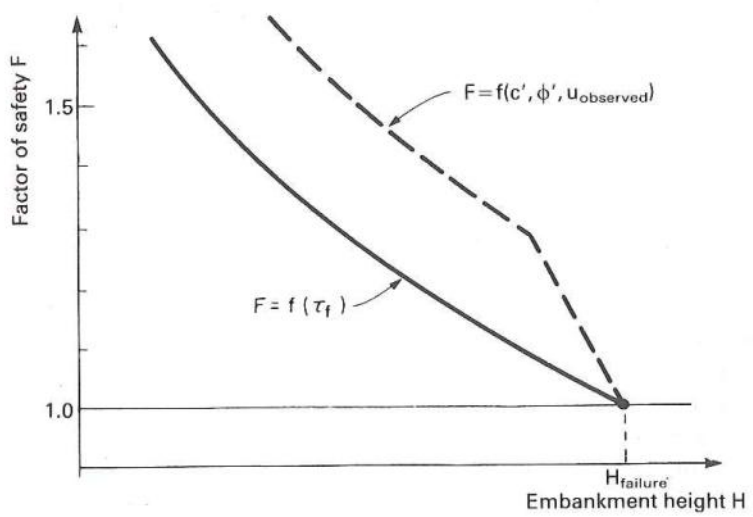

Figure 4.2. Variations in safety factors in corresponding total stress and undrained effective stress analyses as a function of embankment height (Leroueil et al 1990, p. 200)

There may however be some situations where the inherent assumptions of traditional ESA could apply. As ESA assumes no further shearing-induced pore pressure generation between the design state and failure, it corresponds to very slow shearing "with complete dissipation of shear induced pore pressure" (Ladd 1991 p. 550). Essentially this would mean drained shearing while maintaining the initial excess pore pressure level from loading to the design state. Another theoretical possibility could be moderately slow shearing during consolidation, where shearing-induced excess pore pressure is precisely counteracted by simultaneous pressure dissipation from consolidation. Whether these scenarios would be plausible is questionable.

Another issue to consider when modelling excess pore pressure in LEM is that external loads are not distributed as they are in reality, but they act directly on the slice bottoms below. This means that the total stress distribution in the calculation does not correspond to reality. The fact that different LE methods also give different total stress distributions complicates the situation further. To obtain a realistic effective stress distribution (and thus a realistic strength distribution), load-induced excess pore pressure should be modelled only for slices upon which an external load is acting. If pore pressure is modelled based on in situ measurements the pore pressured distribution should be accordingly adjusted. This means that the user should ideally be able to decouple the stress-induced and yielding-induced excess pore pressure components and the distribution of external loading in the soil.

Some geotechnical programs (e.g. Slope/W) utilizing LEM also give the option to model pore pressure with FEM. The accuracy of such a pore pressure profile would then be dependent on the particular calculation model used.

Svanø (1981) proposes a fairly simple method of calculating excess pore pressures based on stress changes. The method UESA (Undrained Effective Stress Analysis) uses Janbu's excess pore pressure equation (after Janbu 1976, referred in Svanø 1981):

$$\Delta u = \Delta p - D \cdot (\Delta\sigma_1 - \Delta\sigma_3) \tag{4.10}$$

where Δp is change in total mean stress, D is a dilatancy parameter, and $\Delta\sigma_1$ and $\Delta\sigma_3$ are changes in the respective total principal stresses. The term $D \cdot (\Delta\sigma_1 - \Delta\sigma_3)$ effectively describes the shear-induced pore pressure component which is dependent on the volume change tendencies of the soil during shearing. Thus it is analogous to the component $\delta p'$ in equation 4.6. The parameter D is determined by triaxial testing (secant value).

A method of calculating shear-induced excess pore pressure in LEM is the parameter r_u' (Länsivaara 2010). The shear-induced pore pressure component is calculated as a function of the initial consolidation pressure. The parameter is defined as:

$$r_u' = \frac{\Delta u_s}{\sigma'_{v0}} \tag{4.11}$$

$$\Leftrightarrow$$

$$\Delta u_s = r_u' \cdot \sigma'_{v0} \tag{4.12}$$

where Δu_s is the shear-induced component of excess pore pressure and σ'_{v0} is the initial effective vertical stress acting on a slice. The value of r_u' is derived from an assumed initial yield surface (Figure 4.3a), with further assumptions of triaxial compression, normal consolidation (OCR = 1) and initial K_0 conditions. This means that the shear-induced component of excess pore pressure is a function of consolidation pressure. Furthermore, it is assumed that the effective stress path between the initial state (intersection of the yield surface and the K_{0NC} line) and failure state (intersection of the yield surface and the failure line) travels along the initial yield surface. In normalized (p',q) space, r_u' is the change of effective mean stress between the initial state and failure, or $\Delta p'$.

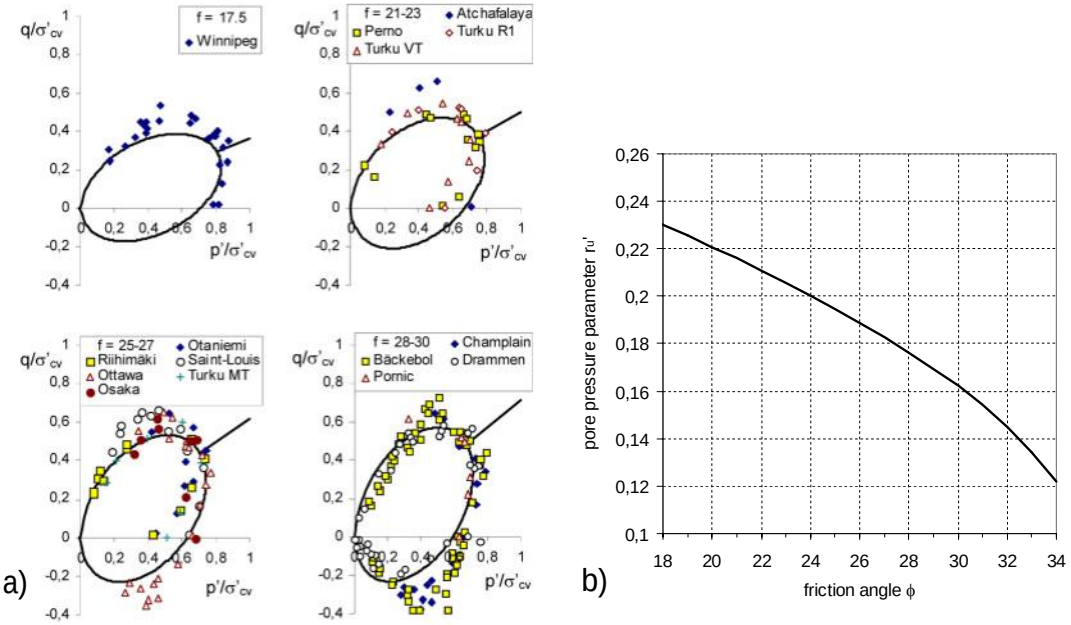

Figure 4.3. a) Estimates of yield surfaces based on friction angle, normalized by vertical preconsolidation stress. b) Solution for the parameter r_u' as a function of φ' (Länsivaara 2010)

With the made assumptions, the value of r_u' becomes simply a function of φ' (Figure 4.3b). The solution only gives the estimated shear-induced excess pore pressure, so the load-induced component needs to be separately taken into accound (e.g. with the r_{uq} parameter).

4.4 Undrained strength analysis

Ladd (1991) differentiates a third type of undrained stability analysis, the Undrained Strength Analysis (USA). USA considers effective stresses acting on the failure plane as *consolidation stresses* (i.e. in situ effective stress before the start of undrained loading). These consolidation stresses can be used to estimate undrained shear strength without knowledge of the excess pore pressures caused by the subsequent undrained loading. Therefore USA can be described as a hybrid between ESA and TSA: the shear strength is solved based on effective (consolidation) stress, but the stability calculation itself can be treated as a total stress analysis because excess pore pressure calculation is not necessary.

USA as defined by Ladd (1991) is very much connected to the SHANSEP (Ladd and Foott 1974) and Recompression (Bjerrum 1973) concepts, as well as Casagrande's QRS method, where undrained shear strength is expressed as a function of effective consolidation stress (Casagrande & Wilson 1960). For more discussion on the effect of preconsolidation pressure on undrained shear strength, see Section 3.4.

Both SHANSEP (Stress History And Normalized Soil Engineering Properties) and Recompression methods contain the same basic steps (after Ladd 1991):

1. The initial stress history of the soil is obtained (in situ effective vertical stress σ'_{v0} and preconsolidation stress σ'_c).

2. Stress changes due to proposed construction are evaluated.

3. Undrained strength is related to consolidation stresses using CK_0U testing (ideally) with relevant failure modes (compression, direct shear, extension). Testing is done at various values of overconsolidation ratio (OCR). Undrained strength is expressed as e.g. s_u/σ'_{v0} = f(OCR).

4. Strength profiles resulting from points 2. and 3. are used as input in stability analyses.

SHANSEP entails consolidating the soil sample to stress states well beyond initial in situ stresses to reliably reach the normally consolidated state. Testing at different levels of overconsolidation is then done by unloading the sample to desired OCR value.

SHANSEP assumes that the strength of the soil can be reliably normalized by e.g. consolidation stress. This is not the case for structured clays where strength will suddenly drop when preconsolidation stress is exceeded and the soil structure is destroyed. The Recompression method takes this into account by not going past the in situ preconsolidation stress at any point so as to preserve the soil structure. (It should be noted that the two methods were developed independently and fairly simultaneously.)

The advantage of USA with SHANSEP and Recompression methods is that the effect of changing consolidation stress on shear strength can readily be estimated, which is not possible with "traditional" total stress analyses (TSA) where shear strength is typically determined solely for the initial in situ stress state. Soil investigations are typically carried out before constructing an embankment, but subsequent investigations from below the embankment can be difficult. The change in consolidation stress can however be fairly

accurately estimated based on the initial (pre-construction) consolidation stress, permeability, load and time.

The methodology also attempts to minimize the effect of sample disturbance. SHANSEP deals with this by first consolidating the sample well beyond its natural preconsolidation pressure, thus creating a new "virgin" state for the sample. This naturally destroys any cementation or aging found in structured natural clays. It can be argued that the Recompression method may be more sensitive to sample quality because its very idea is to run the tests so that the original in situ structure of the sample is retained.

In undrained strength analyses (USA), soil strength is based on correlations with effective consolidation stresses. The stability analysis itself remains a total stress analysis in the sense that strength is given as a "fixed" undrained shear strength that is not affected by effective stresses in the equilibrium calculations. As in traditional TSA, the factor of safety in USA is obtained by comparing the mobilized equilibrium shear stress with a strength that is actually available in failure. This avoids the inherent overestimation of shear strength that happens in traditional undrained effective stress analyses.

The definition of undrained shear strength in USA is however different from the Tresca criterion used in traditional TSA. The Tresca criterion relates strength simply to maximum deviator stress, which is independent of effective stresses. The theoretical failure plane orientation is 45° from both principal stress directions.

USA as defined by Ladd (1991) does not implicitly define the failure criterion. The failure envelope may correspond either to Tresca or Mohr-Coulomb, depending on the test type used to obtain the strength - consolidation stress relationship. The resulting undrained shear strengths are often termed s_u and c_u, respectively (Figure 4.4). The strength s_u is solely defined by the radius of the Mohr's circle at failure:

$$s_u = \tau_{\max} = \frac{\sigma'_{1f} - \sigma'_{3f}}{2} \tag{4.12}$$

The "effective stress" undrained shear strength c_u represents the strength on a failure plane inclined $\theta = 45° + \varphi'/2$ from the minor principal stress direction. It can easily be derived (e.g. using Mohr's circle geometry) that:

$$c_u = \tau_{ff} = \cos\varphi' \cdot \frac{\sigma'_{1f} - \sigma'_{3f}}{2} = \cos\varphi' \cdot s_u \tag{4.13}$$

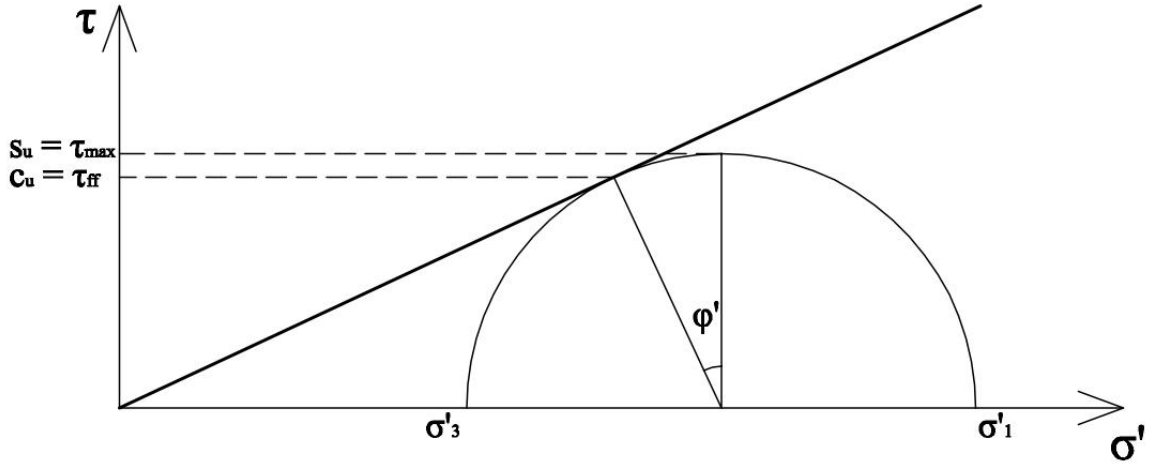

Figure 4.4. Definitions of s_u and c_u

The strength c_u therefore corresponds to the strength at failure, acting on a shear surface consistent with the assumptions of effective stress analyses. According to Bishop & Bjerrum (1960), s_u with a failure surface 45° to horizontal gives the same failure height for a vertical cut as c_u with with a failure surface 45° + φ'/2. From this it could be concluded that if the failure surface corresponds to the assumptions used in a total stress analysis (i.e. $\varphi = 0$), s_u should be used. Correspondingly, c_u should be used if an effective stress slip surface is used.

It can be argued that the strength c_u, corresponding to τ_{ff}, would be a more realistic shear strength input for calculations as it is theoretically the "true" strength that can be mobilized on the "true" failure surface at failure. According to Ladd (1991) this is exactly what an undrained strength analysis should predict, which is why he advocates the use of c_u as defined by Equation 4.13.

It can be noted that the actual stability calculation in LEM using USA works like a typical total stress analysis, as pore pressure is not explicitly accounted for. Additionally, the c_u (or s_u) strength profile determined e.g. by the SHANSEP methodology acts solely an input parameter value. From the standpoint of the equilibrium calculation, the USA strength value functions identically to the s_u value used in "traditional" TSA. The friction angle input needs to be $\varphi = 0$, as in TSA. It is possible that a software-generated critical slip surface will then correspond to TSA assumptions, and in that case the strength $s_u = \tau_{max}$ could just as well be applicable.

5 Proposed modelling approach

5.1 Basic premises and definitions

This thesis presents a new method for calculating undrained shear strength and excess pore pressure in soft clays. The premise is that both can be calculated from stress changes between the initial ("unloaded") state and the failure state.

While one can unquestionably determine the strength of soils by extensive laboratory testing programs, it is not always possible due to time or financial constraints. There is also the question of anisotropy of shear strength, which may be difficult to take into account without rather rarely used laboratory tests such as extension or DSS testing. On the other hand, the critical state friction angle can be determined (for example) with fairly straightforward CIU tests. In addition, oedometer tests to determine the preconsolidation pressure and compressibility properties are routine in typical medium to large construction projects.

The proposed Hybrid s_u (HSU) method uses effective strength parameters and consolidation pressure coupled with a constitutive soil model to

- derive the undrained shear strength for use in total stress stability analyses
- derive excess pore pressure at failure for use in undrained effective stress stability analyses in a manner that is compatible with total stress analyses

The general modelling premise is that both undrained shear strength and excess pore pressure can be accurately and analytically calculated in LEM with a closed form or iterative solution. This is achieved using a fairly simple constitutive soil model and applying suitable assumptions and boundary conditions to reduce the number of unknown factors.

The *initial state* (hereby denoted by subscript "$_0$" means the stress state acting on a soil element before applying an undrained stress change. An example is an existing embankment upon which a traffic load is applied. The initial state then corresponds to the stress state before applying the traffic load. The initial state also corresponds to the in situ consolidation stress state before undrained loading.

The *failure state* (hereby denoted by subscript "$_f$") is in this thesis generally considered to represent the critical state of the soil. In the context of employing soil models for calculation of s_u or Δu, failure stress state is defined as the point in a stress space where the effective stress path reaches the failure envelope. The model does not take strain softening into account.

The *mobilized state* (hereby denoted by subscript "$_{mob}$") is simply the stress state that results from a given undrained loading. Mobilized and failure stress states coincide for $F = 1$.

The (p', q) stress space (Cambridge definition) is used for representing stress states and stress paths. It is especially useful because elastic behaviour of soil results in a constant p' effective stress path, making it easy to decouple load- and shear-induced pore pressure changes.

For sake of brevity in the text, undrained conditions are implicitly assumed unless stated otherwise.

5.2 The S-CLAY1 soil model

To calculate undrained shear strength or excess pore pressure the effective stress path up to failure needs to be modelled. To achieve this, certain selected features of the soil model S-CLAY1 (Wheeler et al 2003) are used.

S-CLAY1 is essentially a derivative of the Modified Cam Clay (Roscoe and Burland 1968) soil model, with an anisotropic initial yield surface (Figure 5.1), coupled with volumetric and rotational hardening of the yield surface. Further refinements of the model also added strain softening caused by destructuration (S-CLAY1S, Koskinen et al 2002), and creep effects (EVP-SCLAY1S, Karstunen et al 2008). What follows is a brief outline of the original S-CLAY1 model, after Wheeler et al (2003).

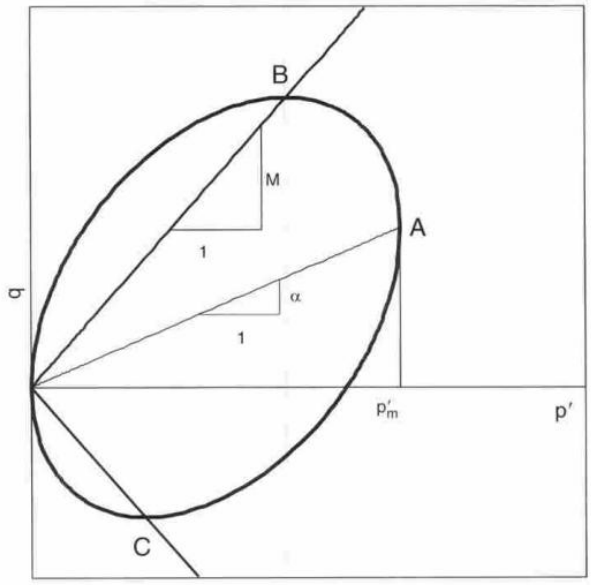

Figure 5.1. The anisotropic yield surface predicted by S-CLAY1 (Wheeler et al 2003)

S-CLAY1 is intended for use with normally or slightly overconsolidated soft clays where yielding is likely caused by small deformations. Therefore isotropic elasticity within the initial yield locus can be assumed with reasonable accuracy. The elastic strain increments are the same as used in MCC:

$$d\varepsilon_v^e = \frac{\kappa dp'}{vp'} \tag{5.1}$$

$$d\varepsilon_d^e = \frac{dq'}{3G'} \tag{5.2}$$

where *p'* and *q* are effective mean stress and deviatoric stress (Cambridge definition), *v* is the specific volume, κ is the slope of the elastic swelling line in (*v*, ln *p'*) coordinates and *G'* is the elastic shear modulus.

The general **yield function** is:

$$f_S = \frac{3}{2}(\{\underline{\sigma'_d} - p'\underline{\alpha_d}\}^T\{\underline{\sigma'_d} - p'\underline{\alpha_d}\}) - (M^2 - \frac{3}{2}\{\underline{\alpha_d}\}^T\{\underline{\alpha_d}\})(p'_m - p')p' \quad (5.3)$$

where M is the critical state strength envelope in (p', q) space, p'_m is the size parameter of the yield surface (see Fig. 5.1). $\underline{\sigma'_d}$ and $\underline{\alpha_d}$ are the deviatoric stress vector and deviatoric fabric tensor, respectively:

$$\underline{\sigma'_d} = \begin{bmatrix} \sigma'_x - p' \\ \sigma'_y - p' \\ \sigma'_z - p' \\ \sqrt{2}\tau_{xy} \\ \sqrt{2}\tau_{yz} \\ \sqrt{2}\tau_{xz} \end{bmatrix} \quad (5.4)$$

$$\underline{\alpha_d} = \begin{bmatrix} \alpha_x - 1 \\ \alpha_y - 1 \\ \alpha_z - 1 \\ \sqrt{2}\alpha_{xy} \\ \sqrt{2}\alpha_{yz} \\ \sqrt{2}\alpha_{xz} \end{bmatrix} \quad (5.5)$$

In triaxial conditions, the yield function is reduced to:

$$f = (q - \alpha_{rot}\, p')^2 - (M^2 - \alpha_{rot}^2)(p'_m - p')\, p' = 0 \quad (5.6)$$

where

$$q^2 = \frac{3}{2}\underline{\sigma_d}^T\underline{\sigma_d} \quad (5.7)$$

$$\alpha_{rot}^{\ 2} = \frac{3}{2}\underline{\alpha_d}^T\underline{\alpha_d} \quad (5.8)$$

The parameter α_{rot} describes the rotation angle of the yield curve in triaxial conditions.

S-CLAY1 assumes **associative flow**, which leads to the following flow rule between the deviatoric and volumetric plastic strain components:

$$\frac{d\varepsilon_d^p}{d\varepsilon_v^p} = \frac{2(\eta - \alpha_{rot})}{M^2 - \eta^2} \quad (5.9)$$

where η is the stress ratio q/p'.

The initial value of α_{rot} can be calculated by assuming cross-anisotropic K_0 consolidation. The normally consolidated K_{0NC} value can be calculated e.g. with the simplified Jaky's equation:

$$K_{0NC} = 1 - \sin\varphi' \tag{5.10}$$

In one-dimensional K_0 straining ($d\varepsilon_r$ = 0) during sedimentation the following relation applies:

$$\frac{d\varepsilon_d}{d\varepsilon_v} = \frac{2}{3} \tag{5.11}$$

If plastic strains are assumed to dominate during the consolidation process (i.e $d\varepsilon^p >> d\varepsilon^e$), it can be estimated that:

$$\frac{d\varepsilon_d^p}{d\varepsilon_v^p} = \frac{2}{3} \tag{5.12}$$

By applying this expression to the flow rule (5.9), the initial value of α_{rot} can be given as:

$$\alpha_{rot0} = \frac{\eta_{K0}^2 + 3\eta_{K0} - M^2}{3} \tag{5.13}$$

where η_{K0} is the stress ratio during K_0 consolidation. This can be calculated from K_{0NC}:

$$\eta_{K0} = \frac{q_{K0}}{p'_{K0}} = \frac{\sigma'_c(1 - K_{0NC})}{\sigma'_c(1 + 2\cdot K_{0NC})/3} = \frac{3 - 3\cdot K_{0NC}}{1 + 2\cdot K_{0NC}} \tag{5.14}$$

If Jaky's equation is thought to apply, both η_{K0} and M are functions of φ'. Thus the shape of the initial yield surface is determined solely by the critical state friction angle, while its size is given by the parameter p'_m. By comparison, Länsivaara (1999) presents data that states that normalized yield surfaces can be determined based solely on friction angle (see Figure 4.1).

There are two hardening laws in S-CLAY1; volumetric and rotational. The **volumetric hardening law** changes the size of the yield surface during yielding (namely, the parameter p'_m). This change is related to plastic volumetric strains (as in Modified Cam Clay):

$$dp'_m = \frac{v\cdot p'_m \cdot d\varepsilon_v^p}{\lambda - \kappa} \tag{5.15}$$

The **rotational hardening law** of S-CLAY1 describes the assumed change in structural anisotropy with plastic straining. Essentially, rotational hardening changes the value of α_{rot} during yielding. It is proposed that plastic strains result in a rearrangement of the soil particles in a way that the eventual arrangement has a different level of anisotropy compared to the initial state. It is also assumed that plastic volumetric strain attempts to "drag" the value of α_{rot} towards a certain instantaneous target value $\chi_v(\eta)$ (Wheeler et al

2003). At the same time, plastic deviatoric strains try to set α_{rot} to an instantaneous target value of $\chi_d(\eta)$. The proposed rotational hardening law of S-CLAY1 is:

$$d\alpha_{rot} = \mu\left[(\chi_v(\eta) - \alpha_{rot}) < d\varepsilon_v^p > + \beta(\chi_d(\eta) - \alpha_{rot})\left|d\varepsilon_d^p\right|\right] \tag{5.16}$$

where μ is a parameter that controls the rate at which α_{rot} is approaching its target value, and β controls the ratio of the effects of $\chi_v(\eta)$ and $\chi_d(\eta)$. Wheeler et al (2003) propose expressions for $\chi_v(\eta)$ and $\chi_d(\eta)$ for Otaniemi clay:

$$\chi_v(\eta) = \frac{3\eta}{4} \tag{5.17}$$

$$\chi_d(\eta) = \frac{\eta}{3} \tag{5.18}$$

5.3 Rotational hardening and choice of failure criteria in HSU

While rotational hardening caused by plastic strains is a valid and fairly intuitive concept, it may be problematic to implement in practice due to the number of parameters and assumptions that are needed. This is contrasted by relatively little available experimental data suitable for determining the rotational hardening parameters. Therefore it is useful to consider if rotational hardening needs to be implemented into HSU. In the intended use of the HSU method there are no resources for actually determining the rotational hardening parameters so these would need to be assumed.

To illustrate the effect of rotational hardening on predicted shear strength, a theoretical example using S-CLAY1 is presented. Shear strength is calculated in triaxial compression and extension with and without rotational hardening, using Mohr-Coulomb and Drucker-Prager failure criteria.

As the overall philosophy of the calculation method proposed in this thesis is "relative simplicity", further discussion of rotational hardening is omitted here. Taking rotational hardening into account would present several additional parameters to determine and assumptions to make, and would perhaps complicate the calculation unnecessarily. However, the effect of (assumed) rotational hardening can be (crudely) counteracted by universally using the critical state line M for triaxial compression for all stress states, as shown in this example. Normally consolidated clay with parameters given in Table 5.1 is simulated. Effective stress paths calculated with S-CLAY1 are presented for the following cases:

A) No rotational hardening applied, Drucker-Prager fitted for compression
B) Rotational hardening applied, Drucker-Prager fitted for compression
C) No rotational hardening, Mohr-Coulomb
D) Rotational hardening, Mohr-Coulomb

Table 5.1. S-CLAY1 model parameters used in the example

property	value	description
φ' [°]	30	friction angle
M_c	1.2	CSL slope for triaxial compression
M_e	0.857	CSL slope for triaxial extension
OCR	1	overconsolidation ratio
K_{0NC}	0.5	K_0 for 1-D consolidation
η_{K0NC}	0.75	q/p' for 1-D consolidation
α_{rot0}	0.458	initial inclination of the yield surface (Eq. 5.13)
λ^*	0.05	modified compression index (arbitrary value)
κ^*	0.01	modified swelling index (arbitrary value)
β	0.5M	relative rotational parameter
μ	300	absolute rotational parameter ($\mu = 15/\lambda^*$)

The parameters K_{0NC}, η_{K0NC}, and α_{rot0} are determined using equations 5.10, 5.13, 5.14.

The parameters λ^* and κ^* are chosen arbitrarily so that the ratio $\lambda^*/\kappa^* = 5$. As strains are not considered in the example, only the ratio $\lambda^*/\kappa^* = \lambda/\kappa$ has an effect on the stress paths, not the absolute values.

The parameters β and μ are chosen based on suggestions given in literature. Wheeler et al (2003) give an expression for β:

$$\beta = \frac{3(4M^2 - 4\eta_{K0}^2 - 3\eta_{K0})}{8(\eta_{K0}^2 - M^2 + 2\eta_{K0})} \tag{5.19}$$

However, Mansikkamäki (2015) notes that this expression is sensitive to the value of K_{0NC}. If the value of K_{0NC} deviates from the simplified Jaky's equation (Eq. 5.10), the value of β calculated using Eq. 5.19 changes rapidly, and can even get very high positive or slightly negative values. Wheeler et al (2003) suggest a value β = 0.5…1. In this example, an arbitrary value of $\beta = 0.5M$ is chosen.

The rotational parameter μ is chosen as $15/\lambda^*$. This falls in the middle of the range $\mu = 10/\lambda^*$…$20/\lambda^*$ proposed by Zentar et al (2002).

If the Mohr-Coulomb failure criterion is thought to apply, the value of M is different for triaxial compression (M_c) and extension (M_e):

$$M_c = \frac{6\sin\varphi'}{3-\sin\varphi'} \tag{5.20}$$

$$M_e = \frac{6\sin\varphi'}{3+\sin\varphi'} \tag{5.21}$$

This can be modelled in triaxial applications by using $M = M_c$ for $\eta \geq \alpha$, and $M = M_e$ for $\eta < \alpha$ (Wheeler et al 2003). This is illustrated in Fig. 5.2. Note the "squishing" of the yield surface on the extension side.

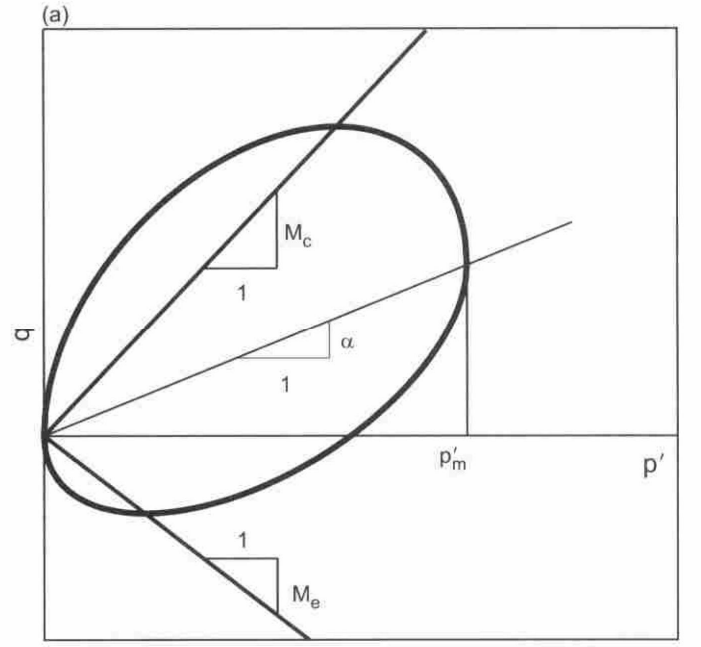

Figure 5.2. S-CLAY1 yield surface with anisotropic failure criteria (Wheeler et al 2003)

In the cases where Mohr-Coulomb failure is assumed, the value of M is changed accordingly depending on the value of η (i.e. if $\eta < 0$, M will correspond to extension and vice versa). This affects all equations that are dependent on M. The resulting effective

stress paths and initial yield surfaces for the various cases are presented in Figure 5.3. The corresponding undrained shear strengths are given in Table 5.2.

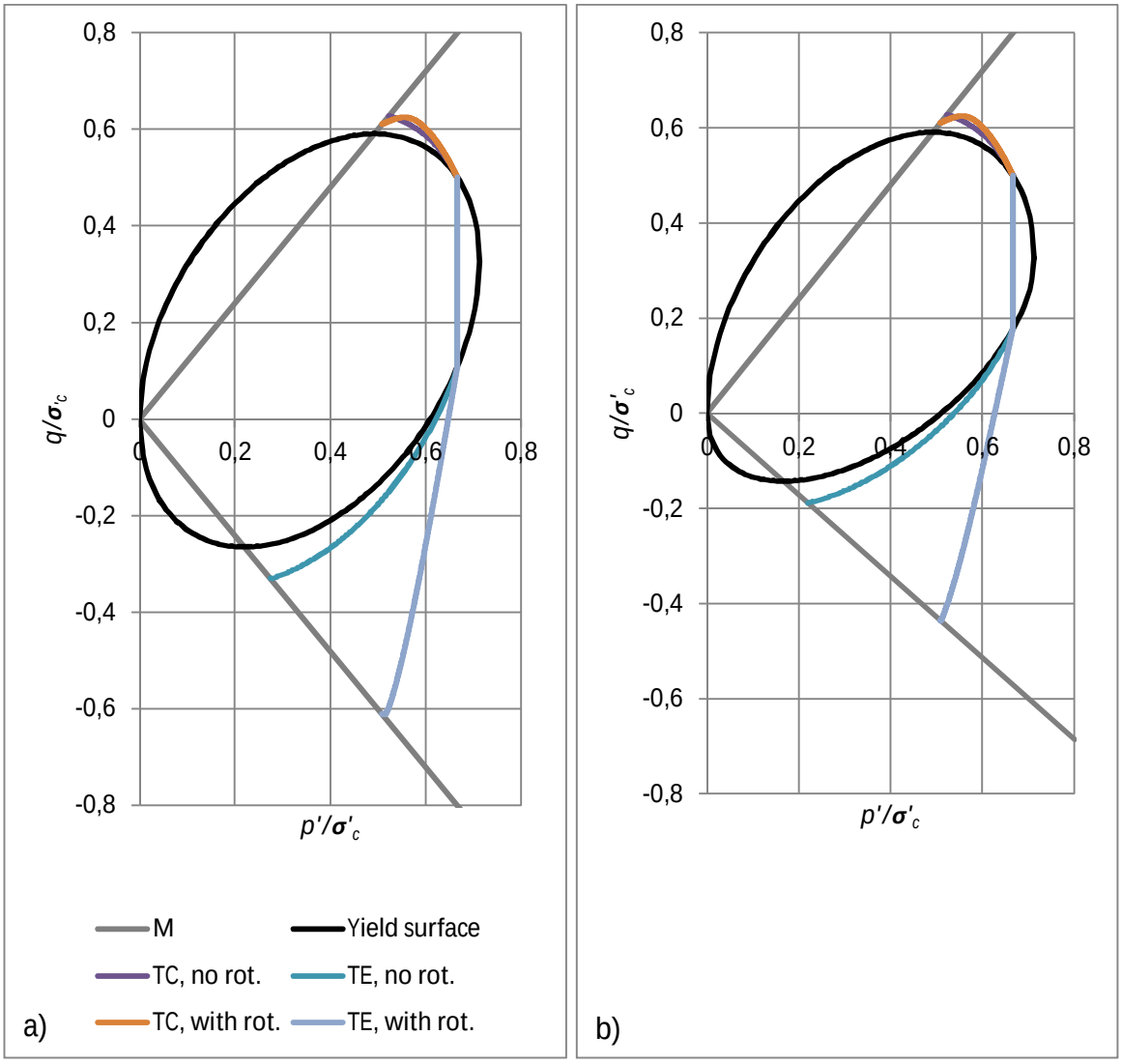

Figure 5.3. Calculated stress paths for the various cases. a) Drucker-Prager fitted for compression, b) Mohr-Coulomb with fitted initial yield surface

Table 5.2. Normalized s_u calculated with the different assumptions.

	No rot. hard. DP	Rot. hard. DP	No rot. hard. MC	Rot. hard. MC
s_{uC}/σ'_c	0.314	0.305	0.314	0.305
s_{uE}/σ'_c	0.165	0.305	0.132	0.218
s_{uE}/s_{uC}	0.526	1.000	0.419	0.714

The results of this arbitrary example show fairly small shear strength differences for compression when applying rotational hardening as proposed for S-CLAY1, or when rotational hardening is left out of the model. This is an expected result, because the stress path in the elastoplastic zone (i.e. outside the initial yield surface) is short, and rotational hardening is relatively minor.

The differences are more notable for triaxial extension. Rotational hardening caused by plastic straining pushes the yield surface towards a more isotropic state, which consequently leads to a more vertical stress path and isotropic shear strength. It seems that in this example, applying rotational hardening results in complete shear strength isotropy (s_{uC}/s_{uE} = 1) for the Drucker-Prager failure criterion. This appears to be caused by a coincidental "perfect" combination of parameters, and for a different set of parameters the anisotropy would be different. By using the Mohr-Coulomb failure criterion where the appropriate M value for extension is used, shear strength anisotropy is higher.

It may be argued that while proper selection of the rotational hardening parameters can allow for quite accurate predictions of shear strength, it seems very difficult to determine these parameters without a very extensive laboratory testing program. By relying on the sparse parameter value recommendations found in literature one may not always expect good accuracy.

From the standpoint of making the proposed model simple but still "accurate enough", rotational hardening can be omitted, but the failure criterion is set to Drucker-Prager. This choice has some advantages over the "proper" use of rotational hardening and Mohr-Coulomb. First, the Drucker-Prager criterion is mathematically convenient as it results in a continuous and constant M value for all Lode angles. Omitting rotational hardening further simplifies the model and reduces the number of unknown parameters.

Additonally, the use of Drucker-Prager fitted for compression slightly counteracts the possible error that occurs in triaxial extension (and nearby stress states) if rotational hardening is omitted from the model. This "corrective" effect is admittedly difficult to quantify except in single cases, but can be seen as a qualitative improvement.

5.4 On the assumptions made in the Hybrid s_u method

The new calculation method named "Hybrid s_u" (HSU) is intended to be used with LEM to calculate an appropriate undrained shear strength in total stress analyses. For undrained effective stress analyses, the method can be used to calculate excess pore pressure so as to arrive to a correct shear strength value.

The goal is to find a closed form solution with few enough input parameters, while at the same time giving the ability to model the anisotropy of undrained shear strength with reasonable accuracy. The parameters needed would have to be such that they can either be determined with simple laboratory testing or readily estimated by other means.

The HSU solution is based on the S-CLAY1 soil model (described in Section 5.2). S-CLAY1 is used here due to its relative mathematical simplicity and potential for accurately modelling anisotropy of shear strength. A notable departure from the original S-CLAY1 is that in this application, **rotational hardening is altogether omitted**. Reasons for this are:

- There is still relatively little experimental data to support certain model assumptions made regarding fabric anisotropy and rotational hardening. There is also still some ongoing debate on certain theoretical aspects (e.g. existence of fabric anisotropy in critical state). This is briefly discussed by e.g. Dafalias and Taiebat (2014).

- Even if all theoretical aspects of rotational hardening were universally accepted and the given model could as such be considered very accurate, determining parameter values remains a problem. In typical design projects where testing resources are limited, the parameters β and μ cannot in practice be determined reliably, and literature values would need to be relied upon. The rotation target value functions $\chi_v(\eta)$ and $\chi_d(\eta)$ seem to have expressions based only on one Finnish clay as described by Wheeler et al (2003), and cannot as such be considered universally valid.

- The intended use for the model is predicting shear strength. As such, there is no pressing need to model strains and the entire stress path between the initial state and failure all that accurately, as long as the eventual shear strength can be obtained. Within this framework, additional "obscure" parameters can even be considered a distraction for the user.

The omission of rotational hardening from the method may induce errors especially in determining shear strength in extension, as modelling changes in fabric anisotropy is left out. It can however be argued that using rotational hardening with wrongly determined parameters may also induce errors. It can be better to use a simpler model with fewer parameters than to use a complex model whose parameters are difficult to determine correctly.

There is however a LEM-specific approach that is applied in the HSU method: By disregarding strains in the LEM application, an additional degree of freedom in modelling stress paths is obtained in the use of compression and swelling indices λ and κ. *By "decoupling" these parameters from their original physical meaning, the ratio λ/κ can*

now be used to control the direction of the stress path. With this approach, the ratio λ/κ effectively becomes a control parameter for s_u. This is illustrated in Figure 5.4, where undrained "S-CLAY1-like" (no rotational hardening, Drucker-Prager) stress paths using different λ/κ ratios are drawn.

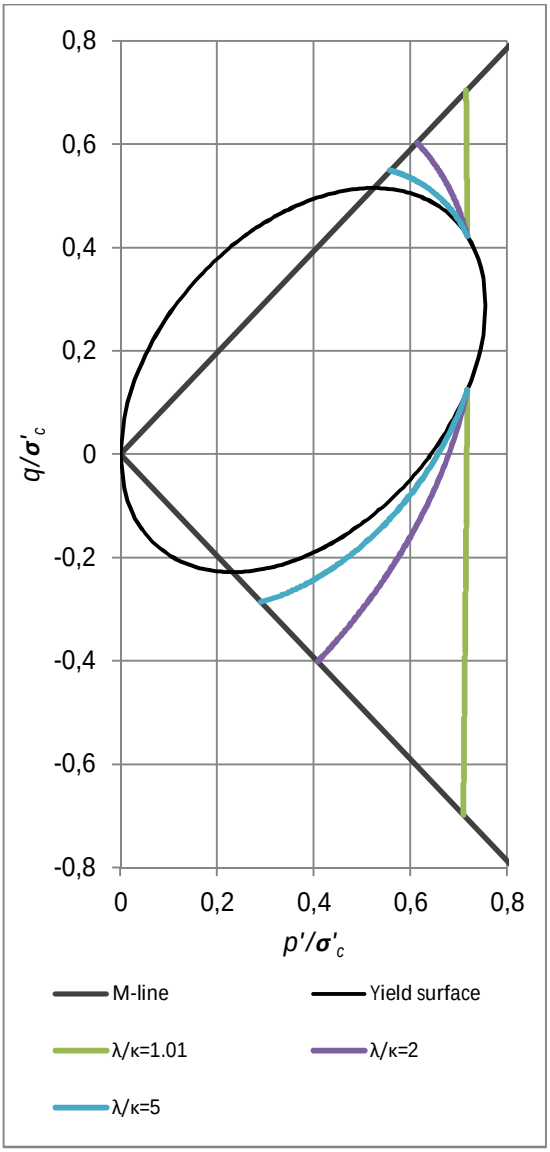

Figure 5.4. Effective stress paths from S-CLAY1 (sans rotational hardening). φ' = 30°, OCR = 1

As the physical meaning of λ/κ is to some extent ignored, it can even be given physically impossible negative values if needed for controlling the effective stress path. This makes the parameter somewhat arbitrary as it becomes something that cannot be readily determined in the laboratory. λ/κ can however be considered a fairly "transparent" and direct parameter as its effect on the stress path is quite apparent, even by sheer trial and error.

λ/κ can for example be chosen so that HSU fits a known (measured) undrained strength value, such as triaxial compression strength or field vane strength. The method is then essentially used to predict the anisotropy of shear strength based on the measured value. If no "desired" shear strength value is available, λ/κ can be chosen so as to give a cautious or conservative estimate of undrained shear strength. The value of λ/κ can also be based on laboratory testing, but this is by no means a necessity.

Another important assumption made in HSU is that the chosen failure criterion is the Drucker-Prager envelope for triaxial compression, i.e. $M = M_c$ for all stress states.

This departure from more "universally" applicable failure criteria (e.g. Mohr-Coulomb or Matsuoka-Nakai criteria) has two main reasons:

- Convenience. Assuming constant M for all combinations of stress states greatly simplifies the analytical solution as no Lode angle dependence needs to be incorporated for M.
- An attempt to counteract the omission of rotational hardening in the model. While there may be difficulties in obtaining proper rotational hardening parameters, the basic concept of rotational hardening is at least qualitatively valid. In extension, some decrease of anisotropy can be expected due to the changes in principal stress directions. The omission of rotational hardening in the model, coupled with the Mohr-Coulomb (or similar) failure criterion, would lead to low predicted shear strengths. By using the Drucker-Prager criterion matching triaxial compression this effect can be counteracted.

The general approach in making these assumptions is that if parameters needed to model a given physical phenomena cannot be reliably determined or assumed, it is better to leave the property out of the model. In addition, assumptions are made so that any induced errors would at least tend to cancel each other. A single, reasonably transparent "control" parameter in the form of λ/κ is retained to give the user an ability to fine-tune or fit the model to give appropriate results.

5.5 Closed form solution of p'_f

For the purpose of this thesis, a "stripped down" derivative of the original S-CLAY1 model is used. The applied solution retains volumetric hardening, but omits the rotational hardening properties for the sake of simplicity. The main goal of the calculation is to calculate the effective mean stress p'_f at failure using easily obtainable parameters and plausible assumptions. The value of p'_f is then used to calculate either s_u in total stress analyses, or excess pore pressure at failure Δu_f in undrained effective stress analyses.

The general form of the S-CLAY1 yield function is expressed in terms of Cartesian stresses. These can in turn be expressed in terms of principal stresses and principal stress rotation angle θ using known properties of continuum mechanics.

Using simple substitutions and rearranging (see Appendix A), the S-CLAY1 yield function can first be solved for σ'_1, where the unknown variables are effective mean stress p', intermediate principal stress parameter b, principal stress rotation angle θ and the size of the yield surface at failure p'_{mf}. The critical state line parameter M and the yield surface inclination α_{rot} are considered constants. They are solved as functions of φ' (eq's 5.20 and 5.13) and do not depend on any other parameters. The M value used is for triaxial compression. α_{rot} is calculated assuming cross-anisotropic K_0 consolidation (and in this application, no rotation of the yield surface). As discussed in previous chapters, these assumptions regarding M and α_{rot} somewhat balance their corresponding errors.

The S-CLAY1 yield function solved for σ'_1, (for the derivation, see Appendix A):

$$\sigma'_{1S} = \sigma'_{1S}(p', b, \theta, p'_m) = \frac{2/3 \cdot \alpha_{rot} - \alpha_{rot} \cdot \sin^2\theta + \alpha_{rot} \cdot b \cdot (b/6 - 2/3 + (\sin^2\theta)/2) + B}{B} \cdot p'$$
$$\pm \frac{(b-2)\sqrt{p'}\sqrt{4B \cdot M^2 \cdot p' + (b^2 + 6b \cdot \sin^2\theta - 4b + 9 \cdot \sin^4\theta - 12 \cdot \sin^2\theta + 4) \cdot \alpha_{rot}^2 \cdot p' + 4B(M^2 + \alpha_{rot}^2) \cdot p'_m}}{6B} \tag{5.22}$$

where

σ'_{1S}	major principal stress solved from the S-CLAY1 yield function [kPa]
α_{rot}	yield surface rotation parameter (Eq. 5.13)
b	intermediate principal stress parameter (Eq. 3.11)
θ	principal stress rotation angle [°] (Eq. 5.43)
p'	effective mean stress [kPa]
M	CSL parameter
p'_m	yield surface size parameter [kPa]

The term B is used to shorten the overall expression, and is defined as:

$$B = b^2 - b + 1 \tag{5.23}$$

As the aim is to solve the effective mean stress *at failure* (p'_f), a failure envelope needs to be introduced. While an anisotropic effective stress failure envelope could be considered accurate, for the sake of simplicity, the Drucker-Prager failure criterion corresponding to triaxial compression is used here. In addition, no cohesion is assumed (at this point - see Section 5.9 for an HSU formulation with cohesion). The assumption here is that in critical state, any structuration that would cause true cohesion will be destroyed by large shear straining.

Essentially, the stress state at failure is calculated as the point in stress space where the effective stress path (a point on a volumetrically expanding yield surface) intersects the Drucker-Prager failure surface.

The Drucker-Prager envelope corresponding to triaxial compression with no cohesion can be formulated as

$$f_{DP} = \sqrt{J_2} - \frac{2\sqrt{\sin\varphi'}}{\sqrt{3}(3+\sin\varphi')} \cdot 3p' = \sqrt{J_2} - C_1 \cdot 3p' \tag{5.24}$$

where the deviatoric invariant:

$$J_2 = -(\sigma'_1 - p')(\sigma'_2 - p') - (\sigma'_1 - p')(\sigma'_3 - p') - (\sigma'_2 - p')(\sigma'_3 - p') \tag{5.25}$$

The term C_1 is defined as:

$$C_1 = \frac{2\sin\varphi'}{\sqrt{3}(3-\sin\varphi')} \tag{5.26}$$

The Drucker-Prager criterion can then be solved for σ'_1, eventually resulting in:

$$\sigma'_{1DP}(p', b) = \frac{B - \sqrt{3}(\pm 2 + b) \cdot C_1 \cdot \sqrt{B}}{B} p' \tag{5.27}$$

At failure, the S-CLAY1 and Drucker-Prager criteria coincide (i.e. the stress state at failure lies both on the S-CLAY1 yield surface and the Drucker-Prager failure surface). By assuming:

$$\sigma'_{1DP} = \sigma'_{1S}$$

i.e. the major principal stresses at failure are equal, the mean effective principal stress at failure p'_f can be solved:

$$p'_f(b, \theta, p'_{mf}) = \frac{B(M^2 - \alpha_{rot}{}^2)}{M^2 + M^2 b^2 - b(M^2 - C_2) + 27C_1{}^2 \cdot B - 2C_2 + 3C_2 \cdot \sin^2\theta} p'_{mf} \tag{5.28}$$

where

$$C_2 = 3\sqrt{3} C_1 \sqrt{B} \cdot \alpha_{rot} \tag{5.29}$$

The final unknown variable here is p'_{mf}. To calculate this, the S-CLAY1 volumetric hardening law (eq. 5.15) is applied. After solving a differential equation (Appendix A), for undrained conditions it can be written that:

$$p'_{mf} = \frac{p'_f{}^A \cdot p'_{m0}}{p'_0{}^A} \tag{5.30}$$

where

$$A = -\frac{\kappa}{\lambda - \kappa} = \frac{\kappa}{\kappa - \kappa \cdot \frac{\lambda}{\kappa}} = \frac{1}{1 - \frac{\lambda}{\kappa}} \tag{5.31}$$

Finally, inserting this expression into Eq. 5.30 and solving for p'_f results (when trivial solutions are omitted) in:

$$p'_f = e^{\ln(1/E)/(A-1)} \tag{5.32}$$

where

$$E = \frac{M^2 - \alpha_{rot}{}^2}{2M^2 + \frac{M \cdot \alpha_{rot}}{\sqrt{B}} \cdot (3\sin^2\theta + b - 2)} \cdot \frac{p'_{m0}}{p'_0{}^A} \tag{5.33}$$

M	CSL inclination for triaxial compression (Eq. 5.20)
α_{rot}	yield surface inclination parameter (Eq 5.13)
b	intermediate principal stress parameter (Eq 3.11)
θ	principal stress rotation angle [°](Eq. 5.43)
p'_0	initial effective mean stress [kPa] (Eq. 5.37)
p'_{m0}	initial size of the yield surface [kPa] (Eq. 5.40)

5.6 Review of HSU parameters

Table 5.3 gives a brief description of the various parameters used in Eqs. 5.31 and 5.33.

Table 5.3. List of parameters used in calculating p'$_f$.

parameter	description	notes
M	inclination of critical state line	soil parameter, function of $\boldsymbol{\varphi'}$
α_{rot}	inclination of yield surface	soil parameter, function of $\boldsymbol{\varphi'}$
b	intermediate principal stress ratio	state parameter, function of stress changes during loading
θ	principal stress rotation angle	state parameter, function of $\boldsymbol{\varphi'}$and slip surface inclination $\boldsymbol{\alpha}$
p'_0	initial effective mean stress	state parameter, function of $\boldsymbol{\varphi'}$, $\boldsymbol{\sigma'_{v0}}$ and $\boldsymbol{\sigma'_c}$
p'_{m0}	initial size of the yield surface	state parameter, function of $\boldsymbol{\varphi'}$, $\boldsymbol{\sigma'_{v0}}$ and $\boldsymbol{\sigma'_c}$
λ (or λ*)	compression index in (ln p', e) space	soil parameter
κ (or κ*)	swelling index in (ln p', e) space	soil parameter

As is evident from Table 5.3, the basic input parameters needed for the model are the critical state friction angle $\boldsymbol{\varphi'}$, initial vertical (consolidation) stress $\boldsymbol{\sigma'_{v0}}$, preconsolidation pressure $\boldsymbol{\sigma'_c}$, compression and swelling indexes λ and κ (or more specifically, their ratio $\boldsymbol{\lambda/\kappa}$), and intermediate principal stress ratio at failure $\boldsymbol{b}$.

As discussed in various chapters, the following assumptions are made:

- No cohesion at failure, all structuration is assumed to be broken down before reaching critical state
- The initial stress state is cross-anisotropic, with K_0 conditions
- Isotropic elasticity inside the yield locus (constant p' stress path)
- The Drucker-Prager failure criterion fitted for triaxial compression is used, no cohesion
- Rotation of the yield surface is omitted. The value of α_{rot} is constant.

The aforementioned parameters are calculated with a sequence of equations presented next. Two additional parameters are introduced: the parameters "*C*" and "*D*" can be used to adjust the values of K_{0NC} and K_0, respectively.

The M value for triaxial compression is used for all stress states:

$$M = \frac{6 \cdot \sin\varphi'_c}{3 - \sin\varphi'_c} \tag{5.20bis}$$

The NC value of K_0 is obtained with a modified version of the Jaky equation:

$$K_{0NC} = C(1 - \sin(\varphi'_c)) \tag{5.34}$$

where C is a coefficient. By default it can be set to $C = 1$, but in many cases it can vary. By adjusting the value of C, any known K_{0NC} value can be replicated.

The in situ value for $_{K0}$ is obtained by slightly modifying the equation suggested by Mayne & Kulhawy (1982):

$$K_0 = K_{0NC} \cdot OCR^{D\cdot\sin(\varphi'c)} = K_{0NC} \cdot \left(\frac{\sigma'_c}{\sigma'_{v0}} \right)^{D\cdot\sin(\varphi'c)} \tag{5.35}$$

where D is a coefficient. By default it can be set to $D = 1$, but in many cases it can vary. By adjusting the value of D, any known K_0 value can be replicated.

Vertical preconsolidation pressure:

$$\sigma'_c = OCR \cdot \sigma'_{v0} \tag{5.36}$$

Initial effective mean stress:

$$p'_0 = \frac{\sigma'_{v0}(1 + 2 \cdot K_0)}{3} \tag{5.37}$$

Mean preconsolidation pressure:

$$p'_c = \frac{\sigma'_c(1 + 2 \cdot K_{0NC})}{3} \tag{5.38}$$

Deviatoric preconsolidation stress (i.e. deviator stress obtained at preconsolidation pressure):

$$q_c = \sigma'_c(1 - K_{0NC}) \tag{5.39}$$

Stress ratio during consolidation:

$$\eta_{K0NC} = \frac{q_c}{p'_c} = \frac{\sigma'_c(1 - K_{0NC})}{\frac{\sigma'_c(1 + 2 \cdot K_{0NC})}{3}} = \frac{3 \cdot (1 - K_{0NC})}{1 + 2 \cdot K_{0NC}} \tag{5.14bis}$$

The inclination of the yield surface:

$$\alpha_{rot} = \frac{\eta_{K0NC}^2 + 3\eta_{K0NC} - M^2}{3} \tag{5.13bis}$$

The size of the initial yield surface can be solved from the triaxial yield function (eq. 5.6), which results in:

$$p'_{m0} = \frac{M^2 \cdot p'^2_c - 2 \cdot \alpha_{rot} \cdot p'_c \cdot q_c + q_c^2}{p'_c(M^2 - \alpha_{rot}^2)} \tag{5.40}$$

The value of the principal stress rotation angle θ (i.e. angle of σ'_1 from the vertical direction) can be derived from the theory of plasticity. It is established that at failure, the critical shear plane is at an angle of 45° - $\varphi'/2$ from the major principal stress. It can be assumed that the critical slip surface corresponds to the critical shear plane. For a situation where σ'_1 is vertical (i.e. $\theta = 0$), the inclination of the slip surface α would then need to be 45° + $\varphi'/2$ from horizontal (Fig. 5.5)

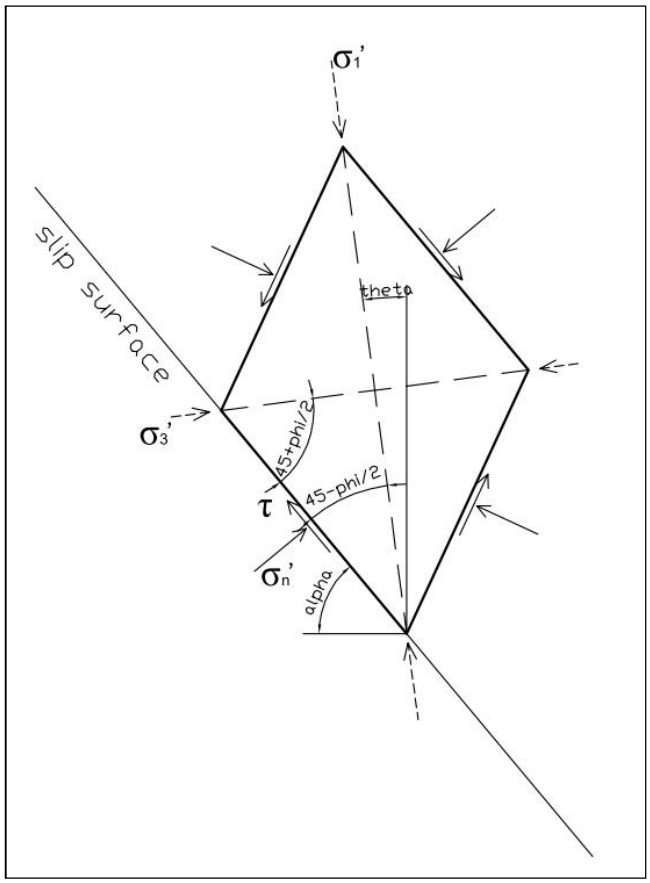

Figure 5.5. The relationship between principal stress direction and the inclination of the slip surface (failure plane)

The principal stress rotation value is then

$$\theta = 45° + \varphi'_c/2 - \alpha \qquad (5.41)$$

where α is the inclination of the critical slip surface at a given point (Figure 5.6).

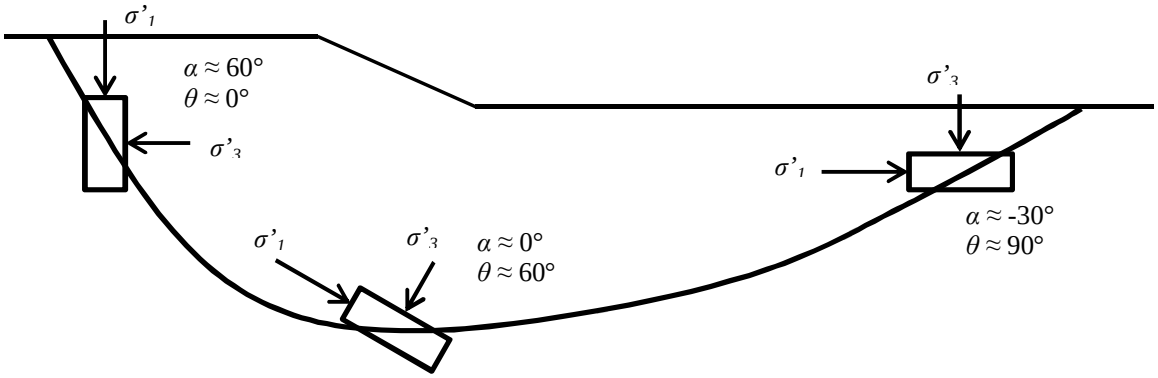

Figure 5.6. Principal stress rotation angle at various parts of a slip surface.

In LEM context the changes in total stresses could be calculated iteratively: First an initial assumption of b is made, and the equilibrium is calculated. Then, the stress state on the slip surface is used to calculate an updated value of b. This process would then be repeated until b converges.

While stress changes in LEM could be calculated using an iterative process, it may not be feasible. As discussed in Chapter 2, limit equilibrium methods do not necessarily give realistic stress distributions along the slip surface, as they only consider static equilibrium requirements. In addition, external loads are not distributed at all inside the soil. Due to this inaccuracy, just using a good assumption for b can well be justified. Such an assumption should be realistic for the general loading pattern. The assumed value should also be chosen so as to minimize the resulting errors, should the actual value of b be significantly different from the assumption. The proposed value of b to be used in stability calculations is $b = 0.3$. This choice is discussed further in Section 6.4.

5.7 Calculating undrained shear strength in LEM context

In Section 5.5 a solution for the effective mean stress at failure p'_f was given (Eq. 5.28). For a total stress stability calculation using undrained shear strength, HSU effectively uses the von Mises criterion. This is consistent with the use of Drucker-Prager in calculating p'_f. The undrained shear strength obtained this way corresponds to the effective stress shear strength at p'_f. The undrained shear strength s_u is defined as:

$$s_u = \frac{q_f}{2} = \frac{p'_f \cdot M}{2} \tag{5.42}$$

This definition of undrained shear strength, or s_u, corresponds to the commonly used definition of shear strength used in total stress analyses where the strength is solely determined by the radius of the Mohr's circle at failure (see e.g. Wood 1990 pp. 179-181).

The calculated value of s_u can be used as a completely normal strength parameter in a $\varphi = 0$ LEM analysis. It must be kept in mind that this strength depends both on the location and direction of shearing, so the calculation of p'_f and s_u is done for a given slip surface. This does not preclude the search for a critical slip surface, as it only means that s_u needs to be calculated separately for each slice of each slip surface generated by the search algorithm.

The proposed workflow of the calculation in a geotechnical design software utilizing LEM is as follows (Fig. 5.7):

Input:

1. Create the soil geometry, layers, water table, loads etc.
2. For each layer, specify if it employs the calculation method (termed "active layers"), and whether it is a part of the initial stress state. For example, an embankment layer can be included in the initial state (old embankment) or not (new embankment).
3. For each external load, specify whether it is part of the initial state. Loads can be either old (permanent) or new (transient or permanent). New loads are not considered part of the initial stress state.
4. Soil parameter input. Input for active layers: γ, φ', OCR, λ/κ, b (default $b = 0.3$) and a coefficient for K_{0NC} (default $C = 1$). Other soil layers have their relevant parameters.

Calculations:

5. For active layers, calculate the following parameters: M, K_{0NC}, η_{K0NC}, α_{rot}
6. Define a slip surface and slices according to the search algorithm utilized by the software
7. For each slice bottom that is located in an active layer, calculate the initial stresses σ'_{v0}, p'_0; preconsolidation stresses σ'_c, p'_c, q_c; size of initial yield surface p'_{m0}; principal stress rotation at failure θ; effective mean stress at failure p'_f.
8. For each slice bottom that is located in an active layer, calculate s_u
9. Conduct a $\varphi = 0$ limit equilibrium calculation using the desired limit equilibrium method.
10. Continue according to the search algorithm, repeat steps 6-10 if necessary.

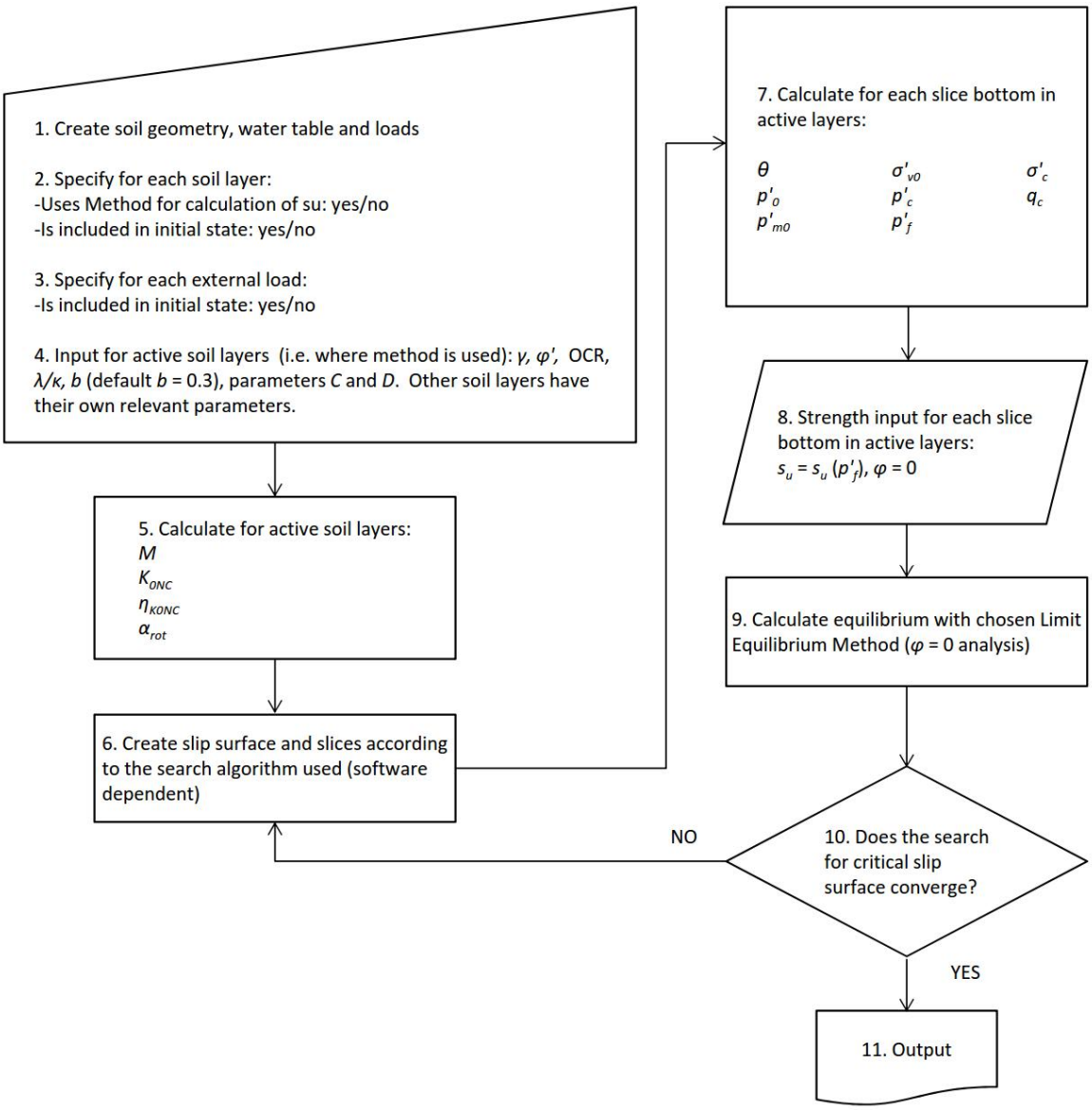

Figure 5.7. Proposed workflow for a total stress calculation with modeling of s_u

A key issue here is that the parameters calculated in step 7 are calculated according to the *initial state*, i.e. the effective stress state prior to short-term loading. Calculations involving the initial state consider that layers and loads not present in the initial state have zero unit weight and magnitude, respectively. The initial effective vertical stress σ'_{v0} at the slice bottom is calculated based on the unit weight and thickness of the overlying layers initially present (and old permanent loads, if applicable):

$$\sigma'_{v0} = q_{app\,0} + \Sigma \gamma'_0 \cdot d_0 \qquad (5.53)$$

where q_{app0} is the applied external long-term loading present in the initial state; γ'_0 and d_0 are effective unit weights and layer thicknesses for layers present in the initial state.

As in any LEM calculations, there will admittedly be errors as the effects of non-horizontal geometry on vertical stress are not taken into account. For geometries with horizontal soil surface and layers, the calculation can be considered accurate.

It needs to be recognized that when using the method to calculate s_u, friction angle φ' is not treated as a strength input parameter *per se*, but as a *calculation parameter for* s_u. The equilibrium calculation itself is carried out as a traditional $\varphi = 0$ analysis.

After calculating the undrained shear strength along the slip surface, a normal limit equilibrium calculation can be made using the desired method. In this calculation, all loads and layers are taken into account with their proper unit weights and magnitudes.

5.8 Calculating Δu_f in LEM context

5.8.1 Introduction

In addition to calculating undrained shear strength, the HSU method can also be used to calculate excess pore pressure at failure. Ideally, an undrained effective stress analysis would give the same result as the corresponding total stress analysis using s_u (assuming that the result given by the total stress analysis is the correct one).

As was noted in Section 4.3, traditional undrained effective stress analyses suffer from the inherent assumption that further excess pore pressure between the mobilized (design) state and failure is not considered. This results in an unrealistic effective stress path, and an overestimation of τ_f and F when $F > 1$.

The main problem in traditional undrained ESA is that the factor of safety F is obtained by comparing the mobilized shear stress τ to a theoretical shear strength τ_f that in reality cannot be mobilized at failure. Thus, even if mobilized excess pore pressure is calculated correctly, the resulting shear strength is incorrect. Further difficulties can arise from the fact that in typical LEM applications, external loads are not realistically distributed within the soil, but any *measured* pore pressure profile results from the true distribution of stresses in the soil. This can, again, result in an unrealistic shear strength distribution along the slip surface.

To circumvent these issues, an approach is proposed *where emphasis is put on obtaining a realistic shear strength distribution* instead of modelling the excess pore pressure as accurately as possible. In a certain sense, pore pressure needs to be deliberately calculated incorrectly, so that the resulting shear strength distribution is correct.

The following chapters present two approaches for calculating excess pore pressure in undrained effective stress analyses: 1) forcing Δu to obtain a realistic value of τ_f; and 2) calculating Δu based on stress changes at failure.

5.8.2 Δu_f based on "forcing" τ_f

If everything else is kept constant, the key parameter that affects the result of a limit equilibrium analysis is the shear strength on the slip surface. Thus if the shear strength distribution resulting from an undrained effective stress analysis is identical to the s_u distribution in a corresponding total stress analysis, one can expect the same results from the two types of analyses. By assuming that the shear strength given by the HSU method is correct (and that in the critical state, no cohesion is apparent), the following condition can be set:

$$s_u = \tau_f = \sigma'_n \cdot \tan \varphi_c' = (\sigma_n - u_0 - \Delta u) \cdot \tan \varphi_c' \tag{5.54}$$

$$\Delta u = \sigma_n - u_0 - \frac{s_u}{\tan \varphi_c'} \tag{5.55}$$

where σ_n is the total normal stress acting on a slice bottom, u_0 is the initial pore pressure, s_u is the undrained shear strength calculated with the HSU method, and φ'_c is the critical state friction angle of the soil. Note that here s_u is assumed to match the effective stress shear strength (Drucker-Prager failure envelope) instead of the total stress shear strength (Tresca/von Mises failure envelopes).

The profile of σ_n on the slip surface depends on the specific limit equilibrium method chosen. More specifically, the σ_n values satisfy the equilibrium conditions with the set of assumptions used by the limit equilibrium method. Thus, the *total stress* distribution may not always reflect the true stress distribution in the soil. However, by forcing the *effective stresses* to their assumed value at failure, (i.e. the value of σ'_n where the resulting shear strength τ_f matches the calculated value of s_u), the *shear strength* profile represents the "correct" values available at failure.

In this sense, the values of total normal stress σ_n and the corresponding calculated Δu can be notably different from reality, but the resulting σ'_n value should in principle correspond to reality.

The proposed workflow for the "forced" effective stress calculation is as follows:

Input:

1. Create the soil geometry, layers, water table, loads etc.
2. For each layer, specify if it employs the calculation method (termed "active layers"), and whether it is a part of the initial stress state. For example, an embankment layer can be included in the initial state (old embankment) or not (new embankment).
3. For each external load, specify whether it is part of the initial state. Loads can be either old (permanent) or new (transient or permanent). New loads are not considered part of the initial stress state.
4. Soil parameter input. Input for active layers: γ, φ'_c, *OCR*, λ/κ, b (default b = 0.3) and a coefficient for K_{0NC} (default C = 1). Other soil layers have their relevant parameters.

Calculations:

5. For active layers, calculate the following parameters: M, K_{0NC}, η_{K0NC}, α_{rot}

6. Define a slip surface and slices according to the search algorithm utilized by the software
7. For each slice bottom that is located in an active layer, calculate the initial stresses σ'_{v0}, p'_0, p_0; preconsolidation stresses σ'_c, p'_c, q_c; size of initial yield surface p'_{m0}; principal stress rotation at failure θ; effective mean stress at failure p'_f undrained shear strength s_u.

   Δu iteration loop:
8. Make a first assumption for Δu.
9. Conduct an undrained c'-φ' limit equilibrium calculation using the desired limit equilibrium method.
10. From the output of the equilibrium calculation, take σ_n values for active slices
11. Calculate new value for Δu (Eq. 5.55)
12. Check if Δu converges
13. a) If Δu converges, continue according to the slip surface search algorithm OR
    b) if Δu does not converge, use the new Δu value as input for next iteration then return to Step 9.

For a given slip surface, this effective stress calculation will give the exact same result as a corresponding total stress calculation. Arguably, the use of an effective stress calculation where the shear strength is fixed to a predetermined value is redundant, as the exact same result can be acquired by using a much simpler total stress analysis using the same "target" s_u value. This approach to undrained effective stress analyses is however included here as a conceptual example, and not so much as a proposed calculation method. The "forced" Δu results can also be used as reference values for Δu results calculated with other means (see next section).

5.8.3 Δu based on stress changes

A more "traditional" way of conducting an undrained effective stress analysis with the HSU method is calculating excess pore pressure at failure based on stress changes. Now excess pore pressure is not forced to give a "fixed" undrained shear strength. The HSU method is used to derive the shear-induced component (through calculating effective mean stress at failure p'_f) of the excess pore pressure response. Two submethods of calculating the load-induced component are proposed.

The principle of effective stresses states that at failure:

$$p_f' = p_f - u_f \tag{5.56}$$

$$\Delta p' = \Delta p - \Delta u \tag{5.57}$$

$$u_f = p_f - p'_f \tag{5.58}$$

$$\Delta u = \Delta p - \Delta p' \tag{5.59}$$

$$\Delta u = (p_f - p_0) - (p'_f - p'_0) \tag{5.60}$$

Excess pore pressure Δu at failure is therefore a sum of total and effective stress change components. The total stress change component Δp is, by definition, a result of increase in total mean stress acting on a soil element (or, the direct result of increasing external stresses). In undrained conditions an increase in total mean stress is compensated by an equal increase in excess pore pressure, resulting in constant volume (assuming isotropic elasticity). The component Δp can therefore be termed as the *load-induced component* of excess pore pressure.

The effective stress change component $\Delta p'$ depends on the volumetric tendencies of the soil as a result of changing deviatoric stresses. A soil on the wet side of the critical state line (CSL), such as normally consolidated or slightly overconsolidated clays, will have a tendency for plastic volumetric compression when subjected to increasing deviatoric stresses (i.e. shearing). In undrained conditions this tendency for compression is then compensated by equal tendency for elastic expansion, i.e. excess pore pressure. The opposite is true for shearing in the dry side of critical.

The link between $\Delta p'$ and deviatoric stress change can be illustrated with a slightly modified expression for Δu (Wood 1990 p. 35):

$$\Delta u = \Delta p - D \cdot \Delta q \tag{5.61}$$

where Δq is change in deviator stress and D is a pore pressure parameter. Using this notation compressive behaviour corresponds to negative values of D, and vice versa. Isotropically elastic behaviour corresponds to $D = 0$, and a constant p' stress path.

For overconsolidated soil (where the initial stress state lies inside the initial yield locus) the response is often assumed elastic, i.e. p' remains constant. When the clay starts to yield and the stress state moves outside the initial yield surface, p' will change according to the structural tendencies of the clay so that constant volume is maintained during

undrained shearing. As $\Delta p'$ is coupled with an increase in deviator stresses, it can be considered the *shear-induced component* of excess pore pressure.

As is the case with calculating undrained shear strength directly, effective mean stress at failure (p'_f) needs to be calculated to be able to calculate $\Delta p'_f$. This can be done with the HSU method as shown in Section 5.5. In addition, the load-induced pore pressure component Δp_f needs to be calculated.

Here two approaches for iteratively calculating Δp_f are suggested. Approach A is based on deriving the total mean stress p from the normal stress distribution acting on the slip surface, while approach B derives p based on calculated vertical stresses. Approach A is slightly modified from an approach suggested for the method UESA (Svanø 1980) in the manual for the software BEAST (Clausen 2003). Approach B is the author's own suggestion.

Approach A:

The total mean stress at failure p_f can, in principle, be calculated iteratively by using the limit equilibrium assumptions. The result of the stress distribution on the slip surface will however depend on the specific limit equilibrium method used (see Chapter 2).

The mean stress components p'_f (from the HSU method), and the initial stresses p'_0 and p_0 are considered known at this point.

An initial assumption for Δu needs to be made. A good assumption will result in fast convergence, but any realistic value should be sufficient. The suggested value of Δu_{ass} for each active slice bottom is:

$$\Delta u_{ass} = \Delta q_{app} - \Delta p'_f \tag{5.62}$$

where

$$\Delta p'_f = p'_f - p'_0 \tag{5.63}$$

Δq_{app} is the sum of vertical loading (in kPa) applied on the slice in undrained conditions.

Then, an equilibrium analysis using the desired limit equilibrium method is run. The pore pressure input for each active slice bottom should be

$$u = \Delta u_{ass} + u_0 \tag{5.64}$$

where u_0 is the initial (long-term) water pressure.

From the output data of the equilibrium analysis, values of σ'_n and τ_f are used to calculate principal stresses at failure, using continuum mechanics. The following equations assume zero cohesion, as the critical state assumption is thought to apply. Refer to Fig.5.8 for the geometry used to derive the equations.

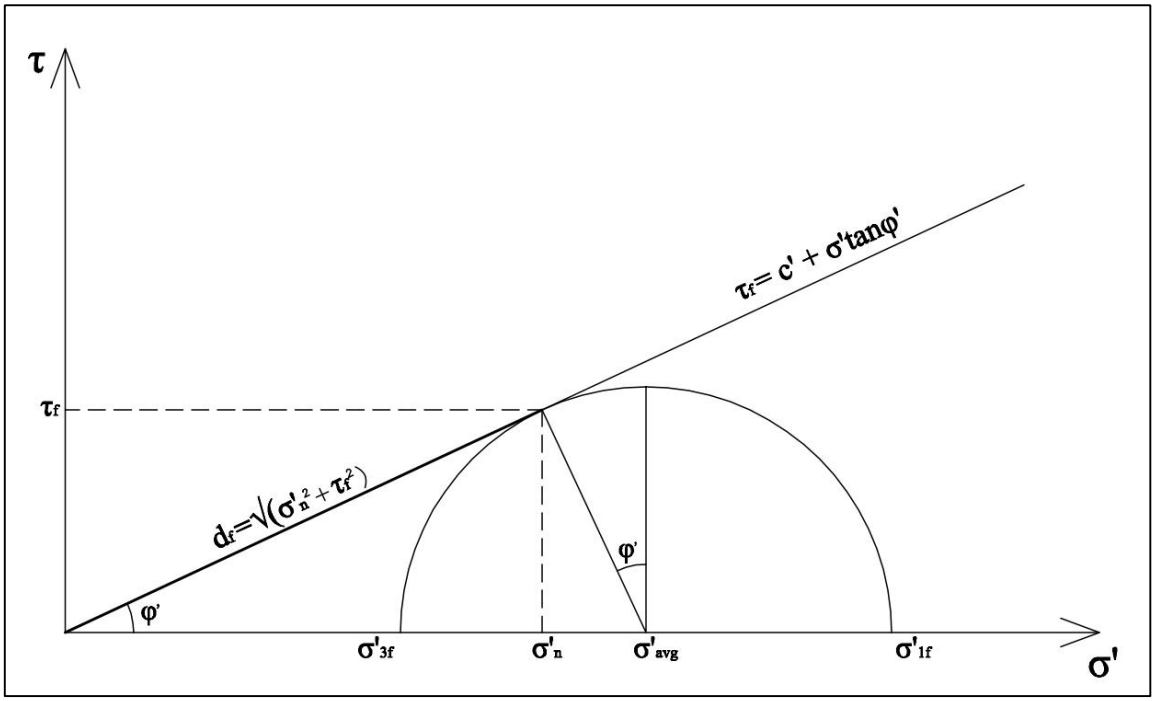

Figure 5.8. The geometry used to derive needed values for Approach A.

$$d_f = \sqrt{\sigma'_n{}^2 + \tau_f{}^2} \tag{5.65}$$

$$\tau_{\max} = \frac{\sigma'_{1f} - \sigma'_{3f}}{2} = d_f \cdot \tan\varphi' \tag{5.66}$$

$$\sigma'_{avgf} = \frac{\sigma'_{1f} + \sigma'_{3f}}{2} = \sqrt{d_f^2 + \tau_{\max}^2} \tag{5.67}$$

$$\sigma'_{1f} = \sigma'_{avg} + \tau_{\max} \tag{5.68}$$

$$\sigma'_{3f} = \sigma'_{avg} - \tau_{\max} \tag{5.69}$$

$$\begin{aligned} p_f &= \frac{\sigma'_{1f} + \sigma'_{2f} + \sigma'_{3f}}{3} + u_f \\ &= \frac{\sigma'_{1f} + (\sigma'_{3f} + b(\sigma'_{1f} - \sigma'_{3f})) + \sigma'_{3f}}{3} + u_f \\ &= \frac{\sigma'_{1f} + 2\sigma'_{3f} + b(\sigma'_{1f} - \sigma'_{3f})}{3} + u_f \end{aligned} \tag{5.70}$$

Finally, a new value for Δu_f can be calculated:

$$\Delta u_f = \Delta p_f - \Delta p'_f = (p_f - p_0) - (p'_f - p'_0) \tag{5.71}$$

The new Δu_f value is then applied as the new assumption, and the iteration loop is continued until Δu_f converges.

While the total stress change calculation is quite straightforward, basing it on limit equilibrium results can be problematic for two reasons: First, the calculated value of p_f is dependent on the specific limit equilibrium method used. Second, the calculated value of σ_n will vary with each updated iteration of Δu, which can potentially cause convergence problems.

The author's own attempts to apply Approach A have been characterised by very frequent convergence issues. Nearly invariably, at some point during the iteration loop of Δu the calculated values of σ_n and τ_f may get very high or very low values, leading to a total divergence in the iterations. This might be remedied by using better iteration algorithms, but for the purposes of this thesis, Approach A is presented as a concept only and no actual calculation results will be presented.

Approach B:

Instead of iteratively using the limit equilibrium results for calculating Δp, Approach B derives the total stresses from vertical stresses and the given slip surface geometry. While an iteration loop is still needed to solve Δp, the result is now obtained independently of the limit equilibrium calculations, which makes the calculation much more robust.

Again the initial stress state is considered known. An initial assumption Δu_{ass} is made for the excess pore pressure at failure. In the loaded state, the "failure" effective vertical stress is simply calculated as:

$$\sigma'_v = W / \Delta x - u_0 - \Delta u_{ass} \tag{5.72}$$

where W is the slice weight and Δx is the slice width. This does not take any distribution of stress in the soil into account and as such is compatible with the general assumptions made in LEM.

It is known that vertical stress and principal stresses are connected by:

$$\sigma'_v = \frac{\sigma'_1+\sigma'_3}{2} + \frac{\sigma'_1-\sigma'_3}{2}\cos 2\theta \tag{5.73}$$

where θ is the rotation angle of the principal stresses.

The principal stress ratio at failure is:

$$PSR = \sigma'_1 / \sigma'_3 = \tan^2(45° + \varphi'/2) \tag{5.74}$$

Based on Eq.5.73 and 5.74, the major and minor principal stresses can be solved as:

$$\sigma'_1 = \frac{2 \cdot PSR \cdot \sigma'_v}{PSR - \cos 2\theta + PSR \cdot \cos 2\theta + 1} \tag{5.75}$$

$$\sigma'_3 = \sigma'_1 / PSR \tag{5.76}$$

The intermediate principal ratio b can be assumed. The default assumption that is used in the HSU method is b = 0.3, which for the sake of consistency can be used here as well. Then the corresponding total mean stress at failure is:

$$p_f = \frac{\sigma'_1+(\sigma'_3+b\cdot(\sigma'_1-\sigma'_3))+\sigma'_3}{3} + u_0 + \Delta u_{ass} = \frac{\sigma'_1+2\sigma'_3+b\cdot(\sigma'_1-\sigma'_3)}{3} + u_0 + \Delta u_{ass} \tag{5.77}$$

Then, an updated assumption for Δu is calculated using Eq. 5.59. The process is repeated until Δu converges. After a desired convergence criterion is satisfied, the resulting Δu value is used as input in the effective stress limit equilibrium calculation.

The proposed iterative algorithm for an undrained effective stress limit equilibrium analysis, using Approach B for calculating Δp is as follows:

Input:

1. Create the soil geometry, layers, water table, loads etc.
2. For each layer, specify if it employs the calculation method (termed “active layers”), and whether it is a part of the initial stress state. For example, an embankment layer can be included in the initial state (old embankment) or not (new embankment).
3. For each external load, specify whether it is part of the initial state. Loads can be either old (permanent) or new (transient or permanent). New loads are not considered part of the initial stress state.
4. Soil parameter input. Input for active layers: γ, φ'_c, OCR, λ/κ, b (default $b = 0.3$) and a coefficient for K_{0NC} (default $C = 1$). Other soil layers have their relevant parameters.

Calculations:

5. For active layers, calculate the following parameters: M, K_{0NC}, η_{K0NC}, α_{rot}
6. Define a slip surface and slices according to the search algorithm utilized by the software
7. For each slice bottom that is located in an active layer, calculate the initial stresses σ'_{v0}, p'_0, p_0; preconsolidation stresses σ'_c, p'_c, q_c; size of initial yield surface p'_{m0}; principal stress rotation at failure θ; effective mean stress at failure p'_f.

   Δu iteration loop:
8. Make a first assumption for Δu.
9. Calculate Δp, update Δu assumption, repeat until Δu converges.

   Limit equilibrium calculation:
10. Use previously calculated Δu as input.
11. Conduct an undrained c'-φ' limit equilibrium calculation using the desired limit equilibrium method.

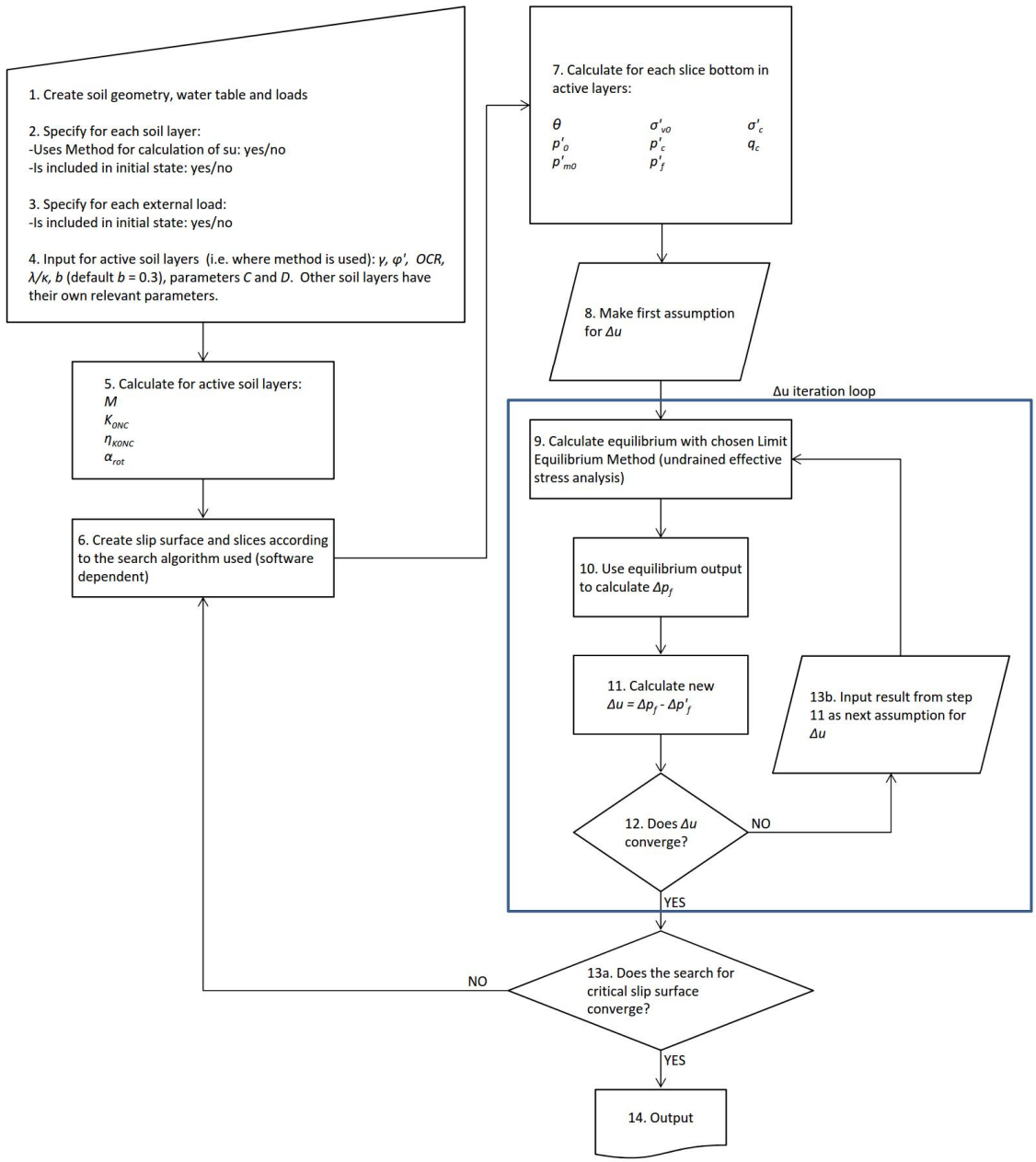

Figure 5.9. Proposed workflow for calculation of an undrained effective stress analysis with calculation of Δu

5.9 Modelling effective cohesion in critical state

While thus far it has been considered that in critical state, there is zero effective cohesion at critical state, it can be useful to give the possibility of modelling cohesion in the HSU method. While the model S-CLAY1 itself assumes zero cohesion, a fairly simple coordinate conversion can be used to include critical state cohesion in HSU if necessary.

No claims about the existence of critical state cohesion are made here, but the procedure is presented to increase the flexibility of the model. The steps taken are as follows:

1) All data is input as usual.

2) From the cohesion value c', the corresponding (p', q) space intercept value q_{int} (q value at p' = 0) is calculated:

$$q_{\text{int}} = \frac{2 \cdot c'}{\cos \varphi'} \tag{5.78}$$

3) The initial mean stress p'_0 and mean preconsolidation stress p'_c are calculated as usual. However, in subsequent calculations these are replaced with calculation values p'_{0calc} and p'_{ccalc}:

$$p'_{0calc} = p'_0 + p'_{att} \tag{5.79}$$

$$p'_{ccalc} = p'_c + p'_{att} \tag{5.80}$$

where p'_{att} is the value of attraction in the (p',q) space (i.e. p' value at q = 0). p'_{att} is defined as follows:

$$p'_{att} = \frac{q_{\text{int}}}{M} \tag{5.81}$$

This conversion has the effect of moving the coordinate system so that the distance between the initial stress state variables and the "tip" of the failure envelope corresponds to the assumed "true" situation with cohesion. The shape of the initial yield surface changes slightly from the corresponding "c' = 0 situation" because the assumed K_0 is now different (q values remain unchanged).

4) Subsequent calculations are done as usual, using the values of p'_{0calc} and p'_{ccalc} as relevant.

5) For illustrative purposes (e.g. drawing yield surfaces and stress paths) the resulting p' coordinates are converted back to their "true" values by subtracting p'_{att} from the calculation values.

The resulting initial yield surface is conceptually illustrated in Figure 5.10.

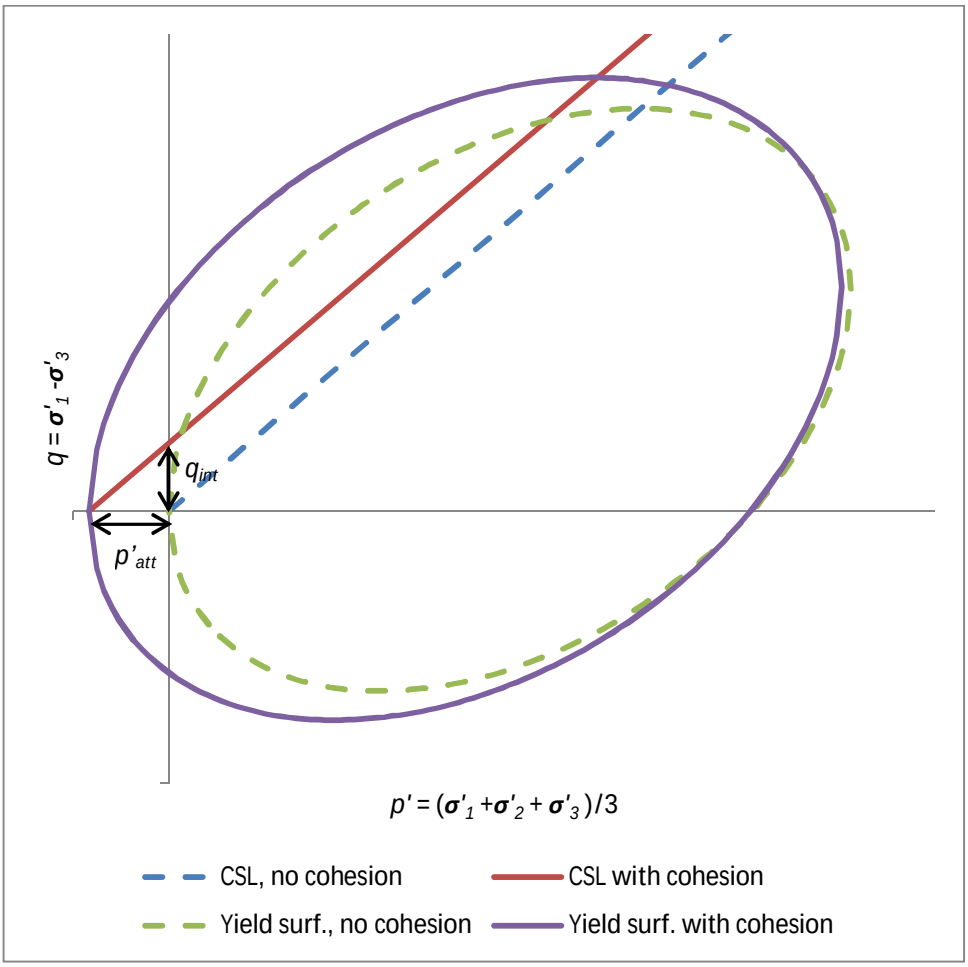

Figure 5.10. Normal initial yield surface without cohesion, and a corresponding yield surface with cohesion, resulting from the coordinate shift procedure.

In Figure 5.10, the yield surface with cohesion has been calculated with zero cohesion and the "calculation" values of *p'*. Then, the *p'* coordinates have been shifted back to their "true" values.
Undrained shear strength is calculated as normal by using the resulting value p'_{fcalc} in Equation 5.42. This gives the same result for s_u as first converting the "calculation" value to the "true" value and separately adding the q_{int} value (i.e. cohesion).

When HSU with cohesion is used to calculate excess pore pressure (based on stress changes), cohesion needs to be accounted for when using the relations between principal stresses and the failure criterion. In the suggested Approach B (section 5.8.3), equations 5.75 and 5.76 are substituted with the Equations 5.82 and 5.83 that use cohesion:

$$\sigma'_v = \frac{\sigma'_1+\sigma'_3}{2} + \frac{\sigma'_1-\sigma'_3}{2}\cos 2\theta \qquad (5.73\text{bis})$$

$$\sigma'_1 = \sigma'_3 \cdot \tan^2(45° + \varphi'/2) + 2c'\tan(45° + \varphi'/2) \qquad (5.82)$$

By combining 5.73 and 5.82 we can write:

$$\sigma'_3 = \frac{2\sigma'_v - 2\cdot\tan(45° + \varphi'/2)\cdot c'\cdot(1+\cos 2\theta)}{\tan^2(45° + \varphi'/2) - \cos 2\theta + \tan^2(45° + \varphi'/2)\cdot\cos 2\theta + 1} \qquad (5.83)$$

6 Parametric studies

6.1 General

The main use of the Hybrid s_u (HSU) method is to calculate the undrained shear strength at a given point of a slip surface. Even the suggested approaches for its use in undrained effective stress calculations entail first calculating s_u or p'_f (which is directly related to s_u). Therefore it is suitable to perform sensitivity analyses with regards to normalized s_u (s_u/σ'_{v0} or s_u/σ'_c).

Sections 6.2-6.6 study different parameter combinations and their effects on the predicted strength. Section 6.8 presents sensitivity analyses. The analyses include OFAT (One Factor At a Time), as well as Monte Carlo simulations on various parameters.

Baseline values for the sensitivity analyses are chosen as:

$\varphi' = 25°$
$\lambda/\kappa = 2$
$\theta = 0$, $b = 0$ (triaxial compression)
$\theta = 90°$, $b = 1$ (triaxial extension)
$C = 1$ (coefficient for K_{0NC})
$D = 1$ (coefficient for K_0)

The baseline values of φ' and λ/κ are in a sense arbitrary, but they can be considered to represent "averages" of the conceivable values of the said parameters. It is worth mentioning that a value of $\lambda/\kappa = 2$ can be considered low relative to typical laboratory values (Plaxis 2014), but for use with this soil model, it seems quite reasonable (see Chapters 7 and 8). The choice of a λ/κ value is discussed further in Chapter 9.

The baseline value for K_{0NC} ($C = 1$) is chosen to match the simplified Jaky equation due to its widespread use in geotechnical engineering. The baseline value of D corresponds to the basic Mayne & Kulhawy (1982) equation for overconsolidated K_0 conditions.

For general reference, HSU effective stress paths resulting from different parameter combinations are presented here.

The stress paths are presented (Figure 6.1) for triaxial compression and extension with OCR = 1 and OCR =2.5; and $\lambda/\kappa = 1.001$, $\lambda/\kappa = 2$ and $\lambda/\kappa = 5$. Other parameters are kept at their baseline values ($\varphi' = 25°$, $C = 1$, $D = 1$).

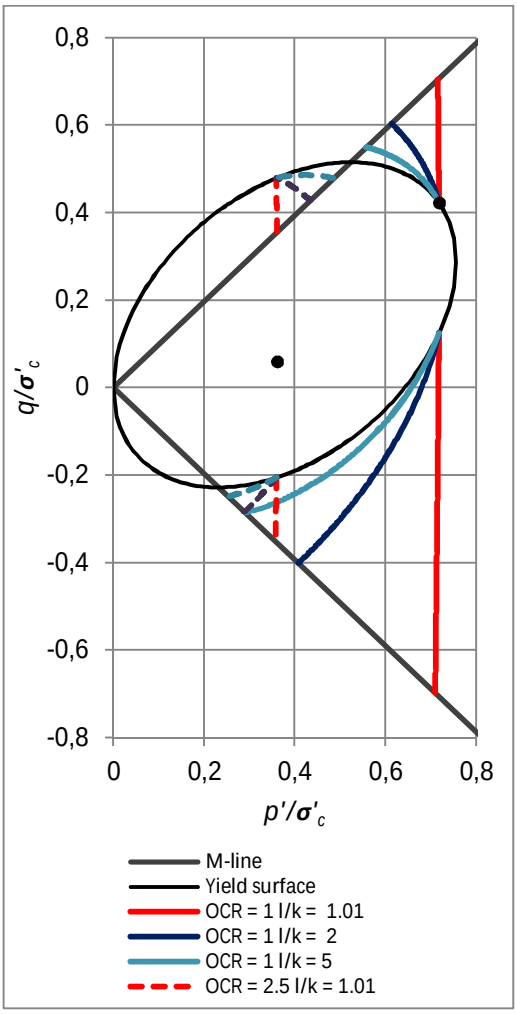

Figure 6.1. Examples of effective stress paths using HSU.

The effective stress paths for OCR = 1 begin from the initial stress state (i.e. intersection of the K_{0NC}-line and the initial yield surface). For triaxial compression, yielding starts immediately, and the stress paths are directed towards the critical state line (M-line). Lower λ/κ values result in more vertical stress paths and vice versa. For triaxial extension at OCR = 1 it is assumed that the effective stress path first travels inside the initial yield surface (decreasing q, constant p') until reaching the yield surface on the opposite side. From there, yielding commences and the stress path curves to the M-line.

For OCR = 2.5, triaxial compression occurs on the dry side of critical. Starting from the initial stress state, the stress path proceeds at constant p' to the initial yield surface. Now the stress path falls back to the critical state line. In terms of undrained shear strength, the effect of λ/κ is now reversed compared to shearing on the wet side of critical. For triaxial extension at OCR = 2.5, the shearing still occurs on the wet side of critical and the behaviour is similar to the situation at OCR = 1.

6.2 Effect of φ'

The effective critical state friction angle φ' is obviously an important parameter affecting the shear strength of a soil. It can be considered a fairly easy parameter to determine with laboratory testing. In addition, it can be considered quite fundamental in the sense that its value remains constant for a given soil deposit regardless of the stress history. φ' is a "primary" parameter in the sense that it in turn affects the "secondary" parameters M, K_{0NC}, K_0 and α_{rot} that are employed in the HSU method.

Figure 6.2 shows normalized undrained shear strength as a function of critical state friction angle. In this example, φ' is varied from 18° to 35°, which can roughly be considered conceivable boundary values for soft clays. In addition, the values are calculated for λ/κ values of 1.001 (roughly resulting in an upper boundary value for s_u), 2 (an arbitrary "intermediate" value for s_u) and 1000 (rough lower boundary value for s_u). Note that using a value of λ/κ approaching unity results in linear elastic behaviour, i.e. identical s_u values for all modes of shearing. The effect of λ/κ is further discussed in Section 6.3.

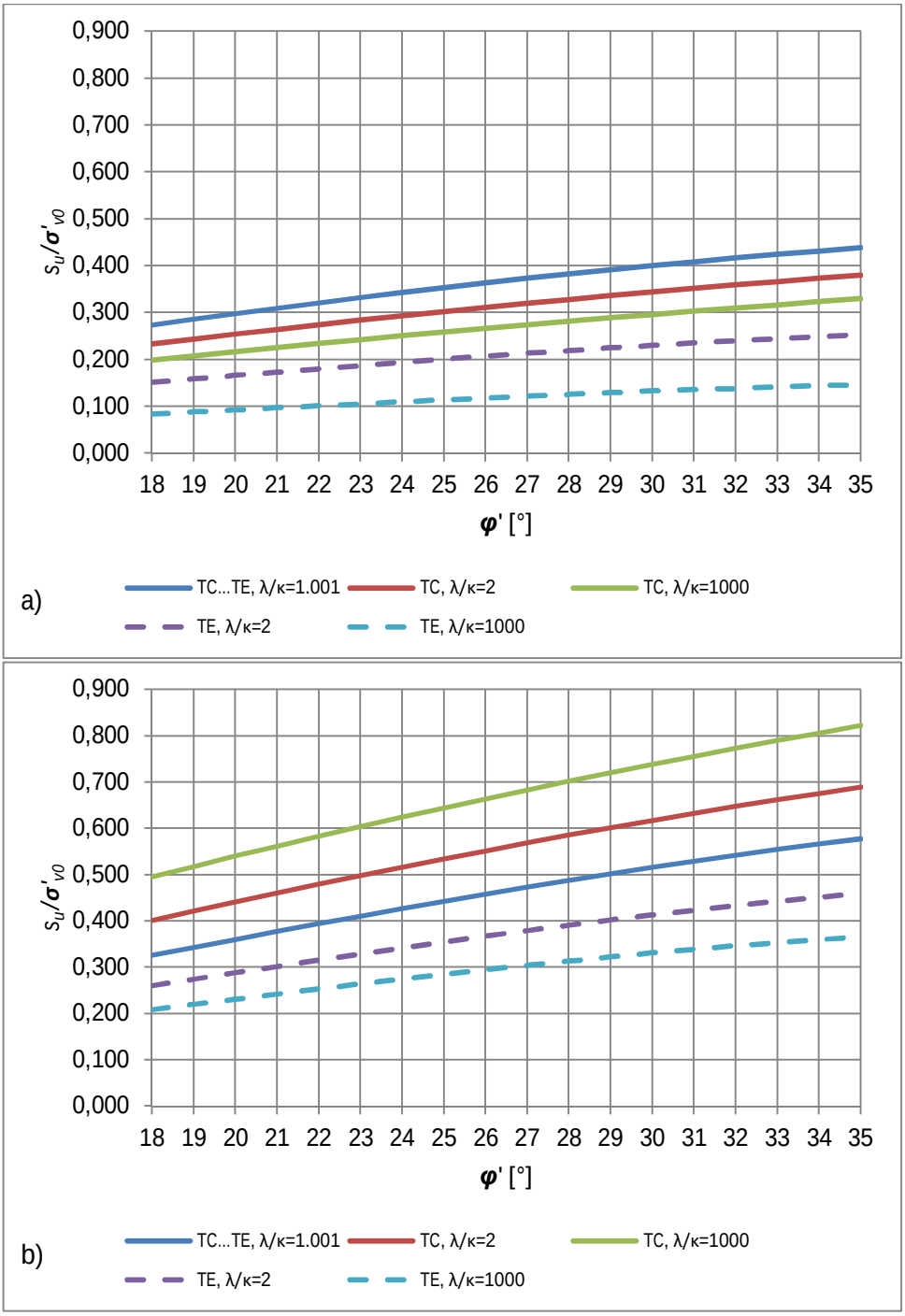

Figure 6.2. Normalized s_u versus φ' for λ/κ values of 1.001, 2 and 1000. Figure a) shows values for OCR = 1 and b) for OCR = 2.5.

As can be seen in Figures 6.2a and 6.2b, friction angle has a considerable effect on undrained shear strength predicted by the method. This is of course highly consistent with the fact that *φ'* can be considered the main strength parameter of a soil.

6.3 Effect of λ/κ

Figure 6.3 shows the effect of varying the value of λ/κ for various values of OCR, for triaxial compression (a) and extension (b). The range here is λ/κ = 1.001…10. This can be considered a "natural" range for the parameter. Higher values are possible, but as is evident from the results, increasing λ/κ further has practically no effect on s_u. Unless otherwise mentioned, other parameters are kept at their baseline values defined at the start of Chapter 6.

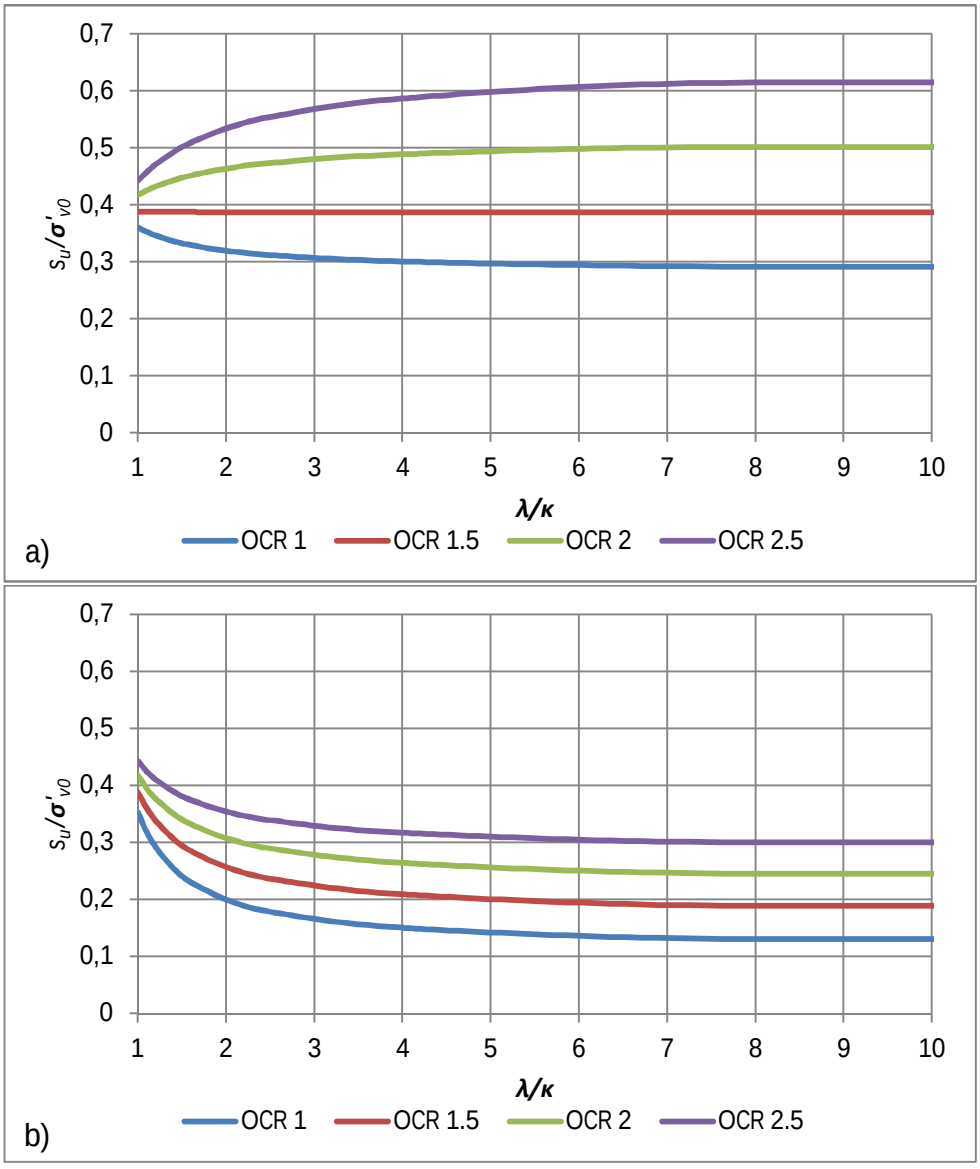

Figure 6.3. Normalized s_u versus λ/κ for a) triaxial compression and b) triaxial extension

It is apparent from Figure 6.3a that for triaxial compression in normally consolidated or slightly overconsolidated soils, increasing λ/κ will quickly decrease s_u. At OCR ≈ 1.5 s_u will be independent from λ/κ. This happens because at this state, the initial stress p'_0 corresponds to the intersection point between the initial yield surface and the failure surface. As linear elasticity (constant p' stress path) inside the yield locus is assumed, the stress path will terminate very close to the point of yielding. Thus the length of the elastoplastic part of the stress path is very short and the effect of volumetric hardening remains negligible.

For overconsolidated soils (*OCR* > 1.5) increasing *λ/κ* results in higher triaxial compression strength. It is however good to note that the OCR value where the trend is reversed (i.e. the *OCR* value where $p'_0 = p'_{yield} = p'_f$) depends on the assumptions made about K_0. In this example, it is assumed that C =1 and D = 1, i.e.

$$K_{0NC} = 1 - \sin\varphi'_c \tag{5.10bis}$$

$$K_0 = K_0^{NC} \cdot OCR^{\sin(\varphi')} = K_0^{NC} \cdot \left(\frac{\sigma'_c}{\sigma'_{v0}} \right)^{\sin(\varphi')} \tag{6.1}$$

For triaxial extension, increasing *λ/κ* generally results in decreasing shear strength for low to moderate values of *OCR* (up to ca. *OCR* = 4). Again, the *OCR* value where the trend changes depends on assumptions made about K_0 conditions.

6.4 Effect of *b*

The intermediate principal stress parameter *b* is defined as follows:

$$b = \frac{\sigma'_2 - \sigma'_3}{\sigma'_1 - \sigma'_3} \tag{3.11ter}$$

The value of *b* can be slightly problematic to calculate in a LEM framework. However, the expected range of *b* can, with some simplifications, be derived as follows: Due to the assumption of cross-anisotropic K_0 initial conditions, initially $\sigma'_{20} = \sigma'_{30}$ and thus $b_0 = 0$. If plane strain conditions during undrained ($\nu = 0.5$) loading are then assumed (along with the assumption of isotropic linear elasticity), the change in σ'_2 can be estimated:

$$\Delta\sigma_2 = \frac{\Delta\sigma_1 + \Delta\sigma_3}{2} \tag{6.2}$$

while the new total intermediate principal stress is:

$$\sigma_2 = \sigma_{20} + \frac{(\sigma_1 - \sigma_{10}) + (\sigma_3 - \sigma_{30})}{2} \tag{6.3}$$

With these assumptions (initial $b = 0$, subsequent undrained loading in plane strain conditions) the value of *b* will vary between 0 and 0.5 depending on the relative amount of stress increase needed to reach failure.

As a theoretical example, let us consider a soil element with the initial major principal stress $\sigma'_{10} = 100$ kPa. In undrained conditions, σ_1 is then gradually increased until failure occurs, while σ_3 is kept constant. For sake of simplicity it is assumed that $\Delta u = \Delta p$ (elastic behaviour). Figures 6.4a and 6.4b show *b* as a function of $\Delta\sigma_1$ for various initial values of K_0, for $\varphi' = 30°$. The plotted curves end at failure.

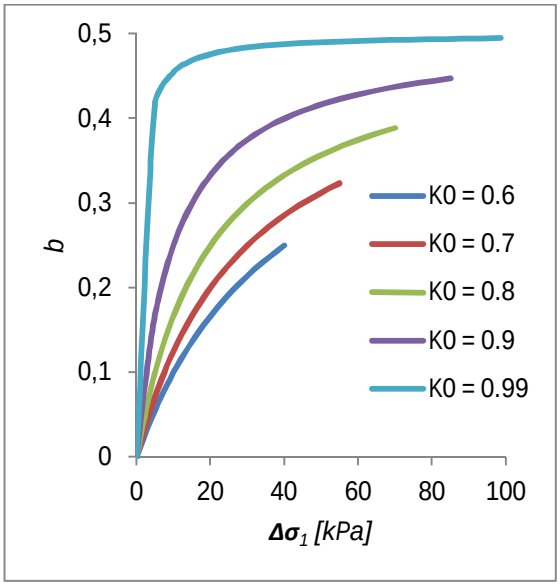

Figure 6.4. Intermediate principal stress parameter b versus increase of major principal stress for φ' =30°. The curves are plotted for different initial K_0 values.

From this theoretical exercise it is evident that the value of *b* at failure depends on the initial anisotropy as well as friction angle (and pore pressure response, which is not varied in the example). All of these factors govern the relative amount of deviatoric stress change needed to cause failure for a given soil element. Higher the stress change needed for failure, higher the value of *b* at failure. As a sidenote, increasing σ_3 as well does not affect the value of *b* at failure with these assumptions.

Accurately calculating the value of *b* in a LEM framework can be difficult. Stresses given by the limit equilibrium may not be very accurate. In addition, calculating *b* based on stresses given by a limit equilibrium will require an additional iteration loop (make an assumption for *b* -> calculate equilibrium -> calculate *b* again -> repeat until *b* converges) which complicates the overall analysis.

The value for *b* can however be simply set to an arbitrary value with reasonable accuracy. It can be assumed that possible values for *b* range from 0 to 0.5 in plane strain conditions, and likely values lie somewhere close to 0.1…0.4, depending on the initial K_0 value.

The *b* value used in LEM calculations should be chosen so that it is plausible and minimizes possible errors, preferably so that the potential for unsafe errors is small. Based on the author's studies, a good assumption that minimises the error potential either way seems to be $b = 0.3$. Figure 6.5 shows the relative error in predicted s_u from assuming $b = 0.3$.

The curves are plotted for $\varphi' = 25°$; $C = 1$; $D = 1$; θ values of 0°, 45° and 90°; and λ/κ values of 2 and 1000 (Fig 6.5a and 6.5b, respectively). Note that *OCR* does not have any influence on the relative effect of *b*. Varying φ' would also have only a very small influence on the relative effect of the *b* value.

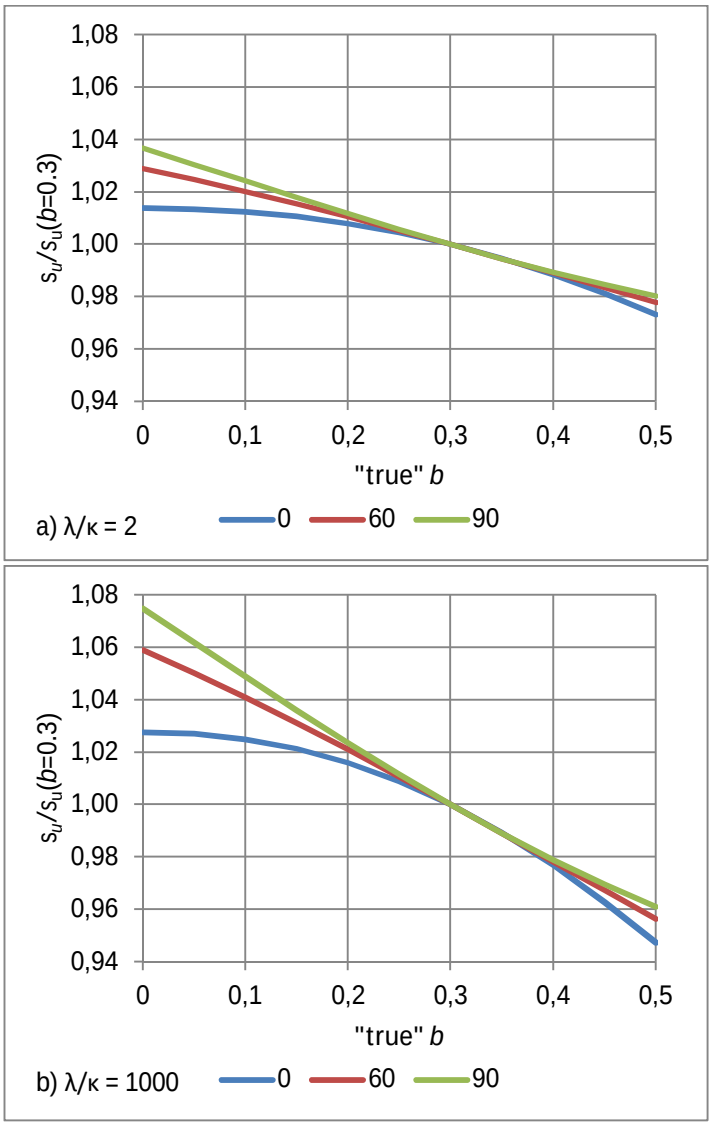

Figure 6.5. Relative difference in predicted shear strength for assumed vs "known" b value. Calculations made with a) λ/κ = 2 and b) λ/κ = 1000.

By assuming $b = 0.3$, the maximum error would be obtained for a true value of $b = 0$ at $\theta = 90°$. This error is on the safe side. The maximum unsafe error would be at $b = 0.5$, $\theta = 0°$. The error is highest at large λ/κ values. Overall, typical calculated errors that might be caused by assuming $b = 0.3$ are small, in the range of few percent in either direction.

Because this simple assumption allows the omission of a whole iteration loop in the algorithm, it can be considered quite helpful. In any case, accurately calculating b in LEM would be difficult without making several simplifying assumptions, which makes simply assuming a value for b all the more valid.

6.5 Effect of θ

As has been demonstrated by numerous authors (Chapter 3.5) that the direction of shearing has a large effect on undrained shear strength. Correspondingly, principal stress direction θ is a key model parameter that affects the anisotropy of shear strength in the HSU method. Figure 6.6 shows the effect of varying θ from 0 to 90°. The data is plotted for φ'=25°; OCR = 1; C = 1. The figure shows curves for b values of 0, 0.3 and 1; and λ/κ values of 1.001, 2 and 1000.

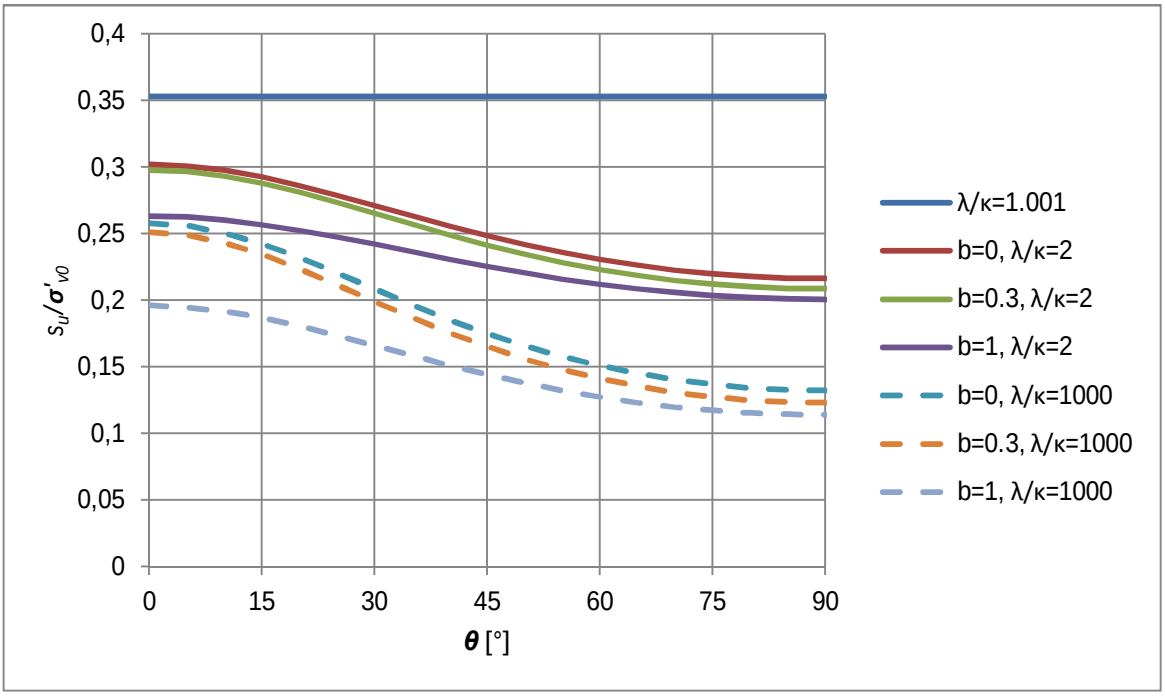

Figure 6.6. Normalised s_u versus θ for various combinations of b and λ/κ.

Due to the anisotropy of the yield surface, increasing the principal stress rotation angle leads to decreasing s_u. This is highly consistent with data available from literature (Chapter 3.5). It is also evident that in terms of anisotropy, θ is a much more critical model parameter than b (see previous section).

6.6 Effects of K_0 assumptions

In HSU, the value of K_{0NC} governs the inclination of the yield surface. The value of K_{0NC} is calculated as

$$K_{0NC} = C \cdot (1 - \sin\varphi') \qquad (5.34bis)$$

where C is a coefficient. The baseline (default) value is set as C = 1, which corresponds to the simplified Jaky equation (Jaky 1948). While the simplified Jaky equation is generally accepted, there is always the chance that for a given soil, the measured K_{0NC} value will be different. Ladd et al (1977) show (Figure 6.7) that for normally consolidated undisturbed of remoulded clays, most values fall in the range of:

$$K_{0NC} = 1 - \sin\varphi' \pm 0.05 \qquad (6.4)$$

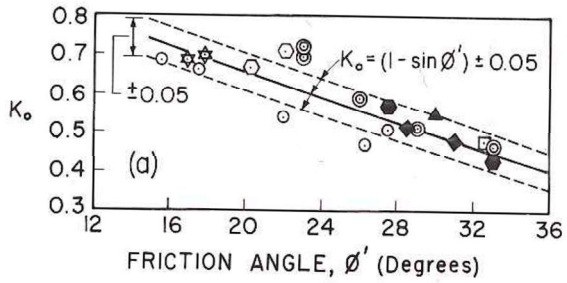

Figure 6.7. K_0 versus friction angle for several normally consolidated soils (Ladd et al 1977)

It also needs to be acknowledged that the original equation proposed by Jaky (1948) was slightly different from the simplified version:

$$K_{0NC} = (1 - \sin\varphi') \cdot \frac{1 + \frac{2}{3}\sin\varphi'}{1 + \sin\varphi'} \qquad (6.5)$$

Figure 6.8a shows the calculated K_{0NC} values for Jaky's simplified equation (with additional ± 0.05 values), as well as Jaky's original equation. Figure 6.8b shows the corresponding C values to use with Eq. 5.34.

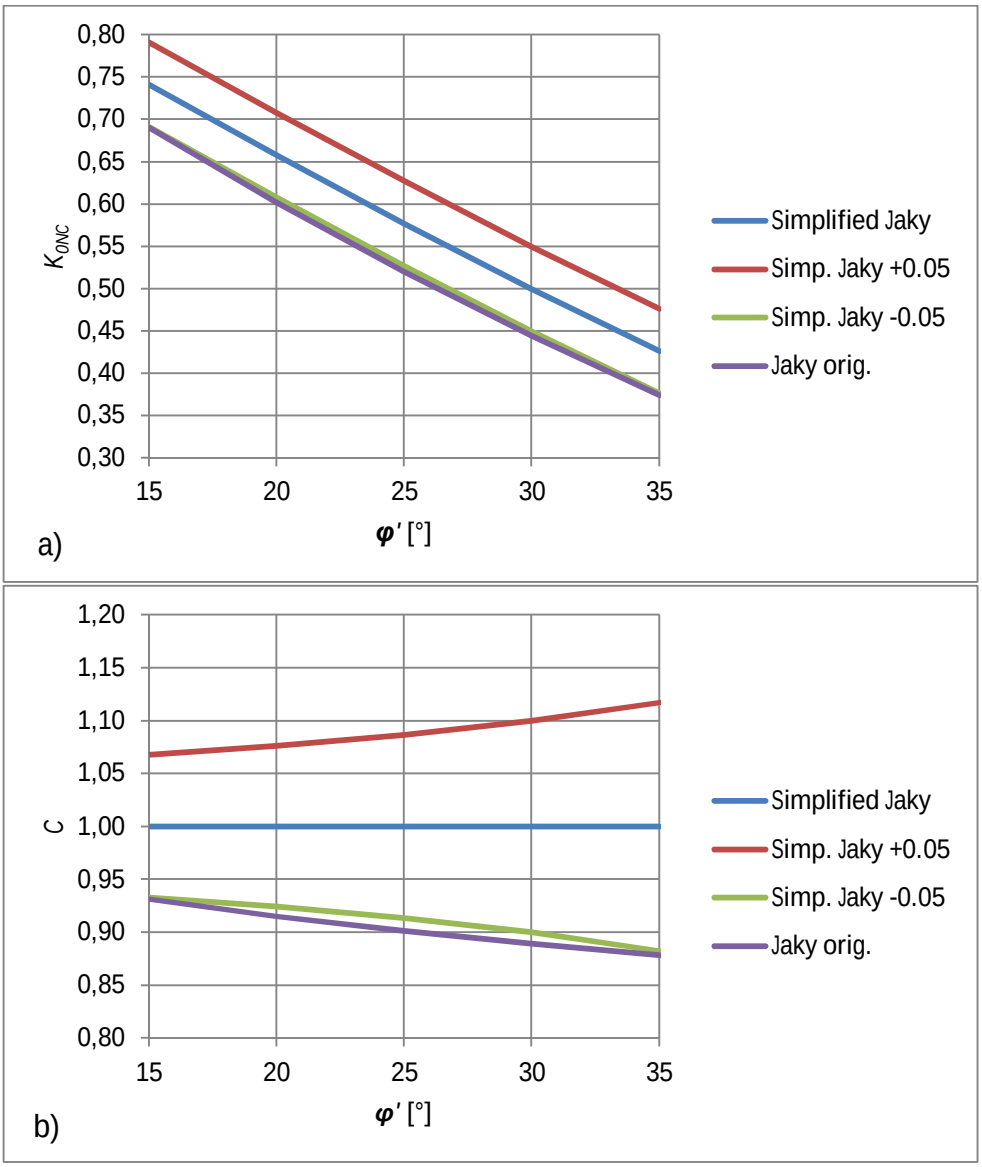

Figure 6.8. a) K_{0NC} versus friction angle with different assumptions. b) HSU parameter C value required to match the given K_{0NC} values with the different assumptions.

It is apparent that with these assumed K_{0NC}-φ' relationships, possible values for C can range from ca. 0.88 to 1.12. It is not however impossible to encounter values even outside these limits. Figure 6.9 shows an example of assumed initial yield surfaces for φ' = 25°, with C = 0.9, C = 1 and C = 1.1.

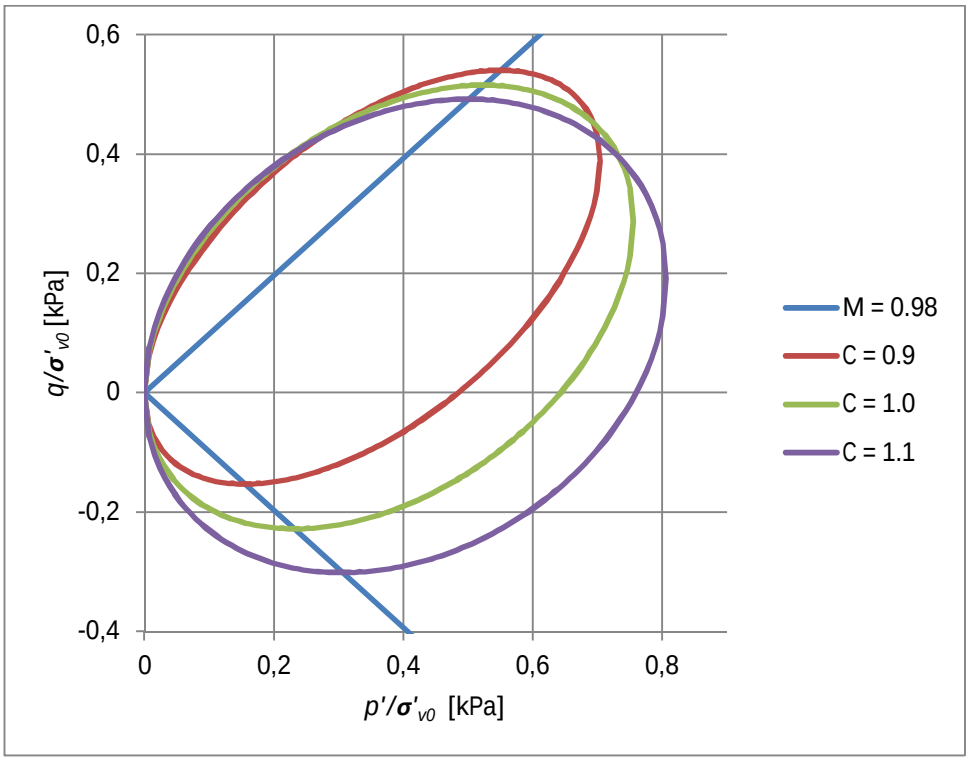

Figure 6.9. Effect of varying* C *value on the initial yield surface (φ' = 25°).

The effect of varying the C value is the most evident in the passive (extension) side of the yield surface, while the relative effect is much smaller in the active side.

Varying the value of K_{0NC} has a large influence on calculated shear strength, especially close to the passive side (triaxial extension). As an example, Figure 6.10 shows the effect of varying the coefficient *C* in HSU. The values are plotted for triaxial compression and extension; φ' = 25°; *OCR* = 1; λ/κ values 1.001, 2 and 1000.

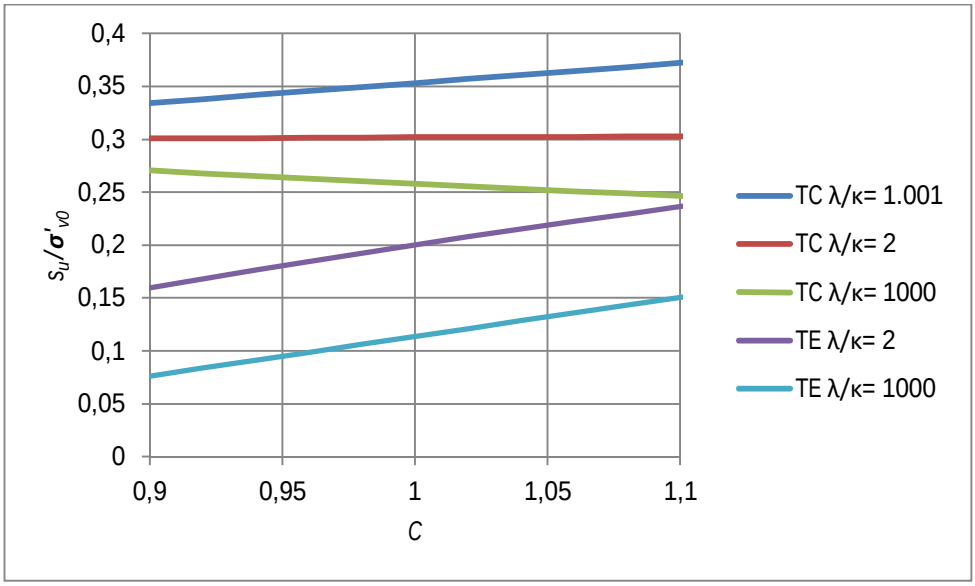

Figure 6.10. Effect of varying the parameter C.

As seen in Figures 6.9 and 6.10, the effect of varying *C* is most evident for triaxial extension, where decreasing C from the default value of 1 will decrease s_u quite

drastically. For triaxial compression, s_u may either increase or decrease with decreasing C, depending on λ/κ.

Figure 6.11 shows the corresponding relative effect of varying C, in relation to the s_u value at C = 1.

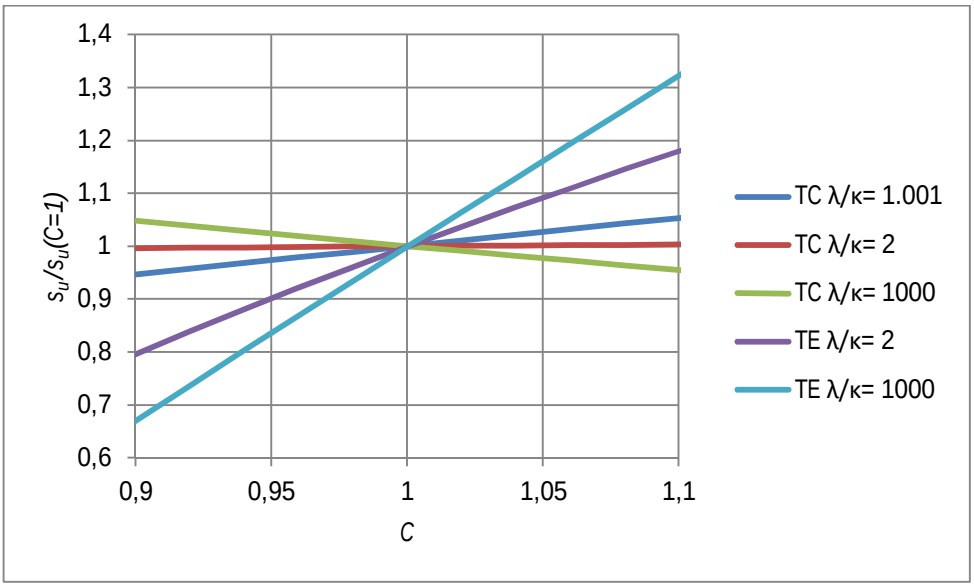

Figure 6.11. Relative effect of varying the parameter C.

For triaxial extension, even a plausible value of C = 0.9 can result in a >20% difference in s_u from C = 1.0. The relative trends are similar for different values of φ' (not plotted), with smaller friction angles being slightly more sensitive to changes in C. OCR has a very small effect on the relative sensitivity to C.

The model is generally quite sensitive to specified the value of K_{0NC}, especially for modes of shearing close to triaxial extension. Care must be taken when selecting the value of C. It is suggested here that if at all possible, the results given by the method should be compared to laboratory results, or at least available literature data for similar clays.

The model is not very sensitive to changes in the relationship between K_0 and OCR (that occur independently from K_{0NC}). It is often assumed that K_0 in the overconsolidated region after primary unloading is a function of K_{0NC} and OCR (Schmidt 1966):

$$K_0 = K_{0NC} \cdot OCR^m \qquad (6.6)$$

where m is a curve fitting exponent. A commonly used value is m = sin φ' (Mayne & Kulhawy 1982). Note that this equation is valid for simple unloading problems only, but for reloading problems K_0 seems to be significantly lower (Ladd et al 1977).

In the HSU method, the OCR-dependency of K_0 is modelled with the equation:

$$K_0 = K_{0NC} \cdot OCR^{D\cdot\sin(\varphi'c)} = K_{0NC} \cdot \left(\frac{\sigma'_c}{\sigma'_{v0}}\right)^{D\cdot\sin(\varphi'c)} \qquad (5.35bis)$$

where D is a control parameter.

It is somewhat tricky to determine "conceivable" limits for the parameter *D*. Here *D* is varied from *D* = 0 to 2. *D* = 0 corresponds to a situation where the K_0 value is equal to the value of K_{0NC} for all OCR values, while *D* = 2 is an arbitrary but somewhat plausible choice.

The relative effect of varying the parameter *D* is illustrated in Figure 6.12. The curves are plotted for φ' = 25°, *C* = 1, and show results for *OCR* = 2 and *OCR* = 4. For normally consolidated clays the value of *D* has, of course, no effect.

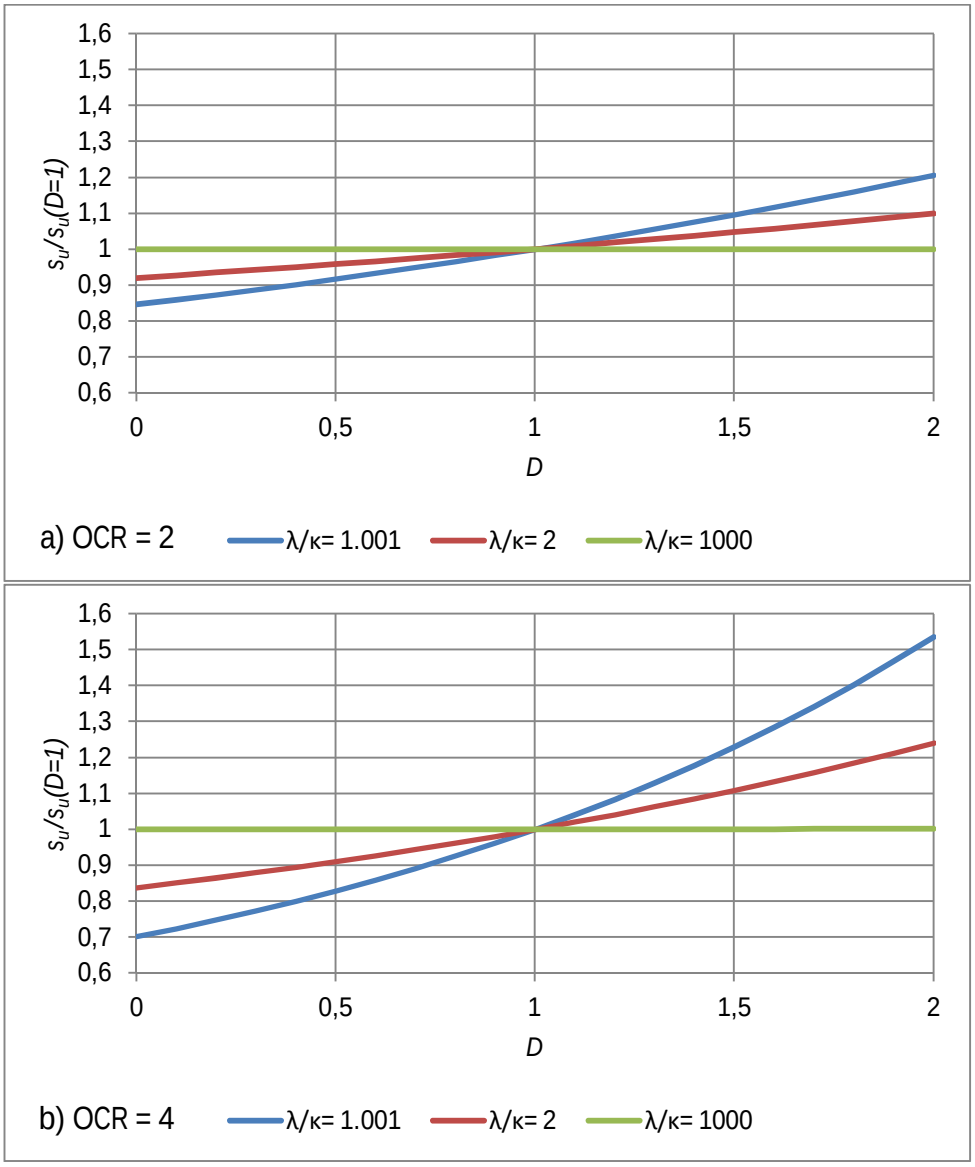

Figure 6.12. Relative effect of varying D for a) OCR = 2, and b) OCR = 4. Note that the relative strength differences are the same for all stress combinations (e.g. for TC or TE)

The sensitivity to changes in *D* increases slightly with increasing friction angle. Increasing *OCR* increases the sensitivity to changes in *D*, which is very logical. For low *OCR* values (say *OCR* < 2) for which the calculation method is primarily intended for, the overall effect of varying *D* remains within ± 20%, even for "extreme" combinations of *D* and λ/κ. The effect is relatively minor as D only affects the initial stress level p'_0, not the shape of the yield surface.

In any case, the actual value of D for a given soil with its unique stress history is somewhat difficult to ascertain without extensive soil testing. Therefore the HSU method is intended for use with $D = 1$, which in light of available literature can be considered a plausible assumption.

6.7 Effect of Eurocode 7 partial factor for φ'

In typical design codes partial factors for materials may be used. In using effective strength parameters, the partial factor is then applied to them instead of the resulting strength. It is valuable to examine what effect the use of a partial factor has on the output of the method. In other words, if a partial factor is applied to φ', what would the corresponding partial factor be for calculated s_u?

For example, Eurocode 7 (EN-1997-1) states that the following material partial factors are to be used (in design approaches that incorporate such factors):

Table 6.1. Partial factors for soil parametes (EN-1997-1)

Table A.2 - Partial factors for soil parameters (γ_M)

Soil parameter	Symbol	Value
Angle of shearing resistance[a]	$\gamma_{\varphi'}$	1,25
Effective cohesion	$\gamma_{c'}$	1,25
Undrained shear strength	γ_{cu}	1,4
Unconfined strength	γ_{qu}	1,4
Weight density	γ_{γ}	1,0
[a] This factor is applied to tan φ'		

The partial factor $\gamma_{\varphi'}$ is applied to tan φ'_k. The resulting design friction angle φ'_d is then:

$$\varphi'_d = \arctan\left(\frac{\tan\varphi'_k}{\gamma_{\varphi'}}\right) \tag{6.7}$$

All other parameters are kept at their baseline values:

$b = 0.3$ (proposed assumption for LEM)
$C = 1$ (corresponds to Jaky's simplified equation, Eq. 5.34)
$D = 1$ (corresponds to assumption made by Mayne & Kulhawy (1982), Eq. 5.35)

The corresponding "output" partial factor γ_{su} is calculated as:

$$\gamma_{su} = \frac{s_{u,\varphi k}}{s_{u,\varphi d}} \tag{6.8}$$

To study the "resultant" reduction of undrained shear strength when a partial safety factor is applied to the friction angle, a set of calculations was run. Various characteristic friction angles from $\varphi'_k = 15°$ to $\varphi'_k = 35°$ were studied at OCR = 1 and OCR = 2. The calculations were done with λ/κ = 1000, 2, and 1.001; and $\theta = 0°$, 45° and 90°. Other

parameters were kept at their baseline values of b = 0.3, C = 1 and D = 1.The results are given in Table 6.2a and 6.2b, for OCR = 1 and OCR = 2 respectively.

Table 6.2.Partial safety factors for s_u, calculated by using EN-1997-1 partial factors for φ'.

a) OCR = 1		φ'_k = 15°; φ'_d = 12.1°	φ'_k = 20°; φ'_d = 16.2°	φ'_k = 25°; φ'_d = 20.5°	φ'_k = 30°; φ'_d = 24.8°	φ'_k = 35°; φ'_d = 29.3°
λ/κ	θ	$\gamma_{su} = s_{u\varphi'k}/s_{u\varphi'd}$				
1000	0°	1.21	1.19	1.17	1.15	1.13
	45°	1.23	1.22	1.19	1.16	1.13
	90°	1.24	1.23	1.20	1.17	1.13
2	0°	1.21	1.19	1.17	1.15	1.12
	45°	1.22	1.20	1.18	1.15	1.12
	90°	1.23	1.21	1.18	1.15	1.12
1.001	0°	1.21	1.19	1.16	1.14	1.11
	45°	1.21	1.19	1.16	1.14	1.11
	90°	1.21	1.19	1.16	1.14	1.11

b) OCR = 2		φ'_k = 15°; φ'_d = 12.1°	φ'_k = 20°; φ'_d = 16.2°	φ'_k = 25°; φ'_d = 20.5°	φ'_k = 30°; φ'_d = 24.8°	φ'_k = 35°; φ'_d = 29.3°
λ/κ	θ	$\gamma_{su} = s_{u\varphi'k}/s_{u\varphi'd}$				
1000	0°	1.21	1.19	1.17	1.15	1.13
	45°	1.23	1.22	1.19	1.16	1.13
	90°	1.24	1.23	1.20	1.17	1.13
2	0°	1.22	1.20	1.18	1.16	1.13
	45°	1.23	1.22	1.19	1.16	1.13
	90°	1.24	1.22	1.20	1.17	1.13
1.001	0°	1.23	1.22	1.19	1.16	1.13
	45°	1.23	1.22	1.19	1.16	1.13
	90°	1.23	1.22	1.19	1.16	1.13

It can be seen from the results that the resulting "output" partial factors γ_{su} are in fact smaller than the partial factor γ_{cu} that is prescribed by Eurocode 7, and even slightly smaller than the "input" partial factor $\gamma_{\varphi'}$. This means that with the HSU method, the "effective" reduction of undrained strength is slightly smaller than when using a total stress model where a larger partial factor is applied directly to the undrained shear strength. This may allow slightly more economical designs.

Admittedly, there are further sources of variability in the other input parameters. Design codes however often put all of the material uncertainties into a measured strength parameter, as is done in this example.

6.8 Sensitivity analyses

6.8.1 OFAT sensitivity analysis

To study the relative sensitivity of HSU to its various parameters, a simple one-factor-at-a-time (OFAT) sensitivity analysis is conducted. First, a set of baseline parameter values and the corresponding value of s_u/σ'_{v0} are established. Each relevant parameter is then in turn varied to its predetermined minimum or maximum value, and the result is compared to the baseline value.

The baseline values can be thought to represent an "average" soil with parameters that result roughly in "average" values of s_u throughout the conceivable range of a given parameter. The baseline values are as follows:

$\varphi' = 25°$	(arbitrary "average" value)
$\lambda/\kappa = 2$	(arbitrary "average" value)
$b = 0.3$	(proposed assumption for LEM)
$C = 1$	(corresponds to Jaky's simplified equation, Eq. 5.34)
$D = 1$	(corresponds to assumption made by Mayne & Kulhawy (1982), Eq. 5.35)

The relative changes from baseline are calculated by changing one parameter at a time from its baseline value. The chosen minimum and maximum values are as follows:

$\varphi' = 20°…30°$	(plausible 20% variance from baseline, corresponds to a 95% tolerance interval for $\sigma = 2.5°$)
$\lambda/\kappa = 1.001…1000$	(possible theoretical range from very fast to very slow rate of shearing)
$b = 0.0…0.5$	(possible theoretical range for plane strain loading)
$C = 0.9…1.1$	(the range presented by Ladd et al (1977))
$D = 0.0…2.0$	(arbitrary)

The data is plotted for principal stress rotation values of 0°, 45° and 90°, and the average of the three values. Fig. 6.13a presents data for OCR = 1; Fig. 6.13b for OCR = 2; and Fig. 6.13c for OCR = 4.

It is apparent that most crucial parameters are friction angle φ', hardening parameter λ/κ, and coefficient C (i.e coefficient for K_{0NC}). The importance of friction angle for undrained shear strength is quite self-explanatory. The hardening parameter λ/κ as it is used in HSU is not a soil parameter *per se*, but more like a control parameter that controls the shape of the effective stress path. The parameter C controls the shape of the initial yield surface, and has the largest effect for extension ($\theta = 90°$)

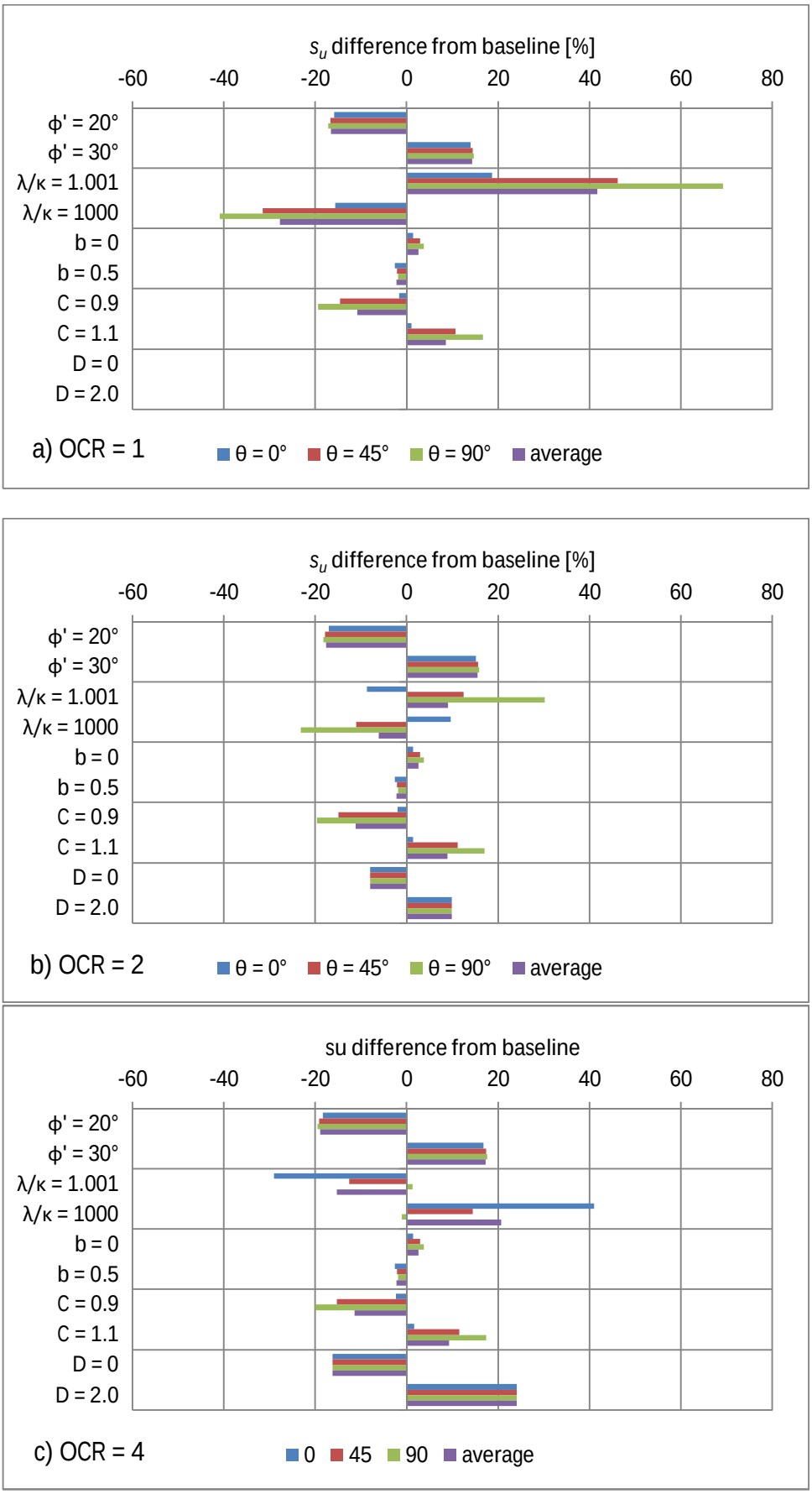

Figure 6.13. OFAT sensitivity analysis results for a) OCR = 1, b) OCR = 2, c) OCR = 4

6.8.2 Monte Carlo simulation with varying φ'

In the following Monte Carlo sensitivity analyses both λ/κ and θ are treated as "known" model parameters.

A distribution for the state parameter λ/κ is difficult to obtain, as its value is highly dependent on the elasto-viscoplastic properties of the soil, and importantly, *time* (i.e. the rate and duration of loading). The strength output is also a highly non-linear function of λ/κ (see Section 6.3), and any realistic frequency distribution for λ/κ should be asymmetric. Choosing a correct distribution and suitable parameters cannot be done here with enough credibility. As such, no attempt is made to randomly generate values for λ/κ, but the simulation is conducted separately for "very conservative", "intermediate" and "highly non-conservative" cases (respective λ/κ values 1000, 2, and 1.001).

To further examine the sensitivity of HSU to its main strength parameter φ', a pseudo-random Monte Carlo simulation is conducted by generating normally distributed φ' values. The distributions of s_u/σ'_{v0} are examined for the following combinations:

θ = 0°, 45° and 90° (active, direct, passive)
λ/κ = 1000, 2 and 1.001 ("very conservative", "intermediate" and "highly non-conservative")
OCR = 1 and 2.

All other parameters are kept at their baseline values:

b = 0.3
C = 1
D = 1

In the simulation, 50,000 normally distributed values were generated for φ' with the following normal distribution:

$\mu_{\varphi'}$ = 25°, $\sigma_{\varphi'}$ = 2.5°

The normalized undrained shear strength s_u/σ'_{v0} was then calculated using the generated dataset of φ' values. The resulting statistical properties from generated datasets are presented in Tables 6.3a (OCR = 1), and 6.3b (OCR = 2). The tables also give values of s_{ud}/σ'_{v0} ("design value" for normalized s_u) and the corresponding cumulative percentage taken from the dataset. Note that for λ/κ = 1.001, only the case θ = 0° is shown, as HSU gives identical shear strengths for all angles at this λ/κ level.

The design value s_{ud}/σ'_{v0} is calculated for a given case by applying the baseline values for b, C and D, and the design value for friction angle φ'_d:

$$\varphi'_d = \arctan\left(\frac{\tan\varphi'_k}{\gamma_{\varphi'}}\right) = \arctan\left(\frac{\tan 25°}{1.25}\right) \approx 20.46° \qquad (6.9)$$

The cumulative percentage $\Phi(s_{ud}/\sigma'_{v0})$ represents the percentage of values in the output dataset that have a value < s_{ud}/σ'_{v0}.

Table 6.3. Simulation results for varying φ'.

OCR = 1

λ/κ	θ	Sample mean $\bar{X}$	Sample standard deviation s_N	COV	s_{ud}/σ'_{v0} (for $\gamma_{\varphi'}$=1.25)	Φ (s_{ud}/σ'_{v0})
1000	0°	0.251	0.019	0.078	0.214	3.4 %
	45°	0.165	0.014	0.084	0.139	3.4 %
	90°	0.123	0.011	0.088	0.102	3.4 %
	(s_u average)	0.179				
2	0°	0.297	0.022	0.075	0.255	3.4 %
	45°	0.241	0.019	0.079	0.205	3.4 %
	90°	0.208	0.017	0.080	0.176	3.4 %
	(s_u average)	0.249				
1.001	0°	0.352	0.026	0.073	0.303	3.4 %

OCR = 2

λ/κ	θ	Sample mean $\bar{X}$	Sample standard deviation s_N	COV	s_{ud}/σ'_{v0} (for $\gamma_{\varphi'}$=1.25)	Φ (s_{ud}/σ'_{v0})
1000	0°	0.501	0.039	0.077	0.428	3.4 %
	45°	0.329	0.028	0.084	0.277	3.4 %
	90°	0.245	0.021	0.087	0.205	3.4 %
	(s_u average)	0.358				
2	0°	0.457	0.037	0.080	0.387	3.4 %
	45°	0.370	0.031	0.084	0.311	3.4 %
	90°	0.320	0.027	0.085	0.268	3.4 %
	(s_u average)	0.382				
1.001	0°	0.417	0.035	0.083	0.351	3.4 %

The resulting s_{ud}/σ'_{v0} frequency histograms (Shown for the OCR = 1 case in Fig. 6.14a, 6.14b) are very close to normally distributed. COV does not vary greatly from between the different values of λ/κ, θ and OCR (not illustrated here).

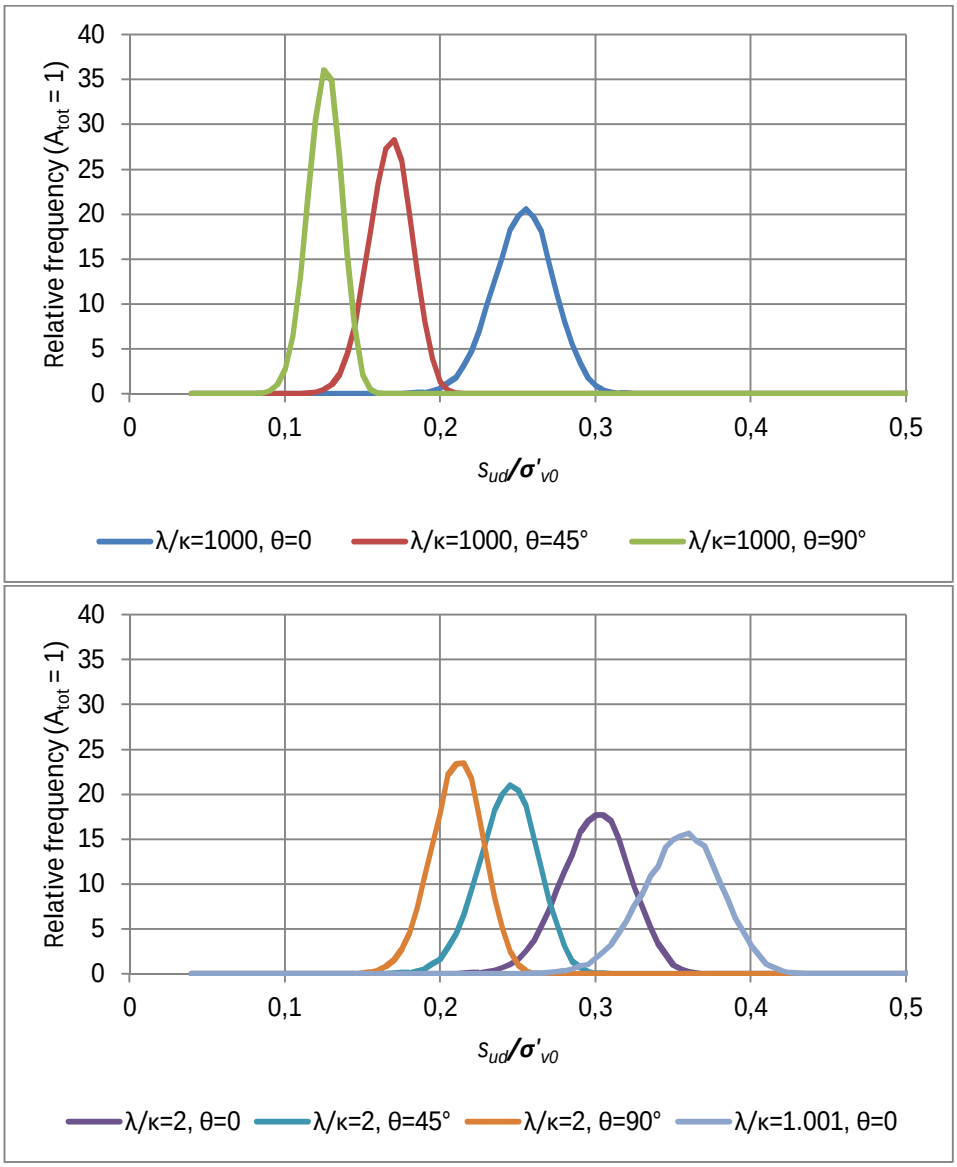

Figure 6.14. Frequency histograms for different λ/κ values for OCR = 1.

It is evident that the model response to variations in φ' is straightforward and fairly robust: For a normally distributed input, the output is also normally distributed. The resulting COV values of s_{ud}/σ'_{v0} for the presented cases are also smaller than the COV of the φ' population.

With the given φ' distributions, the calculated design value s_{ud}/σ'_{v0} represents a cumulative percentage of 3.4 %. This corresponds to a reliability index $\beta = 1.89$. For a φ' population with a smaller COV the reliability index would be higher, and vice versa.

6.8.3 Monte Carlo simulation with varying *C*

In this simulation the K_{0NC} coefficient C is varied. 50,000 normally distributed values for C were generated. The distribution used to generate C is a normal distribution ($\mu_C = 1$, $\sigma_C = 0.05$) that is truncated at $C = 0.85$ and 1.15. The distribution is truncated to avoid numerical issues associated with very low values of C. In addition, available literature (see Chapter 6.6) seems to indicate that C values outside these limits would be fairly unreasonable. With the given distribution only a very small percentage of the population would otherwise lie outside these limits.The distributions of s_u/σ'_{v0} are examined for the following combinations:

θ = 0°, 45° and 90° (active, direct, passive)
λ/κ = 1000, 2 and 1.001 ("very conservative", "intermediate" and "highly non-conservative")
OCR = 1 and 2.

All other parameters are kept at their baseline values:

φ' = 25°
b = 0.3
D = 1

Tables 6.4a and 6.4b show statistical parameters for the s_u/σ'_{v0} distributions. Figures 6.15a and 6.15b show the resulting s_u/σ'_{v0} frequency histograms for OCR = 1 cases.

Table 6.4. Simulation results for varying C.

OCR = 1

λ/κ	θ	Sample mean $\bar{x}$	Sample standard deviation s_N	COV
1000	0°	0.251	0.003	0.014
	45°	0.164	0.016	0.099
	90°	0.123	0.018	0.150
	(s_u average)	0.179		
2	0°	0.297	0.002	0.007
	45°	0.240	0.015	0.063
	90°	0.208	0.019	0.089
	(s_u average)	0.249		
1.001	0°	0.353	0.009	0.027

OCR = 2

λ/κ	θ	Sample mean $\bar{x}$	Sample standard deviation s_N	COV
1000	0°	0.501	0.007	0.014
	45°	0.328	0.032	0.099
	90°	0.245	0.037	0.150
	(s_u average)	0.358		
2	0°	0.457	0.004	0.008
	45°	0.370	0.024	0.065
	90°	0.320	0.029	0.091
	(s_u average)	0.382		
1.001	0°	0,418	0,013	0,030

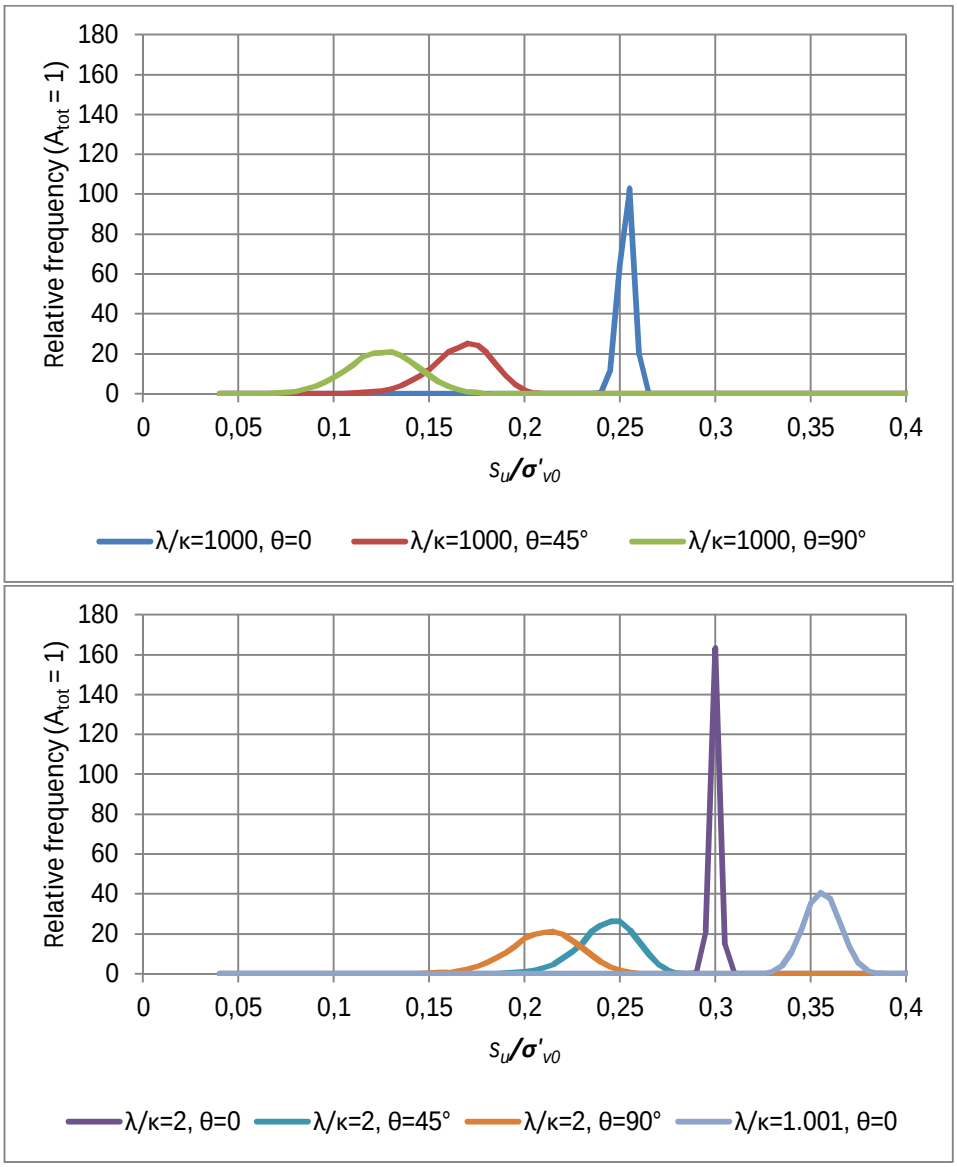

Figure 6.15. Frequency histograms for different λ/κ values at OCR = 1.

It is apparent that for active shearing (θ = 0°), HSU is quite insensitive to changes in *C*, but the sensitivity increases notably when principal stress rotation is increased. The variability for extension is rather high at COV = 0.15 at λ/κ = 1000. This is due to the fact that changing C can dramatically change the size of the initial yield surface, specifically on the extension side (or in more general terms “not in compression”). This is discussed in Chapter 6.6. With this in mind, a poor choice of C can give dangerously high or overconservatively low shear strengths.

6.8.4 Monte Carlo simulation with varying OCR

In the previous examples OCR has been treated as a constant, but there can be considerable uncertainty in determining OCR. An attempt is made here to model the sensitivity of HSU to fluctuations in OCR with a Monte Carlo simulation. For example, sample disturbance and rate effects can affect the value of σ'_c obtained in the laboratory. According to Graham et al (1983) a tenfold difference in strain rate will generally result in a 10-20 % difference in apparent σ'_c. According to data from Holtz et al (1986), 85 mm piston samples (presumably somewhat disturbed) give very slightly lower σ'_c values and higher scatter in oedometer testing than block samples. According to Berre et al (1969, as referred to by Karlsrud & Hernandez-Martinez 2013), yield stresses given by 54 mm and 95 mm samples are not very different, but scatter of the results was higher for the 54 mm samples.

For generating OCR values in a simulation, it can be difficult to validate the choice of a distribution. In this example a normal distribution truncated at OCR = 1 is assumed. This is admittedly a fairly arbitrary assumption, but can be considered "good enough" as there does not seem to be much data available about statistical variability of OCR or σ'_c. It can however be argued that COV should probably be around 10-20 % based on available literature, and the mode of the truncated distribution should represent the mean of the corresponding "non-truncated" normal distribution.

The following baseline parameter values were used in the Monte Carlo analysis:

φ' = 25°
b = 0.3
C = 1
D = 1

OCR = 1.3 was chosen as the assumed baseline value. Results are plotted for λ/κ values 1.001, 2 and 1000; and θ values 0, 45° and 90°.

In the analysis 50,000 values of OCR were generated. The distribution used was a normal distribution with $\mu = 1.3$ and $\sigma = 0.2$ (COV ≈ 0.16). The distribution was then truncated at OCR = 1. The resulting OCR distribution (Fig. 6.16) of the generated 50,000 point sample has the following statistical parameters:

μ = 1.328
σ = 0.176
COV = 0.133

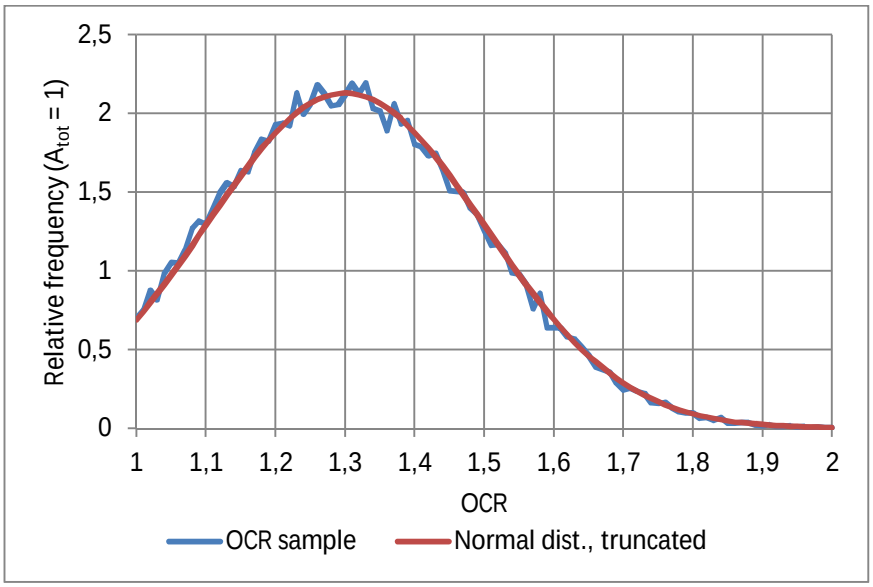

Figure 6.16. Frequency histogram of the generated OCR data set.

Statistical parameters for the output (s_u/σ'_{v0}) are given in Table 6.5. It is evident that COV does not depend on θ, but the value of λ/κ has a large effect. COV is largest for large λ/κ values. The 2.28 % quantile (2σ) and the corresponding partial safety factor for s_u are given. Overall, the γ_{su} values with the given assumptions are quite small.

Table 6.5 Simulation results for varying OCR.

λ/κ	θ	Sample mean $\bar{x}$	Sample standard deviation s_N	COV	2.28% quantile $q_{2.28}$	γ_{su}
1000	0°	0.333	0.044	0.132	0.259	1.29
	45°	0.219	0.029	0.132	0.170	1.29
	90°	0.164	0.022	0.132	0.127	1.29
	(s_u average)	0.239				
2	0°	0.354	0.029	0.082	0.303	1.17
	45°	0.287	0.023	0.082	0.246	1.17
	90°	0.248	0.020	0.082	0.212	1.17
	(s_u average)	0.296				
1.001	0°	0.377	0.012	0.032	0.356	1.06

Figures 6.17a and 6.17b show the resulting frequency histograms of s_u/σ'_{v0}. Now the histograms are not normally distributed, but exhibit a notable skew to the right. The distributions do not have a tail on the left, as the smallest value of a distribution corresponds to OCR = 1.

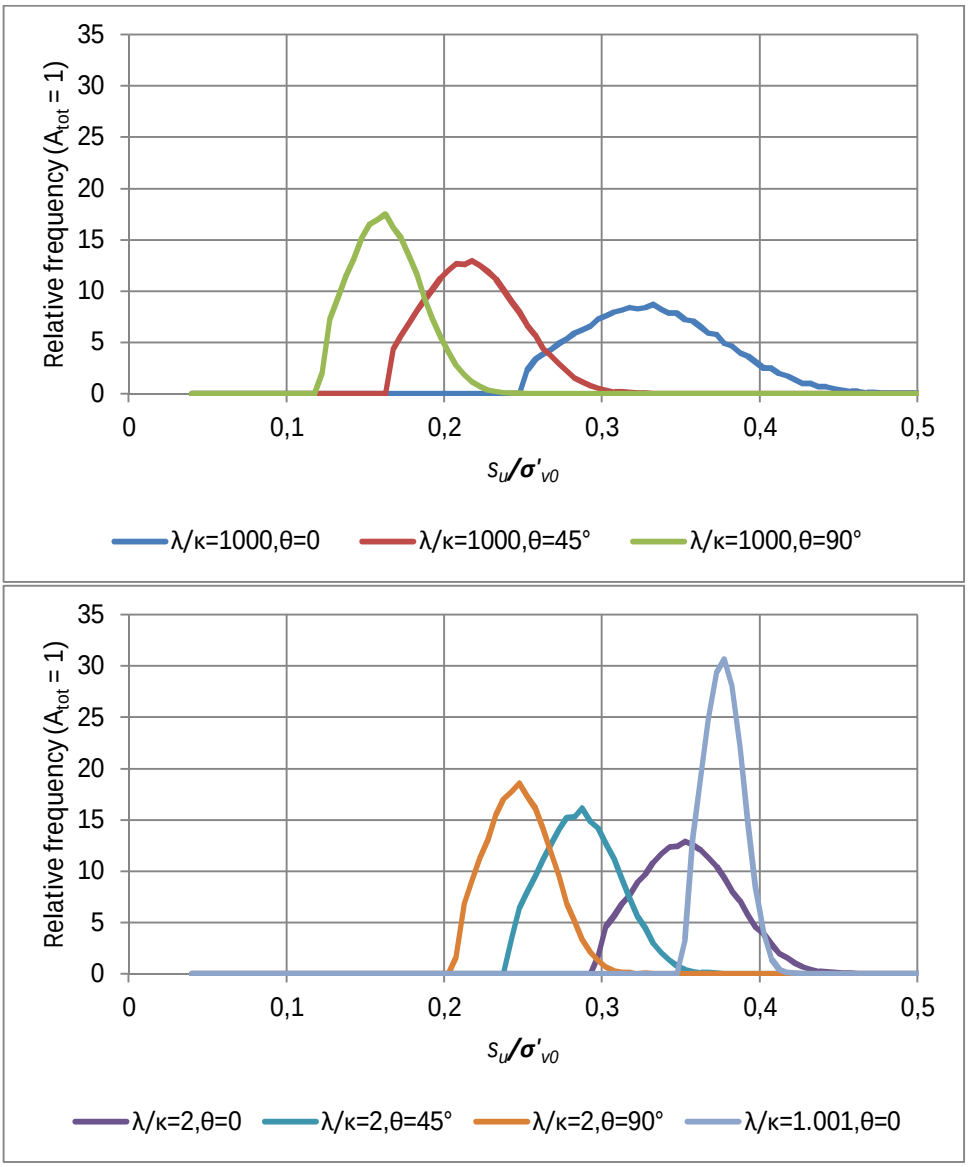

Figure 6.17. Frequency histograms for different λ/κ values.

7 HSU results compared with data on various clays

7.1 Perniö clay

Clay from the site of Perniö, Finland has been extensively researched from 2009 onwards. Perniö is located in the municipality of Salo, near the southern coast of Finland. A full-scale embankment failure test was conducted at the site in 2009 to study the ultimate bearing capacity of a small railway embankment. A description of the experiment can be found in Lehtonen et al (2015).

Samples have been taken from two locations that differ mostly by the stratigraphy of their topmost layers. In 2009 samples were taken at the site of the failure experiment (Location A). The layers from top down consist of a sand fill, a stiff crust that at the time of sampling was located under the ground water table, soft plastic clay, varved silty clay, and sand and moraine followed by bedrock. Undisturbed samples were taken using 50 mm and 54 mm piston tube samplers.

In 2013 large diameter (d = 84 mm) piston samples were taken from a nearby field (Location B). The general stratigraphy is the similar to Location A, but instead of a sand fill the topmost layer is an organic agricultural layer followed by the crust and other layers.

The 2009 laboratory testing program for samples taken from Location A included index tests, CRS oedometer tests and triaxial (mostly CAU) compression tests. The main aim of the triaxial testing was to determine the initial yield surface and friction angle. With this in mind, all but one sample were consolidated to or beyond the initial stress state, typically to 1.5…2 times σ'_{v0}.

Mansikkamäki (2015) gives a friction angle of φ' = 25°-26° (c' = 0) when fitted through the peaks of the effective stress paths (Figure 7.1). When fitted for maximum principal stress ratio, the friction angle seems similar, but with some apparent cohesion . There may have been some issues with sample disturbance due to the small diameter sample tubes, as suggested by Lunne et al (1997). The sample quality was deemed as “Poor” or “Good to fair” based on volume change during oedometer sample reconsolidation, as categorized by Lunne et al (1997).

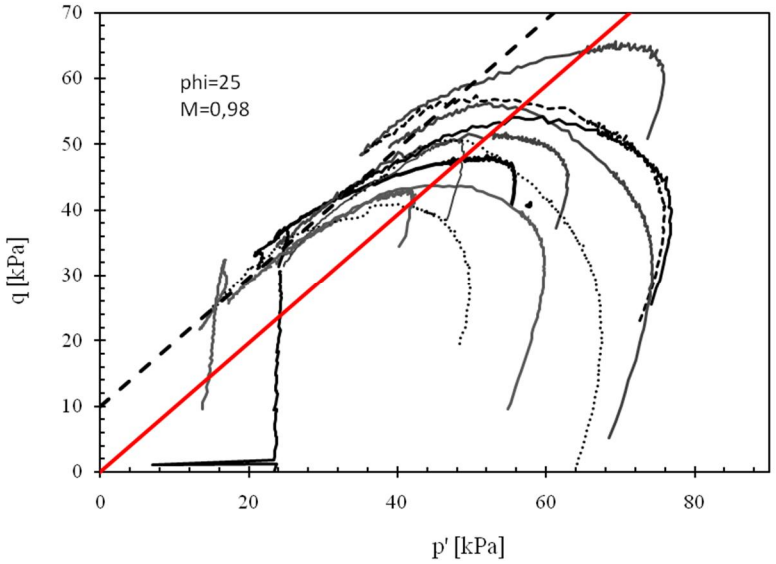

Figure 7.1. Effective stress paths from triaxial testing, failure line fitted through the peaks (Mansikkamäki 2015)

In 2013-2014 a new testing program for samples taken from Location B was conducted to study the strength anisotropy of Perniö clay. More emphasis was based on the determination of the undrained shear strength at various values of OCR.

CRS oedometer tests were used to determine the in situ preconsolidation pressure. Sensitivity and liquid limit were determined with fall cone tests. Hydrometer tests were run to establish the clay content, and burn tests were used to determine organic content from the samples. Additional field vane tests and CPTU borings were conducted at the site as well.

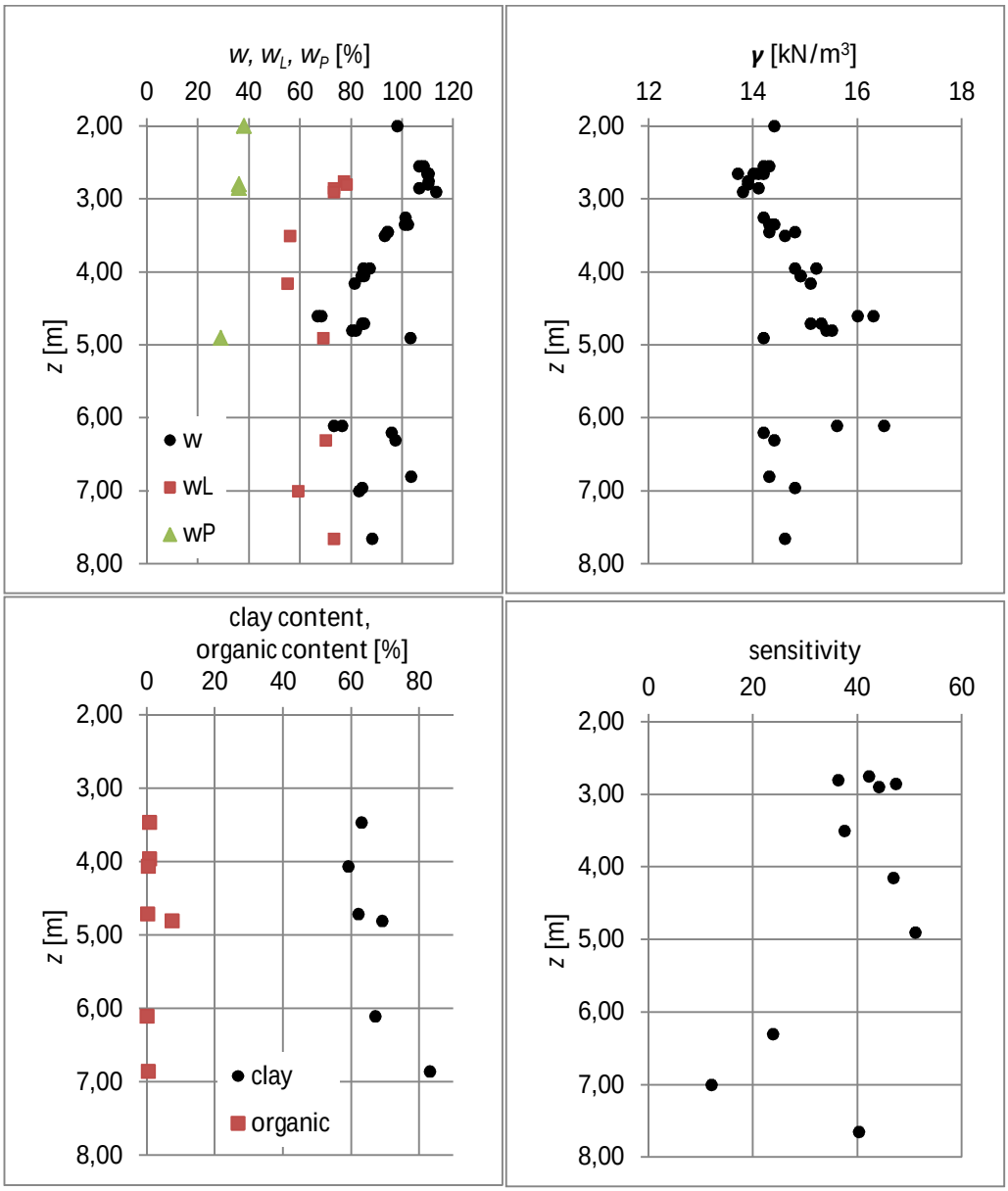

Figure 7.2. Selected properties of Perniö clay, Location B.

As is evident in Figure 7.2, the measured water content and unit weight have linear but opposite trends from 2.5 to 4 meter depths, after which there is considerable scatter in all measured quantities. Below 4 meters a single sample tube could contain several different layers especially with regards to water content/void ratio. The clay content (fraction of <0.002 mm particles) determined by hydrometer tests was around 60 %.

The clay layer most relevant for the stability analysis for the embankment failure experiment is located between about 2.5 m to 4.3 m depths at Location B. This layer contains the same soft clay that is found at Location A.

Triaxial compression and extension tests were conducted with anisotropic consolidation to the approximated in situ stress state. Two parallel 35.8 mm diameter triaxial samples were trimmed from 84 mm tube samples so that a pair of compression and extension tests could be run from the same exact depth. A stress path controlled loading frame was used to consolidate the compression samples close to the in situ stress state. Extension samples were consolidated to the same anisotropic stress state by using external weights. This was necessary due to certain mechanical limitations that precluded the use of the stress path

controlled frame for extension tests. The value of σ'_r / σ'_a in the tests was slightly higher than the approximate in situ value of K_0. This was decided as a precaution as a few samples almost failed during consolidation. Undrained shearing was conducted at a constant rate of $\dot{\varepsilon}_a = 1\%/h$ for most samples. Exceptions were compression test samples 4P3 and 4P4, which were sheared at $\dot{\varepsilon}_a = 0.1\%/h$. The extension failure occurred by decreasing the applied axial stress.

In addition to tests at the slightly overconsolidated in situ stress state (OCR = 1.2…1.5), some NC and high OC tests were done to determine a s_u/σ'_{v0} versus OCR curve. The NC tests were consolidated to stresses higher than the initial preconsolidation pressure, while all OC tests were consolidated so that the initial preconsolidation stress was never achieved during consolidation (as opposed to the "proper" SHANSEP methodology where σ'_c is first surpassed, after which the sample is unloaded to the desired OCR).

Despite the relatively large diameter sample tubes, sample disturbance was an issue with some tubes, especially for those taken from a depth of 4.5 m and below. Below this level the soil becomes increasingly inhomogenous, with occasional stripes of silt or sand, as well as organic layers. High scatter was observed in index properties and unit weight as well. Typically entire tubes taken from below 4.5 m exhibited symptoms of sample disturbance (low initial stiffness both for oedometers and triaxials, preconsolidation pressure not readily visible as a change in stiffness, low peak strengths), which suggests that the disturbance may have occurred already during sampling. There was no difference in observed disturbance effects between laboratory samples were trimmed from the center of the 84 mm sample or near the edge.

Figures 7.3a and 7.3b show the normalized stress-strain curves for compression and extension, respectively for samples taken from the fairly homogenous clay layer (sample depths from 2.55 to 4.05 meters). Typical s_u/σ'_c for compression values are close to 0.35, which is fairly well in line with typical literature values for similar clays (see following chapters). The corresponding extension strength is on both sides of s_u/σ'_c = 0.2 with considerable scatter. There are differences with initial stiffness in the tests. At least for compression tests, the least stiff samples were from tube 4 (samples named 4Px), which would indicate sample disturbance in that tube.

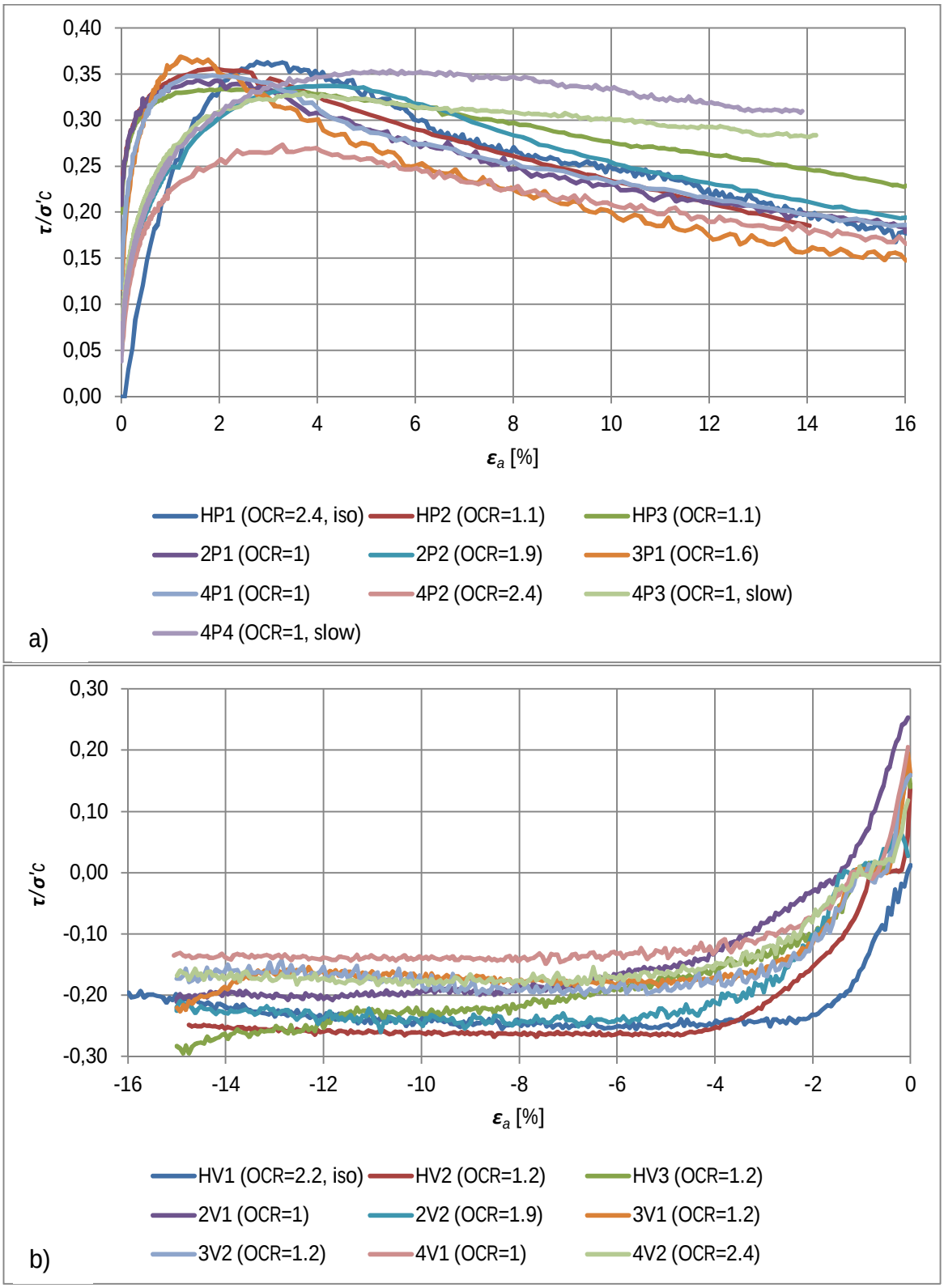

Figure 7.3. Triaxial test results from Perniö Location B. a) compression tests, b) extension tests.

Table 7.1. Triaxial test results, Perniö Location B.

			In situ stress state (approx.)			Consolidation state (test)			Test results		
Test ID	type	depth [m]	σ'_{v0}	σ'_c	OCR	σ'_1	σ'_3	OCR (test)	s_u	s_u/σ'_{v0}	s_u/σ'_c
HP1	CIUC	2.75	25	36	1.44	15.0	15.0	2.40	13.1	0.873	0.364
HP2	CAUC	2.65	25	36	1.44	31.8	16.8	1.13	12.8	0.403	0.356
HP3	CAUC	2.55	24	35	1.46	30.5	16.5	1.15	11.7	0.383	0.334
2P1	CAUC	2.65	25	36	1.46	51.4	30.0	1.00	17.7	0.344	0.344
2P2	CAUC	2.55	24	35	1.46	18.5	14.0	1.90	12.1	0.656	0.345
3P1	CAUC	3.45	28	38	1.36	24.2	15.5	1.57	13.7	0.564	0.359
4P1	CAUC	4.05	31	41	1.31	52.0	40.5	1.00	18.5	0.355	0.355
4P2	CAUC	3.95	30	40	1.32	16.5	12.5	2.42	10.7	0.647	0.267
4P3	CAUC	3.85	30	40	1.33	46.5	41.5	1.00	15.3	0.330	0.330
4P4	CAUC	3.85	30	40	1.33	60.5	55.5	1.00	21.4	0.354	0.354
HV1	CIUE	2.75	25	36	1.44	16.5	16.5	2.18	9.18	0.556	0.255
HV2	CAUE	2.65	25	36	1.44	29.3	19.0	1.23	9.64	0.329	0.268
HV3	CAUE	2.55	24	35	1.46	29.1	19.0	1.24	8.56	0.294	0.238
2V1	CAUE	2.65	25	36	1.46	52.0	31.0	1.00	11.0	0.211	0.211
2V2	CAUE	2.55	24	35	1.46	18.9	14.0	1.85	8.7	0.460	0.249
3V1	CAUE	3.45	28	38	1.36	31.1	19.0	1.22	7.1	0.227	0.186
3V2	CAUE	3.35	28	38	1.36	32.1	20.0	1.18	7.6	0.236	0.199
4V1	CAUE	4.05	31	41	1.31	61.6	37.5	1.00	9.1	0.148	0.148
4V2	CAUE	3.95	30	40	1.32	16.9	13.0	2.37	7.4	0.438	0.184
Note: test 3P2 (not shown) failed during consolidation with valve open, results omitted Tests 4P2 and 4V1 are likely badly disturbed as their measured shear strength is quite low.											

Table 7.1 presents some further triaxial test results. The given s_u values correspond to peak τ values for the strain range shown in Figure 7.4. Exceptions were extension tests 3V1 and HV3, where at high strains (ε_a > 11 %) the measured shear stress started to increase after being at a plateau for some time. This has been attributed to the membrane around the sample, which may have started to stretch at high axial strains, adding to the deviator stress. In these cases, the peak τ value is simply taken for the strain range before the obvious stress increase.

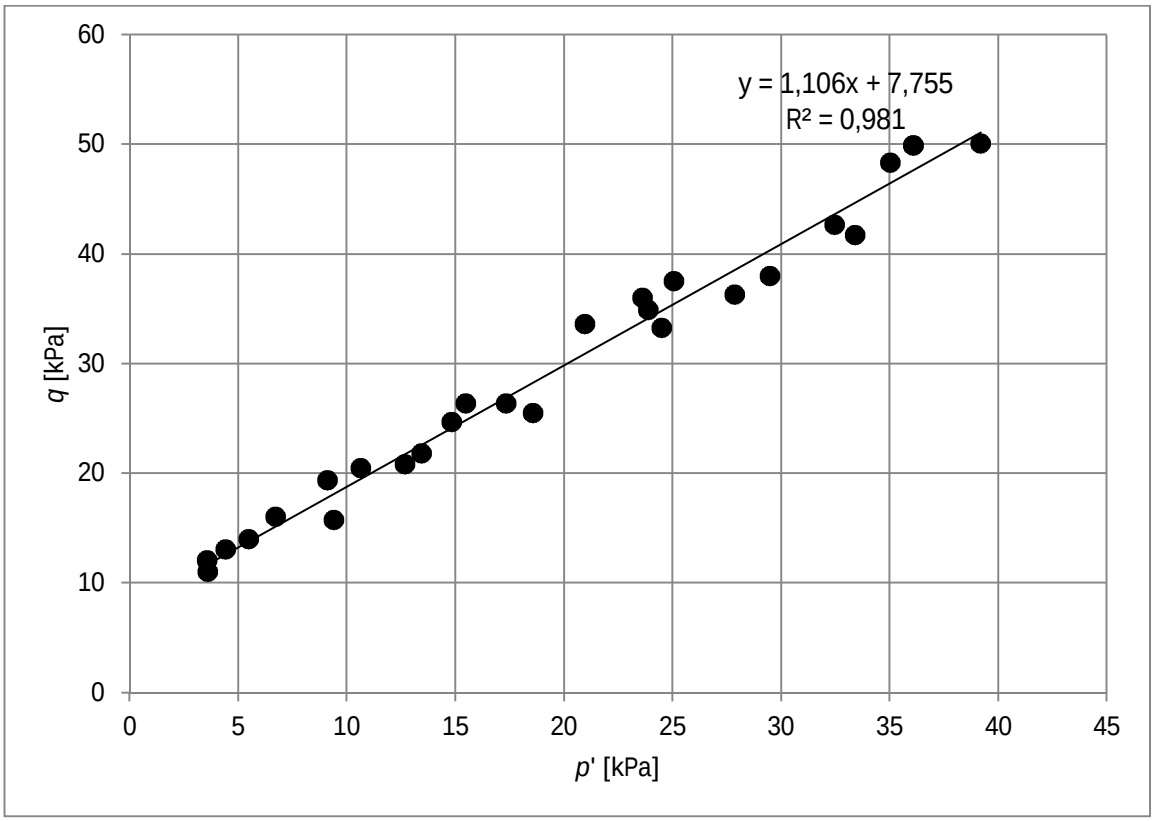

Figure 7.4. Perniö clay failure line fitted through points of maximum obliquity.

To determine the critical state friction angle for compression, a line is fitted through stress points at maximum obliquity, i.e. stress points corresponding to the maximum *q/p'* value. The data is taken from both locations A and B, totaling 27 CIUC and CAUC tests. The stress points and the corresponding linear fit through the points are shown in Figure 7.4. The linear fit indicates the following effective critical state strength parameters in (*p'*,*q*) space:

$M = 1.106$
$q_{int} = 7.76$ kPa

The linear fit is very good ($R^2 = 0.98$). There is however some uncertainty regarding the accuracy of the pore pressure measurements (which is done from the end of the sample, not from the failure plane). Also at large strains the assumed corrections for the sample cross-section area and membrane stress may not always be accurate. The above numbers are nevertheless what laboratory testing indicates, and the linear fit through the data points is excellent. It is however unclear if the apparent cohesion really exists or whether it is an artifact of testing.

The (*p'*,*q*) strength parameters correspond to the following effective strength parameters :

$\varphi' = 27.8°$

$$c' = \frac{q_{\text{int}}}{2} \cdot \sin(90° + \varphi') = 7.76kPa \cdot \sin(90° + 27.8°) = 3.4kPa$$

In slight contrast, Mansikkamäki (2015) has determined the peak friction angle (fitted for maximum deviator stress) for Perniö clay to be φ' = 25-26° (from Location A tests, see Figure 7.1).

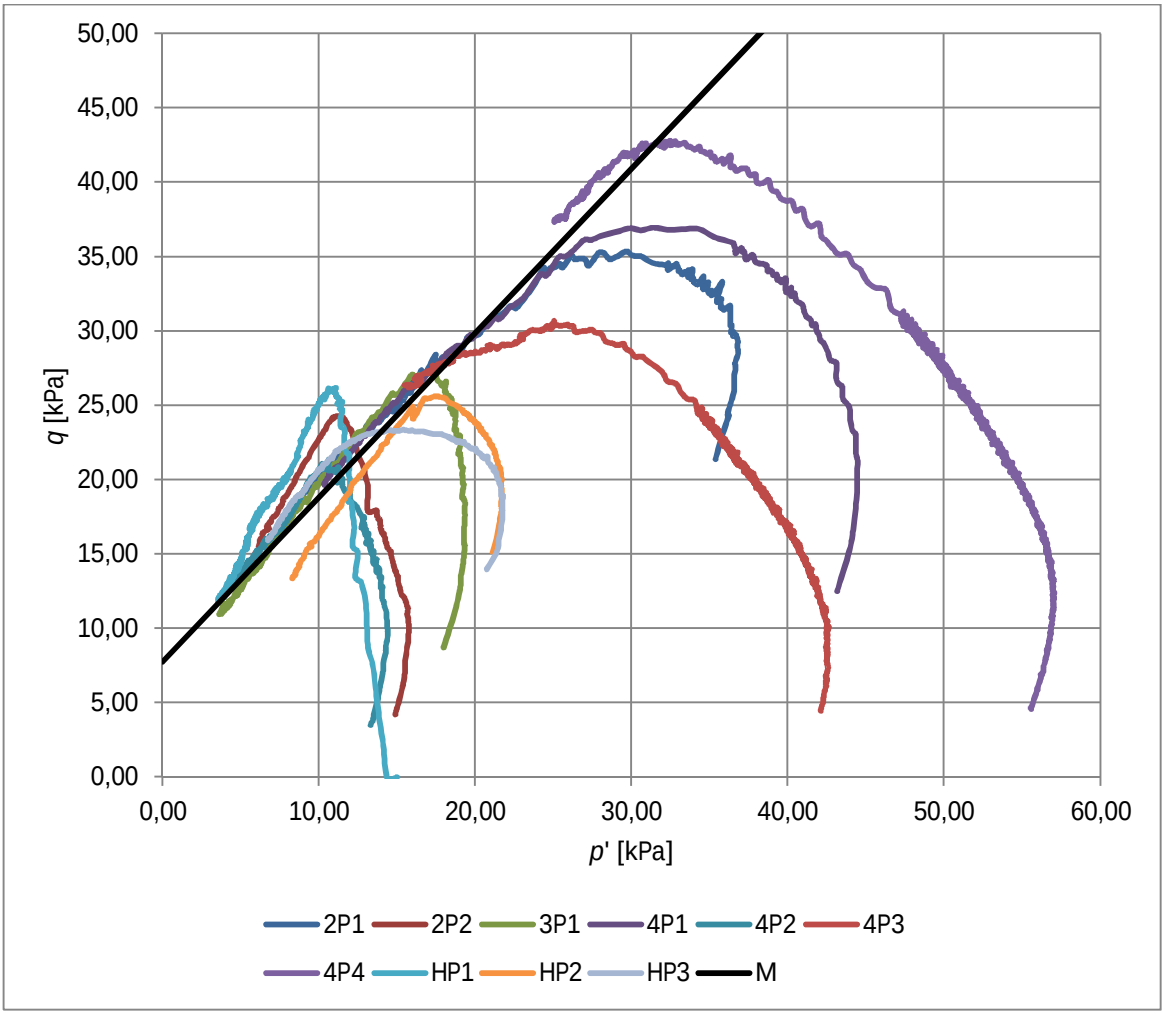

Figure 7.5. Effective stress paths of compression tests, Location B.

Figure 7.5 shows effective stress paths for tests from Location B. Additionally, the critical state M-line for M = 1.106, q_{int} = 7.76 kPa is shown. Overall, the visual fit between the assumed M-line and the tail parts of the stress paths is quite good.

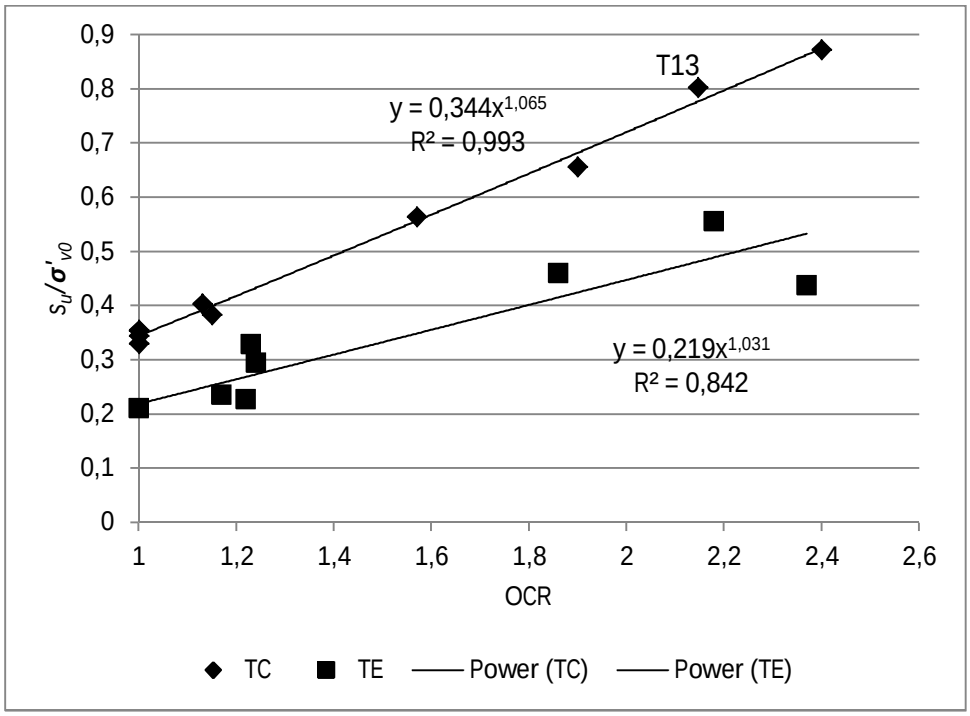

Figure 7.6. SHANSEP-type curve fit, Location B

Figure 7.6 shows the Location B normalized shear strengths versus OCR. The data is supplemented with a single OC compression test from Location A (marked as "T13"), which was added to get better data coverage for the larger OCR values. The likely badly disturbed samples 4P2 and 4V1 were omitted from the data set. The SHANSEP parameters (although not resulting from a "pure" SHANSEP procedure) are obtained by the standard MS Excel curve fit for a power function, and as is shown in the figure, are:

Triaxial compression (TC): $S = 0.344$, $m = 1.065$
Triaxial extension (TE): $S = 0.219$, $m = 1.031$

It must be acknowledged that the apparent SHANSEP parameters for triaxial extension are quite high when compared to typical values found in literature (see e.g. Sections 7.2 and 7.3). An obvious caveat is that the laboratory data consistently indicates cohesion at high strain levels (Figures 7.4 and 7.5). If cohesion is present in the data, the measured strengths are difficult to normalize either by σ'_{v0} or σ'_c. This is so because the *relative* strength contribution of cohesion depends on the *absolute* magnitude of the consolidation stress level, as is illustrated in Figure 7.7. Therefore samples that share the same OCR value but have differing in situ consolidation stresses cannot, in theory, share the same locations on the (s_u/σ'_{v0}, OCR) plot.

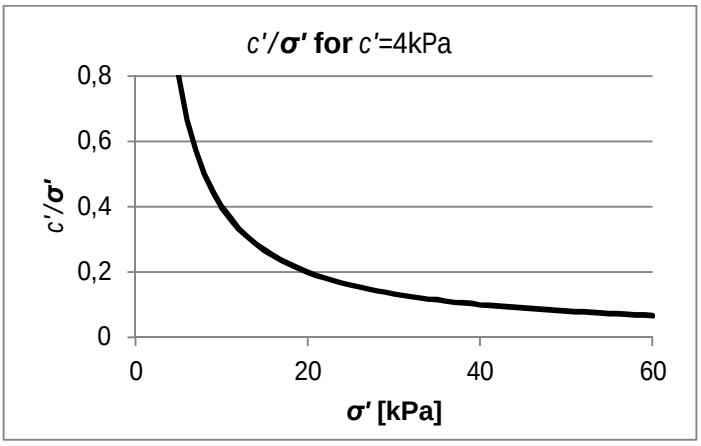

Figure 7.7. Relative strength contribution of a given amount of cohesion versus stress level

If φ' = 27.8° is accepted and c' = 0 is assumed, coupled with the measured K_{0NC} = 0.52, the HSU parameters for Perniö clay become:

φ' = 27.8°
C = 0.97
D = 1 (basic assumption).

Mansikkamäki (2015) gives the following compressibility parameters for Perniö clay:

λ = 0.50-0.60
κ = 0.045-0.060

These values would then amount to $\lambda/\kappa \approx 10$.

A non-normalized model fit (i.e. an attempt to recreate the measured stress paths at laboratory stress levels) using the HSU method is quite possible. The basic concept is described in section 5.9. The steps taken are as follows:

1) A preconsolidation stress level is chosen. In this case σ'_c = 36 kPa is chosen as the in situ preconsolidation stress of the samples was at or close to that number. All data is first normalized by their actual σ'_c values, and then multiplied by the new value σ'_c = 36 kPa to normalize the dataset to the same preconsolidation pressure. This is necessary to be able to present the data in relation to a single initial yield surface.

2) Necessary data is input as usual.

3) The initial mean stress p'_0 and mean preconsolidation stress p'_c are calculated as usual. However, in subsequent calculations these are replaced with calculation values p'_{0calc} and p'_{ccalc}:

$$p'_{0calc} = p'_0 + p'_{att} \tag{7.1}$$

$$p'_{ccalc} = p'_c + p'_{att} \tag{7.2}$$

where p'_{att} is the value of attraction in the (p',q) space. p'_{att} is defined as follows:

$$p'_{att} = \frac{q_{int}}{M} \tag{7.3}$$

4) Undrained shear strength is calculated as usual, using the values of p'_{0calc} and p'_{ccalc} as relevant.

5) The stress path resulting from this calculation corresponds to the calculation values of p'. To draw the proper stress path, the stress paths are moved back to the left by p'_{att}.

Figure 7.8 shows some selected effective stress paths from Location B, normalized to σ'_c = 36 kPa when necessary. NC tests with much higher consolidation pressures have been omitted, as the apparent cohesion makes accurate normalization difficult when the stress states differ greatly. In addition, effective compression and extension stress paths predicted by the HSU method are shown (σ'_c = 36 kPa, OCR = 1.2, λ/κ = 10).

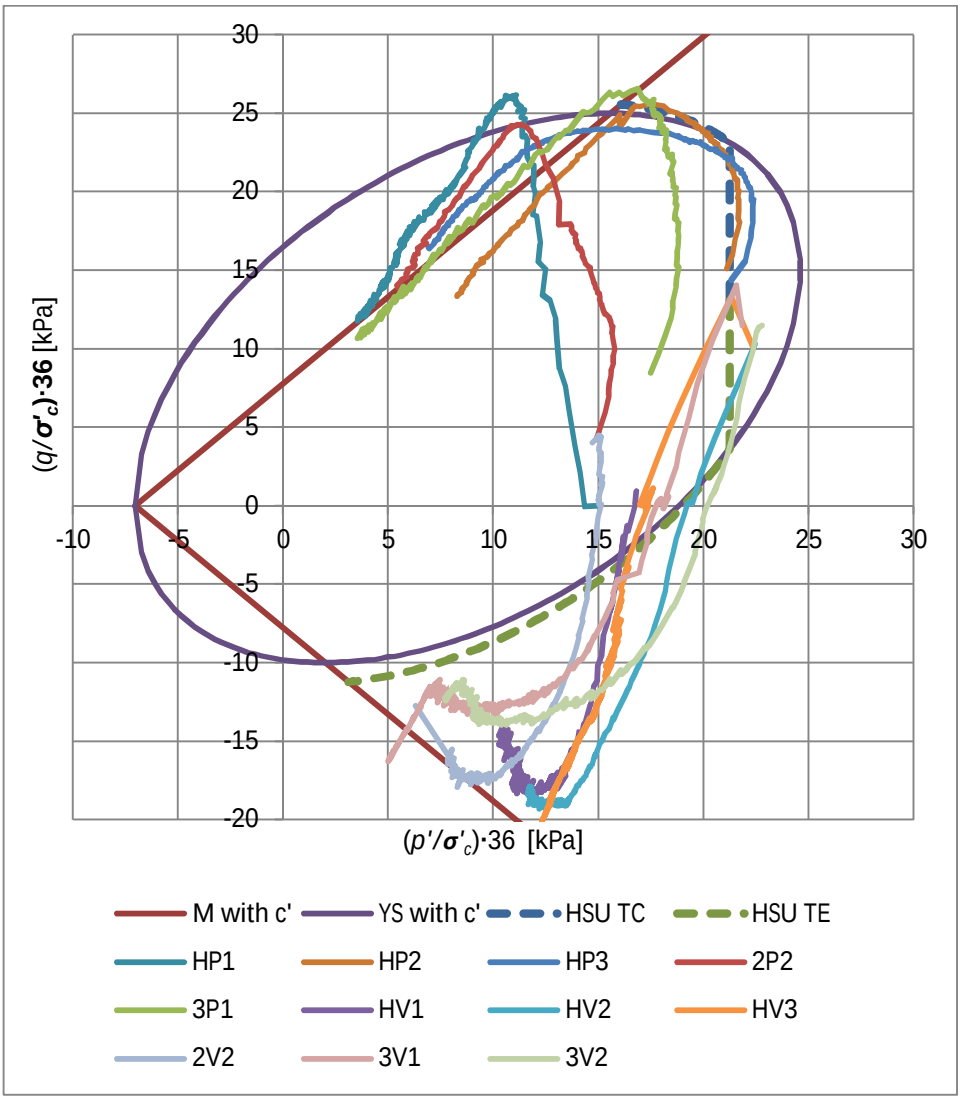

Figure 7.8. HSU stress paths and yield surface with measured stress paths.

The HSU method matches the compression strength at OCR = 1.2, λ/κ = 10 very well. On the other hand, using the same λ/κ results in low extension strength when compared to the laboratory data. Apparently, a much lower λ/κ value would be needed to match the indicated extension strength of 5-10 kPa. For example, λ/κ = 2 would result in s_{uE} = 8.9 kPa, which is close to what many stress paths starting from the same initial stress levels would indicate.

Finally, each test from Location B is modelled using HSU. Now, the value of λ/κ is treated as an unknown, and is chosen so as to match the s_u value of each individual test. This is done to study which λ/κ values would be applicable. The initial stress states are matched as accurately as possible. The apparent cohesion is taken into account as described previously.

The strength parameters for all modelled tests are:

$\varphi' = 27.8°$
$q_{int} = 7.8$ kPa

For each modelled test, the preconsolidation stress σ'_c and OCR were directly set to match the conditions in the laboratory. If OCR > 1 in the test, σ'_c is set to the approximate in situ value. If OCR = 1, $\sigma'_c = \sigma'_{10}$.

For tests where the in situ preconsolidation stress was not surpassed (i.e. OCR > 1), the value of C = 0.97 was used to match the measured K_{0NC} value. For tests that were consolidated beyond the in situ preconsolidation stress, the C value was chosen so as to match the initial stress state in the test.

The parameter D was chosen to match the initial stress state with the laboratory conditions. Note that in many tests the K_0 value was significantly higher than in situ, which explains the high D values needed. For OCR = 1, D was set to 1, as the parameter does not affect anything at OCR = 1.

Finally, λ/κ was set to match the undrained shear strength given by the corresponding test. The results are presented in Table 7.2.

Table 7.2. Summary of HSU strength predictions compared to the test results.

		consolidation state				HSU parameters		Measured s_u and corresponding λ/κ		Strength with λ/κ = 10	
Test ID	type	σ'_c [kPa] (in situ)	σ'_{10} [kPa] (test)	σ'_{30} [kPa] (test)	OCR (test)	C	D	s_u^{meas} [kPa]	λ/κ	s_u^{HSU} [kPa]	s_u^{HSU} / s_u^{meas}
HP1	CIUC	36	15.0	15.0	2,40	0.97	1.61	13.1	*)	12.5	0.95
HP2	CAUC	36	31.8	16.8	1,13	0.97	0.36	12.8	9,50	12.8	1.00
HP3	CAUC	35	30.5	16.5	1,15	0.97	0.68	11.7	-5,38	12.5	1.07
2P1	CAUC	36	51.4	30.0	1,00	1.09	1	17.7	3,91	16.6	0.94
2P2	CAUC	35	18.5	14.0	1,90	0.97	1.27	12.1	-1,25	12.3	1.01
3P1	CAUC	38	24.2	15.5	1,57	0.97	1.01	13.7	1,53	13.1	0.96
4P1	CAUC	41	52.0	40.5	1,00	1.46	1	18.5	2,48	14.9	0.80
4P2	CAUC	40	16.5	12.5	2,42	0.97	0.92	10.7	**)	13.4	1.25
4P3	CAUC	40	46.5	41.5	1,00	1.67	1	15.3	3,4	12.7	0.83
4P4	CAUC	40	60.5	55.5	1,00	1.72	1	21.4	2,4	15.8	0.74
HV1	CIUE	36	16.5	16.5	2,18	0.97	1.81	9.18	1,59	5.5	0.60
HV2	CAUE	36	29.3	19.0	1,23	0.97	2.33	9.64	1,80	5.6	0.58
HV3	CAUE	35	29.1	19.0	1,24	0.97	2.31	8.56	2,20	5.6	0.66
2V1	CAUE	36	52.0	31.0	1,00	1.12	1	11.0	10,68	11.1	1.01
2V2	CAUE	35	18.9	14.0	1,85	0.97	1.25	8.7	1,63	5.4	0.62
3V1	CAUE	38	31.1	19.0	1,22	0.97	1.79	7.1	3,76	5.9	0.82
3V2	CAUE	38	32.1	20.0	1,18	0.97	2.4	7.6	3,16	5.9	0.77
4V1	CAUE	41	61.6	37.5	1,00	1.14	1	9.1	-2,91	13.3	1.47
4V2	CAUE	40	16.9	13.0	2,37	0.97	0.98	7.4	2,52	5.9	0.80
*) Measured strength not reached with any λ/κ value (measured strength too high) **) Measured strength not reached with any λ/κ value (measured strength too low)											

It is evident that by varying λ/κ, the measured s_u values can be predicted with HSU in most cases. Sometimes, a negative λ/κ value may be needed. If shearing occurs in the wet side, a negative λ/κ value causes the effective stress path to fall back inside the initial yield

surface. In the dry side, a negative λ/κ value causes the effective stress path to go outside the initial yield surface. This can be useful if the result of a given test needs to be matched, but there is no physical meaning for negative λ/κ values. The samples that require negative λ/κ values for matching s_u may be disturbed or there may have been unrecognized errors in the test (pore pressure measurements, incorrect zero values for axial stress, contact problems between the sample and the pedestal etc.).

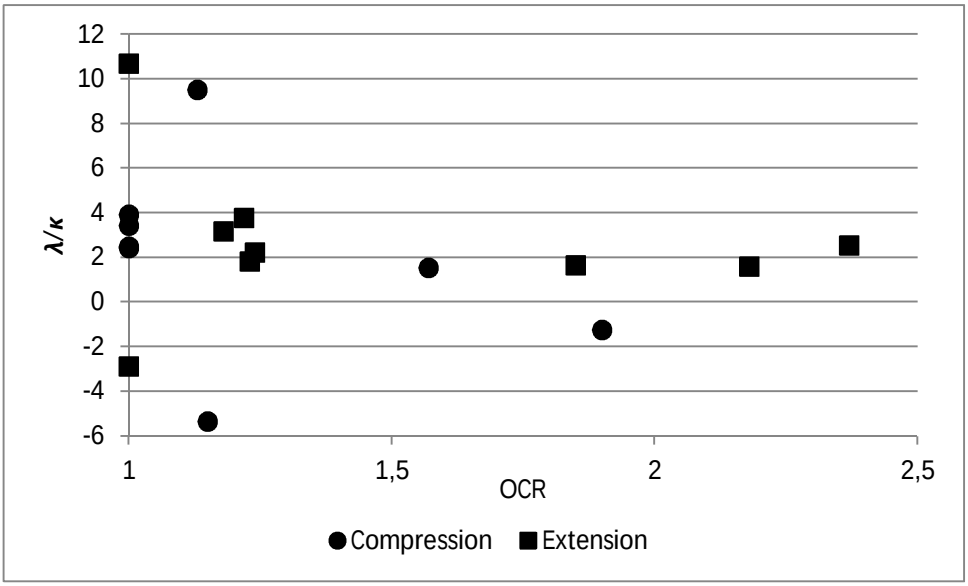

Figure 7.9. λ/κ values needed to match the measured undrained shear strengths versus OCR.

Figure 7.9 shows the λ/κ values required for the HSU method to match the measured s_u values. There is no visible trend with OCR, and no difference between the compression and extension tests. When the outliers are ignored, it appears that the applicable range is λ/κ = 1.5…3.

When the value of λ/κ = 10 (Mansikkamäki 2015) is used, the compression strength predicted by HSU is well in line with the measured values from tubes H, 2 and 3. This is because the model is not very sensitive in triaxial compression, so varying λ/κ has a relatively small effect on predicted compression strength (see Section 6.3). Tube 4 results do not match as well as tubes 2 and 3. The likely reason for poor results in modelling the tube 4 was that tests 4P1, 4P3 and 4P4 were normally consolidated with quite high K_0 values that did not occur in situ, and the resulting model yield surfaces can be considered unrealistic because HSU assumes K_0 consolidation. In addition, sample 4P2 (OCR = 2.4) is likely disturbed.

The HSU method does not predict the measured extension strengths well with λ/κ = 10, but generally underestimates the extension strength. Much better results are obtained with values of λ/κ = 2…4. It can well be that the model does not capture the hardening properties in extension all that well, but it must be noticed that the plasticity of Perniö clay is quite high. As is generally seen from literature (see e.g. Section 7.3), especially the extension strength is quite sensitive to plasticity. As such the HSU value of λ/κ in extension might be needed to be adjusted accordingly so that higher plasticity requires lower λ/κ in extension. This issue is further addressed in Chapter 9, where the choice of λ/κ is discussed.

7.2 Strength fits based on data on Norwegian clays

7.2.1 General

There are some correlations for normalized shear strengths gathered from inorganic Scandinavian clays. A recent paper by Karlsrud & Hernandez-Martinez (2013) presents data collected from several sites in Norway (22 sites) and UK (1 site) between 1982 and 2010. High-quality block samples were taken using the Sherbrooke sampler (Lefebvre & Poulin 1979). Triaxial compression, extension and DSS test were carried out. The sample quality was determined to be superior to typical piston samples. As such, the data presented in the paper can well be used to verify the results given by the HSU method.

Figure 7.10 shows normalized compression and extension s_u versus OCR plots and inferred SHANSEP (see Section 4.4) curves from the test series (Karlsrud & Hernandez-Martinez 2013). Similar DSS results are omitted here for brevity and because the regressions derived from DSS results are based on a relatively low number of tests.

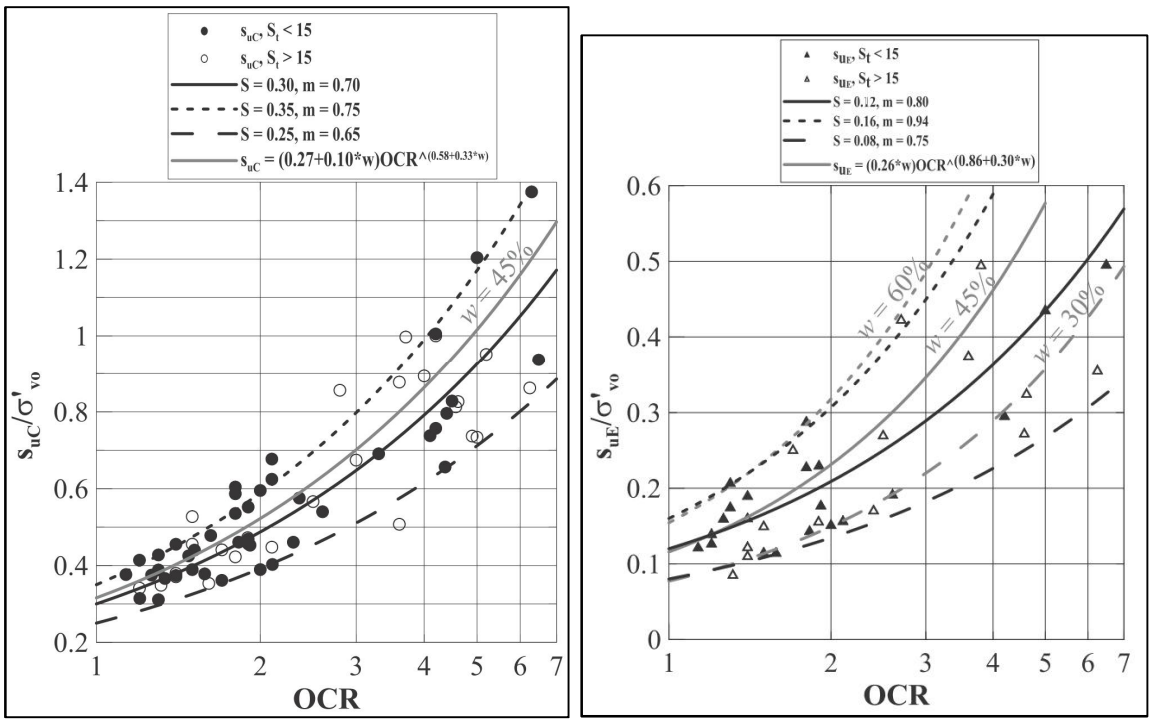

Figure 7.10. Peak strengths for Norwegian clays, a) compression, b) extension (Karlsrud & Hernandez-Martinez 2013)

Figures 7.10a and 7.10b show results for from triaxial compression and extension tests, respectively. Based on this data, three "cases" can be distinguished (Table 7.3).

Table 7.3.Representative SHANSEP parameter values for Norwegian clays (Karlsrud & Hernandez-Martinez 2013)

case		Triax. comp		Triax. ext		
		S	*m*	*S*	*m*	S_{ext}/S_{comp}
"Low"		0.25	0.65	0.08	0.75	0.32
"Average"		0.30	0.70	0.12	0.80	0.40
"High"		0.35	0.75	0.16	0.94	0.46

There is of course the question whether the regression is valid for clays with higher water content (up to or above w = 100 %). Additionally, there is quite a lot of scatter with the extension strength data, and the regression parameters are based on a relatively low number of measurements. The given regression parameters are still used as the basis for a HSU fit as they are generally based on a reasonably robust data set from high quality samples.

The HSU method can be used to predict similar SHANSEP curves. At this point, φ', λ/κ and C can be considered unknown. The parameter D is set at its default value $D = 1$.

While the friction angles for the single data points are not explicitly given, Karlsrud & Hernandez-Martinez (2013) give maximum friction angles obtained by assuming zero attraction intercept (i.e. zero cohesion):

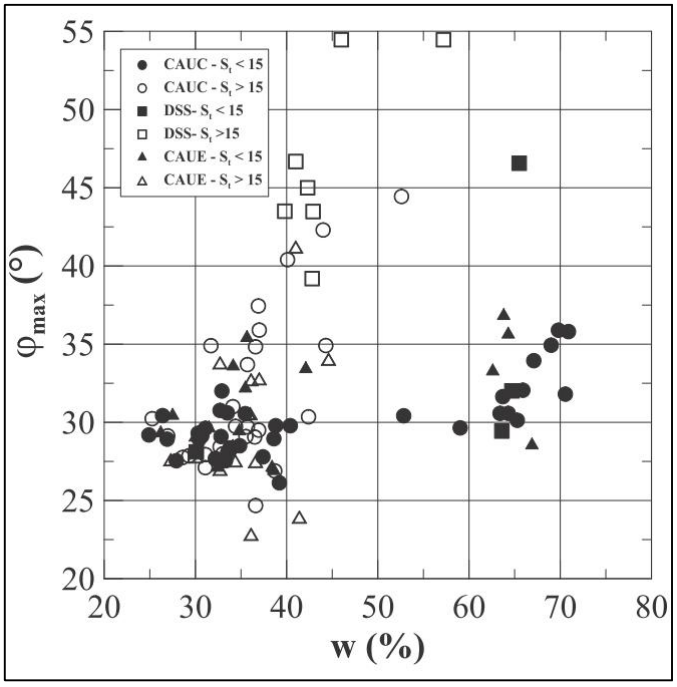

Figure 7.11. Peak friction angle versus water content (Karlsrud & Hernandez-Martinez 2013)

It is apparent from Figure 7.11 that the applicable "wet side" peak friction angles generally range from 25° to 35°, which is a typical range for Scandinavian clays. The highest friction angles in the figure most likely correspond to tests exhibiting apparent effective stress cohesion at low stress levels. Fitting such data with the assumption of $c' = 0$ results in very high apparent friction angle.

7.2.2 HSU fitted for both compression and extension

Here, an HSU fit is produced by iteratively varying the values of φ', λ/κ and C. The aim is to achieve a fit as good as possible for both triaxial compression and extension.

When φ' and λ/κ are varied together, it becomes apparent that varying λ/κ has a large effect on the SHANSEP exponent m. Thus the HSU fit can be done in an iterative fashion by first setting λ/κ to produce the desired m value, changing the φ' to obtain the desired strength ratio S, and then repeating the process until a desired fit for triaxial compression is achieved.

After this, the model is fitted for triaxial extension. The parameter C controls the level of anisotropy by controlling the inclination of the yield surface. Its effect is fairly slight for triaxial compression, but quite notable for extension. First, the λ/κ value is chosen for extension to set the exponent m after which the parameter C is chosen to set the stress ratio S.

After this, some further iterative tweaking is done to set the parameters to give the desired result.

Overall, the process of fitting was:

1. Set λ/κ in compression to give the desired m value
2. Set φ' to give the desired S value in compression
3. Set λ/κ in extension to give the desired m value
4. Set C to give the desired S value in extension
5. Repeat steps 1-4 until the fit is satisfactory (here no explicit requirements were set, but an overall "good" fit was attempted)

Table 7.4 shows the HSU parameters obtained in the fitting process and the corresponding SHANSEP parameters. Some boundary conditions were applied: The range of the parameter C was restricted to $C = 0.9…1.1$, as values beyond this range can be considered unlikely (see Section 6.6). Additionally, the value of λ/κ was restricted to 1000. This was a slight issue in fitting HSU for extension, as negative λ/κ would have been required for $m >$ 1.

Table 7.4. HSU fit results.

				compression			extension		
case	φ'	C	D	λ/κ	S	m	λ/κ	S	m
"low"	20.0°	0.90	1	2.24	0.251	0.650	3.13	0.095	0.750
"average"	25.9°	0.91	1	2.43	0.300	0.699	3.60	0.123	0.798
"high"	33.1	1.01	1	2.64	0.36	0.750	11.0	0.160	0.940

When the results of Table 7.4 are compared with the target values given in Table 7.3, it is evident that HSU could be fitted to perfectly produce the SHANSEP compression parameters, but the extension parameters could not quite be attained. Figure 7.12 shows the "target" SHANSEP curves and those resulting from the HSU fit for triaxial extension.

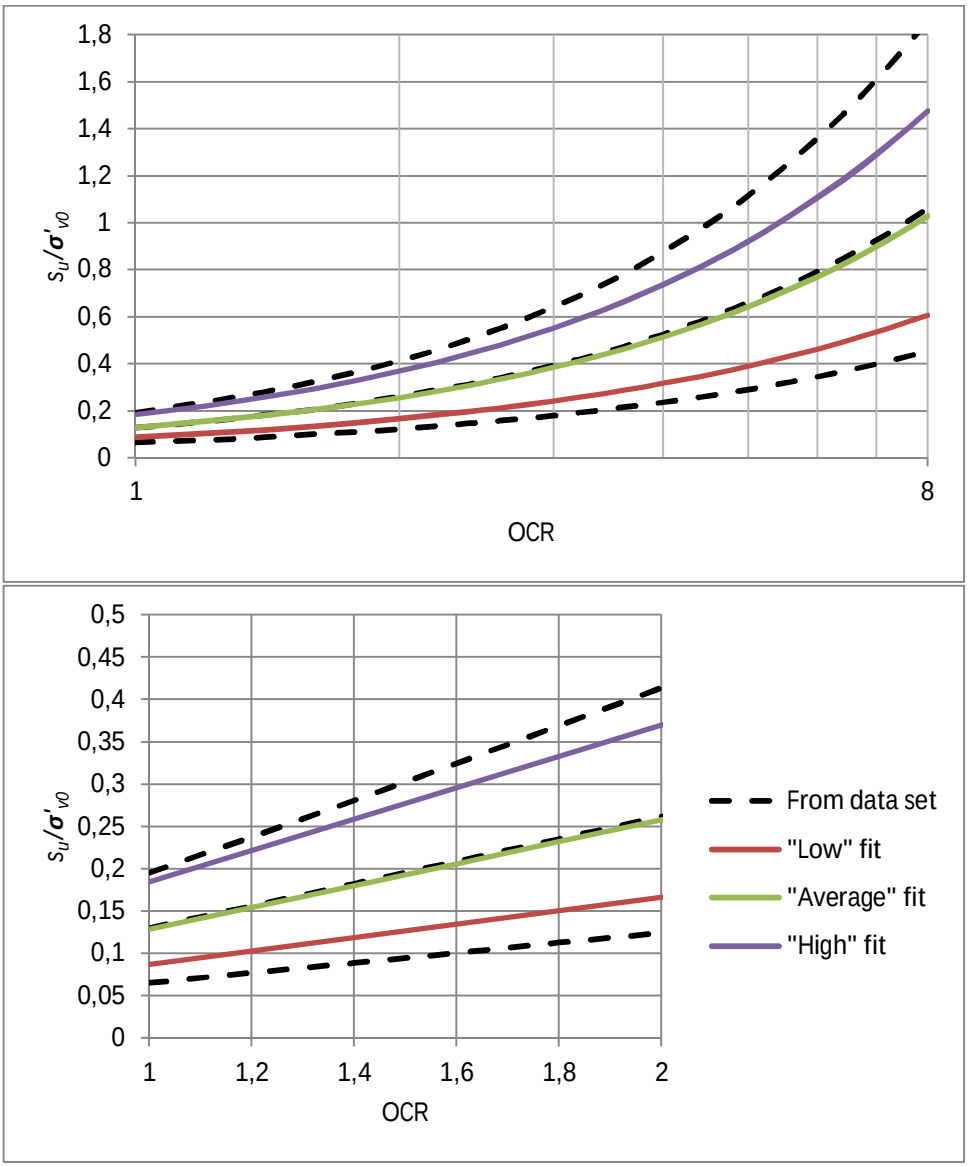

Figure 7.12. Target SHANSEP curves and HSU fits for a) compression and b) extension.

Fitting HSU for compression was simple, and the parameter values required were quite reasonable. However, in extension the fitting is not quite as straightforward. If the "reasonable" ranges of parameter values are respected, the fit is not perfect. In the "low" case, a low enough strength ratio S (high enough strength anisotropy) could be achieved only by decreasing the C value below $C = 0.9$. In the "average" and "high" cases, an m value over 1 could only be achieved with negative λ/κ values. It should however be noted that the m values given by Karlsrud & Hernandez-Martinez (2013) are based on relatively sparse data with large scatter, which reduces the reliability of the given regression parameters.

A notable issue here is that the data given by Karlsrud & Hernandez-Martinez (2013) corresponds to peak strengths of good quality samples, whereas the HSU method does not account for any post-peak strain softening. Therefore in practical engineering use it should be considered somewhat unwise to fit HSU directly to peak strengths, as in reality peak strengths are not simultaneously achieved along the slip surface. The HSU method is intended to be used so that its predicted shear strengths correspond to reasonable post-peak strengths that can be used in design. As such, HSU is not necessarily capable for

capturing the extremely high strength anisotropy exhibited by good quality low plasticity samples.

HSU is mainly intended for normally consolidated or slightly overconsolidated clays. Practical model fitting should focus on predicting the undrained shear strength over a relatively small OCR range (e.g., OCR = 1…2). As such, properly predicting the strength ratio *S* can be considered more important than the exponent *m* when compromises need to be made.

As shown in Figure 7.11, there is no clear trend between water content and friction angle in the original data. In the model fits there is however a clear correlation between these parameters (high SHANSEP parameter values correlate with high water content, and require high friction angle in the HSU method). As such the fit can be considered somewhat artificial. This fitting exercise however shows that HSU can be readily adapted for predicting the strength of various clays. The friction angles required for fitting HSU to the given data fall quite well in the general range of ca. $\varphi' = 25°…35°$ given by Karlsrud & Hernandez-Martinez (2013).

7.2.3 HSU fit with baseline values

A SHANSEP fit that may be closer to the intended real life usage (where few parameters are known) is presented for comparison. Here only the friction angle is considered known. Values $\varphi' = 25°$, $\varphi' = 30°$ and $\varphi' = 35°$ are studied. These values are well in line with the range presented in the data (when the very high φ' values for samples exhibiting cohesion are omitted). Parameters C and D are considered unknown, and by default they are set at their baseline values $C = D = 1$ as no better information is available. Now only λ/κ is varied and the results are compared to the target SHANSEP parameters presented by Karlsrud & Hernandez-Martinez (2013), (see Section 7.2.1, Table 7.3).

Furthermore, λ/κ is set to the same value for both compression and extension to reflect more simplified "real life" (consultant) usage where choosing individual values would not be feasible. This results in the same m value for triaxial compression and extension. Overall, the fit would then have to be a compromise between the S and m parameters, and between compression and extension strengths.

As HSU is mainly intended for use with normally or slightly overconsolidated clays, the fitting is done here only for the range OCR = 1…2. This makes obtaining an overall fit somewhat easier and more in line with the intended usage.

Based on the fits with varying φ' (Section 7.2.1), no specific attempt is made to match the "Low" boundary values suggested by Karlsrud & Hernandez-Martinez (2013), as it is clear that quite low friction angles are needed to match the lower boundary of the data. Instead, the SHANSEP parameter range "available" with the given friction angles is studied.

Figure 7.13 shows the effect on the calculated SHANSEP parameters S and m when λ/κ is varied. Additionally, the "Low", "Average" and "High" S and m values presented by Karlsrud & Hernandez-Martinez (2013) are shown in the respective figures.

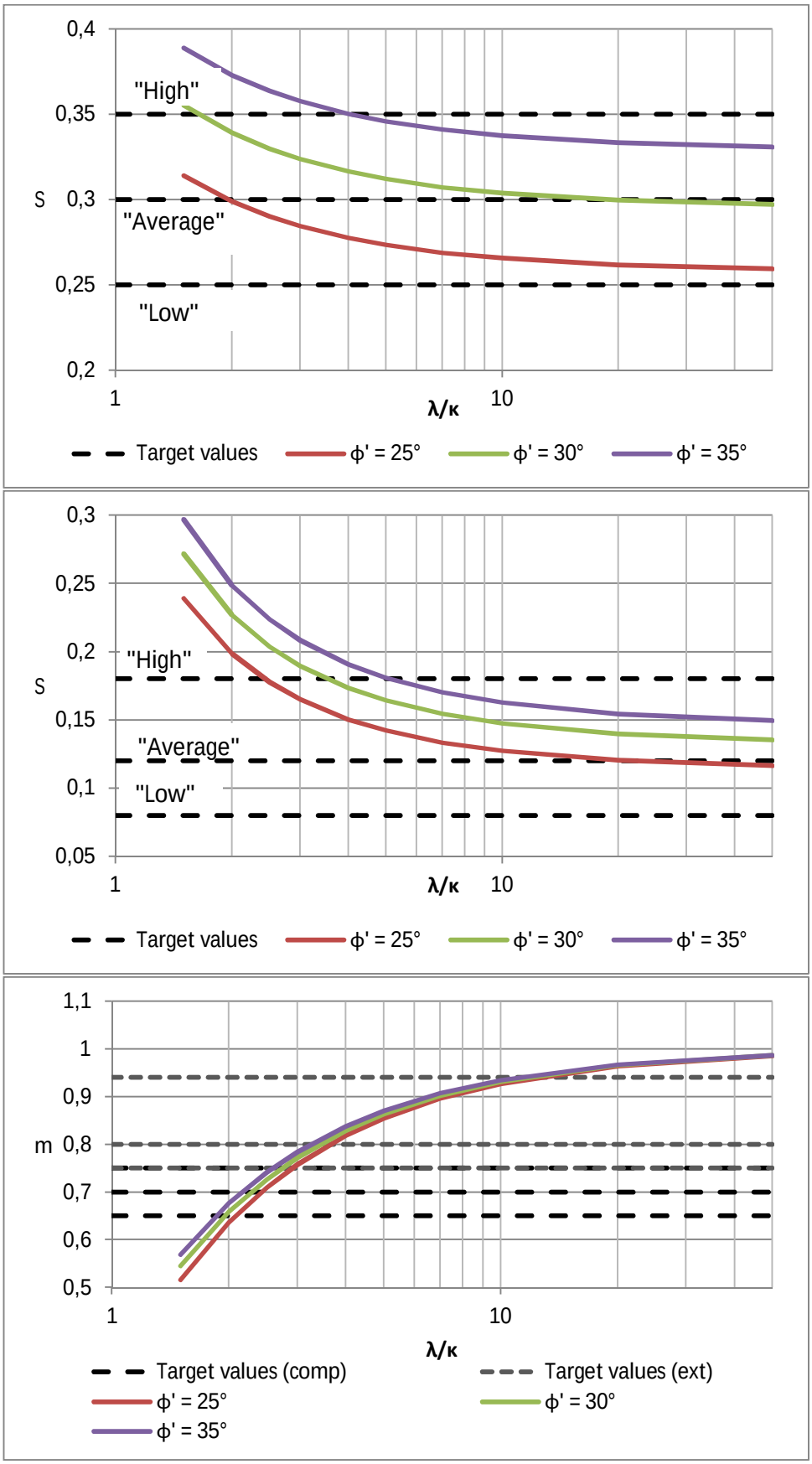

Figure 7.13. SHANSEP parameters as functions of λ/κ: a) S for compression; b) S for extension; c) m (shared). The "target values" correspond to the "Low", "Average" and "High" parameters suggested by Karlsrud & Hernandez-Martinez (2013).

It is apparent from Figure 7.13 that the exponent m can be matched by using a fairly small λ/κ value in all cases. The range of λ/κ values capable of matching a given case is considerably larger (and with the given friction angles, the "low" case cannot be matched with any value of λ/κ between 1 and infinity).

Thus the choice of λ/κ value to match a given set of SHANSEP-type data should be a compromise between a "local" fit at a given OCR (especially the parameter S), and fitting over a large OCR range (parameter m). For example, if HSU is fitted to give accurate s_u values at low OCR (i.e. fitted for S), the results will be notably worse at high OCR levels.

As an example, the case of $\varphi' = 30°$ with a high water content (typical of inorganic clays found in Southern Finland) could plausibly correspond to the "High" case of the Karlsrud & Hernandez-Martinez (2013) data set. The "target" parameters would then be $S = 0.35$, $m = 0.75$ for compression, and $S = 0.18$, $m = 0.94$ for extension. Using the combination of baseline values $C = D = 1$ and $\varphi' = 30°$, the "High" SHANSEP target values could be matched with the following λ/κ values:

S for compression: $\lambda/\kappa = 1.63$
S for extension: $\lambda/\kappa = 3.41$
m for compression: $\lambda/\kappa = 2.73$
m for extension: $\lambda/\kappa = 11.3$

For reference, the two "extremes", or curves resulting from $\lambda/\kappa = 1.63$ and $\lambda/\kappa = 11.3$ are plotted in Figure 7.14, along with the "High" target SHANSEP curves. In addition, a rough compromise value $\lambda/\kappa = 5$ that results in a good extension fit is shown as well.

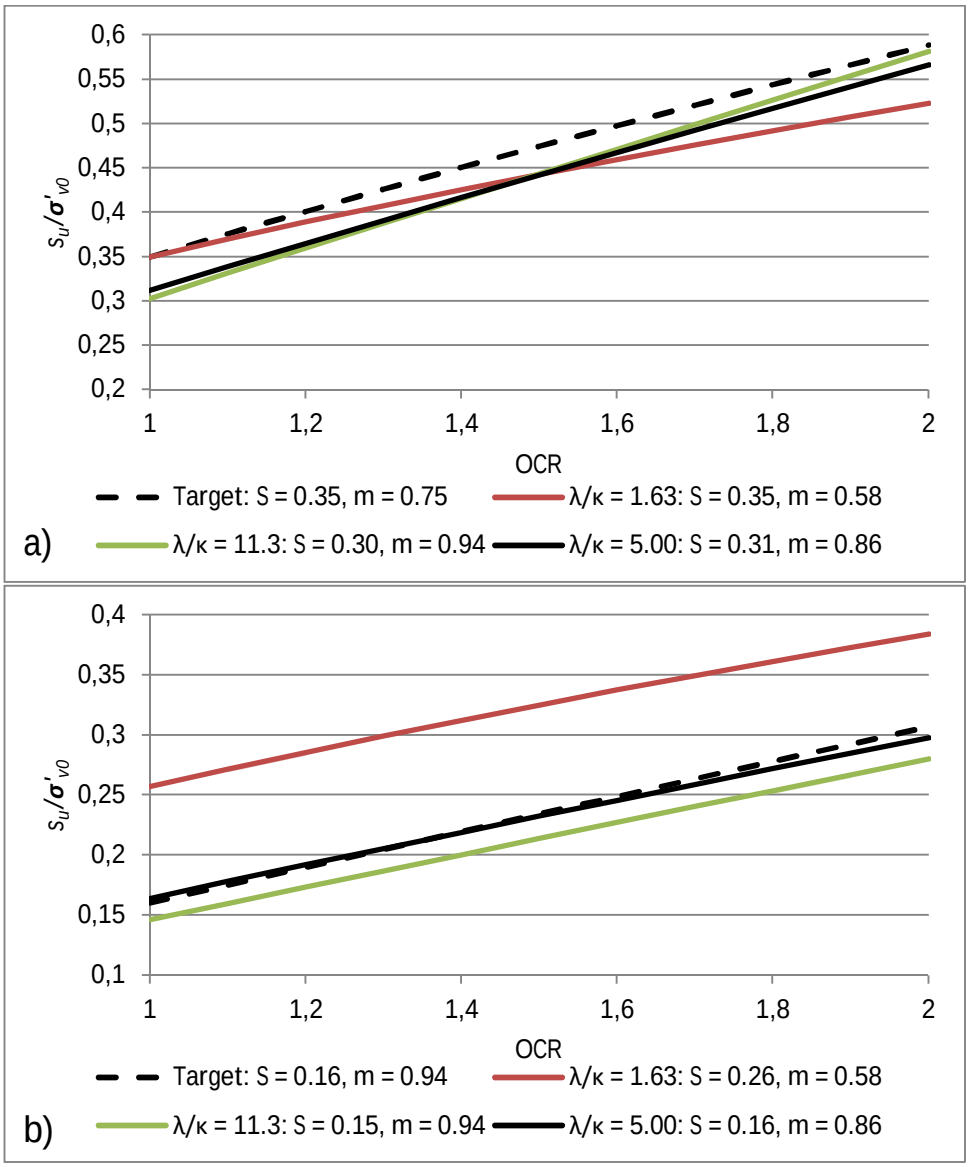

Figure 7.14. SHANSEP target values and curve fits for a) triaxial compression, and b) triaxial extension.

When the resulting compression and extension curves are examined together, it becomes apparent that the best overall fit is obtained by placing emphasis on fitting HSU for extension. If HSU is accurately fitted for compression (low λ/κ values), the extension strength becomes too large, which can be dangerous. On the other hand, fitting for extension results in slightly "too low" compression strength.

However, it needs to be remembered that the data is for peak strengths, which should not be directly used as design values due to strain softening and strain compatibility. Karlsrud & Hernandez-Martinez (2013) recommend a reduction of 10-15 % for the compression strength to account for these issues in design. In this view, the "too low" predicted compression strengths become quite beneficial.

7.3 Various Scandinavian clays

Larsson (1980) presents well-known correlations between plastic properties and normalized undrained shear strengths of some Scandinavian clays. The data (Table 7.5) shows fairly clear trends of s_u/σ'_c versus w_L or I_p for triaxial compression, simple shear and triaxial extension (Figure 7.15).

Table 7.5. Plasticity and normalized undrained shear strength data from various Scandinavian clays (Larsson 1980).

Place	w_L	I_p	Triaxial tests CAU τ_{fu}/σ_p' and τ_{CR}/σ_p', respectively: Compression	Triaxial tests CAU τ_{fu}/σ_p' and τ_{CR}/σ_p', respectively: Extension	Simple shear tests CAU τ_{fu}/σ_p'	Reference
Studenterlunden	37	20	0.32	0.09	0.19	Berre and Bjerrum (1973)
Ellingsrud	25	4	0.30	0.08	0.16	Aas (1976*a*,*b*)
Drammen plastic	60	31	0.27	0.11	0.215	Berre and Bjerrum (1973)
Drammen lean	33	10	0.26	0.06	0.17	Berre and Bjerrum (1973)
Sundland	58	28	0.31	—	0.23	Berre and Bjerrum (1973)
Vaterland	47	20	0.30	0.105	0.225	Berre and Bjerrum (1973)
Manglerud	28	9	0.29	0.13	0.18	Berre (1972)
Mastemyr	29	7	0.30	0.125	0.22	Berre (1972)
Olav Kyrres Plass	25	4.5	0.32	0.08	0.19	Karlsrud and Myrvoll (1976)
Bäckebol	80	50	0.34	0.235	0.29	Unpublished
Lilla Mellösa	85	53	0.35	0.22	0.27	Larsson (1977)
Fävren	50	26	0.33	0.21	—	Larsson (1977)
Kallebäck	85	49	0.33	0.26	0.29	Unpublished

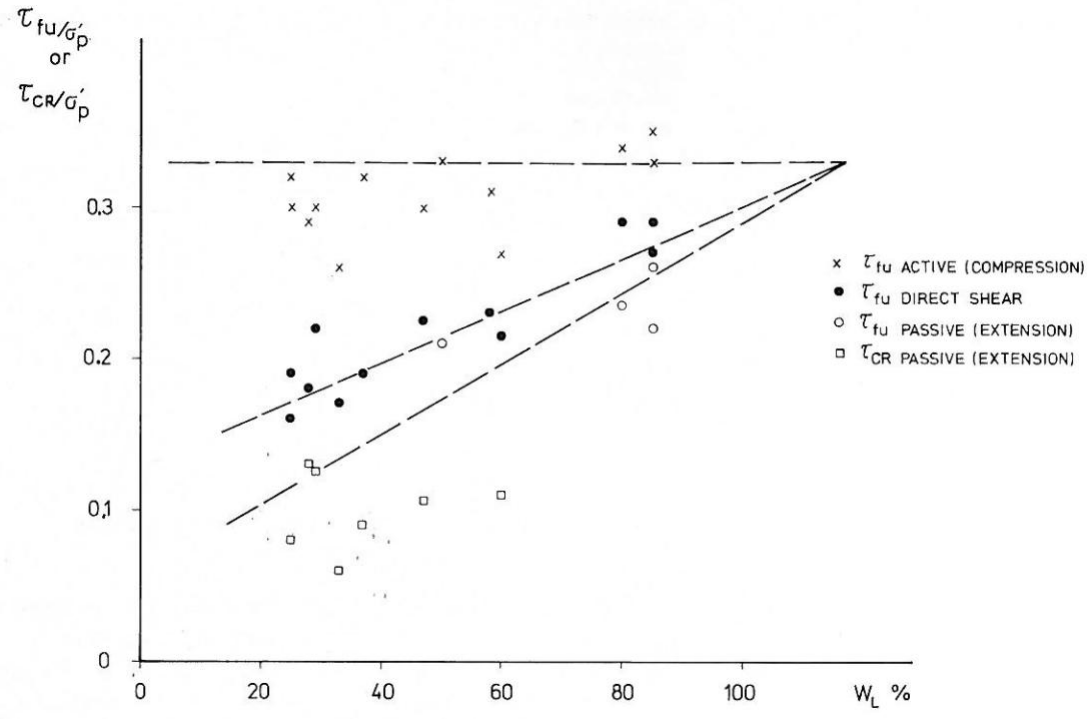

Figure 7.15. Undrained shear strength versus liquid limit (Larsson 1980)

Larsson (1980) concludes from the data that for triaxial compression, the normalized undrained shear strength is a constant s_u/σ'_c = 0.33 independent from liquid limit or

plasticity index. Simple shear and extension strengths are functions of plasticity. Larsson (1980) does not mention friction angles for his data, but the original sources mentioned by Larsson indicate friction angles of about $\varphi' = 30\ldots32°$. OCR values are not specified by Larsson (1980), but at least the results taken from Berre & Bjerrum (1973) have OCR values from 1.25 to 1.5. The fact that the data is normalized with preconsolidation pressure with no regard to OCR can be problematic, as this ratio seems not to be constant with OCR. In the SHANSEP approach for example, it can be derived that:

$$\frac{s_u}{\sigma'_{v0}} = S \cdot OCR^m \Leftrightarrow \frac{s_u}{\sigma'_c} = S \cdot OCR^{m-1} \tag{7.4}$$

Therefore the ratio s_u/σ'_c is constant with OCR only if the exponent $m = 1$. Typically this seems not to be the case (see e.g. data presented in Section 7.2).

HSU is then fitted to Larsson's (1980) data, which is taken at face value. The chosen HSU parameters are:

$\varphi' = 30.5°$ (an average of values given by Berre & Bjerrum (1973) and Larsson (1977))
OCR = 1.3 (an average of values given by Berre & Bjerrum (1973))
$C = 0.9$ or 1 (arbitrary but plausible, calculated for both cases)
$D = 1$ (base assumption)

The compression and extension values for θ and b are the basic $\theta = 0$, $b = 0$, and $\theta = 90°$, $b = 1$, respectively. For simple shear principal stress rotation is set to $\theta = 60°$, which corresponds to horizontal shearing for $\varphi' = 30°$. The intermediate principal stress parameter is set to $b = 0.3$, which is just the basic assumption used in HSU for design purposes.

The value of λ/κ is then varied to fit HSU to Larsson's (1980) data. The range of $\lambda/\kappa = 1.5\ldots5$ seems to give values that fit the given data fairly well. The results are plotted in Figure 7.16, for cases of $\lambda/\kappa = 1.5$ and $\lambda/\kappa = 5$, and for $C = 0.9$ and $C = 1.0$. The calculated strengths are superimposed on Larsson's data of s_u/σ'_c versus w_L, where w_L is chosen so that the data point for extension matches the correlation line given by Larsson (1980). It needs to be remembered that HSU does not explicitly include any measure of plasticity, but the calculated data points are simply placed so that the points "line up" with the original measured data.

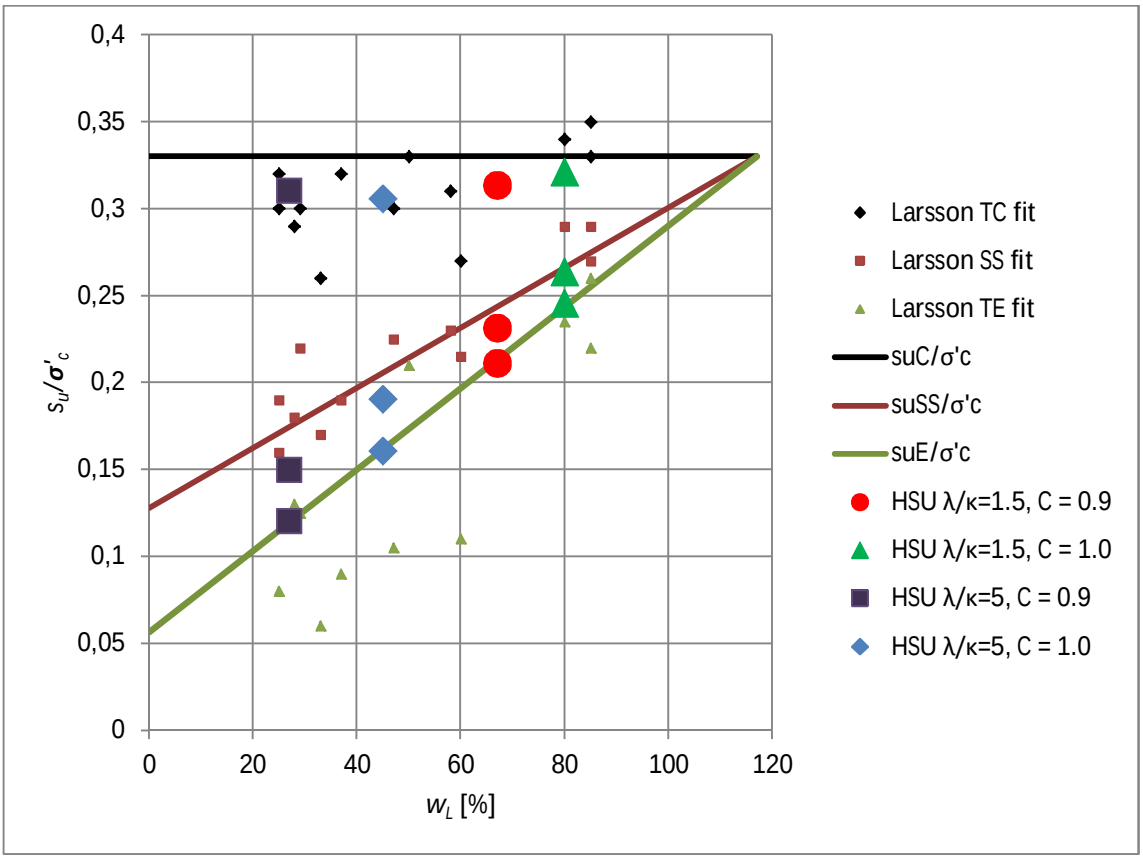

Figure 7.16. HSU results plotted with the data from Larsson (1980). Note that the HSU data points have been manually placed on a w_L ***coordinate where the strengths "line up" with Larsson's (1980) data.***

HSU can well be fitted to the data presented by Larsson (1980). While the predicted compression strengths are lower than the constant s_u/σ'_c line proposed by Larsson, the points fit very well to the measured data. The caveat here is that the yield point for compression at OCR = 1.3 is very close to the critical state line, which makes the predicted compression strength relatively immune to changes in either λ/κ or C. Changing these two parameters has an effect mostly on the extension strength, and many parameter combinations fitting the measured extension strength data can be found. That being said, the parameter combinations resulting in the shown values can be considered highly plausible.

7.4 Drammen Clay

Drammen clay deposits in Drammen, Norway have been extensively researched. The Drammen clay deposit contains several different clay layers. Typically plastic and lean clay layers are distinguished in the stratigraphy. The plastic clay layer lies at a depth of ca. 6.3…9.3 meters, while the lean clay lies at ca. 6.0…12.5 meters (Berre & Bjerrum 1973).

Table 7.6 presents some selected properties and test results of Drammen Plastic and Drammen Lean clays as reported by Berre & Bjerrum (1973).

Table 7.6. Properties of Drammen clay (Berre & Bjerrum (1973)

	w [%]	w_L [%]	w_P [%]	I_p [%]	S_t	OCR	K_{0NC}	K_0	K_0 in triax. tests	τ_{TC}/σ'_{v0}	τ_{TE}/σ'_{v0}	φ' [°]	τ_{SS}/σ'_{v0}	τ_{FV}/σ'_{v0}
Drammen (plastic)	52	60	29	31	8	1.5	0.49	0.61	0.50	0.40	0.16	31.7	0.32	0.36
Drammen (lean)	32	33	23	10	8	1.3	0.49	0.64	0.50	0.34	0.07	30.0	0.22	0.14

In Table 7.6 there are normalized undrained shear strengths from CK_0U triaxial (compression and extension), simple shear and field vane tests. The laboratory tests were consolidated to the in situ vertical effective stress σ'_{v0} to match the field conditions.

Further results (Berre & Bjerrum 1973) for the Drammen Plastic clay are presented in Fig. 7.17a (effect of strain rate in undrained compression tests) and Fig. 7.17b (stress-strain curves for triaxial compression and extension).

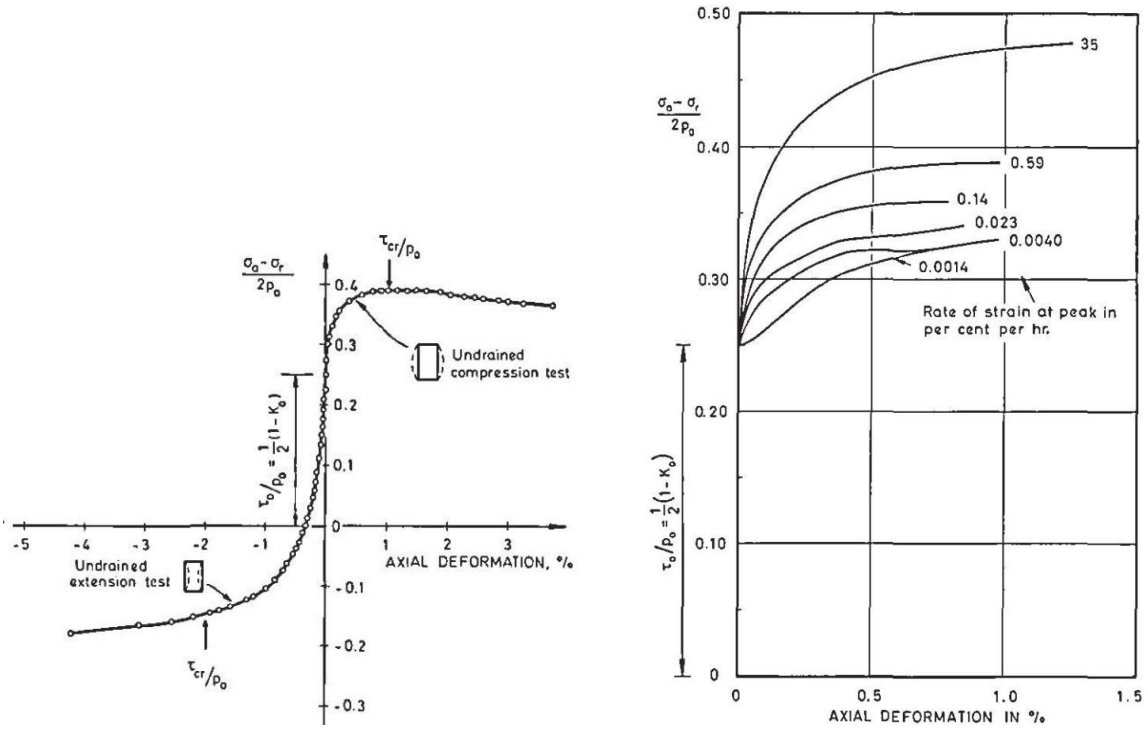

Figure 7.17. Stress-strain curves for Drammen clay (Berre & Bjerrum 1973)

HSU can in principle be fitted using the data given by Berre & Bjerrum (1973). There is however data available on the yield surface of plastic Drammen clay (Larsson 1977, data from Länsivaara 1999) that can be used to fit the model. The yield points indicate a yield surface that is somewhat smaller than what has been determined for other clays with

similar friction angles (see Fig. 7.24 in Section 7.6), especially on the extension side. The best yield surface compromise for $\varphi' = 30°$, at least for triaxial compression, seems to be $C = 1$, which results in $K_{0NC} = 0.500$. The yield stress points for the extension side are well inside the HSU yield surface. Choosing the friction angle $\varphi' = 31.7°$ that is given for plastic Drammen clay results in a HSU yield surface ($C = 1.05$, $K_{0NC} = 0.498$) with even higher discrepancies. The two yield surfaces and the yield point data are shown in Fig. 7.18.

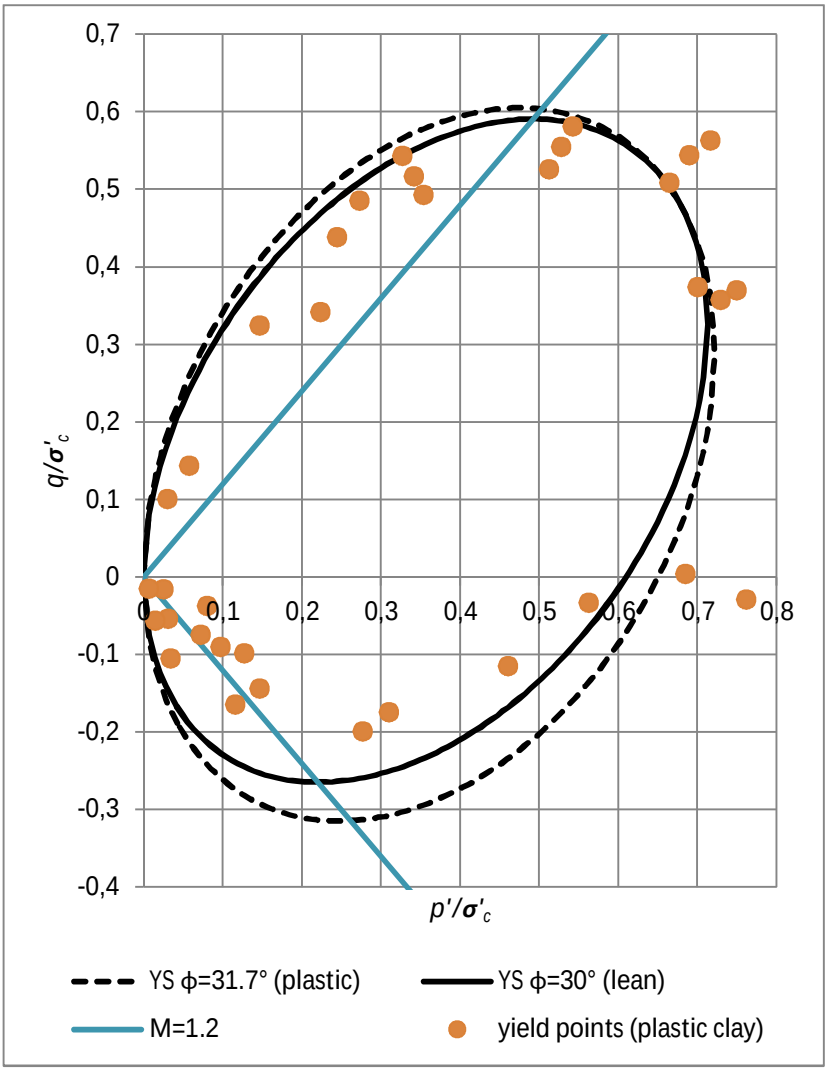

Figure 7.18. Yield points and modelled yield surfaces for Drammen clay.

Based on the yield surface fit, both Drammen clays are modelled using $\varphi' = 30°$ and $C = 1$. The D values are chosen to match the given K_0 values. The only "free" control variable is λ/κ, which is used to match the strengths given by Berre & Bjerrum (1973). Table 7.7 shows the resulting λ/κ values. The experimental shear strengths (plotted on the lines of $M = 1.2$, which corresponds to $\varphi' = 30°$), the yield surface used and the stress paths predicted by HSU are shown in Fig. 7.19.

Table 7.7. HSU results for Drammen clay.

	φ' (model)	OCR (model)	K_{0NC} (model)	K_0 (model)	C	D	λ/κ_{TC}	λ/κ_{TE}	s_{uTC}/σ'_{v0}	s_{uTE}/σ'_{v0}	s_{uTC}/σ'_c	s_{uTE}/σ'_c
Drammen (plastic)	30.0°	1.5	0.5	0.61	1.00	0.98	-1.01	-3.78	0.442	0.160	0.295	0.107
(experimental results given by Berre & Bjerrum 1973)									0.40	0.16	0.27	0.11
Drammen (lean)	30.0°	1.3	0.5	0.64	1.00	1.88	-1.42	-1.09	0.340	0.070	0.261	0.054
(experimental results given by Berre & Bjerrum 1973)									0.34	0.07	0.26	0.05

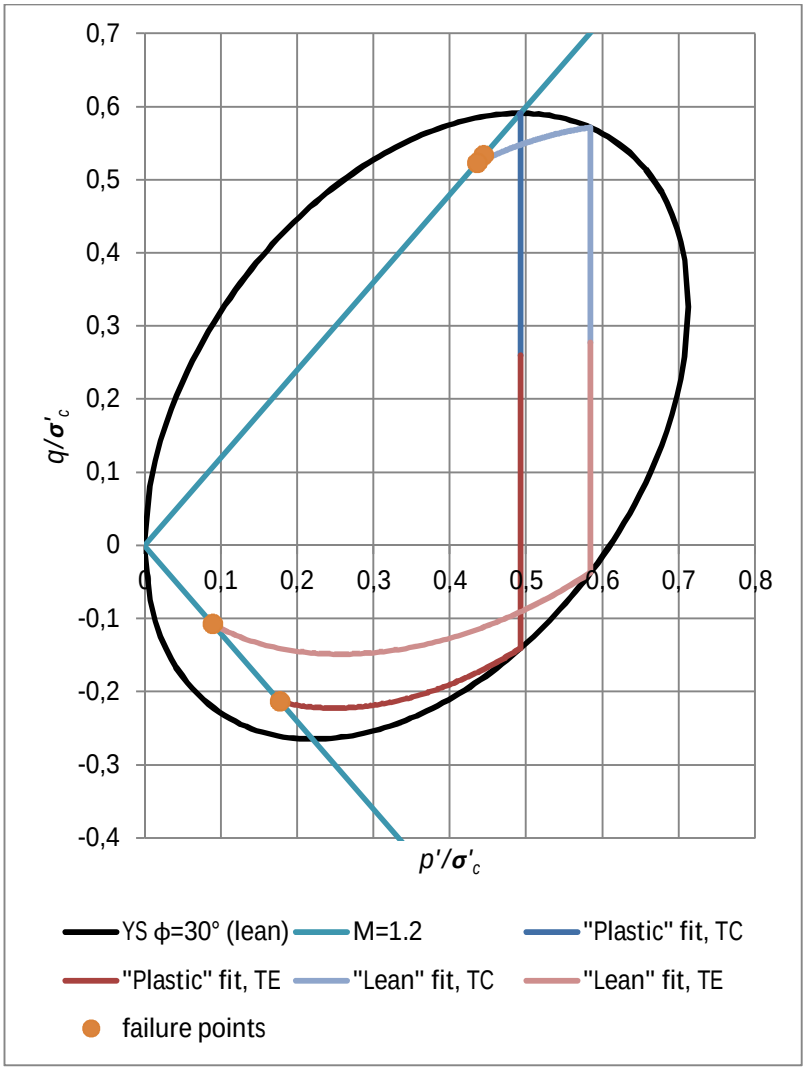

Figure 7.19. Modelled effective stress paths for Drammen clay.

It is obvious that to reach the measured strengths of Drammen plastic and lean clays, the HSU method needs to resort to "impossible" negative values of λ/κ. Model fitting is especially difficult for the plastic clay, as the in situ stress state lies very close to the boundary between the wet and dry sides of critical. This results in a very short effective stress path outside the initial yield surface, and consequently low ability to control the stress path with a choice of λ/κ. It can be noted that the compression and extension shear strengths given by Berre & Bjerrum (1973) lie on or inside the initial yield surface determined for Drammen clay (Fig. 7.18), and well inside the yield surface predicted by the HSU method (Figure 7.19). They can be also seen as low outliers in Larsson's (1980) correlation data (see Section 7.3). There is therefore some reason to doubt the reliability of these results.

7.5 Resedimented Boston Blue Clay

Sheahan et al (1996) describe a test series of 25 CK_0U tests on resedimented Boston Blue Clay (BBC) that were conducted to study undrained rate effects of the clay. A resedimented clay mass was consolidated to a vertical stress of σ'_{v0} = 100 kPa, and then rebounded to 25 kPa. The resulting soil had an average water content w = 39.9 %; liquid limit w_L = 45.4 %; and plastic limit w_P = 23.7 %. The resedimented samples were then anisotropically consolidated to high vertical stresses and then rebounded to desired OCR values, as per the SHANSEP approach.

CK_0U triaxial compression tests were performed at OCR values of 1, 2, 4 and 8; using axial strain rates of 0.05, 0.5, 5 and 50 %/h. The obtained test results are summarized in Table 7.8 (Sheahan et al 1996). Note that the *p'* and *q* values given in the table follow the MIT (Lambe) notation, and thus correspond to *s'* and *t* in Cambridge notation.

Table 7.8. Test results on resedimented Boston Blue Clay (Sheahan et al 1996)

TABLE 2. Results of CK_oUC Tests on Normally Consolidated BBC

Test no. (1)	σ'_{vc}, kPa (K_o)[a] (2)	OCR (3)	$\dot{\varepsilon}_a$[b] (%/h) (4)	At Peak Shear Stress: ε_a (%) (5)	q/σ'_{vc} (6)	p'/σ'_{vc} (7)	$\Delta u_s/\sigma'_{vc}$[c] (8)	ϕ' (9)	At Maximum Obliquity: ε_a (%) (10)	q/σ'_{vc} (11)	p'/σ'_{vc} (12)	ϕ' (13)	Comments (14)
CTX-21	284 (0.478)	1.00	0.051	0.22	0.298	0.734	0.018	23.9°	8.70	0.274	0.514	32.1°	Test stopped at ε_a = 8.8%
CTX-23	291 (0.490)	1.00	0.051	0.37	0.300	0.716	0.045	24.8°	9.87	0.277	0.503	33.4°	—
CTX-11	281 (0.472)	1.00	0.50	0.13	0.325	0.757	0.023	25.4°	10.97	0.252	0.450	34.0°	—
CTX-13	276 (0.489)	1.00	0.50	0.18	0.319	0.765	0.003	24.6°	12.18	0.247	0.455	32.9°	—
CTX-33	293 (0.518)	1.00	5.0	0.21	0.342	0.806	−0.012	25.1°	12.76	0.240	0.457	31.6°	Used base Δu measurements
CTX-17	276 (0.491)	1.05	50	0.39	0.379	0.816	−0.049	27.7°	7.84	0.315	0.564	34.0°	—[d]
CTX-18	280 (0.487)	1.05	49	0.41	0.374	0.774	−0.015	28.9°	8.17	0.298	0.547	33.1°	—[d]
CTX-52	292 (0.476)	1.00	49	0.33	0.373	0.806	−0.015	27.5°	7.71	0.295	0.559	31.8°	—

[a] Preshear K_o value.
[b] Axial strain rate based on ε_a-t linear regression.
[c] $\Delta u_s = \Delta u - \Delta\sigma_{oct} = \Delta u - 1/3(\Delta\sigma_v + 2\Delta\sigma_h)$.
[d] Some preshear unloading occurred; σ'_{vm} = 288 kPa and 280 kPa used to normalize CTX-17 and CTX-18 results, respectively.

TABLE 3. Results of CK_oUC Tests on Overconsolidated BBC

Test no. (1)	σ'_{vc}, kPa (K_o)[a] (2)	OCR (3)	$\dot{\varepsilon}_a$[b] (%/h) (4)	At Peak Shear Stress: ε_a (%) (5)	q/σ'_{vc} (6)	p'/σ'_{vc} (7)	$\Delta u_s/\sigma'_{vc}$[c] (8)	ϕ' or q/p'[d] (9)	At Maximum Obliquity: ε_a (%) (10)	q/σ'_{vc} (11)	p'/σ'_{vc} (12)	ϕ' or q/p'[d] (13)	Comments (14)
(*a*) OCR = 2													
CTX-38	298 (0.638)	1.97	0.051	0.78	0.488	1.037	−0.115	28.1°	8.69	0.420	0.788	32.2°	Base Δu used; sh. plane at ε_a = 13%
CTX-40	297 (0.635)	1.98	0.50	0.69	0.518	1.093	−0.164	28.3°	8.52	0.445	0.859	31.2°	Base Δu used; sh. plane at ε_a = 13%
CTX-42	584 (0.641)	1.99	5.0	1.16	0.539	1.116	−0.176	28.9°	NR	NR	NR	NR	Sh. ended at ε_a = 5%
CTX-41	297 (0.632)	1.97	51	0.95	0.585	1.177	−0.229	29.8°	8.83	0.495	0.948	31.5°	—
CTX-60	291 (0.635)	1.98	54	0.99	0.573	1.153	−0.203	29.8°	5.54	0.514	0.987	31.4°	—
(*b*) OCR = 4													
CTX-26	152 (0.836)	3.70	0.051	6.53	0.801	1.548	−0.389	0.517	5.79	0.796	1.485	0.536	—
CTX-35	148 (0.827)	3.95	0.051	4.68	0.851	1.651	−0.471	0.516	7.73	0.836	1.605	0.521	Sh. plane at ε_a = 13%
CTX-16	148 (1.054)	3.97	0.50	2.96	0.864	1.699	−0.370	0.508	13.30	0.782	1.479	0.529	High K_o = 1.054
CTX-29	146 (0.848)	4.02	0.50	3.17	0.843	1.638	−0.458	0.515	8.97	0.787	1.504	0.523	—
CTX-39	148 (0.845)	3.97	5.1	1.84	0.871	1.673	−0.484	0.521	0.70	0.762	1.444	0.528	—
CTX-49	147 (0.849)	4.00	5.0	3.01	0.893	1.717	−0.518	0.520	7.00	0.848	1.621	0.523	Sh. plane at ε_a = 14.8%
CTX-27	148 (0.804)	3.97	52	3.78	0.939	1.761	−0.576	0.533	0.75	0.768	1.416	0.542	—
(*c*) OCR = 8													
CTX-44	75 (1.125)	7.89	0.051	5.94	1.419	2.675	−1.110	0.530	1.52	1.196	2.213	0.541	Sh. plane at ε_a = 7.5%
CTX-47	75 (1.120)	7.92	0.51	4.23	1.425	2.603	−1.035	0.548	1.39	1.223	2.188	0.559	—
CTX-46	74 (1.091)	7.93	5.1	6.45	1.418	2.584	−1.055	0.549	1.52	1.189	2.094	0.568	—
CTX-43	76 (1.092)	7.80	51	4.75	1.563	2.980	−1.382	0.524	1.51	1.363	2.395	0.569	Sh. plane at ε_a = 14%
CTX-45	75 (1.104)	7.82	50	4.51	1.537	2.848	−1.259	0.540	1.52	1.273	2.175	0.585	—

The test results are used for comparison with the HSU method. As HSU is intended for use with NC to slightly OC clays, test results from OCR = 1 and OCR = 2 test are used to determine the model parameters.

The average large strain friction angle (at maximum principal stress ratio) was φ' = 32.4° for tests done at OCR = 1 and OCR = 2. This is directly used as the value of φ' in HSU.

According to Sheahan et al (1996), the samples were first consolidated with zero radial strains (K_0 conditions), and then unloaded so that the value of cell pressure was:

$$\sigma_h = 0.48 \cdot \sigma'_v \cdot OCR^{0.41} + u \tag{7.5}$$

HSU employs the following equation for modelling K_0:

$$K_0 = K_{0NC} \cdot OCR^{D \cdot \sin\varphi'} = C \cdot (1 - \sin\varphi') \cdot OCR^{D \cdot \sin\varphi'} \tag{5.34ter}$$

The coefficients C and D are then calculated based on the given values (based on Eqs. 5.34 and 7.5) as:

$$C = \frac{1 - \sin\varphi'}{K_{0NC}} = \frac{1 - \sin 32.4°}{0.48} = 1.035 \tag{7.6}$$

$$D = \frac{\sin 32.4°}{0.41} = 0.77 \tag{7.7}$$

As the tests were triaxial compression tests, applicable model parameter values are b = 0 and θ = 0.

By setting the values of φ', OCR, b, θ, C and D, the only unknown input variable in the model is λ/κ. Applicable λ/κ values can be back-calculated to match the results given by Sheahan et al (1996). Table 7.9 presents a summary of test results and the corresponding λ/κ value needed for HSU to match that value.

Table 7.9. λ/κ fits for resedimented BBC.

OCR	$d\varepsilon/dt$ (%/h)	s_u/σ'_{v0} (peak)	λ/κ (peak)	s_u/σ'_{v0} (max PSR)	λ/κ (max PSR)
1	0.05	0.299	-*	0.276	-*
1	0.5	0.322	7.90	0.25	-*
1	5	0.342	3.20	0.24	-*
1	50	0.374	1.69	0.297	-*
2	0.05	0.488	-*	0.42	-*
2	0.5	0.518	1.25	0.445	-*
2	5	0.539	1.62	0.495	-*
2	50	0,579	3.45	0.514	1.20
4	0.05	0.826	1.85	0.816	1.79
4	0.5	0.854	2.01	0.785	1.64
4	5	0.882	2.20	0.805	1.74
4	50	0.939	2.71	0.768	1.56
8	0.05	1.419	2.25	1.196	1.72
8	0.5	1.425	2.27	1.223	1.77
8	5	1.418	2.24	1.189	1.70
8	50	1.550	2.68	1.318	1.99

*Measured value too low to be replicated with HSU.
OCR = 1: $s_u/\sigma'_{v0,min} = 0.309$ (@ $\lambda/\kappa = 1000$)
OCR = 2: $s_u/\sigma'_{v0,min} = 0.496$ (@ $\lambda/\kappa = 1.01$)

In the presented test data, the peak strength response is quite consistent. Peak strength generally increases with increasing strain rate and OCR. The strength at maximum principal stress ratio is not quite as consistent. This can be because at large strains the principal stress ratio changes very slightly near its maximum level over a fairly large range of strains, and the exact point where the maximum PSR value is obtained can vary greatly. Therefore in this study fairly little attention is given for the large strain s_u values.

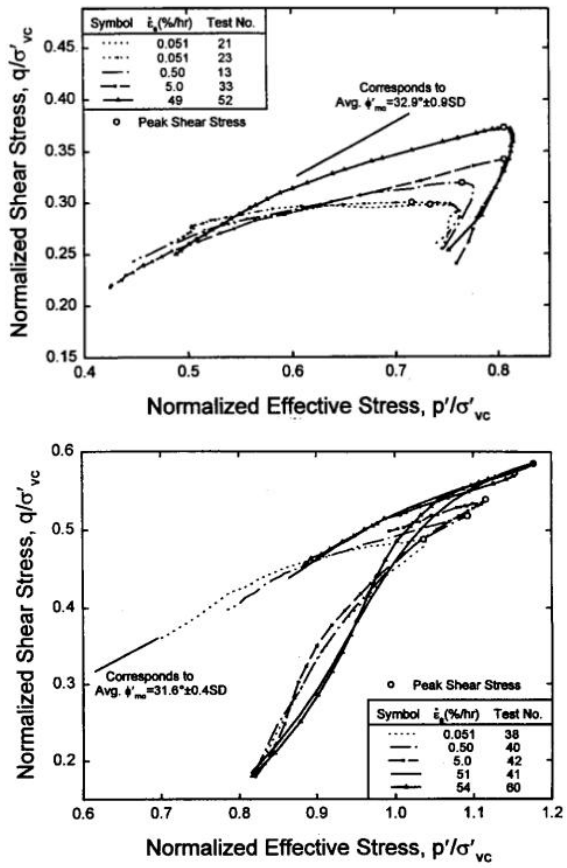

Figure 7.20. Effective stress paths for a) OCR = 1, and b) OCR = 2 (Sheahan et al 1996). Note that the stress space uses the MIT definitions for p' and q.

Figures 7.20a and 7.20b show the measured effective stress paths for OCR = 1 and OCR = 2, respectively (Sheahan et al 1996). Note that the *p'* and *q* in the Fig. 7.20 use the MIT definition.

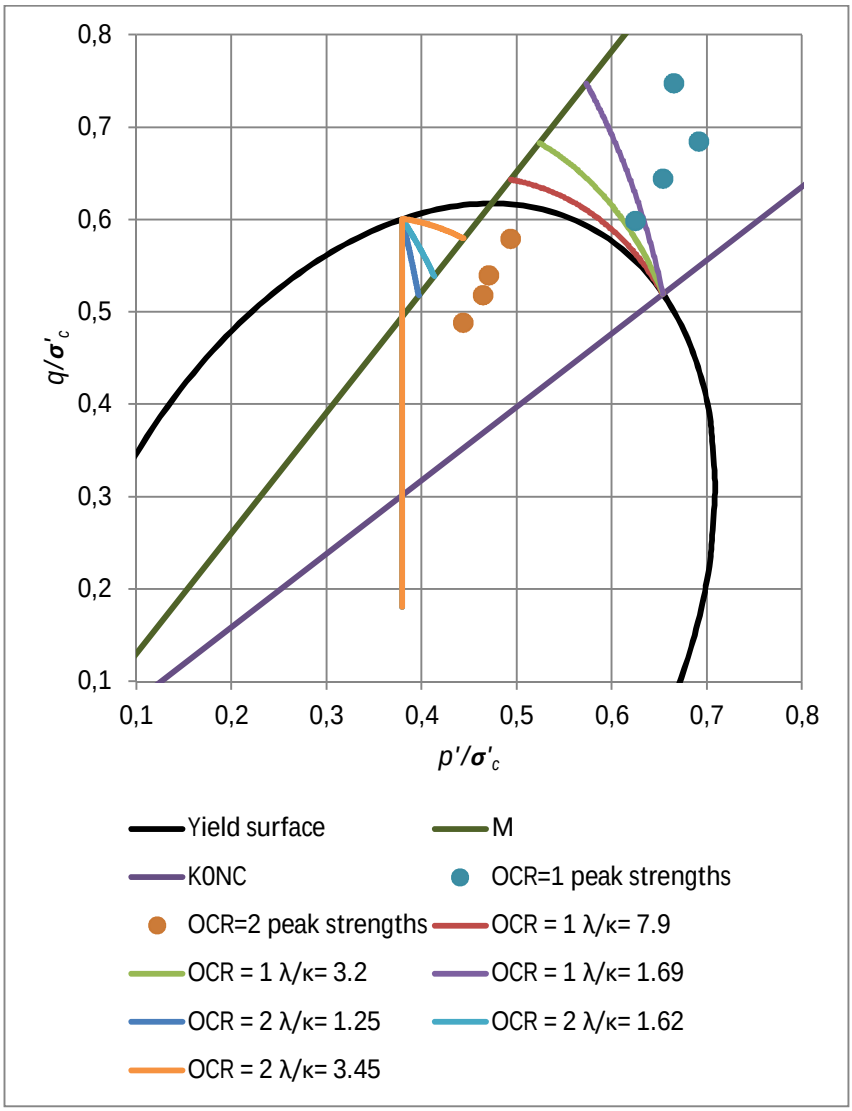

Figure 7.21. HSU effective stress paths and given points of peak strength.

Figure 7.21 shows the yield surface given by HSU, measured peak strength stress points for OCR = 1 and OCR = 2, and the effective stress paths given by HSU using the back-calculated λ/κ values. The (p',q) stress space is plotted with the Cambridge stress definition. The stress paths given by the HSU do not match those measured. This is because the model does not attempt to account for strain softening and peak states. The measured stress paths exhibit an initially elastic behaviour followed by post-peak strain softening before reaching critical state. The measured peak strengths do not therefore lie on the critical state line, whereas HSU always gives its strength value somewhere on the critical state line.

It is apparent that for slow strain rates, HSU is in some cases unable to match the measured s_u/σ'_{v0} values. In addition, the λ/κ response resulting from back-calculation is not consistent: For tests starting on the wet side (OCR = 1), faster rates of shearing result in lower λ/κ values. For higher OCR, the trend is reversed. This is due to the way volumetric hardening is implemented in HSU (and S-CLAY1), and concerns all Cam Clay model derivatives.

Sheahan et al (1996) also provide SHANSEP strength parameters for the different strain rates (Table 7.10). As all other HSU parameters are fixed, curve fitting attempts are made by varying the value of λ/κ.

Table 7.10. SHANSEP parameters based on test results (Sheahan et al 1996)

TABLE 4. SHANSEP Parameters for BBC at Different Strain Rates

Strain rate $\dot{\varepsilon}_a$ (%/h) (1)	S^a (2)	m^b (3)	r^2 (4)	Number of observations n (5)
0.05	0.298	0.757	0.9997	6
0.5	0.320	0.714	0.9993	6
5	0.340	0.689	0.9997	5
50	0.373	0.686	0.9984	8

[a] S = value of s_u/σ'_{vc} at OCR = 1, based on regression analysis.
[b] m = strength increase exponent [refer to Eq. (3)].

First, an attempt is made to fit HSU to match the given SHANSEP curves throughout the entire OCR range up to OCR = 8. Here a single λ/κ value is chosen for the entire OCR range by minimizing the residual sum of squares between the target curve and the HSU curve. Table 7.11 shows the λ/κ value which results in the best fit, and resulting SHANSEP parameters.

Table 7.11. λ/κ values for best fits to target curves (OCR = 1…8) and resulting SHANSEP parameters

$d\varepsilon/dt$ (%/h)	λ/κ	S	m
0.05	2.22	0.354	0.662
0.5	2.17	0.355	0.654
5	2.25	0.354	0.666
50	2.79	0.344	0.731

Figure 7.22 shows the target SHANSEP curves, and the HSU curves for $d\varepsilon/dt$ = 0.5 %/h and $d\varepsilon/dt$ = 50 %/h. The other two model curves are omitted for clarity; they are very close to the 0.5 %/h curve.

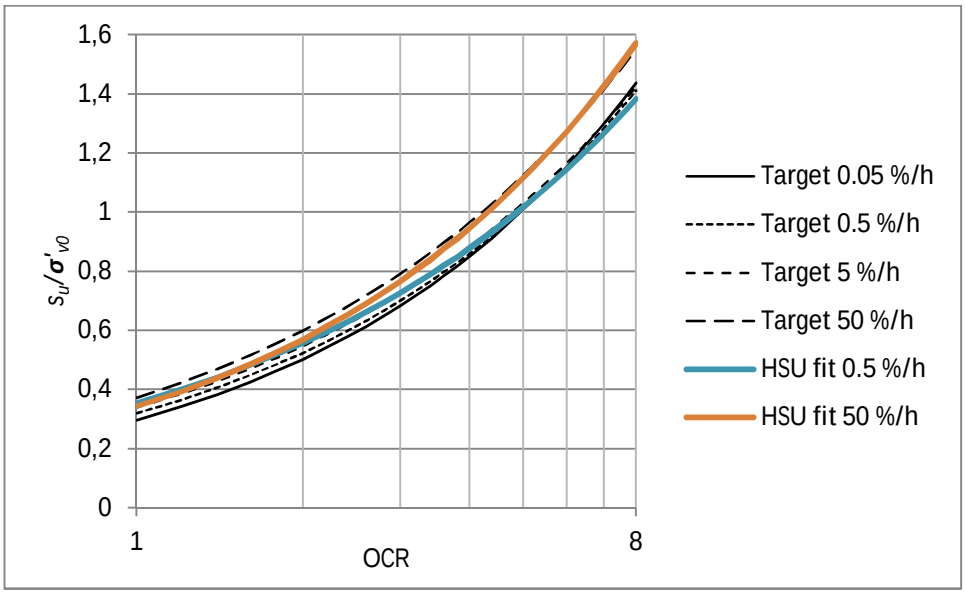

Figure 7.22. Target curves from the data (Sheahan et al 1996) and best fits from the HSU method, OCR = 1…8.

It becomes apparent that using these HSU fits, the resulting SHANSEP parameters are virtually identical, even though the target parameters vary notably with strain rate. The calculated fits between the target curves and the HSU curves are still very good when the whole range of OCR = 1…8 is examined. Especially the fit for $d\varepsilon/dt$ = 5 %/h is excellent.

However, the fit in the intended range of application for the HSU method, say OCR = 1…2, is quite poor. Therefore it is would be beneficial to fit HSU separately for this range. Fitting was again done by varying λ/κ so that the residual sum of squares for the given OCR range is minimized.

Table 7.12 shows the best fits to the given SHANSEP curves for OCR = 1…2. Figure 7.23 shows the target SHANSEP curves, and the HSU method curves for $d\varepsilon/dt$ = 0.05 %/h and $d\varepsilon/dt$ = 50 %/h. The other two model curves are omitted for clarity.

Table 7.12. λ/κ values for best fits to target curves (OCR = 1…2) and resulting SHANSEP parameters

dε/dt (%/h)	*λ/κ*	*S*	*m*
0.05	3.50	0.339	0.776
0.5	2.90	0.345	0.730
5	2.50	0.351	0.687
50	2.30	0.355	0.659

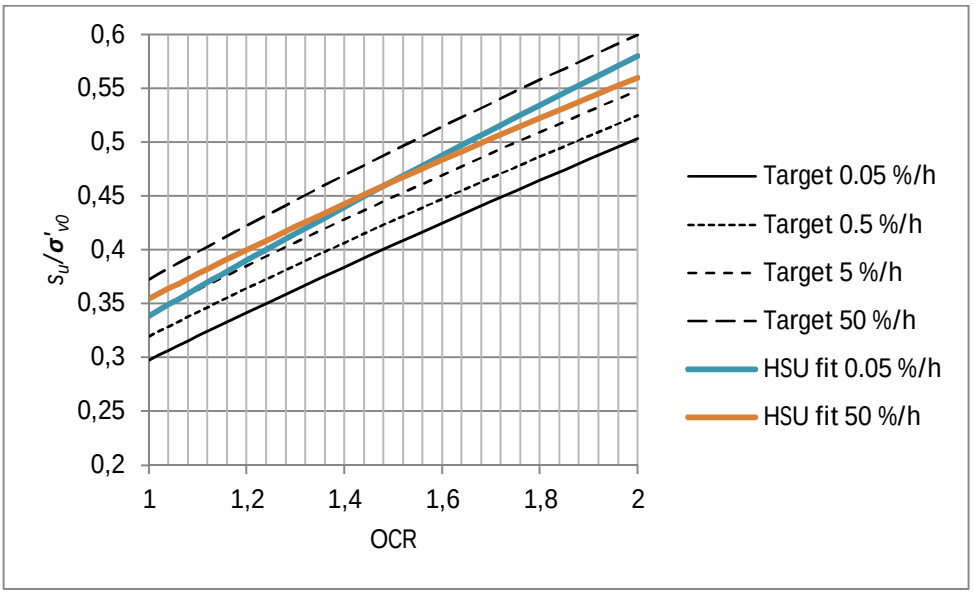

Figure 7.23. Target curves from the data (Sheahan et al 1996) and best fits from HSU, OCR = 1…2.

The fits for OCR = 1…2 are not very good except for the given SHANSEP curve for the 5 %/h tests. In this particular case it seems that HSU is not very well able to match a given SHANSEP curve based on the test data with a single set of parameters. Matching both *S* and *m* to the values given by Sheahan et al (1996) is difficult; a compromise needs to be made so that the average predicted strength over a range of OCR remains acceptable. HSU can however be used to match any single s_u value at a given OCR, provided that the measured value remains within the boundaries prescribed by the boundary values of λ/κ.

It is also good to note that the tests were done for resedimented samples that should lack all structuration effects, and do not necessarily represent a natural clay that exhibits at least some structuration. The measured peak strengths are thus probably lower than what could be expected from a corresponding undisturbed natural sample.

7.6 Yield surface fits on experimental data

Länsivaara (1999) presents data of yield points for various clays measured in triaxial tests. The data is grouped by friction angle.

The data used is collected from the following geographical locations:

φ' = 17.5°: Winnipeg (Canada)
φ' = 21-23°: Atchafalaya (USA), Perno (Finland), Turku (Finland)
φ' = 25-27°: Otaniemi (Finland), Riihimäki (Finland), Saint-Louis (Canada), Ottawa (Canada), Osaka (Japan), Turku (Finland)
φ' = 28-30°: Champlain (Canada), Bäckebol (Sweden), Drammen (Norway), Pornic (France)
φ' = 32°: Favren (Sweden), Saint-Jean-Vianney (Canada), Cubzac-les-Ponts (France)
φ' = 34-35°: Bogota (Colombia), Bothkennar (United Kingdom)

To study the general validity of the HSU (and S-CLAY1) initial yield surface assumptions, the HSU yield surfaces are drawn against the data presented by Länsivaara (1999). The HSU parameters that affect the shape of the yield surface are friction angle φ' and the K_{0NC} parameter C. The data was grouped according to friction angle as presented by Länsivaara (1999). For each group, the HSU friction angle value vas chosen from the middle of the range, if applicable. The parameter C was kept at its baseline value $C = 1$.

The comparisons are shown in Figure 7.24 (also compare to Figure 4.3 for yield surfaces produced with a different model). It is evident that while there is some scatter in the measured data (resulting e.g. from variations in strain rate), the shown HSU fits do not systematically over- or underestimate the size of the initial yield surface. The fit is generally the best for compression in the wet side of critical. Overall, it can be said that the HSU anisotropic yield surfaces match experimental data reasonably well.

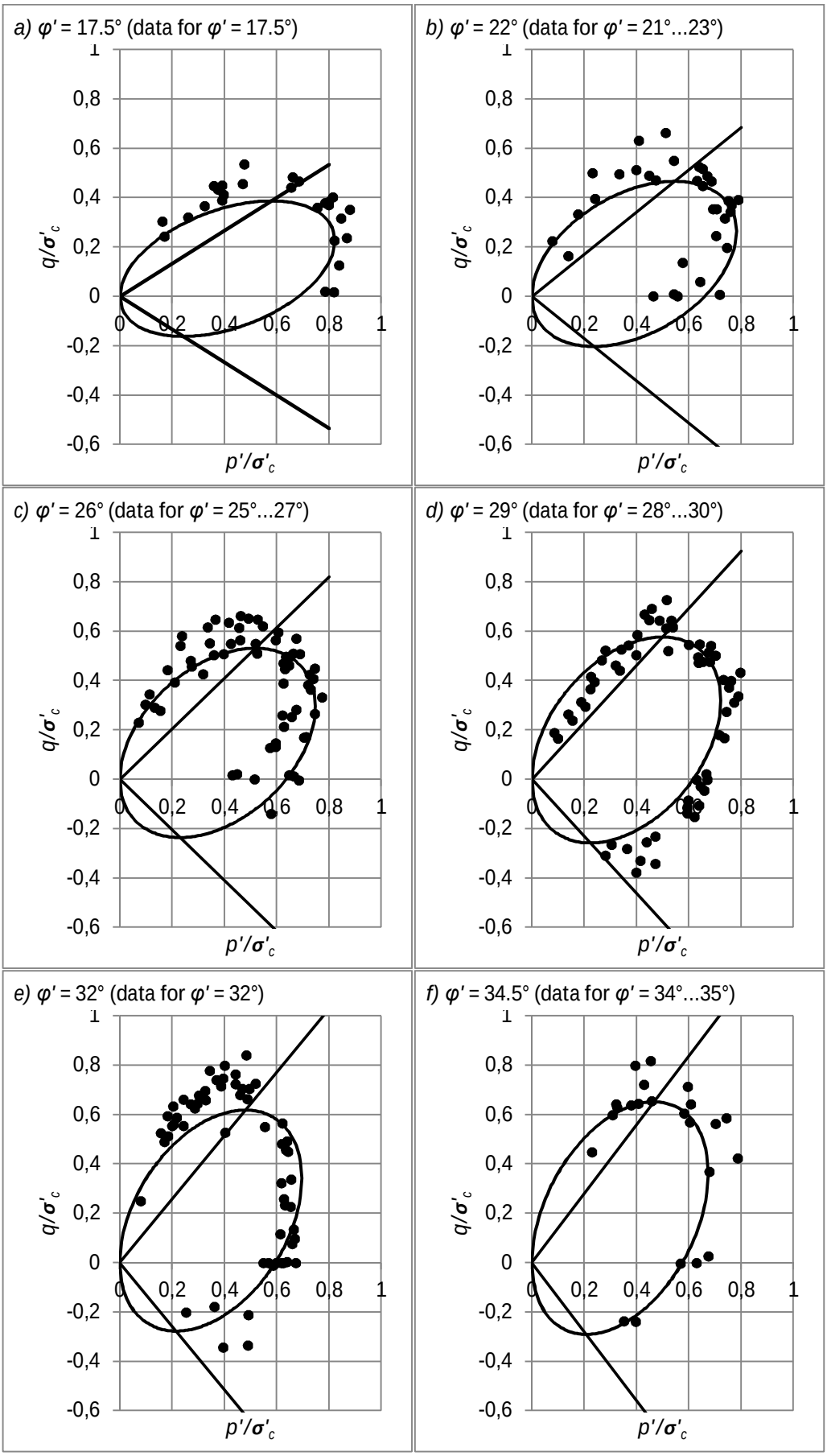

Figure 7.24. HSU yield surfaces compared with experimental data from various sites (collected data from Länsivaara 1999).

8 Calculation examples of failed embankments

8.1 Perniö failure experiment

In 2009 Tampere University of Technology and the Finnish Traffic Agency conducted an experiment where a small trial embankment in Perniö, Finland was brought to failure by rapid loading. The experiment simulated a heavy train coming to a standstill on a small embankment built on clay subsoil. The purpose of the experiment was to gather data of such a loading event, and to test the suitability of various monitoring systems.

This section discusses the experiment in the depth required for a LEM stability analysis using the HSU method. For an outline of the experiment arrangements and instrumentation see Lehtonen et al (2015). Mansikkamäki (2015) presents more detailed laboratory test data, as well as advanced finite element analyses of the experiment using anisotropic, viscoplastic, strain softening soil models.

The soil conditions at the site consisted of a ca. 1.5 m thick sandy fill layer (added some decades ago), a 0.6-0.9 m thick stiff crust, a 3.5-4.5 m thick soft sensitive clay layer, followed by varved silty clay and more coarse layers (sand, moraine). Ground water level was at a depth of ca. 1.3 m. The soil layers and some field vane results are shown in Figure 8.1. The parameters of the clay layer and a corresponding HSU fit are discussed in Section 7.1.

A small embankment (h = 0.55 m) was built on the site in place of old, disused railway tracks. On the embankment new rails on concrete sleepers were installed. Prior to constructing the embankment, roughly two months prior to the experiment, the soil surface was cut on one side of the small embankment. Additionally a 2 m deep, 7 m wide ditch was dug 13.5 m from the embankment centreline to reduce the overall stability and to direct the location of the slip surface.

The embankment was brought to failure by loading modified shipping containers (Figure 8.2) with sand during a period of 30 hours. The containers rested on steel frameworks that simulated the axle configuration of two-bogey freight cars. The frameworks themselves rested on the rail tracks. The loaded length of the embankment was 50 meters.

The test area was extensively instrumented with pore pressure transducers, total stations, inclinometers, settlement tubes and other various instruments. Special emphasis was put on measuring pore pressure close to the predicted slip surface. This was achieved by 37 strain-gauge based pore pressure transducers installed close to the center cross-section of the loaded area. Most instrument readings were automatically recorded throughout the experiment at set time intervals.

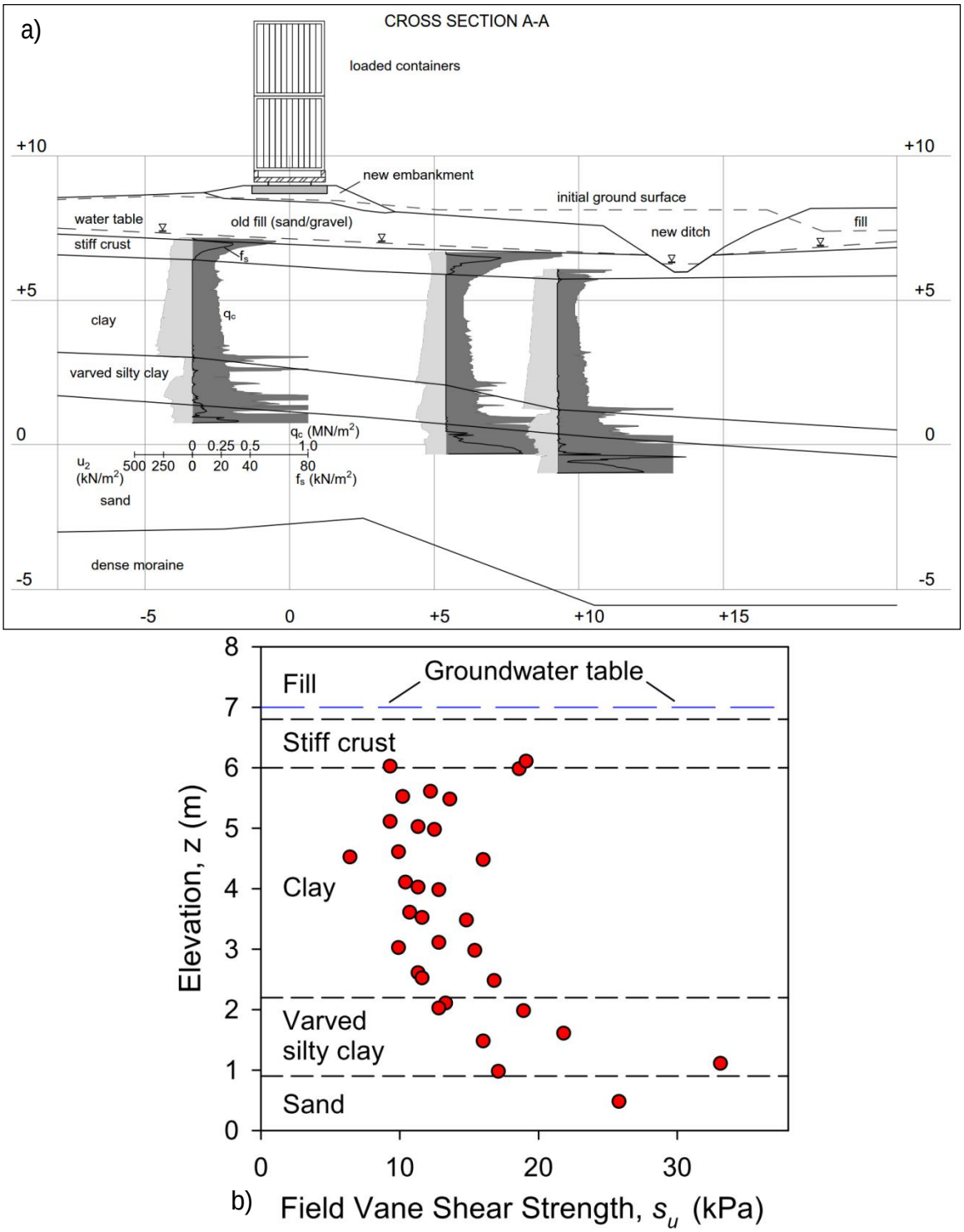

Figure 8.1. a) Soil cross-section from the center of the experiment area. b) Field vane strength along the toe of the new embankment. (Lehtonen et al 2015)

Figure 8.2. The containers before loading. (Lehtonen et al 2015)

During the first hours of loading a load equivalent to 24 kPa (load per length of track divided by the sleeper length of 2.5 m) was added in the two middle cars, and 21 kPa in the two outer cars. Loading was stopped for the night (at t = 3:20 hours from the start of loading), and continued in the following morning (t = 16:45 from the start of loading). During the second day loading was continued an average rate of 5.5 kPa/h until the containers were full at t = 28:04. At this point the center containers were loaded with 87 kPa, and the outer cars with 85 kPa equivalent loads.

The general displacement and pore pressure responses were fairly linear up to ca. t = 26:40, at which point the loading in the center cars was 83 kPa. After this point the displacements and excess pore pressure started to increase at an accelerating rate. This accelerating increase continued without interruptions until failure occurred at t = 29:57, about two hours after loading had ended.

At failure, the cars settled nearly instantaneously about 1 m before falling on their sides. Simultaneously the soil mass between the embankment and the ditch moved upwards and outwards roughly the same amount. After the failure, no further movements were observed, which indicates that the soil mass reached its new equilibrium instantaneously.

No clearly defined slip surface was detected by any means, but a more gradual “shearing band” could be distinguished based on aggregated data from inclinometers, pore pressure transducers and surface displacements. Figure 8.3 shows the likely failure mechanism.

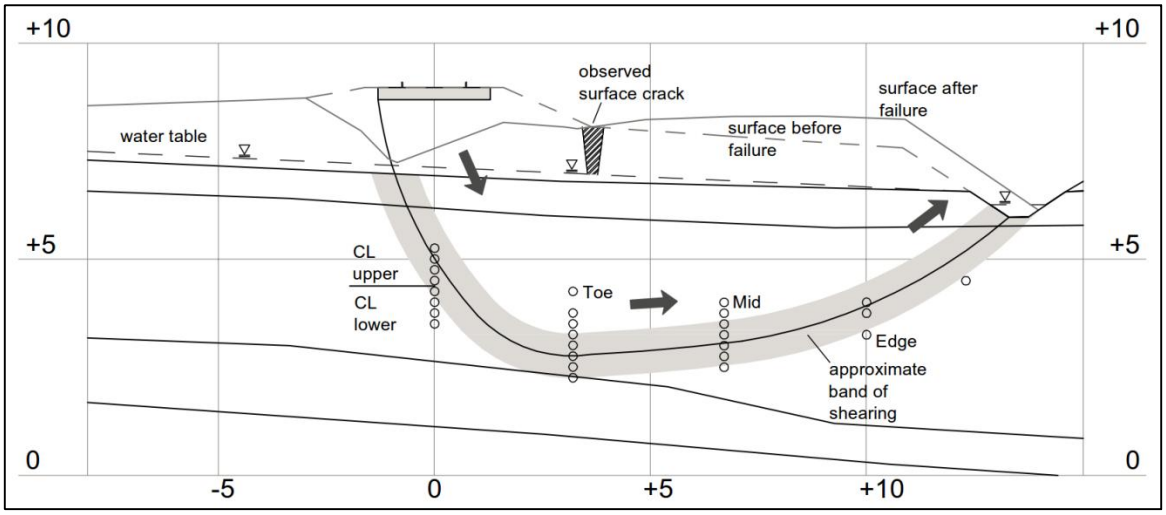

Figure 8.3. Assumed failure mechanism in the Perniö experiment. (Lehtonen et al 2015)

The most probable failure surface is not circular, but rather wedge-like with a steep active wedge, a nearly horizontal direct shear part, and a passive part close to the ditch.

The extents of the failure (Fig. 8.4) could be easily determined from the movements of surveying points installed on the soil surface. These points were surveyed before and after the experiment.

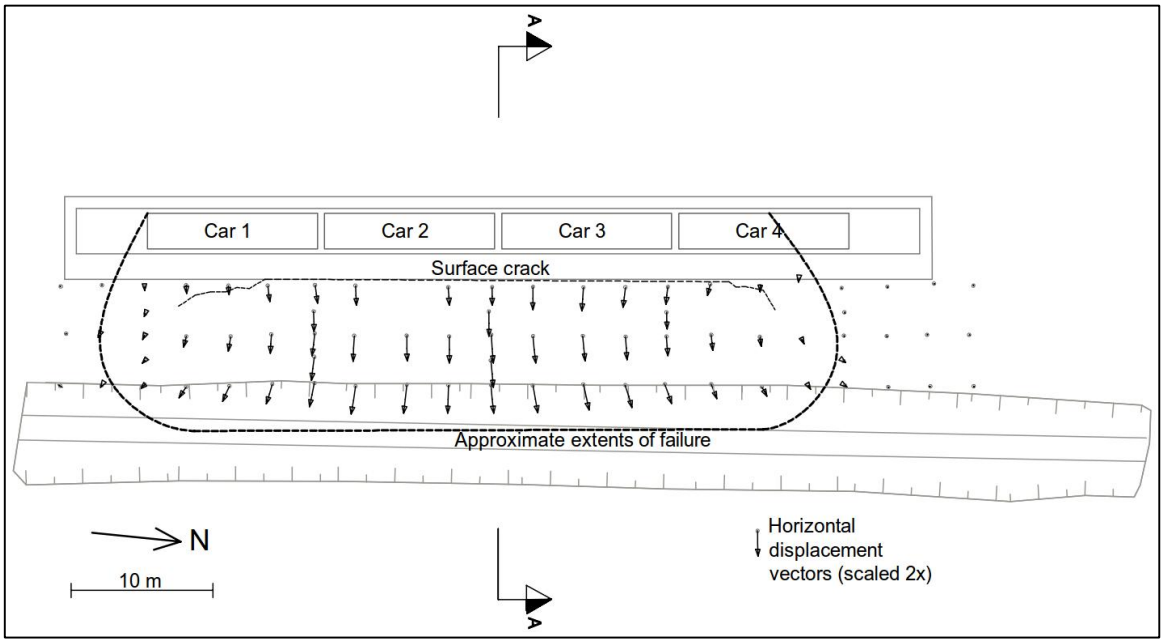

Figure 8.4. The extents of the failure. (Lehtonen et al 2015)

A factor that makes this experiment different from most other failure tests is the rate of loading. Most of pore pressure and displacement increase happened only after loading had ended and the load remained steady. The failure mechanism can thus be termed an undrained creep failure under a constant external load.

It is apparent that the failure could as well have happened at a lower external load level. According to advanced FE back-analyses conducted by Mansikkamäki (2015), the loading rate (and the time that a load is sustained for) has a significant impact on the resulting failure load magnitude. Even though the realized failure load was 87 kPa, failure might well have occurred at a load of ca. 70-75 kPa sustained over a long period. Figure 8.5

shows the failure load calculated using the elasto-viscoplastic, anisotropic, strain softening soil model EVP-SCLAY1S (Mansikkamäki 2015). The model in question is a derivative of the original S-CLAY1 model from which the HSU method is also derived.

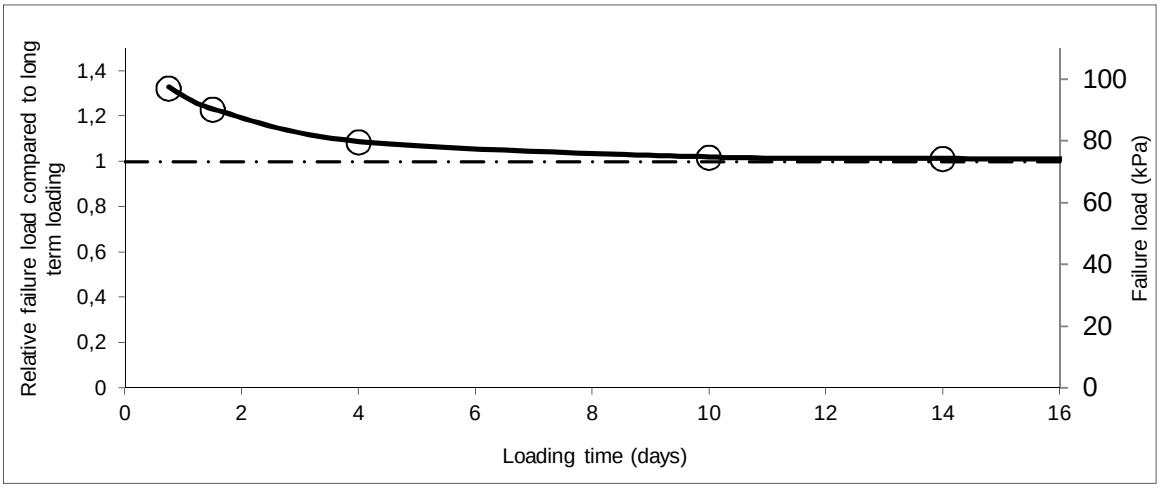

Figure 8.5. Calculated failure load of the Perniö embankment using the EVP-SCLAY1S soil model for the soft clay. (Mansikkamäki 2015).

The layers modelled for the HSU analysis are the embankment, the fill layer, crust, and the clay layer. As the failure did not reach the layer of varved silty clay, there is no need to model it in LEM context. The clay layer is modelled with the HSU method, while the crust is modelled with a given s_u profile. The embankment and fill layers are considered drained, frictional materials.

The friction angle and unit weight of the embankment and fill have been approximated from nuclear density gauge tests done from the finished embankment structure and fill surface, as well as numerous back-calculations and stability analyses conducted since. The strength and unit weight of the crust is based on laboratory testing and vane shear tests.

The OCR values vary with depth in the clay layer. The OCR profile used in the analysis is based on fitting the calculated preconsolidation stress for each slice bottom (which is the product of calculated effective vertical stress and OCR) with the available oedometer test data.

Table 8.1. Soil parameters for Perniö.

	φ' [°]	s_u [kPa]	ds_u [kPa/m]	γ [kN/m3]	γ_{sat} [kN/m3]	OCR	C	D	
Embankment	40	0	0	18	21	-	-	-	
Sand fill	38	0	0	15	19	-	-	-	
Crust	0	35	0	-	17	-	-	-	
Sensitive clay	28	0	0	-	15	*	0.97	1	
*) Set for each slice so that σ'_c matches measured values.									

Based on studies presented in Section 7.1, the HSU parameters φ', C and D for Perniö clay are:

φ' = 27.8°
C = 0.97
D = 1 (basic assumption).

While the laboratory tests (Section 7.1) consistently indicate some cohesion (c' = 3.4 kPa), it remains debatable if this apparent cohesion can be considered "real". It may for example be a testing artefact related to pore pressure measurements, or perhaps the stress-strain states at the final stages of the tests were still too far from a "true", non-cohesive critical state. At this point no strong opinions are adopted either way and the calculations are thus presented with both assumptions of c' = 0, and c' = 3.4 kPa.

The current application of the HSU method requires a predetermined failure surface (i.e. it is not possible to search for the most critical failure surface). The failure surface was determined so that it roughly matches the estimated failure surface in the experiment (Figure 8.3). Limit equilibrium convergence was checked by applying the chosen failure surface in the software GeoCalc and conducting a total stress analysis with Spencer's method, with a rough anisotropic s_u profile. The chosen slip surface and the slice geometry are shown in Figure 8.6.

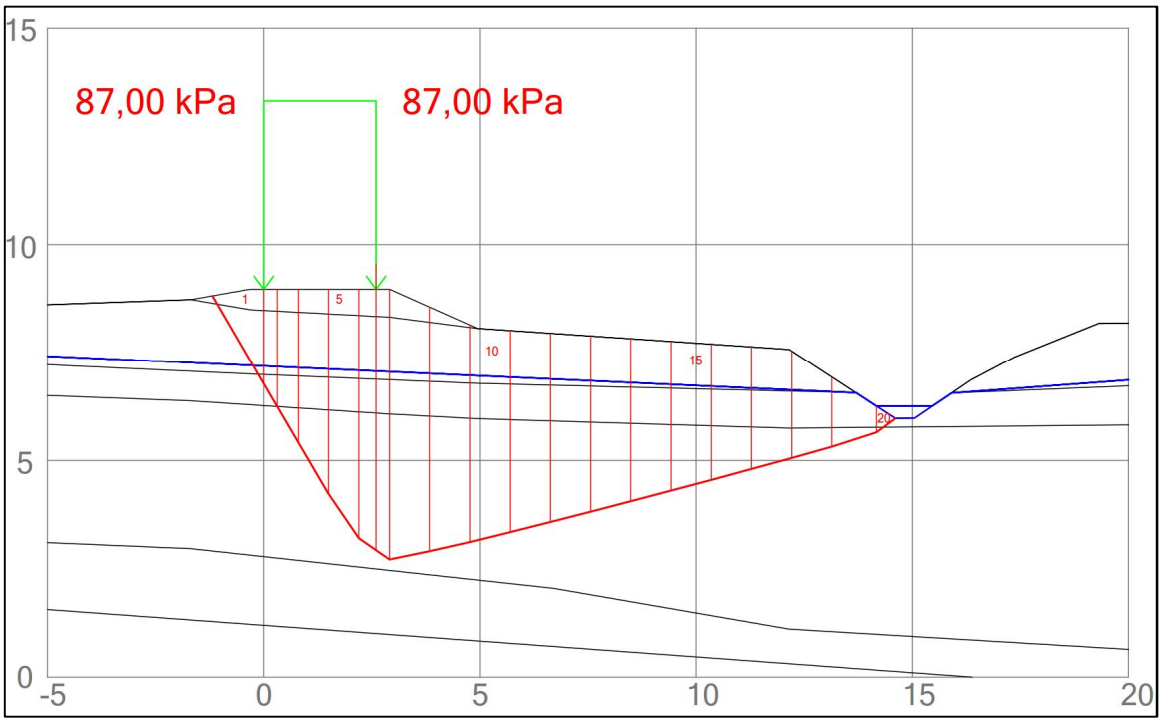

Figure 8.6. The slip surface and slices used in the analysis.

The initial effective vertical stress is calculated directly as the geostatic stress resulting from the calculation geometry. The initial effective stress state is assumed to correspond to the situation after cutting the top soil and excavating the ditch, but before applying the small embankment. Therefore when calculating the initial effective stress state, the embankment is considered weightless.

The OCR values for the slice bottoms were obtained by "hand-matching" the calculated σ'_c values to lab results taken from a corresponding elevation and distance from the embankment. For this purpose, the oedometer results were divided into two groups, "Toe" and "Ditch" according to their sampling location in relation to the cross-section geometry. Roughly half of the samples were taken close to from the toe of the new embankment (before building the said embankment) and half from the edge of the ditch. The slices were divided correspondingly so that slices 4…9 belong to the "Toe" group and slices 10…19 belong to the "Ditch" group. The group division is slightly arbitrary, as the line could be drawn a bit closer to or farther from the ditch, but the overall difference from a slightly different choice would be small. The hand-matched σ'_c values for the slices and the measured values are shown in Figure 8.7. The resulting OCR, σ'_{v0} and σ'_c values that were used as input in the calculations are shown in Table 8.2.

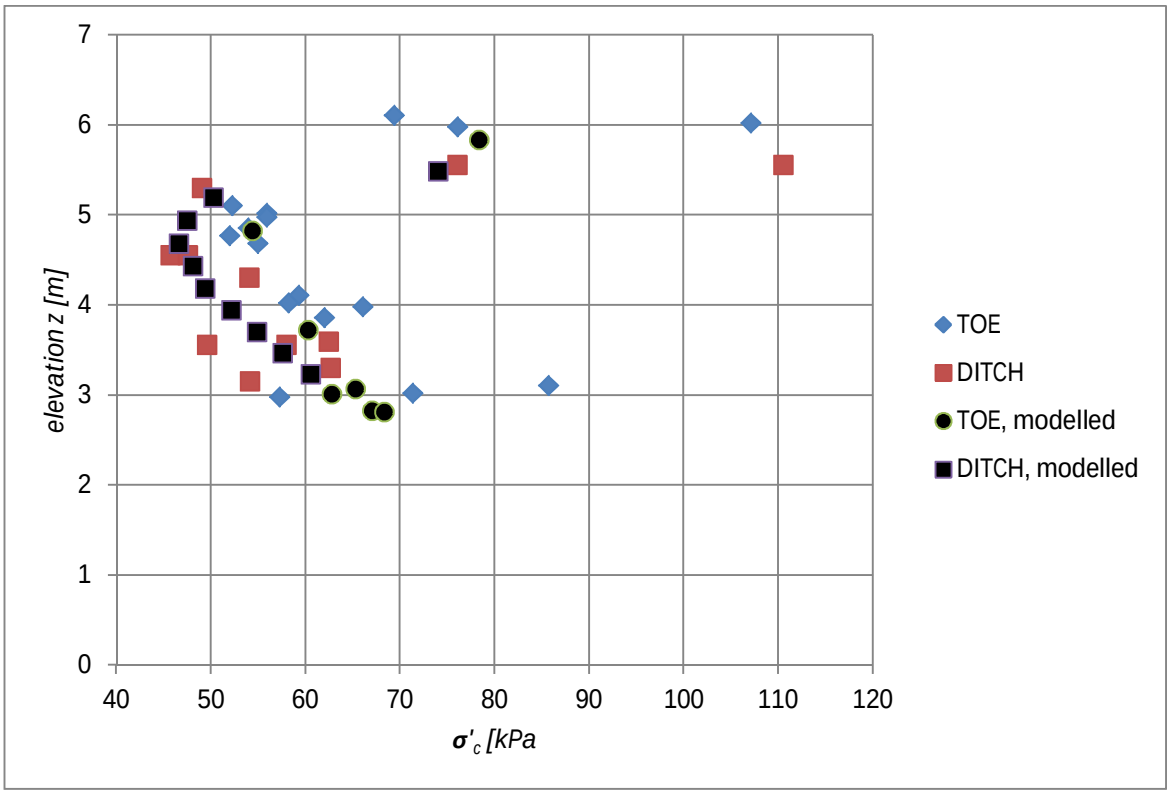

Figure 8.7. Measured and modelled preconsolidation pressure values.

Table 8.2. Consolidation state applied in the analysis.

Slice	Slice bottom layer(s)	x [m]	σ'_{v0} [kPa]	OCR	σ'_c [kPa]
1	Emb/sand/crust	-0.40	12.5	1	12.5
2	Crust	0.16	25.8	1	25.8
3	Clay	0.56	29.8	2.7	80.5
4	Clay	1.15	35.3	1.55	54.7
5	Clay	1.85	39.7	1.6	63.6
6	Clay	2.40	43.3	1.6	69.3
7	Clay	2.76	44.4	1.6	71.1
8	Clay	3.38	43.6	1.6	69.7
9	Clay	4.31	41.2	1.65	67.9
10	Clay	5.24	39.0	1.55	60.5
11	Clay	6.17	37.2	1.55	57.6
12	Clay	7.10	35.4	1.55	54.9
13	Clay	8.03	33.7	1.55	52.2
14	Clay	8.96	31.9	1.55	49.4
15	Clay	9.89	30.1	1.6	48.1
16	Clay	10.82	28.3	1.65	46.6
17	Clay	11.75	26.4	1.8	47.5
18	Clay	12.68	19.4	2.6	50.3
19	Clay	13.66	9.3	8	74.1
20	Crust	14.32	0.7	1	0.7

Unfortunately, in this case there were bad convergence problems with HSU effective stress analyses using Spencer's method (or any other variant of Morgenstern-Price, or GLE, for that matter). TSA calculations using Spencer's method however converged well. The convergence issues in ESA may be due to the fairly complex slip surface and soil layer geometry. Therefore, the following calculations have been done using Janbu's Simplified method (formulation given in Abramson et al 2002), which converges reliably both in TSA and ESA. The given results include the correction factor f_0 used with Janbu's Simplified method. For the chosen slip surface, f_0 = 1.12, which means that F_{corr} = 1 when F = 1/1.12 = 0.893. In other words, a calculated, uncorrected factor of safety F = 0.893 should correspond to a "true", corrected factor of safety F_{corr} = 1.

When effective stress calculations are conducted by forcing the Δu value so that the same s_u value as in TSA is obtained, the ESA and TSA results are inherently similar and mutually redundant. Instead, the ESA results presented in the following tables use Δu calculated from vertical stresses (Approach B, see Section 5.8.3). The stress changes are calculated from the state before adding the small embankment. Additionally, the excess pore pressure distributions with the two methods are later compared for selected calculations.

The first analyses are done with two load levels, q_{app} = 87 kPa and q_{app} = 80 kPa. The embankment failed at 87 kPa, but it is very likely that given enough time, it could have just as well have failed at 80 kPa or below due to undrained creep. If λ/κ is used as an adjustment parameter to account for time/rate effects, HSU should be able to reproduce at least these two failure loads at plausible λ/κ levels.

Table 8.3 shows the calculated factors of safety at 80 and 87 kPa loads, with c' = 0 and c' = 3.4 kPa. Note that the given Janbu's Simplified Method F values include the correction factor.

Table 8.3.Stability calculation results with HSU, using Janbu's Simplified method

q_{app} = 80 kPa c' = 0	λ/κ = 1000	λ/κ = 5	λ/κ = 3	λ/κ = 1.5	λ/κ = 1.01
F (TSA)	0.72	0.77	0.80	0.86	0.93
F (ESA)	0.60	0.62	0.63	0.68	0.74
difference	-16.8 %	-19.7 %	-20.5 %	-20.8 %	-20.4 %

q_{app} = 87 kPa c' = 0	λ/κ = 1000	λ/κ = 5	λ/κ = 3	λ/κ = 1.5	λ/κ = 1.01
F (TSA)	0.67	0.72	0.75	0.81	0.87
F (ESA)	0.56	0.58	0.59	0.64	0.69
difference	-16.7 %	-19.8 %	-20.7 %	-21.0 %	-20.7 %

q_{app} = 80 kPa c' = 3.4 kPa	λ/κ = 1000	λ/κ = 5	λ/κ = 3	λ/κ = 1.5	λ/κ = 1.01
F (TSA)	0.84	0.89	0.93	1.02	1.13
F (ESA)	0.66	0.70	0.72	0.80	0.88
difference	-20.7 %	-22.2 %	-22.4 %	-22.1 %	-21.6 %

q_{app} = 87 kPa c' = 3.4 kPa	λ/κ = 1000	λ/κ = 5	λ/κ = 3	λ/κ = 1.5	λ/κ = 1.01
F (TSA)	0.78	0.84	0.87	0.96	1.06
F (ESA)	0.62	0.65	0.67	0.74	0.83
difference	-20.7 %	-22.5 %	-22.8 %	-22.5 %	-21.9 %

From the results the following is evident:

- If c' = 0 is assumed, HSU is unable to give correct failure loads with any plausible values of λ/κ. It is evident that the predicted strengths are too low (all possible factors of safety are below 1).
- The method of predicting excess pore pressure from vertical stress changes results in too high Δu values, and consequently too low factors of safety.

However, total stress analyses (and effective stress analyses with forced Δu) with c' = 3.4 kPa give good results. Both failure load levels are obtainable with very plausible λ/κ values. **In subsequent analyses the assumption of *c'* = 3.4 kPa is used.**

It is useful to further study the link between calculated failure load and λ/κ. Table 8.4 and Figure 8.8 show calculated failure loads at different λ/κ values.

Table 8.4. λ/κ needed to reach failure at different load levels. Total stress analysis with c' = 3.4 kPa used.

c' = 3.4 kPa	q_{app} = 65 kPa	q_{app} = 70 kPa	q_{app} = 75 kPa	q_{app} = 80 kPa	q_{app} = 85 kPa	q_{app} = 87 kPa	q_{app} = 90 kPa
λ/κ (TSA)	22.1	4.10	2.33	1.67	1.33	1.24	1.13

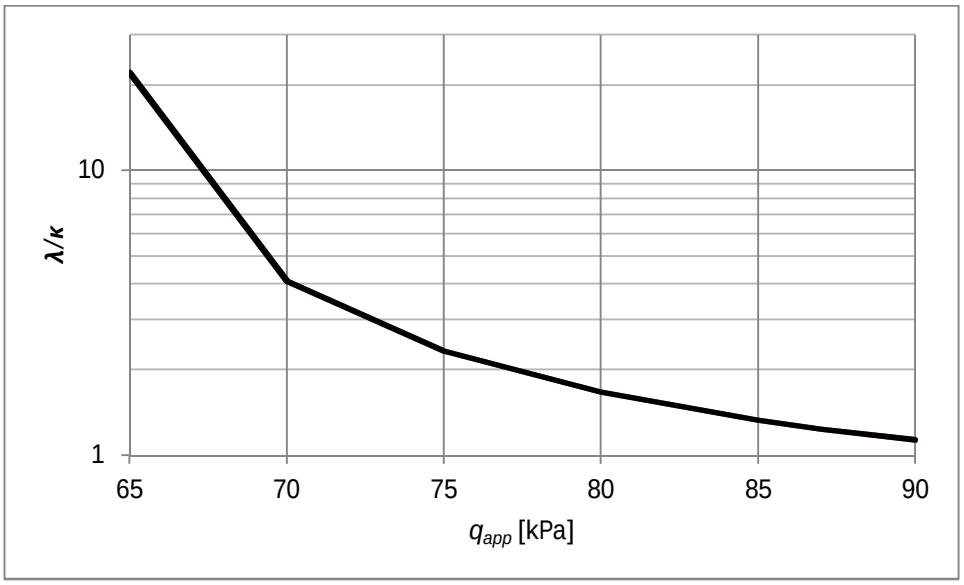

Figure 8.8. λ/κ needed to reach failure at different load levels. Total stress analysis with c' = 3.4 kPa used.

Table 8.5 presents the calculated failure load at different failure loads for total stress analyses with *c'* = 3.4 kPa.

Table 8.5. Failure load q_f at different λ/κ values. Total stress analysis with c' = 3.4 kPa used.

c' = 3.4 kPa	*λ/κ* = 1000	*λ/κ* = 10	*λ/κ* = 5	*λ/κ* = 3	*λ/κ* = 2	*λ/κ* = 1.5	*λ/κ* = 1.2	*λ/κ* = 1.01
q_f [kPa]	63.9	66.4	68.9	72.3	77.0	82.2	88.1	94.4

It is noteworthy that the range of failure loads available by varying *λ/κ* (range *λ/κ* ≈ 10…1.01) compares very well with model results obtained by Mansikkamäki (2015) where loading time was varied (Fig. 8.5). In this case, the largest *λ/κ* values correspond to failure loads that could have caused failure if sustained over a very long period (while still remaining undrained – at some point primary consolidation will begin at a significant enough scale). Smaller *λ/κ* values then correspond to failure loads that are applied very quickly. This suggests that *λ/κ* can indeed be used to model rate effects on undrained shear strength.

Figure 8.9 shows the calculated TSA shear stress distributions at failure for q_{app} = 87 kPa, *λ/κ* = 1.24; and q_{app} = 75 kPa, *λ/κ* = 2.33. The difference in predicted shear strength is most evident in the direct shear/extension part of the slip surface, where changing *λ/κ* has the largest effect (see Section 6.3). In the compression part (ca. *x* = 1…3) the effective stress path from yielding to failure is quite short, so the strength there is almost immune to changes in *λ/κ*.

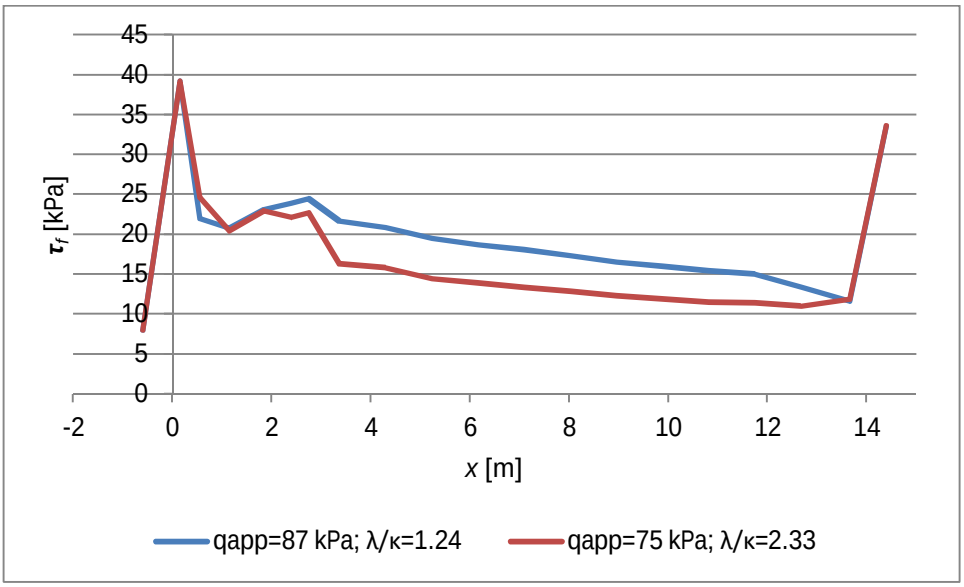

Figure 8.9. Mobilized shear stress at failure for total stress analyses at different load levels.

Pore pressure calculations in effective stress analyses seem slightly problematic. Figure 8.10 shows the distributions of forced excess pore pressure (giving the same factor of safety as TSA) and excess pore pressure calculated from vertical stress changes (Approach B). The calculations are done at q_{app} = 87 kPa, λ/κ = 1.24; and q_{app} = 75 kPa, λ/κ = 2.33, both corresponding to failure at the respective load levels.

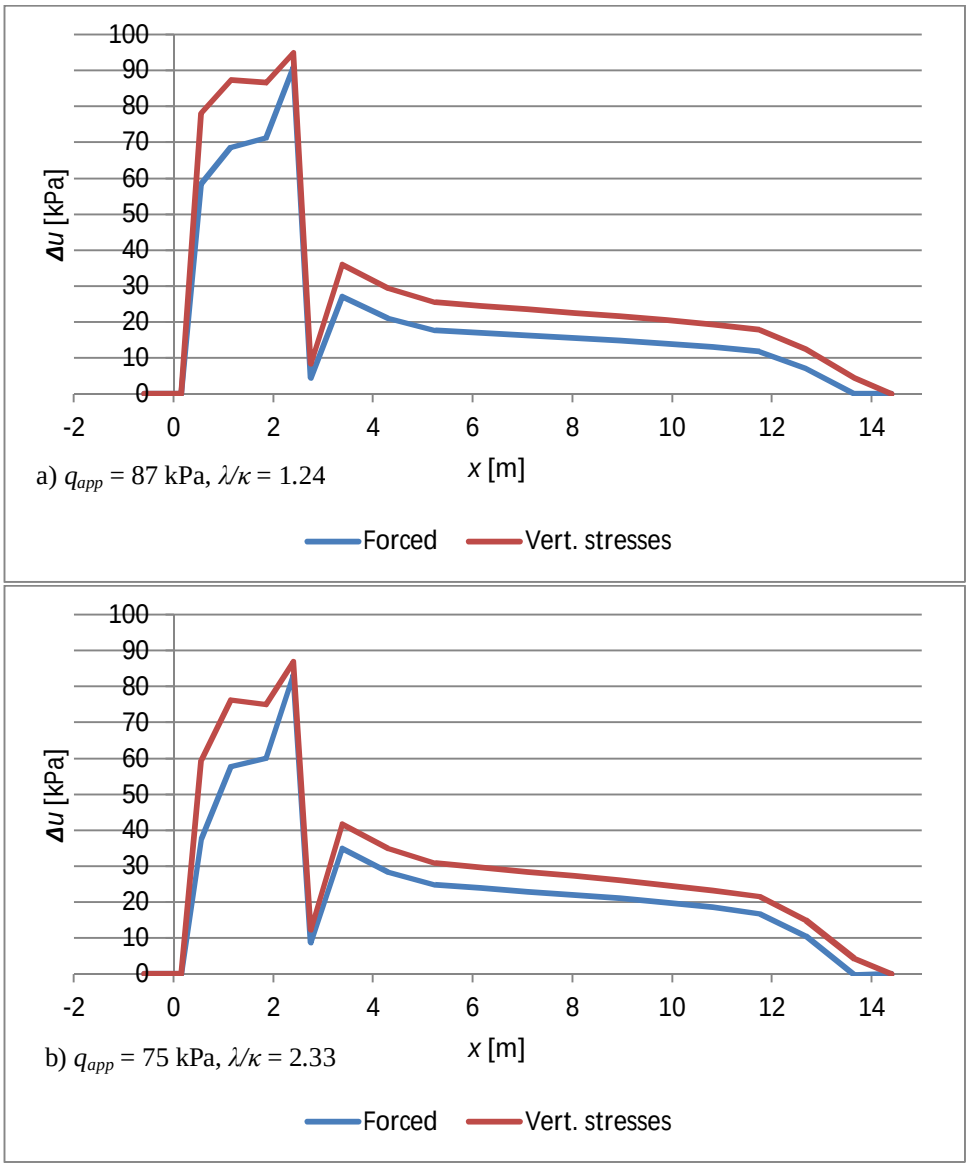

Figure 8.10.Excess pore pressure along the slip surface calculated by forcing to s_u, and based on vertical stresses.

The excess pore pressure calculated based on vertical stress changes is notably higher than the "forced" pore pressure, resulting in much lower factors of safety. In the case of the Perniö failure experiment, it can be said that the proposed method (Approach B) of calculating Δu is too conservative. On the other hand, the "forced" Δu will always give the undrained shear strength that is considered correct by the HSU method, but its use is completely redundant as a total stress analysis with the same s_u is considerably simpler and more reliable in terms of convergence.

For comparison, Figure 8.11 shows measured excess pore pressure from the center cross-section of the experiment area right before failure. It is evident that right under the load, the modelled excess pore pressure is somewhat higher than measured, due to the way external loading is handled by LEM (without any realistic distribution of loads in the soil). On the other hand, the modelled Δu levels are quite well within the correct range of ca. 10-40 kPa, depending on the lateral position.

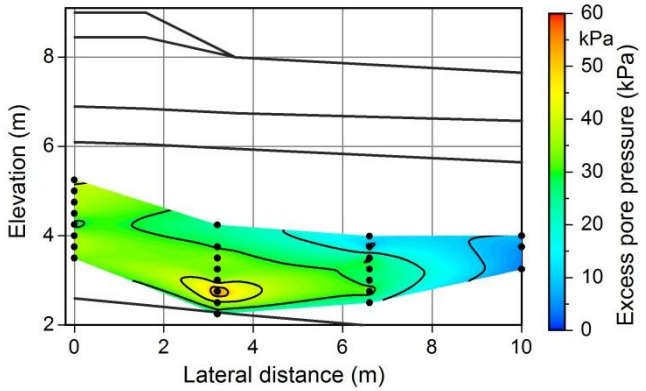

Figure 8.11. Measured excess pore pressure profile at failure. The loaded embankment is located on the top left. Pore pressure transducers are shown as black dots.

Overall, the HSU method gives very good results in total stress analyses of the Perniö failure experiment. Even the undrained creep effects associated with fast loading can be rudimentarily taken into account with proper selection of the λ/κ value. The range of failure loads available by varying λ/κ is well in line with analysis results using advanced elastoviscoplastic soil models (Mansikkamäki 2015). While the total stress analysis results are good, there are some issues with calculating Δu for undrained effective stress analyses.

8.2 Saint Alban Test Fill **A**

An embankment in Saint-Alban, Quebec, Canada was brought to failure as a part of a testing program conducted by Laval University in 1972. An embankment built on sensitive Champlain Sea clay failed after being raised to a height of 3.9 m above the ground surface. The embankment and failure geometries are shown in Figure 8.12.

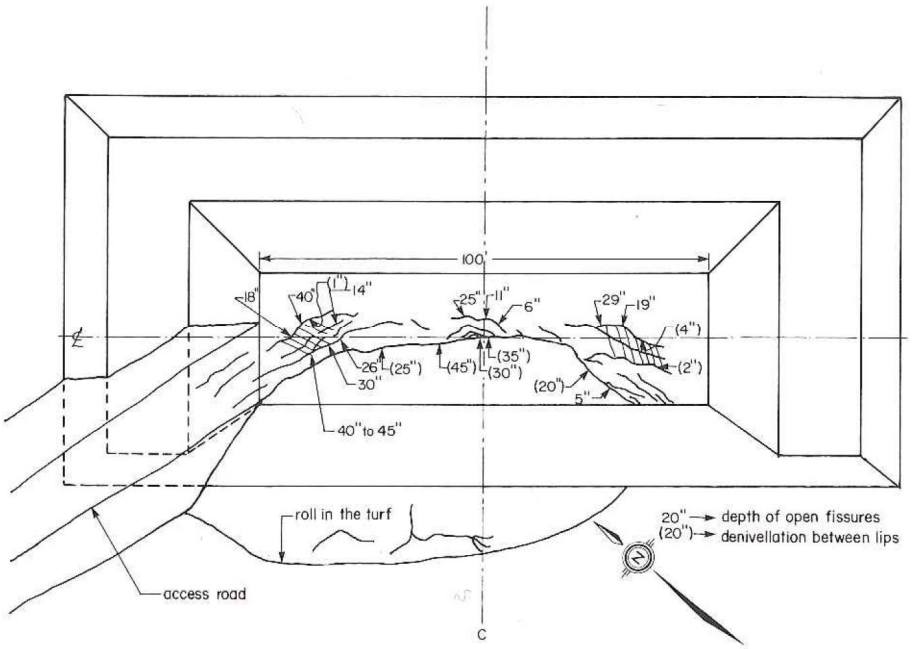

FIG. 8. Pattern of the fissures on the top surface of the embankment.

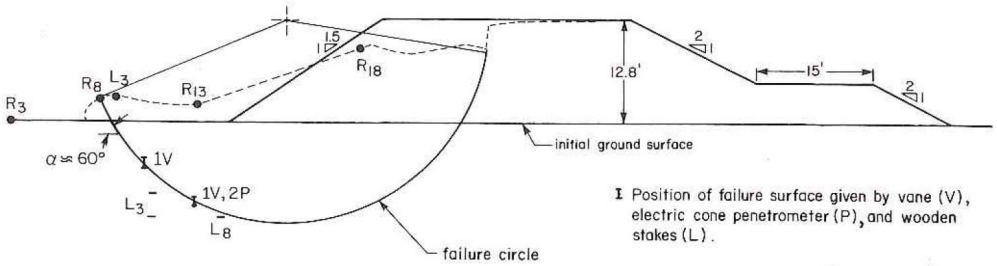

Figure 8.12. Geometry of Saint-Alban Fill A and the failure (La Rochelle et al 1974)

The soil conditions at the site are shown in Figure 8.13.

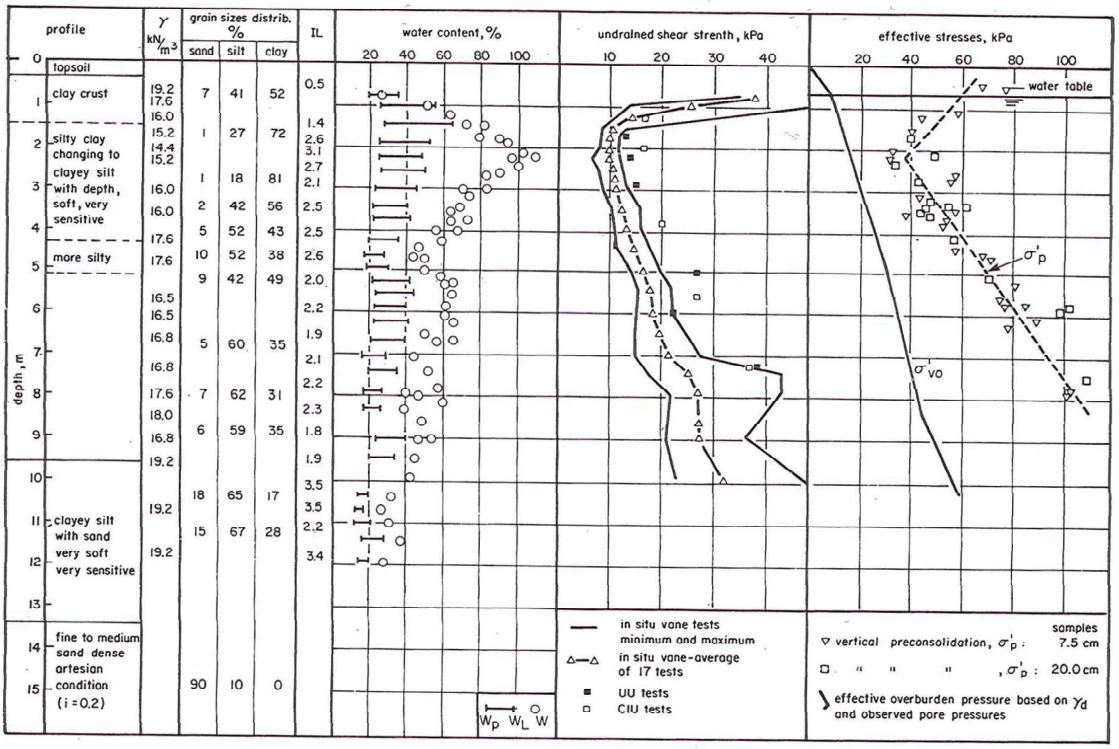

Figure 8.13. The soil profile at Saint-Alban. (Trak et al 1980)

The relevant soil profile consists of a 1.5-2 m thick crust layer, followed by slightly overconsolidated, sensitive silty clay. The stated thickness of the crust seems to vary between sources, for example Trak et al (1980) indicate 1.5 m, while Zdravkovic et al (2002) give 2 m crust thickness. The preconsolidation stress profile given by Trak et al (1980, see Figure 8.12) indicates that the soil from 0 to 2 m depth can be considered as stiff crust. Zdravkovic et al (2002) give a value of OCR = 2.2 for the sensitive clay layer. Very notable is that the in situ water content is at some places double the measured liquid limit, indicating very high sensitivity. The water table lies at a depth of ca. 0.7 m.

The effective friction angle in triaxial compression is φ' = 27°, and K_{0NC} = 0.49 (Zdravkovic et al 2002). This corresponds to HSU parameter value C = 0.9. In their own analyses, Zdravkovic et al (2002) assume the K_{0OC} value according to the Mayne & Kulhawy (1982) equation (Eq. 6.6), which would correspond to D = 1.

The chosen parameters for the soil layers in the HSU analysis are given in Table 8.6. The parameters are determined based on data given by La Rochelle et al (1974), Trak et al (1980) and Zdravkovic et al (2002).

Table 8.6. Soil parameters.

	φ' [°]	s_u [kPa]	ds_u [kPa/m]	γ [kN/m^3]	OCR	C	D
Embankment	44	0	0	19	-	-	-
Crust (0-1 m, active side)	0	30	0	19	-	-	-
Crust (1-2 m, active side)	0	30 (top of layer)	-20	19	-	-	-
Crust (0-2 m, passive side)	0	13 (top of layer)	-4	19	-	-	-
Clay (2 m-)	27	0	0	16	2.2	0.9	1

Both the assumed slip surface (La Rochelle et al 1974) and the mechanism calculated by Zdravkovic et al (2002) are circular or very close to that. A circular slip surface is then

assumed for the HSU analysis as well. The coordinates and other properties of the selected slip surface are given in Table 8.7 and shown in Figure 8.14.

Table 8.7. Properties of the slip surface used in the analysis.

Slice no.	layer	*x* [m]	*y* [m]	width [m]	base length [m]	base angle [°]	*φ'*	*c'*	OCR
1	crust	0.42	-0.58	0.83	1.43	-54.4	0.0	10.7	-
2	crust	1.25	-1.58	0.84	1.18	-44.9	0.0	6.7	-
3	clay	1.98	-2.24	0.62	0.78	-37.9	27.0	0.0	2.2
4	clay	2.60	-2.67	0.62	0.73	-32.4	27.0	0.0	2.2
5	clay	3.21	-3.03	0.62	0.69	-27.2	27.0	0.0	2.2
6	clay	3.83	-3.31	0.62	0.67	-22.3	27.0	0.0	2.2
7	clay	4.50	-3.55	0.73	0.77	-17.1	27.0	0.0	2.2
8	clay	5.24	-3.74	0.73	0.75	-11.7	27.0	0.0	2.2
9	clay	5.97	-3.86	0.73	0.74	-6.3	27.0	0.0	2.2
10	clay	6.70	-3.90	0.73	0.73	-1.0	27.0	0.0	2.2
11	clay	7.43	-3.88	0.73	0.73	4.3	27.0	0.0	2.2
12	clay	8.16	-3.79	0.73	0.74	9.6	27.0	0.0	2.2
13	clay	8.89	-3.63	0.73	0.76	15.0	27.0	0.0	2.2
14	clay	9.62	-3.40	0.73	0.78	20.6	27.0	0.0	2.2
15	clay	10.49	-3.00	1.01	1.14	27.5	27.0	0.0	2.2
16	clay	11.50	-2.37	1.01	1.25	36.2	27.0	0.0	2.2
17	crust	12.35	-1.66	0.69	0.96	44.2	0.0	16.7	-
18	crust	13.04	-0.89	0.69	1.11	51.7	0.0	30.8	-
19	fill/crust*	13.74	0.16	0.69	1.41	60.8	31.4	11.1	-
20	fill	14.43	2.34	0.69	3.20	77.5	44.0	0.0	-
*slice bottom located partly in fill and partly in crust, parameters for the slice are weighted averages									

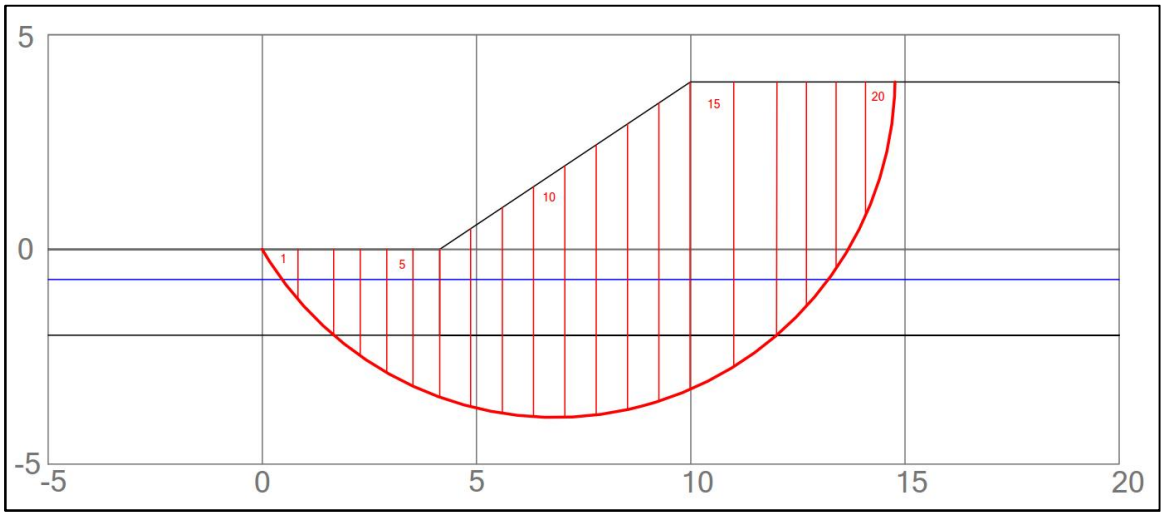

Figure 8.14. Slip surface geometry.

With the given assumptions, the only unknown factor is the value of λ/κ, which is then varied. Calculations are done both by using HSU for calculating s_u (total stress analysis), and for calculating Δu (effective stress analysis).

Figure 8.15a plots factor of safety from TSA as a function of λ/κ using Spencer's Method, while Figure 8.15b shows the corresponding shear strength and normalized shear strength profiles for various values of λ/κ.

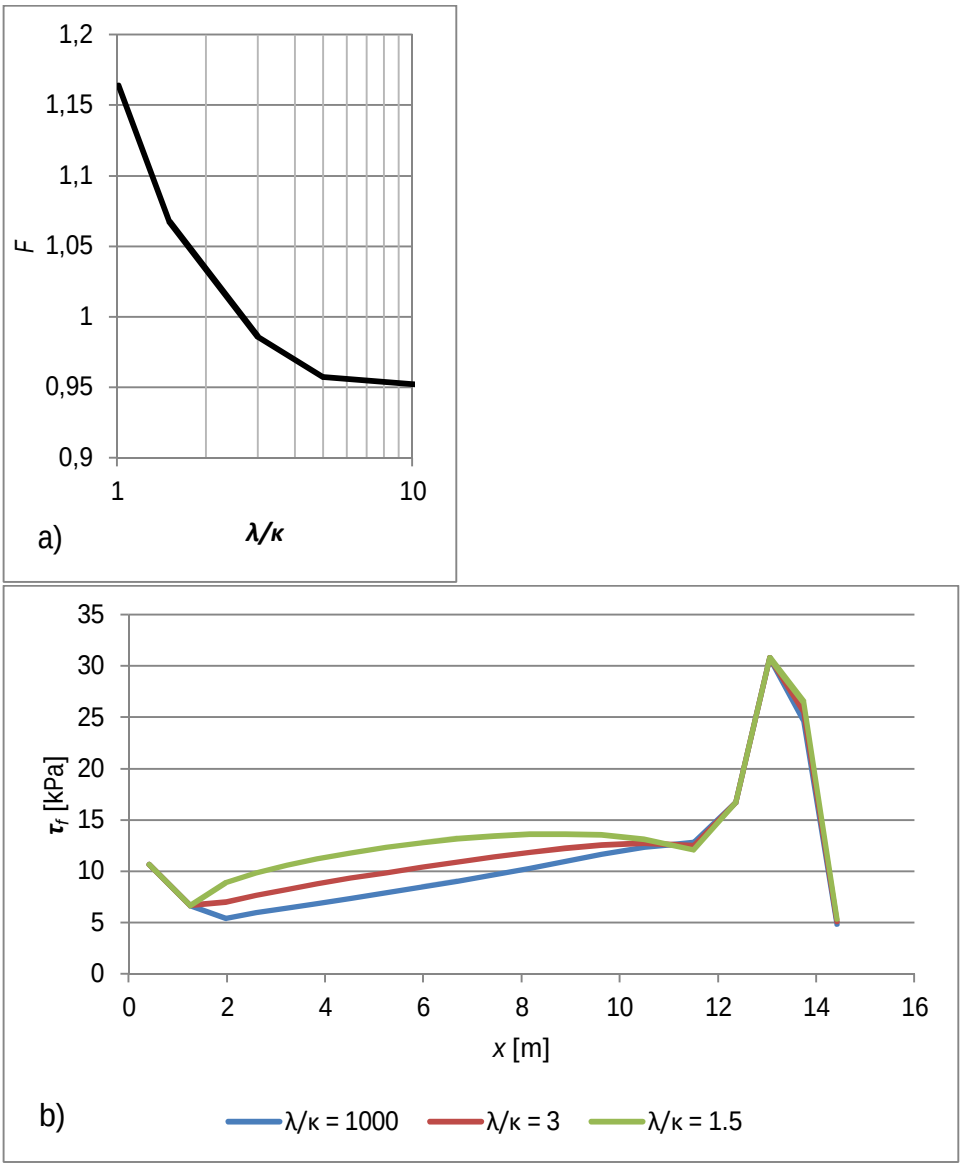

Figure 8.15. a) Factor of safety versus λ/κ, b) Shear strength along the slip surface at different λ/κ values.

The TSA results are quite realistic. By varying λ/κ, the factor of safety remains fairly close to unity. $F = 1$ is achieved with $\lambda/\kappa = 2.53$, which can roughly be considered a plausible "halfway estimate" for λ/κ when using the model with slightly overconsolidated clays.

An interesting graph for comparison is presented by Zdravkovic et al (2002) where they plot the mobilized shear strength along the failure plane as predicted by their FEM analyses using the anisotropic soil model MIT-E3 (Figure 8.16a). Their predicted mobilized shear strength curve is highly similar to that given by the HSU method at $\lambda/\kappa = 2.53$ (Figure 8.16b). Note however that the slip surface geometries are slightly different so the x-coordinates in the two figures are not fully comparable.

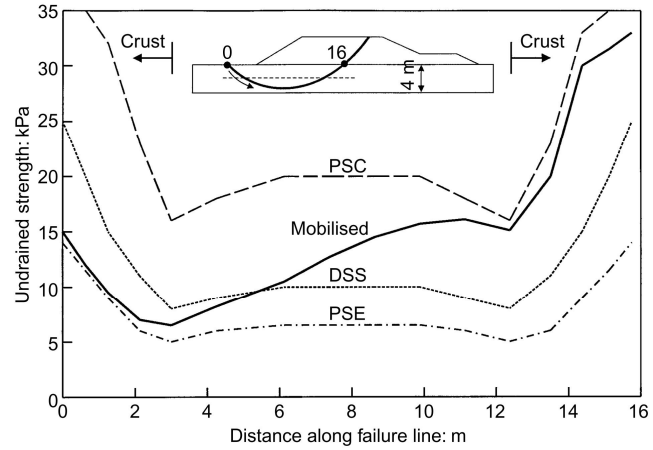

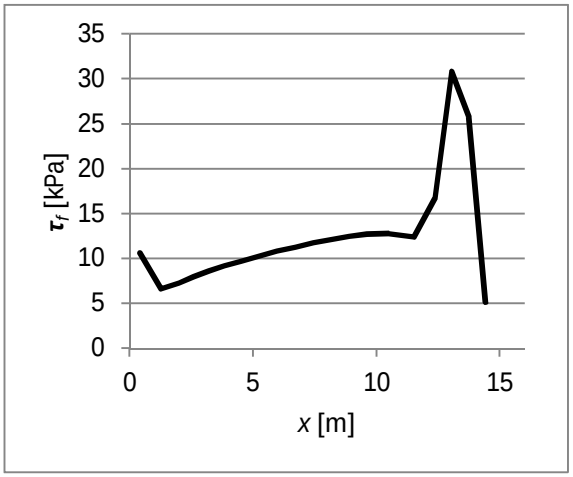

Figure 8.16. a) Shear strength profiles calculated with the MIT-E3 model (Zdravkovic et al 2002). b) HSU strength profile with λ/κ = 2.53 (F = 1)

The ESA results with excess pore pressure calculated based on vertical stress changes are somewhat lower than the TSA results (Table 8.8). To reach F = 1.0, the value λ/κ = 1.42 is needed. This value is quite low, and is fairly close to the theoretical upper boundary of shear strength attainable with HSU.

Table 8.8. TSA and ESA (based on stress changes) results compared.

	λ/κ = 1000	λ/κ = 5	λ/κ = 3	λ/κ = 1.5	λ/κ = 1.01
F (TSA)	0.9188	0.9575	0.9861	1.0680	1.1644
F (ESA)	0.8615	0.8958	0.9208	0.9912	1.0719
difference	-6.2 %	-6.4 %	-6.6 %	-7.2 %	-7.9 %

ESA shear strength profiles at various λ/κ are shown in Figure 8.17. The calculated shear strength in ESA is lower than in TSA (compare to Figure 8.14).

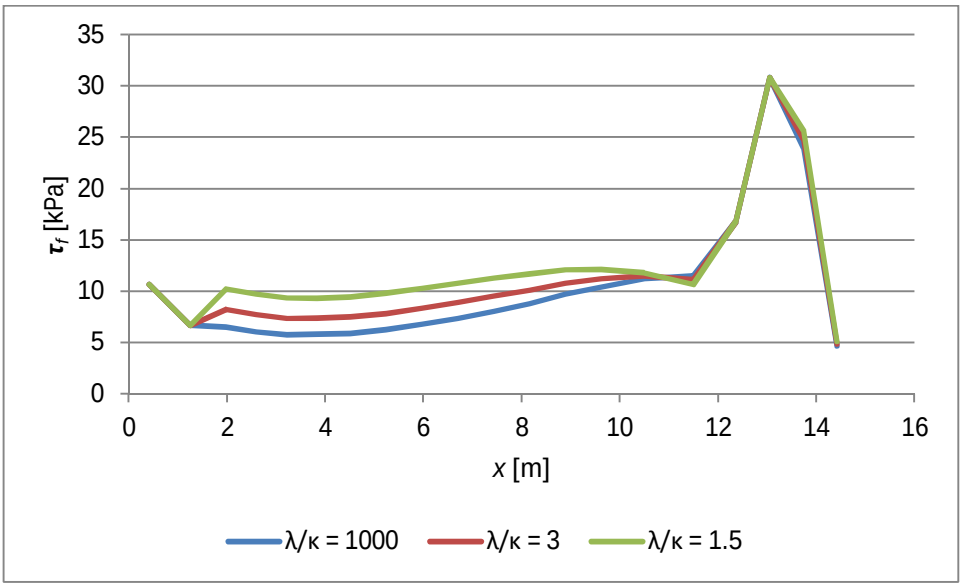

Figure 8.17. ESA strength profiles (based on stress changes)

Figure 8.18 shows the calculated excess pore pressure profile for the ESA at λ/κ = 2.53 (i.e. F = 1.0 for TSA), as well as the "forced" excess pore pressure profile that gives TSA-equivalent shear strength for comparison. Overall, the pore pressure that is derived from calculated stress changes results in higher Δu and lower shear strength than what results from total stress analyses.

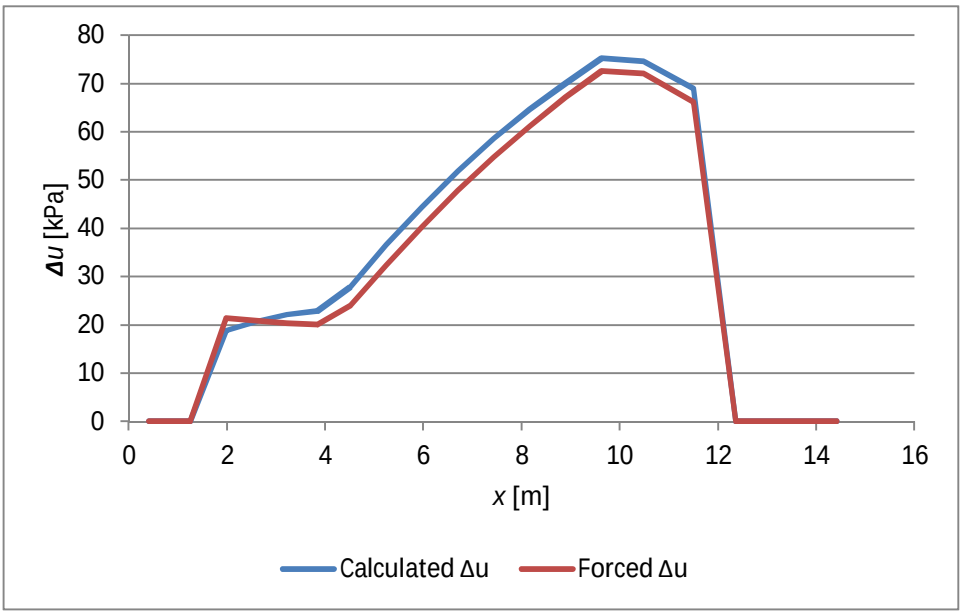

Figure 8.18. Comparison of Δu based on vertical stress changes, and forced based on predicted s_u

The HSU method gives very good results for the Saint-Alban A test fill when it is used to provide strength input for a total stress analysis. There are some issues in calculating Δu for undrained effective stress analyses, but the discrepancy between TSA and ESA are much smaller than in the case of Perniö (Section 8.1).

8.3 New Liskeard embankment

In 1963 in New Liskeard, Ontario, Canada, a highway embankment built on a varved clay deposit failed during construction, right after a lift had been completed. The failure (Figure 8.19) occurred less than one month after the start of construction. The failure length was ca. 105 m. The height of the embankment at the center part of the failure was 5.8-6.1 m. (Lacasse et al 1977)

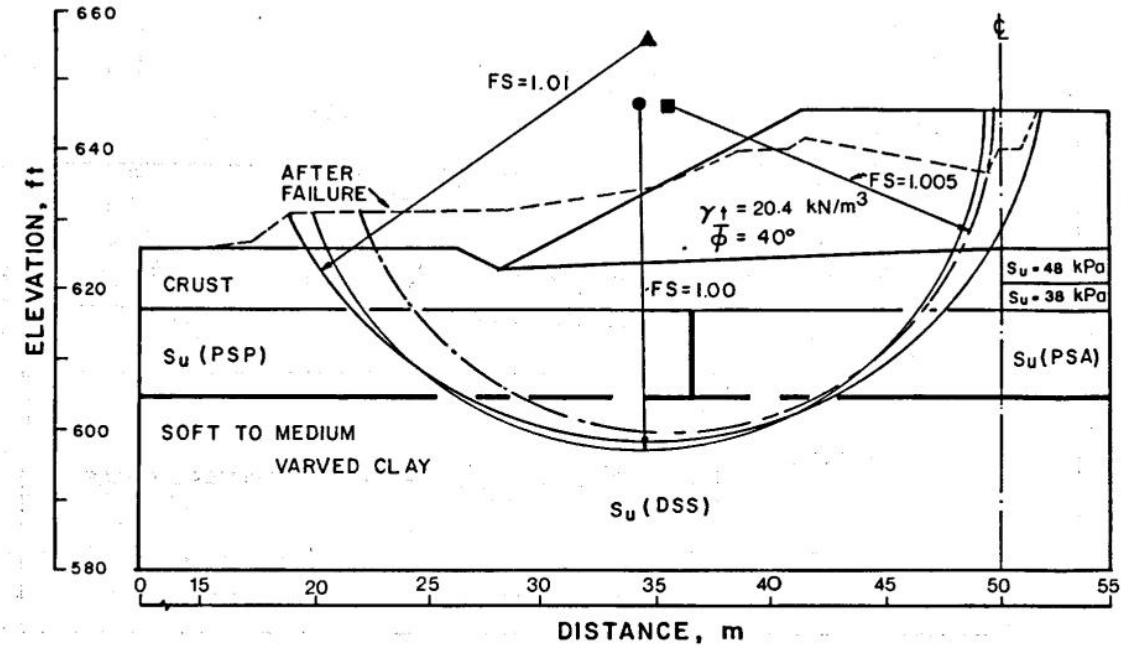

Figure 8.19. Failure and stability analyses of the New Liskeard embankment. DSS = Direct simple shear, PSA = plane strain active, PSP = plane strain passive (Lacasse 1977)

The soil conditions consist of a 2.1-3.7 m thick desiccated clay crust, below which lies a varved layer consisting of alternating clay and silt varves. Soil properties reported by Lacasse et al (1977) are given in Table 8.9. The presence of carbonates in both the clay and silt layers indicates "a high degree of natural cementation" in the soil (Lacasse et al 1977).

Table 8.9. Properties of New Liskeard varved clay (Lacasse et al 1977)

		w (%)	w_L (%)	I_p (%)	OCR
Varved clay	Clay varves	60-80	70±10	47±13	1.1-1.5
	Silt varves	24-30	30±5	10±6	

Stress properties, measured and normalised undrained strength properties and effective strength properties are shown in Figures 8.20-8.22 (Lacasse et al 1977). Interestingly, the measured DSS strength is considerably lower than passive plane strain strength. This is due to the horizontal varving: For active and passive shearing, the shear plane is directed across the alternating silt and clay varves, whereas for horizontal DSS shearing the lower strength of the clay varves determines the strength.

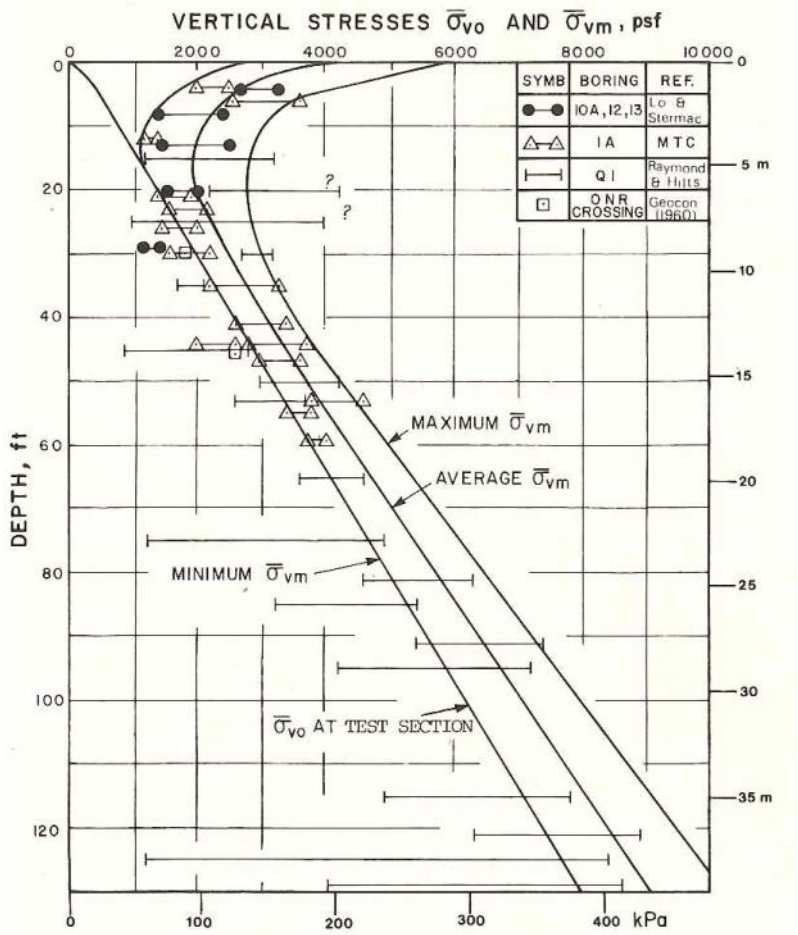

Figure 8.20. Consolidation stress state of New Liskeard clay (Lacasse et al 1977)

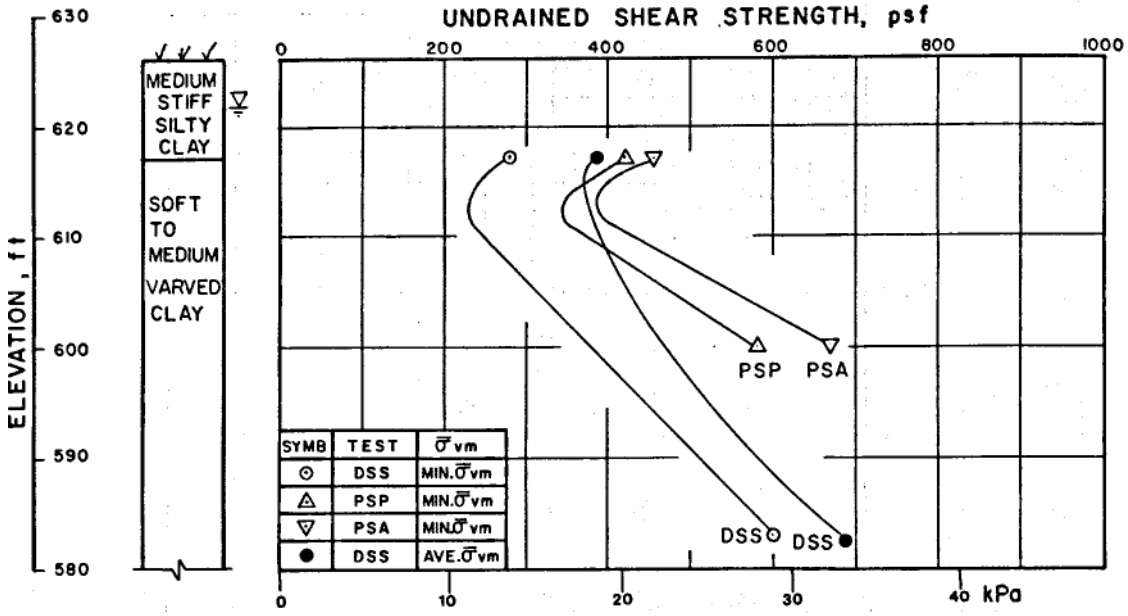

Figure 8.21. Undrained shear strength of New Liskeard clay. DSS = Direct simple shear, PSA = plane strain active, PSP = plane strain passive. (Note: 1 ft = 0.305 m) (Lacasse et al 1977)

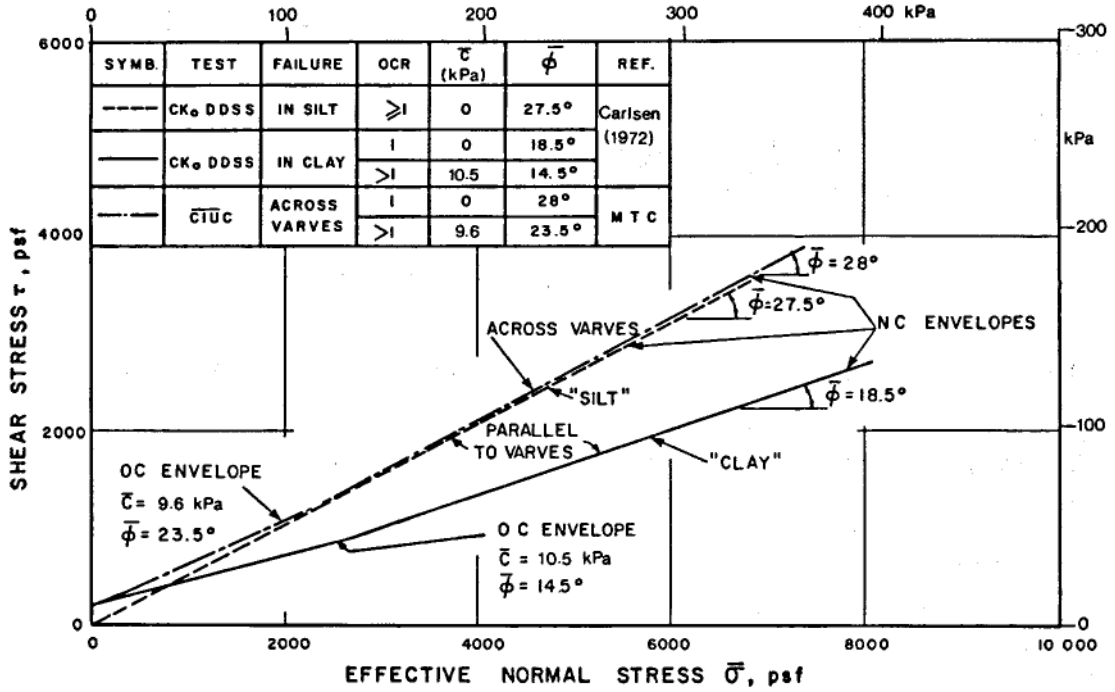

Figure 8.22. Effective strength envelope of New Liskeard clay. (Lacasse et al 1977)

No data of unit weight of the soil or measured water table elevation is given by Lacasse et al (1977). It is however mentioned that due to apparent downward seepage the in situ effective vertical stress level is higher than for hydrostatic conditions.

Lacasse et al (1977) present various stability analyses of their own as well as previous analyses done by several other authors. Depending on assumptions made about the strength of the embankment fill and crust, as well as OCR in the varved clay, the calculated factors of safety are on both sides of $F = 1$. Total stress analyses conducted by Lacasse et al (1977) give $F = 0.99…1.12$, whereas their effective stress analyses result in $F = 1.05…1.23$.

For an analysis using the HSU method quite many assumptions need to be made. Fill and crust properties used by Lacasse et al (1977) in their analyses are used “as is”, since they result in good computed factors of safety by the authors. No data is given about the unit weight of the soil, but setting the water table at a depth of 1.8 m from the initial ground surface as done by Lacasse et al, and using a dry unit weight $\gamma = 15$ kN/m^3 and a saturated unit weigh $\gamma_{sat} = 18$ kN/m^3 results in a σ'_{v0} profile that is highly similar to that given in Figure 8.20. The OCR values used in the analysis are chosen so that they correspond with the “average” σ'_c profile presented by Lacasse et al (1977).

The soil parameters used in the analysis are given in Table 8.10. As there is no explicit data about K_0 conditions, the HSU parameters C and D are left at their default values. The clay is divided into two sections: For slices where the base inclination is low, i.e. $\alpha = -15°…15°$ (arbitrary), the friction angle is set to $\varphi' = 19°$ to reflect the low DSS strength that is governed by the clay varves. Other slices are set to $\varphi' = 28°$. These values correspond to those given by Lacasse et al (1977).

Table 8.10. Model parameters for the analysis

	φ' [°]	s_u [kPa]	ds_u [kPa/m]	γ [kN/m3]	γ_{sat} [kN/m3]	OCR	C	D	
Fill	40	0	0	20.4	20.4	-	-	-	
Crust	0	48	-4.0	15	18	-	-	-	
Clay (direct shear)	19	0	0	15	18	*)	1	1	
Varved clay (across varves)	28	0	0	15	18	*)	1	1	
*) Set for each slice so that σ'_c matches the average profile given by Lacasse et al (1977)									

As the spreadsheet implementation of the HSU method does not allow for slip surface optimization, a preset slip surface is obtained using the GeoCalc software. This is done by conducting a basic total stress analysis where the varved clay is modelled with a field vane strength of s_u = 15 kPa on top of the layer, and an increase of ds_u = 2 kPa/m. Spencer's method is used. The coordinates of the critical slip surface are then imported to the HSU spreadsheet.

The critical slip surface from the initial total stress analysis is shown in Fig. 8.23. Both free-form and circular slip surfaces were used, but the critical slip surface most compatible with the data given by Lacasse et al (1977) was a circular one. It is recognized that no data was available on the shape of the actual surface, but circular surfaces seemed to result in failure dimensions that are most compatible with the measured extents of the failure. Free-form surfaces tended to result in too long critical slip surfaces.

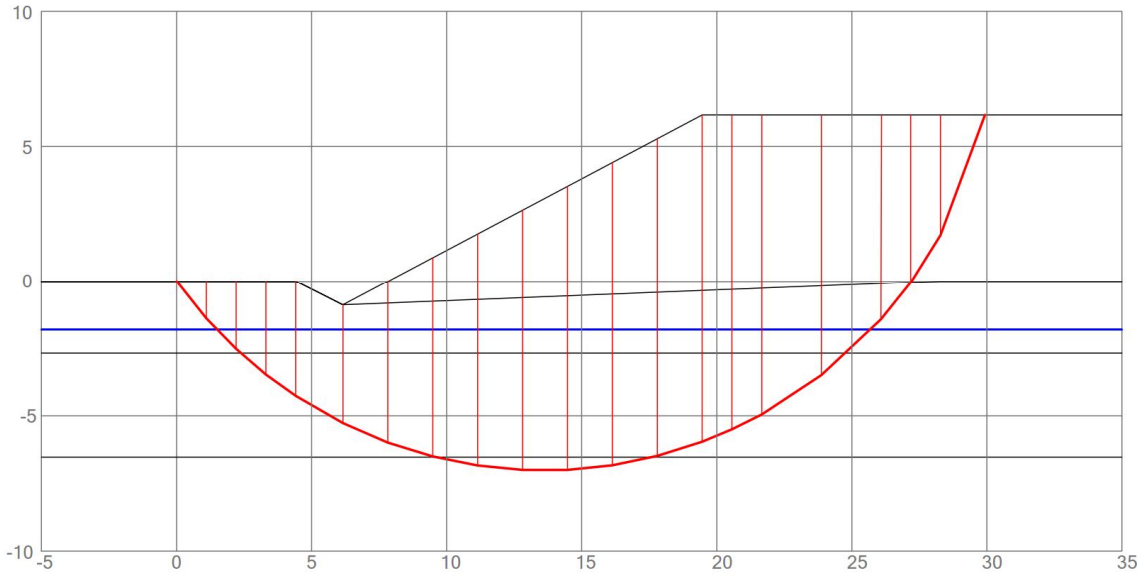

Figure 8.23. Slip surface geometry.

The location and other properties for each slice bottom are given in Table 8.11. The coordinate origin is fixed at the left end of the slip surface, at ground level (i.e. "global" initial ground level).

Table 8.11. Properties of the slip surface used in the analysis.

Slice no.	layer	x [m]	y [m]	width [m]	base length [m]	base angle [°]	φ'	c'	OCR
1	crust	0.55	-0.69	1.10	1.77	-51.5	0.0	45.2	-
2	crust	1.65	-1.95	1.10	1.58	-45.8	0.0	40.2	-
3	varved clay	2.76	-2.99	1.10	1.45	-40.6	28.0	0.0	2.6
4	varved clay	3.86	-3.86	1.10	1.36	-35.8	28.0	0.0	2.1
5	varved clay	5.29	-4.76	1.75	2.02	-30.0	28.0	0.0	1.7
6	varved clay	6.99	-5.63	1.66	1.81	-23.4	28.0	0.0	1.5
7	varved clay	8.65	-6.24	1.66	1.74	-17.3	28.0	0.0	1.4
8	clay (DSS)	10.32	-6.67	1.66	1.70	-11.4	19.0	0.0	1.4
9	clay (DSS)	11.98	-6.92	1.66	1.67	-5.6	19.0	0.0	1.35
10	clay (DSS)	13.64	-7.00	1.66	1.66	0.1	19.0	0.0	1.35
11	clay (DSS)	15.31	-6.91	1.66	1.67	5.9	19.0	0.0	1.35
12	clay (DSS)	16.97	-6.65	1.66	1.70	11.6	19.0	0.0	1.4
13	varved clay	18.63	-6.22	1.66	1.74	17.5	28.0	0.0	1.4
14	varved clay	20.01	-5.73	1.10	1.19	22.6	28.0	0.0	1.5
15	varved clay	21.11	-5.22	1.10	1.24	26.8	28.0	0.0	1.6
16	varved clay	22.77	-4.22	2.21	2.64	33.4	28.0	0.0	2
17	varved clay*	24.97	-2.46	2.21	3.02	43.1	28.0	0.0	3.2
18	crust	26.63	-0.73	1.10	1.77	51.4	0.0	45.3	-
19	fill	27.73	0.84	1.10	2.08	58.0	40.0	0.0	-
20	fill	29.10	3.94	1.65	4.74	69.7	40.0	0.0	-
*slice bottom located partly in the crust, but whole slice treated as varved clay									

With the given assumptions, the only unknown factor is the value of λ/κ, which is then varied in this analysis. Calculations are done both by using HSU for calculating su (total stress analysis, TSA), and for calculating Δu (effective stress analysis, ESA).

Figure 8.24a plots factor of safety from TSA as a function of λ/κ using Spencer's Method, while Figure 8.24b shows the corresponding shear strength and normalized shear strength profiles for various values of λ/κ.

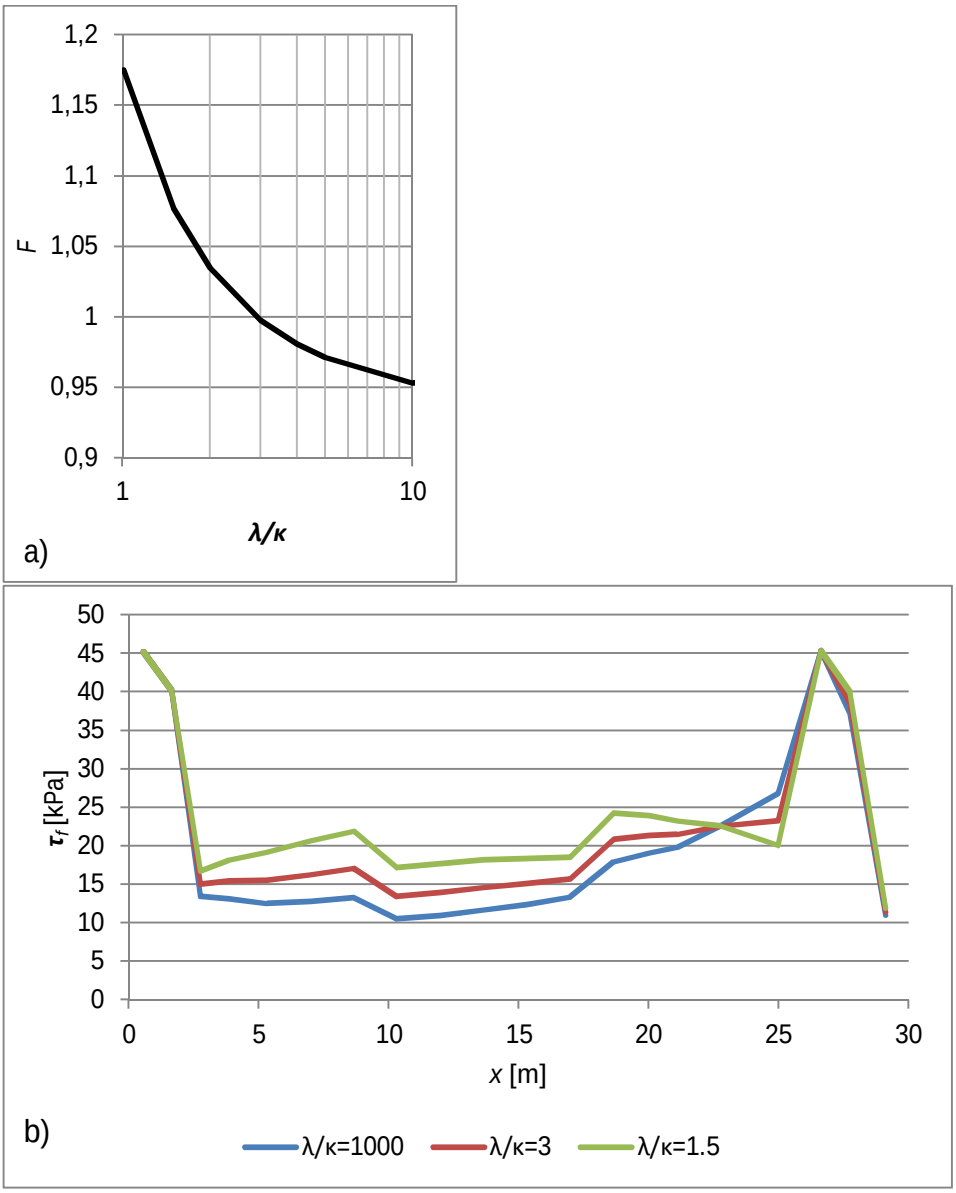

Figure 8.24. a) Factor of safety versus λ/κ, b) Shear strength along the slip surface at different λ/κ values.

Overall, the TSA results with the HSU method are very good. With the given set of assumptions regarding the fill and crust layers, the value $\lambda/\kappa = 3$ gives a calculated factor of safety of $F = 0.998$.

Corresponding undrained effective stress analyses with the HSU method (Approach B) give very similar results. Table 8.12 shows the factors of safety with different λ/κ values for both TSA and ESA. The differences between the analysis types are negligible when close to $F = 1$, but the differences seem to increase when F is increasing.

Table 8.12. TSA and ESA (based on stress changes) results compared.

	$\lambda/\kappa = 1000$	$\lambda/\kappa = 5$	$\lambda/\kappa = 3$	$\lambda/\kappa = 1.5$	$\lambda/\kappa = 1.01$
F (TSA)	0.9367	0.9712	0.9977	1.0773	1.1751
F (ESA)	0.9360	0.9689	0.9938	1.0671	1.1554
difference	-0.1 %	-0.2 %	-0.4 %	-0.9 %	-1.7 %

Figure 8.25 shows the resulting shear strength profiles at various λ/κ values. Overall, the differences between TSA and ESA are very small, as is reflected in the calculated factors of safety as well.

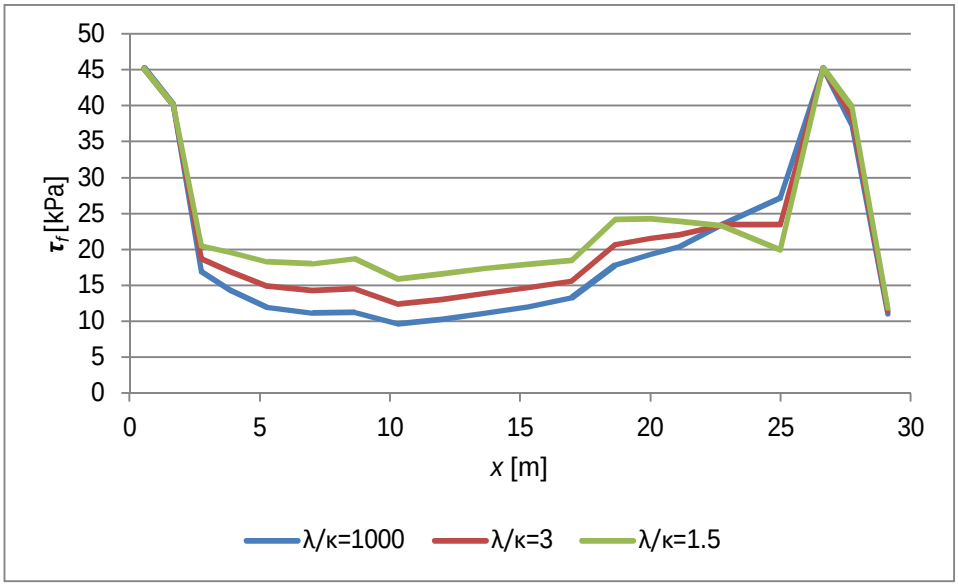

Figure 8.25 ESA strength profiles (based on stress changes)

Figure 8.26 shows the calculated excess pore pressure profile for the ESA at λ/κ = 3, as well as the "forced" excess pore pressure profile that gives TSA-equivalent shear strength for comparison. The profiles are nearly identical, with most differences in the passive part of the slip surface.

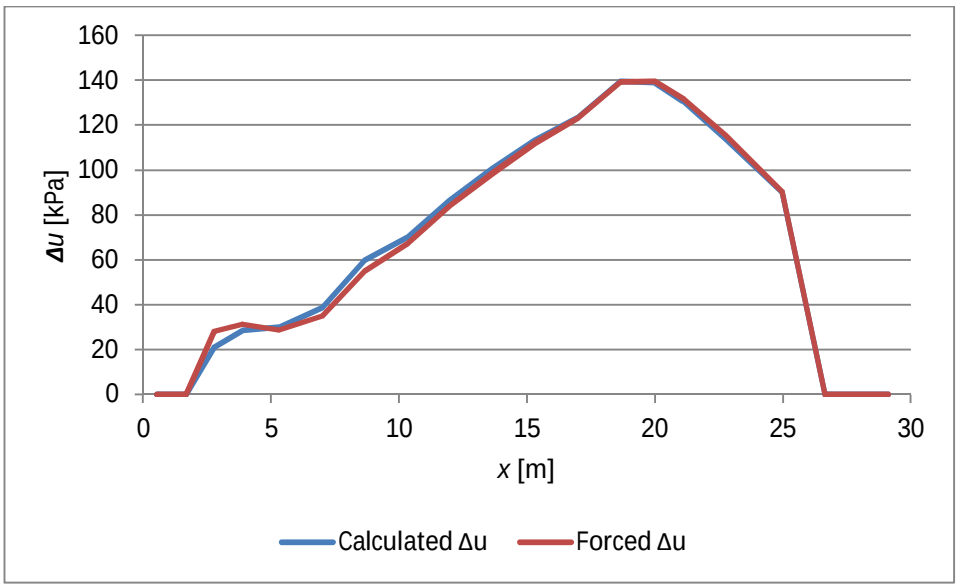

Figure 8.26. Comparison of Δu based on vertical stress changes, and forced based on predicted s_u

Overall, the back.calculation results of applying the HSU method to the New Liskeard embankment are excellent. Failure is attained with very realistic parameter levels and all calculation methods (TSA and the two different ESA approaches) give very similar results.

9 Discussion

9.1 General

The formulation of the HSU method and the proposed modelling approach have been presented in Chapter 5. Formulations have been presented for modelling s_u in total stress stability calculations, and for modelling excess pore pressure in undrained effective stress stability calculations. The different concepts and approaches of the method are schematically presented in Figure 9.1.

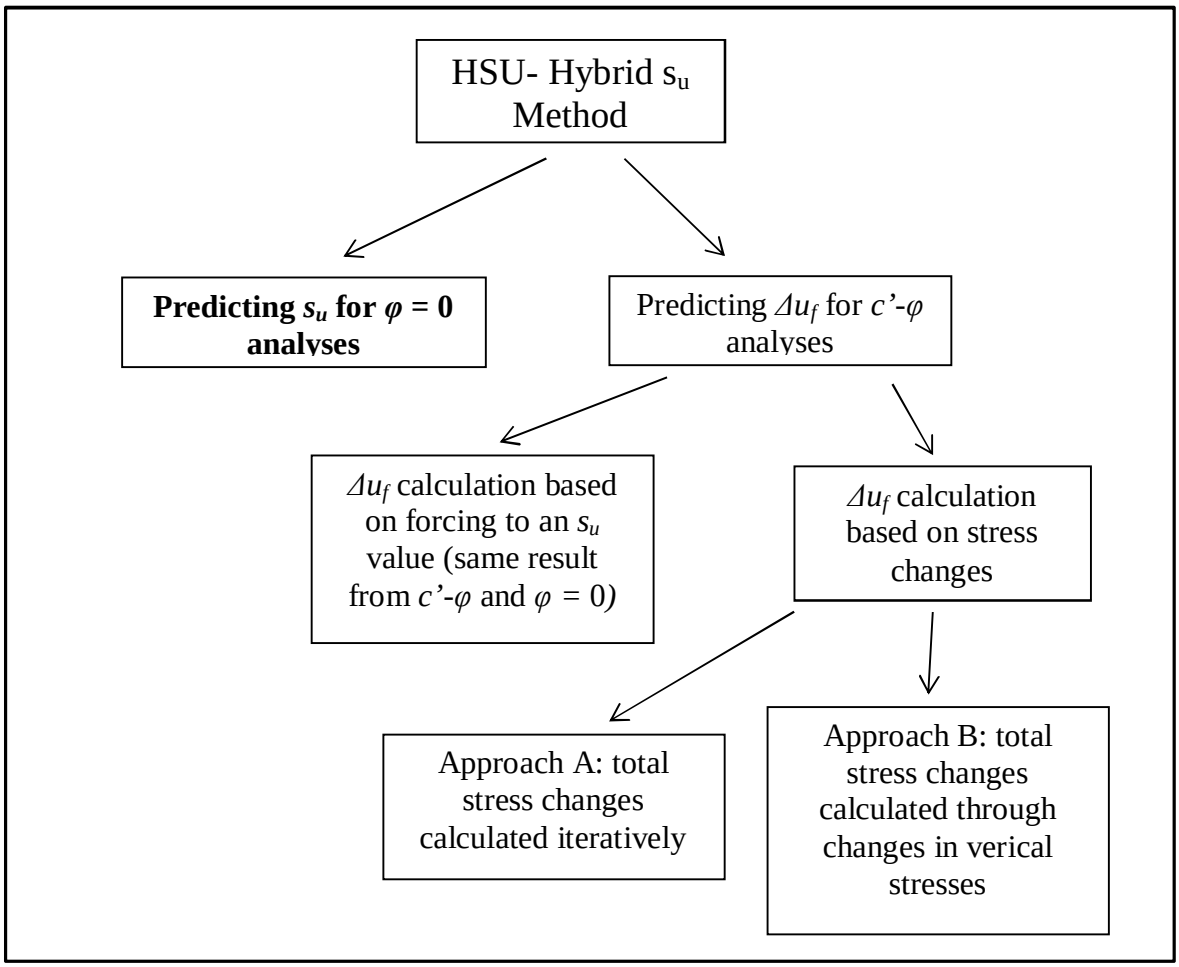

Figure 9.1. "Family tree" for the HSU method

Modelling s_u gives a shear strength value that is directly usable as input strength in the stability calculation. Modelling Δu can be approached in two ways: Δu can be forced to a value so that a given undrained shear strength is obtained. This approach essentially solves the issue of overestimating shear strength when $F > 1$ that occurs in traditional undrained effective stress analyses. The other approach in calculation Δu is done based on assumed stress changes on the failure surface. This approach also attempts to calculate the true pore pressure at failure, resulting in the true undrained strength at failure. These approaches are further discussed in Section 9.2.

Chapter 6 studies the influence of the various model parameters to the undrained shear strength predicted by the method. HSU generally gives plausible results, the various parameters affect the results quite logically. The method does not seem to be overly sensitive to any of the parameters.

The method makes a number of simplifying assumptions to simplify the overall process. Such assumptions are the omission of rotational hardening (present in the original S-CLAY1 model, Wheeler et al 2003), use of the Drucker-Prager failure criterion, and the use of the intermediate principal stress parameter b = 0.3 for stability calculation applications. In the light of the generally good results, these assumptions can be considered good trade-offs between simplicity and accuracy. In the case of rotational hardening, the selection of proper parameters can be considered quite difficult, if not impossible in typical engineering use, which makes its omission all the more acceptable. The assumed effect of rotational hardening is however counteracted to some extent with the use of the Drucker-Prager failure criterion fitted for triaxial compression.

Perhaps the biggest potential issue with the model is the relative sensitivity of the predicted extension strength (or the strength at any stress state where the principal stress rotation is close to $\theta = 90°$). Especially the parameters C (which governs the inclination of the yield surface) and λ/κ which controls the direction of the effective stress path have a quite large effect on the extension strength. The proper choice of parameters to avoid troubles with extension strength is discussed further in the following sections.

In Chapter 7, the HSU method was fitted to laboratory test results on various soft clays using different fitting methods. Based on the studied cases, it can be said that the HSU method can predict the anisotropic undrained shear strength (triaxial compression and extension) quite well with proper parameter selection. Especially for a given OCR value, the model could be fitted in most cases to produce proper undrained strengths. If the model is fitted to predict undrained strength over a range of OCR (e.g. the SHANSEP approach), the fit typically needs to be a compromise, as a given "target" SHANSEP curve is likely very difficult to replicate accurately over a large OCR range.

In Chapter 8, the model was applied to back-calculate some well documented failures. The stability calculation results were very good, with F = 1 reachable with plausible parameter combinations without "forcing" any parameters to unreasonable values.

Overall, it can thus be said that the model works for its intended purpose: calculating the anisotropic undrained shear strength of normally consolidated or slightly overconsolidated soft clays, especially for stability calculations with LEM.

9.2 Total stress versus effective stress applications

The HSU method offers three options for undrained stability calculations (see Chapter 5):

1. Calculating undrained shear strength s_u, which is then used as strength input in LEM stability calculations. The stability calculation can be done as a total stress analysis.

2. Calculating Δu so that the resulting shear strength $\tau_f = s_u$. The stability calculation is an effective stress analysis. As the shear strength is forced to match the undrained shear strength predicted by HSU, the end result is identical to a total stress calculation using s_u. It is good to note that the resulting excess pore pressure is not necessarily correct or even realistic, but instead depends on the target strength and the total stress state given by the limit equilibrium calculation. This approach avoids the overestimation of shear strength at $F > 1$ that is inherent in traditional undrained effective stress analyses. An iteration loop is required as the calculation requires the output of the limit equilibrium as its input.

3. Calculating Δu based on assumed stress changes. Here, the excess pore pressure response is divided into two parts:

$$\Delta u = \Delta p - \Delta p' \tag{9.1}$$

The effective stress component $\Delta p'$ represents the yield-induced excess pore pressure, and is calculated from the HSU method, representing the stress change from the initial state to failure. The total stress component Δp is calculated from assumed stress changes on each slice bottom, again representing the change at failure. As the excess pore pressure is calculated at failure, it should result in shear strength that is the actual strength at failure, which again avoids the overestimation of shear strength for $F > 1$.

This approach also requires an iteration loop for the calculation of Δu.

All approaches have been shown to give good results in the back-calculations presented in Chapter 8. However, the proposed effective stress approaches with calculation of Δu are mainly to be considered as “proof of concept”, whereas the calculation of s_u for total stress stability calculations is intended as a proper engineering tool.

The main reason for this consideration is that in stability calculations (especially using limit equilibrium), the main unknown that has the most effect in the end result is shear strength. The main purpose of a limit equilibrium stability analysis is the correct calculation of the factor of safety F, not so much modelling the stress state along the slip surface. Additionally, the use of the whole HSU method is based on the assumption that the undrained shear strength predicted by HSU is reasonably correct.

If we assume the shear strength predicted by HSU to be correct, this makes the use of Δu based on stress changes less favourable, as the resulting shear strength at failure is not always the “correct” value predicted by HSU (although it can be very close, as evidenced by Sections 8.2 and 8.3).

The use of forced Δu to arrive in a given shear strength does give the "correct" shear strength at failure. An effective stress limit equilibrium calculation using this Δu gives the same overall result as using the predicted s_u in a total stress calculation. However, the effective stress calculation is notably more complicated (including an iteration loop that requires that the limit equilibrium is calculated several times per failure surface) than the total stress calculation. In addition, the iteration of Δu may not always converge, especially with more rigorous limit equilibrium methods (e.g. the Morgenstern-Price method and its special case, Spencer's method). As the total stress calculation with s_u is simpler and more reliable, there simply is no reason to use an undrained effective stress calculation with forced Δu.

There might be an application for calculating Δu with the HSU method, where a rough estimate of excess pore pressure at failure is needed for comparison to measured values on an instrumented low stability embankment. On the other hand, if there is time to instrument and monitor an embankment, there probably is also time to use a more advanced FEM model to calculate pore pressures at failure.

9.3 Guidelines for parameter selection

9.3.1 Friction angle φ'

Friction angle φ' is the basic effective strength parameter and when its value is chosen based directly on laboratory test results, HSU typically gives good results. As HSU is essentially a critical state model, the friction angle should also correspond to high strains /critical state as well as possible to obtain the correct slope of the critical state line *M*. It is recommended that good quality CK_0U triaxial tests sheared to a high enough strain level (e.g. $\varepsilon_a > 15$ %) are used to determine φ'. The test series should preferably include at least one test done at or close to the *in situ* consolidation state to provide a shear strength reference for model fitting.

The consolidation stresses used in testing should preferably be high enough to avoid dilation and shearing on the dry side of critical, which would complicate the determination of the critical state friction angle. The geotechnical engineer should always know which stress and strain levels in laboratory testing are applicable for use with a given soil model.

9.3.2 A note on applying cohesion

As many typical critical state models do, the HSU method by default assumes that at critical state all bonding between the clay particles have been destroyed and the soil acts a completely frictional material, i.e. $c' = 0$. However, in some cases clays can exhibit effective cohesion in triaxial testing, even at high strains on the wet side of critical (see e.g. the results on Perniö clay, Figure 7.4).While no claims of "true" effective cohesion are made here, the option of modelling effective cohesion is offered in the HSU method (see Section 5.9).

In the case of Perniö clay, the stability calculation did not really work without cohesion. On the other hand, applying some cohesion in HSU resulted in very good calculation results. While there is a large number of other variables that might affect the results (e.g. the strengths of the sand fill and dry crust), it seems that modelling cohesion was essential for obtaining good back-calculation results.

It is still recommended that $c' = 0$ is generally assumed in accordance to the general critical state assumptions. However, if laboratory results consistently indicate effective cohesion at large strains, and the corresponding stability calculation results give unrealistically low factors of safety, applying cohesion as described in Section 5.9 can be relevant. Still, careful engineering judgment needs to be exercised when applying cohesion in HSU so as to avoid dangerous overprediction of shear strength.

9.3.3 Preconsolidation stress σ'_c

Another quite essential parameter for HSU is the preconsolidation stress σ'_c. This should be determined by oedometer testing (CRS or traditional), or possibly by K_0NC testing on triaxial samples (i.e. drained test where the stress path is controlled with the requirement of zero lateral strains.

σ'_c is an important parameter in the HSU method (and indeed in any model with a yield surface) as the size of the initial yield surface is directly proportional to σ'_c. The size of the initial yield surface then greatly affects the predicted strength.

Sample quality and strain rate in the test are important issues to consider (and not just restricted to the use of HSU) in determining σ'_c. Poor quality samples make determining preconsolidation stress difficult and unreliable.

It has been established that strain rate affects the apparent preconsolidation pressure (see Section 3.6). High strain rates result in high apparent preconsolidation stress and vice versa. Therefore basing the value of σ'_c on a very fast or slow tests that may not be applicable to the in situ loading case can result in incorrect prediction of shear strength. For example, traditional staged loading oedometer tests are typically much slower than typical CRS oedometer tests, so the preconsolidation stress values determined from CRS tests are typically higher (Länsivaara 1999).

No specific recommendations are given here for applicable strain rates in oedometer testing, as such a discussion is outside the scope of this thesis and not at all restricted to the use of the HSU method. However, one should use their engineering judgment in analysing the problem: is the potential loading case "fast" (e.g. a train coming to a standstill) or "slow" (e.g. a gradually built landfill)? For example, results from a relatively fast CRS test are more applicable to the "stopping train" than the "landfill" case.

9.3.4 "Control parameter" λ/κ

The parameter λ/κ is the ratio between the compression and swelling indices, or the ratio between elastoplastic and elastic strains. In the HSU method its value effectively controls the direction of the effective stress path, and therefore the predicted shear strength. This relationship can be derived from the concept of undrained loading: A high λ value means that the clay has a large tendency for plastic volumetric straining. In undrained conditions this tendency is offset by corresponding elastic expansion, or excess pore pressure. High compressibility therefore results in high excess pore pressure and a "flat" effective stress path. Correspondingly, low λ would result in low Δu and a more vertical effective stress path. For reference, see Figure 6.1.

As strains are not considered in the HSU method, the parameter λ/κ is effectively detached from its physical meaning, and becomes a control parameter for the shape of the effective stress path. Therefore the selection of λ/κ should not necessarily be based on an actual laboratory value (obtainable e.g. from oedometer testing), but on producing relevant stress paths.

Another issue that affects the choice of λ/κ is the rate of undrained shearing. As soil also has viscous properties, high rates of shearing result in less excess pore pressure than slower rates, and thus a more vertical effective stress path (see Section 3.6). Because λ/κ can in this application be decoupled from its physical meaning, it can thus be used also to take rate effects into account to some extent.

When λ/κ is considered a control variable instead of a physical parameter, it becomes an unknown in the model that cannot be determined accurately. However, based on the properties shown in Section 6.3 and Chapters 7 and 8, a reasonable range and recommended values for engineering use can be established.

"Physically" meaningful values of λ/κ are between 1 and infinite. λ/κ = 1 means completely elastic behaviour (i.e. elastic + plastic strain = elastic strain, i.e. no plastic strains, vertical (p',q) stress path), while large λ/κ means large plastic strains (i.e. little volumetric hardening, stress path directed along the initial yield surface). Negative λ/κ values are also mathematically possible and can be used to direct the stress path further, but have no realistic physical meaning.

In terms of undrained shear strength, highest strengths are obtained with $\lambda/\kappa \approx 1.000\ldots$ (a value of unity results in division by zero in the model). Increasing λ/κ quickly decreases the resulting s_u value, and above $\lambda/\kappa \approx 10$, s_u practically reaches a constant value (the stress path closely follows the initial yield surface).

It is good to recognize that λ/κ has a larger effect on extension strength than compression strength. This is because the extension stress path is much longer than in compression, so changing its direction also has a larger influence in s_u.

Some representative values of λ/κ resulting from the model fits and back-calculation examples in Chapters 7 and 8 are collected in Table 9.1. For the details of these fits and calculations, please see the corresponding sections.

Table 9.1. Selection of λ/κ values that result from model fits and back-calculations of failures.

Section	Case	λ/κ	Notes
7.1	Perniö clay compression	2.1	average for compression, Table 7.2
7.1	Perniö clay extension	2.7	average for extension, Table 7.2
7.2	Norwegian clays, compression	2.4	"average" case, Table 7.4
7.2	Norwegian clays, extension	3.6	"average" case, Table 7.4
7.3	Scandinavian clays, fit for comp. and ext.	1.5-5	values that allow the HSU to be fitted to the data
7.4	Drammen clay	negative values	the HSU yield surface fit the data poorly
7.5	Resedimented BBC, compression	2.7	
8.1	Perniö failure experiment, c' = 3.4 kPa	4.1	TSA with s_u; failure at q_{app} = 70 kPa
		1.7	TSA with s_u; failure at q_{app} = 80 kPa
		1.2	TSA with s_u; failure at q_{app} = 87 kPa
8.2	Saint Alban test fill A	2.5	TSA with s_u
8.3	New Liskeard embankment	3.0	TSA with s_u

While the methodology used in obtaining these values varies as the data available in the examples varies somewhat, it can be observed that applicable λ/κ values generally range from close to 1 (e.g. very fast loading in Perniö) to around 4-5. Even if these results remain anecdotal, it may be cautiously said that in engineering purposes a similar range of values would be applicable.

Ideally, the engineer would have some kind of undrained shear strength data to help in fitting the model and choosing the value of λ/κ. If the loading rate can be considered "ordinary", i.e. not extremely fast, applicable values might be in the range of λ/κ = 2.5…5. For a cautious estimate, λ/κ = 5 might be a good starting point.

In the case of very fast loading, a low λ/κ value close to 1 might be applicable. An example could be external loading from a rapidly applied load, such as a train or a heavy container. However, if the quickly applied loading is then sustained for some time, due to

undrained creep effects (see Section 3.6) pore pressure will increase and the "equivalent" effective stress path will correspond to a more slowly applied load (Figure 3.13). Therefore assuming a low λ/κ and consequently a very high undrained strength can be extremely dangerous unless the rapidly applied load is sustained only for a very short time.

No "hard" values for λ/κ are suggested, but the engineer should still use his or her best judgment and ideally vary the value of λ/κ and study its effect on the end results. A good idea would be to plot the yield surface and effective stress path with the chosen model parameters and see if the predicted stress path is realistic. For reference, see e.g. Figure 6.1.

9.3.5 K_0 parameters C and D

The K_0 parameters C and D can be chosen based on known K_0 data, fitting on a sufficiently large strength data set, or in the absence of such data, can be left at their default values.

As there is a fairly reliably established connection between K_{0NC} and φ' in the Jaky equation (see Section 6.6), it can be said that the theoretical range of C varies roughly in the range of C = 0.9…1. However, as C is primarily a parameter that controls the inclination of the yield surface (with the assumption of associated flow), the value of C should also be considered from this viewpoint. The shape of the yield surface especially affects the predicted extension strength.

Based on the examples in Chapters 7 and 8, it appears that applicable C values are broadly in the range of C = 0.9…1.1. When C has been fitted to given data, its value is often close to 1, and the results in terms of predicted strength or factor of safety are also quite plausible. When the overall functionality of the model (including the initial yield surface and resulting effective stress paths) is examined, the following suggestions are given for the choice of C:

a) In the absence of K_{0NC} data, choose C = 1

b) If K_{0NC} is known, choose:

$$C = \frac{K_{0\,NC}}{1 - \sin\varphi'} \tag{9.2}$$

or c) Choose C (together with λ/κ) so that a desired degree of strength anisotropy is obtained, staying within C = 0.9…1.1 if possible (see Section 9.4)

The K_0 parameter D can be considered less important than the others, as in HSU it only has a slight effect on the initial mean effective stress p'_0. The value of D is quite difficult to obtain reliably and *in situ* it is also affected by the loading-unloading history of the soil. Therefore it is recommended here that D is set to its default value D = 1 (corresponding to the equation proposed by Mayne & Kulhawy (1982), see Section 6.6), and changed only if a very specific parameter combination is desired for some reason.

9.4 On strain softening and strain compatibility

It should be noted that the model fits presented in Chapter 7 were done based on peak strength data. Soft clay typically exhibits notable strain softening after the peak strength is attained (Section 3.3), especially in triaxial compression. For direct shearing and extension, the peak is not as pronounced and occurs at much higher strains.

It is known that along a slip surface, these peak strengths are not attained simultaneously: the peak occurs at different strain levels for compression, direct shear and extension, and the strain levels along the slip surface vary as well (e.g. Ladd 1991). Often the active portion (compression) of the slip surface is first mobilized past failure, later followed by other parts of the slip surface.

If a model could accurately capture the strain softening (and the strain level) of the soil, peak strengths could be used in design. HSU does not however model strain softening nor are strains considered in limit equilibrium calculations. Therefore the design strength value should take strain compatibility and softening into account on average. This issue naturally applies to other similar soil models and LEM in general.

In typical engineering practise, peak strengths are however sometimes used as the characteristic strength applied in the design. This perhaps works because of low quality samples that do not exhibit "ideally" high peak strengths that very high quality samples would. Also the required safety factors give some margin for error here.

Ladd (1991) suggests that failure occurs when the maximum average shear strength along the slip surface is mobilised. Therefor the characteristic strength should correspond to the strain level where the average strength reaches its maximum. For this, stress-strain curves from undrained compression and extension tests (at minimum) would be needed. If this thought is applied to HSU, fitting should be done so that the predicted strength corresponds to those "maximum average" strengths determined by laboratory testing.

Karlsrud & Hernandez-Martinez (2013) suggest reducing the measured peak strengths by a given amount to account for strain softening and strain compatibility in design applications. These values would apply for good quality samples.

Table 9.2. Suggested reductions (in %) to peak strengths to account for strain softening and strain compatibilty (Karlsrud & Hernandez-Martinez 2013)

Test type	High sensitivity clays, $S_t > 15$	Low sensitivity clays, $S_t < 15$
CAUC	10–15	0–10
CAUE	0–5	0
DSS	5–10	0–5

If both extension and compression strengths would be available for fitting HSU, the kind of reduction could be achieved by fitting the more accurately for extension (according to the peak extension strength), and with a lower compression strength compared to the peak strength. This can be achieved with a proper combination of C and λ/κ (see Section 9.5).

9.5 Suggested model fitting and parameter choice procedures

In Chapters 7 and 8, many different methods of fitting the HSU parameters to available data were used. It can be said that HSU can in most cases be fitted for both compression and extension at a given OCR level (unless the "target strength" is much lower or higher than what the yield surface geometry allows). If the strength over a broader OCR range is targeted, the fit needs to be a compromise between compression and extension strengths at the different OCR levels.

The fitting procedure also depends on the amount and quality of the data that is available. HSU is completely usable if only friction angle φ', preconsolidation pressure σ'_c and the *in situ* vertical stress σ'_{v0} are known. Assuming these are reliably determined, their input values in HSU should be set at their laboratory/calculated values. In that case the parameters C and D are simply left at their default values $C = D = 1$, and λ/κ can be set at e.g. $\lambda/\kappa = 5$ (although λ/κ should be treated as an unknown that is varied to ascertain its effect on the results).

If in addition to φ', σ'_c and σ'_{v0} undrained shear strength data is available (CK_0U tests, DSS tests etc.), the strength data should be used to choose the value of λ/κ. If extension or direct shear data is available in addition to compression strength data, the value of C can be slightly adjusted to better match the strength in extension. Changing the value of C has a relatively low effect on compression strength (see Section 6.2), so the degree of strength anisotropy can thus be adjusted almost independently. The values of λ/κ and C can be changed iteratively until both compression and extension strengths are matched. Of course, matching compression and extension strengths does not completely ensure that strengths for the in between stress states are correct, but could still be considered "close enough".

If there is data on K_{0NC} and the in situ K_0 value, this data could additionally be used to determine the values of C and D, respectively. In theory, assuming that the assumptions made in the HSU method are correct, this should result in correct predicted strengths. If there is no measured undrained shear strength data, C and D should thus be determined as accurately as possible. If the "correct" C and D values however lead to predicted shear strength that differs from measured strengths, these parameters could be adjusted as needed.

If HSU is fitted over a large OCR range, the parameter fit most likely needs to be a compromise that emphasizes strength at some chosen OCR value. Paradoxically, having "too much" measured data on the different parameters reduces the ability of the method to be fitted well to a given set of SHANSEP parameters. If a SHANSEP parameter fit is attempted, it can generally be said that the value of λ/κ controls the exponent m, while φ' and C control the strength ratio S. While λ/κ also controls S, it should be set to produce the desired m value as other parameters do not affect m effectively.

Good engineering judgment and knowledge of the model parameters' influence is generally required in choosing the parameters for HSU, especially if values other than measured or default are chosen. For the choice of λ/κ, experimentation with different values is recommended to see its effect on the end result. While proper usage is emphasized here, the HSU method should not be thought as an overly complex model (actually it is relatively simple). The same basic principles apply in all aspects of soil modelling.

10 Conclusions

10.1 Present state

The presented Hybrid s_u (HSU) method offers a new approach of conducting an undrained stability analysis based on effective strength parameters. HSU is intended to be used for limit equilibrium stability analyses on soft, normally or slightly overconsolidated clays. It is based on the anisotropic critical state soil model S-CLAY1 (Wheeler et al 2003). The HSU method can take into account the effects strength anisotropy, consolidation state and to some extent the rate of loading on the predicted undrained strength.

The method is shown to effectively predict anisotropic undrained shear strength s_u of soft clays with a relatively small amount of parameters. The equilibrium analysis itself can be carried out just like a typical total stress analysis, with the calculated s_u value acting as strength input for the limit equilibrium. This makes HSU a good compromise between "traditional" total stress analyses and notably more complicated finite element analyses with intricate soil models. Therefore the HSU method can be considered a suitable tool for everyday stability design work. It is not however intended for detailed analyses of soil stress states.

The HSU method also offers the option of undrained effective stress analysis by calculating the excess pore pressure Δu. This can be approached by two ways: Either by forcing Δu so that the strength predicted by HSU is achieved in terms of effective stresses, or by calculating the value of Δu based on the assumed stress changes at the failure state. Both approaches solve the theoretical issue of overpredicting shear strength that is inherent in traditional undrained effective stress analyses when $F > 1$. This is because different approaches of the HSU method always relate shear strength to the actual (assumed) stress state at failure, not the mobilized stress state. This means that the factor of safety given by an undrained effective stress analysis is directly comparable to a corresponding total stress analysis.

While the suggested methods of undrained effective stress stability analysis do generally give good results and solve an important theoretical issue in predicting the shear strength at failure, it is debatable if they offer any extra value over the offered method of using predicted s_u in total stress limit equilibrium calculations. This is because the end result (i.e. factor of safety) is roughly the same between the methods, and if there is a difference, the total stress approach should be considered correct (as the value of Δu is derived from the calculated s_u value). On the other hand, the undrained effective stress calculations are somewhat more complex, time-consuming and prone to errors due to the added iteration loops. Therefore the suggested approach of HSU is to use it to calculate s_u and apply this strength input to a total stress analysis.

Another novelty of the HSU method is that it offers the option of modelling cohesion with a critical state model. This may provide useful if laboratory data consistently indicates cohesion at large strains. By modelling cohesion where relevant, one avoids the need for compensating the high strength with overly large friction angle values, which could then lead to inaccuracies. However, applying cohesion in HSU should be based on careful engineering judgment as it can result in dangerously high predicted strengths if applied erroneously.

10.2 Future research potential

A matter that could not be included in this thesis is the implementation of the HSU method with the search for the most critical slip surface. While calculation algorithms for the different approaches are suggested (Chapter 5), the technical details involved are not complete. While the main purpose of HSU in limit equilibrium applications is “only” to generate strength or pore pressure input for the equilibrium calculation, the strength (or excess pore pressure) depends on the geometry of a given slip surface. Therefore the strength needs to be separately calculated separately for each individual slip surface. While there is no doubt that a working implementation in a geotechnical design software will be found, at the time of writing this has not been tested in practise.

Improvements could also be made in calculating Δu. Improving the iteration procedures might increase the reliability and robustness of the method. The calculation of excess pore pressure based on stress changes could also have potential for improvement. The theoretical approach that solves the inherent overestimation of shear strength that occurs in traditional undrained effective stress analyses could be useful in other applications as well, so research on this issue could be useful.

Finally, the presented HSU method demonstrates the concept of applying a fairly advanced soil model to a limit equilibrium framework. Such an approach could be used to implement even more advanced models that account for e.g. strain softening. With suitable assumptions, the overall complexity of such a model could be kept at a manageable level.

11 References

Abramson, L.W. 2002, *Slope stability and stabilization methods,* Second Edition edn, John Wiley & Sons Incorporated.

Arulanandan, K., Shen, C. & Young, R. 1971, "Undrained creep behaviour of a coastal organic silty clay", *Geotechnique,* vol. 21, no. 4, pp. 359-375.

Atkinson, J. 1993, *An introduction to the mechanics of soils and foundations: through critical state soil mechanics.* McGraw-Hill Book Company (UK) Ltd.

Augustesen, A., Liingaard, M. & Lade, P.V. 2004, "Evaluation of time-dependent behavior of soils", *International Journal of Geomechanics,* vol. 4, no. 3, pp. 137-156.

Barden, L. 1969, "Time dependent deformation of normally consolidated clays and peats", *Journal of Soil Mechanics & Foundations Div,* vol. 95, no. 1, pp. 1-31.

Berre, T. & Bjerrum. L. 1973, "Shear strength of normally consolidated clays", *Proc. 8th ICSMFE, Moscow.*

Berre, T., Schjetne, K., & Sollie, S. 1969, "Sampling disturbance of soft marine clays". *Proceedings of the 7th ICSMFE, Special Session, Mexico, vol. 1, pp. 21-24.*

Bishop, A.W., Bjerrum, L. 1960, "The relevance of the triaxial test to the solution of stability problems", ASCE, also published as Norwegian Geotechnical Institute Publication No. 34

Bjerrum, L. 1973, "Problems of soil mechanics and construction on soft clays", *Proc. of 8th Int. Conf. on SMFE*

Bjerrum, L. 1972, "Embankments on soft ground", *Performance of earth and earth-supported structures.*ASCE

Bjerrum, L. 1967, "Engineering geology of Norwegian normally-consolidated marine clays as related to settlements of buildings", Geotechnique, vol. 17, no. 2, pp. 83-118.

Burland, J. B. 1990, "On the compressibility and shear strength of natural clays." *Géotechnique,* vol. 40, no. 3, pp. 329-378

Burland, J. B., Rampello, S., Georgiannou, V. N., & Calabresi, G. 1996. "A laboratory study of the strength of four stiff clays." *Géotechnique*, vol. 46, no. 3, pp. 491-514.

Casagrande, A., & Wilson, S. D. 1960, "Testing Equipment, Techniques and Error: Moderators' Report, Session 2", In *Proceedings, Research Conference on Shear Strength of Cohesive Soils,* ASCE, pp. 1123-1130.

Cheng, Y.M. 2003, "Location of critical failure surface and some further studies on slope stability analysis", *Computers and Geotechnics,* vol. 30, no. 3, pp. 255-267.

Cheng, Y.M., Länsivaara, T. & Wei, W.B. 2007, "Two-dimensional slope stability analysis by limit equilibrium and strength reduction methods", *Computers and Geotechnics,* vol. 34, no. 3, pp. 137-150.

Cheng, Y. M., & Lau, C. K. 2008, "Slope stability analysis and stabilization: new methods and insight", Taylor & Francis.

Cheng, Y. M., Li, D. Z., Li, L., Sun, Y. J., Baker, R., & Yang, Y. 2011, "Limit equilibrium method based on an approximate lower bound method with a variable factor of safety that can consider residual strength", *Computers and Geotechnics*, vol. 38, no. 5, pp. 623-637.

Clausen, C. 2003, *Program BEAST Documentation*, Report 8302-2, Revision 4.

Craig, R.F. 2004, *Soil Mechanics*, 7th Ed, Spon Press.

Dafalias, Y. F., & Taiebat, M. 2014, “Attributes of rotational hardening rules in clay plasticity”, *Numerical Methods in Geotechnical Engineering*, vol 1, pp. 27-32.

Dascal, O. & Tournier, J. 1975, "Embankments on soft and sensitive clay foundation", *ASCE Journal of the Geotechnical Engineering Division,* vol. 101, no. GT3, pp. 297-314.

Duncan, J.M. & Wright, S.G. 1980, "The accuracy of equilibrium methods of slope stability analysis", *Engineering Geology,* vol. 16, no. 1, pp. 5-17.

Drucker, D. C. and Prager, W. 1952, “Soil mechanics and plastic analysis for limit design”, *Quarterly of Applied Mathematics*, vol. 10, no. 2, pp. 157–165.

Fredlund, D.G. & Krahn, J. 1977, "Comparison of slope stability methods of analysis", *Canadian Geotechnical Journal,* vol. 14, no. 3, pp. 429-439.

Fredlund, D.G., Krahn, J. & Pufahl, D.E. 1981, "The relationship between limit equilibrium slope stability methods", *Proc. 10th International Conference Soil Mechanics, Stockholm, Sweden*, pp. 409.

Graham, J., Crooks, J. & Bell, A. 1983, "Time effects on the stress-strain behaviour of natural soft clays", *Géotechnique,* vol. 33, no. 3, pp. 327-340.

Habib, M. P. 1953, “Influence of the variation of the intermediate principal stress on the shearing strength of soils”, In *Proc of 3rd Int Conf Sial Mech Foundation Eng*, Vol. 1, pp. 131-136.

Helenelund, K.V. 1977, "Methods for reducing undrained shear strength of soft clay", *Swedish Geotechnical Institute, Proceedings*.

Holzer, T.L., Höeg, K. & Arulanandan, K. 1973, "Excess pore pressures during undrained clay creep", *Canadian Geotechnical Journal,* vol. 10, no. 1, pp. 12-24.

Jaky, J. 1948, “Pressure in silos”, 2nd ICSMFE, London, Vol. 1, pp. 103-107

Jamiolkowski, M. 1985, "New developments in field and laboratory testing of soils, State of the Art Report", *Proc. 11th Int. Conf. on SMFE*

Janbu, N. 1957, "Earth pressure and bearing capacity calculations by generalized procedure of slices", *Proceedings of the 4th international conference on soil mechanics and foundation engineering London*London, pp. 207.

Janbu, N. 1954, "Application of composite slip surfaces for stability analysis", *Proc. European Conf. on Stability of Earth Slopes, Stockholm, 1954*, pp. 43.

Janbu, N. 1954, "Stability analysis of slopes with dimensionless parameters", *Harvard Soil Mech. Ser.,* vol. 46, pp. 81 pp.

Karlsrud, K. & Hernandez-Martinez, F.G. 2013, “Strength and deformation properties of Norwegian clays from laboratory tests on high-quality block samples”, *Canadian Geotechnical Journal, vol. 50, no. 12, pp. 1273-1293*

Kirkgard, M. & Lade, P.V. 1993, "Anisotropic three-dimensional behavior of a normally consolidated clay", *Canadian Geotechnical Journal,* vol. 30, no. 5, pp. 848-858.

Krahn, J. 2003, "The 2001 R.M. Hardy Lecture: The limits of limit equilibrium analyses", *Canadian Geotechnical Journal,* vol. 40, no. 3, pp. 643-660.

La Rochelle, P., Trak, B., Tavenas, F. & Roy, M. 1974, "Failure of a Test Embankment On a Sensitive Champlain Clay Deposit", *Canadian Geotechnical Journal, vol 11, no. 1, pp. 142-164*

Lacasse, S.M., Ladd, C.C. & Barsvary, A.K. 1977, "Undrained behavior of embankments on New Liskeard varved clay", *Canadian Geotechnical Journal, vol. 14, no. 3. pp. 367-388*

Ladd, C.C. 1991, "Stability evaluation during staged construction", *Journal of Geotechnical Engineering,* vol. 117, no. 4, pp. 540-615.

Lade, P. V. 1977, "Elasto-plastic stress-strain theory for cohesionless soil with curved yield surfaces", *International Journal of Solids and Structures*, vol 13, no. 11, pp. 1019-1035.

Lade, P.V. & Musante, H.M. 1978, "Three-dimensional behavior of remolded clay", *Journal of the Geotechnical Engineering Division,* vol. 104, no. 2, pp. 193-209.

Länsivaara, T. 2010, "Failure induced pore pressure by simple procedure in LEM", In: Benz, T. et al.(eds.). *Numerical Methods in Geotechnical Engineering. Proceedings of the Seventh European Conference on Numerical Methods in Geotechnical Engineering Numge 2010*, Trondheim, Norway, 2-4 June, 2010.

Länsivaara, T. 1999, "A study of the mechanical behavior of soft clay", *Norwegian University of Science and Technology.NTNU.Doktor ingeniöravhandling,* vol. 85, pp. 191.

Larsson, R. 2007, *Skjuvhållfasthet: utvärdering i kohesionsjord,* Statens geotekniska institut (SGI).

Larsson, R. 1980, "Undrained shear strength in stability calculation of embankments and foundations on soft clays", *Canadian Geotechnical Journal,* vol. 17, no. 4, pp. 591-602.

Larsson, R. 1977,"Basic behavior of Scandinavian soft clays", In *Swedish Geotechnical Institute, Proceedings*, Report No. 4.

Lefebvre, G. & Leboeuf, D. 1987, "Rate effects and cyclic loading of sensitive clays", *Journal of Geotechnical Engineering,* vol. 113, no. 5, pp. 476-489.

Lefebvre, G., & Poulin, C. 1979, "A new method of sampling in sensitive clay", *Canadian Geotechnical Journal*, vol. 16, no. 1, pp. 226-233.

Lehtonen, V., Meehan, C., Länsivaara, T. & Mansikkamäki, J. 2015,"Full-scale embankment failure test under simulated train loading", *Géotechnique.* Published, ahead of print (available online from 29th August 2015).

Leroueil, S., Magnan, J. & Tavenas, F. 1990, *Embankments on soft clays*

Leroueil, S., Kabbaj, M., Tavenas, F. & Bouchard, R. 1985, "Stress–strain–strain rate relation for the compressibility of sensitive natural clays", *Geotechnique,* vol. 35, no. 2, pp. 159-180.

Lunne, T., Berre, T., & Strandvik, S. 1997, "Sample disturbance effects in soft low plastic Norwegian clay." In *Symposium on Recent Developments in Soil and Pavement Mechanics,* Rio de Janeiro, Brazil, pp. 81-102.

Mansikkamäki, J. 2015, "Effective stress finite element stability analysis of an old railway embankment on soft clay", Doctoral thesis, Tampere University of Technology.

Matsuoka, H., & Nakai, T. 1985, “Relationship among Tresca, Mises, Mohr-Coulomb and Matsuoka-Nakai criteria”, *Soils and Foundations*, vol. 25, no. 4, pp. 123-128

Matsuoka, H., & Nakai, T. 1974, “Stress-deformation and strength characteristics of soil under three different principal stresses”, In *Proc. JSCE,* vol. 232, pp. 59-70

Mayne, P.W. 1985, "Stress anisotropy effects on clay strength", *Journal of Geotechnical Engineering,* vol. 111, no. 3, pp. 356-366.

Mayne, P.W. & Kulhawy 1982, F.H, “K_0-OCR relationships in soil”, *Journal of the Geotechnical Engineering Division,* vol. 108, no. 6, pp. 851-872

Morgenstern, N.R. & Price, V.E. 1965, "The analysis of the stability of general slip surfaces", *Geotechnique,* vol. 15, no. 1, pp. 79-93.

Morgenstern, N.R. & Sangrey, D.A. 1978, "Methods of stability analysis", *Transportation Research Board Special Report*, no. 176.

Nishimura, S., Minh, N. & Jardine, R. 2007, "Shear strength anisotropy of natural London clay", *Geotechnique,* vol. 57, no. 1, pp. 49-62.

Nordal, S. 2010, “Soil Modeling”, course material for the Ph.D course BA 8304 Soil Modeling, NTNU Trondheim

Prashant, A. & Penumadu, D. 2004, "Effect of intermediate principal stress on overconsolidated kaolin clay", *Journal of Geotechnical and Geoenvironmental Engineering,* vol. 130, no. 3, pp. 284-292.

Ratahallintokeskus 2005, *Radan stabiliteetin laskenta, olemassa olevat penkereet. Ratahallintokeskuksen julkaisuja B 15*, Ratahallintokeskus, Helsinki.

Ronkainen, N. 2012, *Suomen maalajien ominaisuuksia. Suomen ympäristö 2/2012.*, Suomen ympäristökeskus, Helsinki.

Roscoe, K., & Burland, J. B. 1968, *On the generalized stress-strain behaviour of wet clay.*

Schmidt, B. 1966,” Earth pressures at rest related to stress history” *Canadian Geotechnical Journal*, vol. 3, no. 4, pp. 239-242.

Schofield, A. & Wroth, P. 1968, *Critical state soil mechanics*, McGraw-Hill, London.

Sheahan, T. & Kaliakin, V. 1999, "Microstructural considerations and validity of the correspondence principle for cohesive soils", In: *Proceedings of the 13th conference onengineering mechanics*, Baltimore, MD, USA (eds N. Jones and R. Ghanem), ASCE, Reston, VA, USA

Sheahan, T.C. 1995, "Interpretation of undrained creep tests in terms of effective stresses", *Canadian geotechnical journal,* vol. 32, no. 2, pp. 373-379.

Sheahan, T.C., Ladd, C.C. & Germaine, J.T. 1996, "Rate-dependent undrained shear behavior of saturated clay", *Journal of Geotechnical Engineering,* vol. 122, no. 2, pp. 99-108.

Sheahan, T.C., Ladd, C.C. & Germaine, J.T. 1996, "Rate-dependent undrained shear behavior of saturated clay", *Journal of Geotechnical Engineering,* vol. 122, no. 2, pp. 99-108.

Skempton, A. W. 1954, “The pore-pressure coefficients A and B.” *Geotechnique*, vol. 4, no. 4, pp. 143-147.

Skempton, A. W. 1964, “Long-term stability of clay slopes.” *Geotechnique*, vol. 14, pp. 77-102.

Skempton, A. W. 1977, “Slope stability of cuttings in brown London clay.” In: *Proceedings of the 9th International Conference on Soil Mechanics and Foundation Engineering,* vol. 3, pp. 261-270.

Spencer, E. 1973, "Thrust line criterion in embankment stability analysis", *Geotechnique,* vol. 23, no. 1.

Spencer, E. 1967, "A method of analysis of the stability of embankments assuming parallel inter-slice forces", *Geotechnique,* vol. 17, no. 1, pp. 11-26.

Svanø, G. 1981, *Undrained effective stress analyses*, University of Trondheim.

Tavenas, F. & Leroueil, F. 1980, “The behavior of embankments of clay foundations”, *Canadian Geotechnical Journal,* vol. 17, no. 2, pp. 236-260.

Tavenas, F., Trak, B. & Leroueil, S. 1980, "Remarks on the validity of stability analyses", *Canadian Geotechnical Journal,* vol. 17, no. 1, pp. 61-73.

Thakur, V., Jostad, H.P., Kornbrekke, H.A. & Degago, S.A. 2014, “How well do we understand the undrained strain softening response in soft sensitive clays?”, *Landslides in Sensitive Clays, Advances in Natural and Technological Hazards Research* Volume 36, 2014, pp 291-303, Springer

Trak, B., La Rochelle, P., Tavenas, F. & Roy, M. 1980, “A new approach to the stability analysis of embankments on sensitive clays”, *Canadian Geotechnical Journal,* vol. 17, no. 4, pp. 526-544.

Ukonjärvi, P. 2015, ”Rautatieympäristössä siipikairauksella määritettävän suljetun leikkauslujuuden luotettavuus”, Master’s Thesis, Tampere University of Technology. Unfinished, reference to the draft version during the time of writing. (In Finnish. Title in English: Reliability in determining undrained shear strength using the vane shear test in railway environment)

Vaid, Y.P. & Campanella, R.G. 1974, "Triaxial and plane strain behavior of natural clay", *Journal of Geotechnical and Geoenvironmental Engineering,* vol. 100, no. Proc. Paper 10421.

Vaid, Y., Robertson, P. & Campanella, R. 1979, "Strain rate behaviour of Saint-Jean-Vianney clay", *Canadian Geotechnical Journal,* vol. 16, no. 1, pp. 34-42.

Wheeler, S.J, Näätänen, A., Karstunen, M. & Lojander, M 2003,” An anisotropic elastoplastic model for soft clays”, *Canadian Geotechnical Journal*, vol. 40, no. 2, pp. 403-418.

Wood, D.M. 1990, *Soil behaviour and critical state soil mechanics,* Cambridge University Press.

Wright, S.G., Kulhawy, F.H. & Duncan, J.M. 1973, "Accuracy of equilibrium slope stability analysis", *Journal of the Soil Mechanics and Foundations Division,* vol. 99, no. 10, pp. 783-791.

Zdravkovic, L., Potts, D. & Hight, D.W. 2002, “The effect of strength anisotropy on the behaviour of embankments on soft ground”, *Geotechnique*, vol. 52, no. 6, pp. 447-457

Zentar, R., Karstunen, M., Wiltafsky, C., Schweiger, H.F., Koskinen, M. 2002, “Comparison of two approaches for modelling anisotropy of soft clays”, In *Proceedings of the 8th International Symposium on Numerical Models in Geomechanics (NUMOG VIII)*, Rome. 10–12 April, pp.115–121.

12 Appendix A: Derivation of the HSU method

The general initial yield surface is expressed as (Wheeler et al 2003):

$$f_S = \frac{3}{2}(\{\underline{\sigma'_d} - p'\underline{\alpha_d}\}^T\{\underline{\sigma'_d} - p'\underline{\alpha_d}\}) - (M^2 - \frac{3}{2}\{\underline{\alpha_d}\}^T\{\underline{\alpha_d}\})(p'_m - p')p' \qquad \text{(A.1)}$$

where the deviatoric stress vector and the deviatoric fabric tensor are respectively defined as:

$$\underline{\sigma'_d} = \begin{bmatrix} \sigma'_x - p' \\ \sigma'_y - p' \\ \sigma'_z - p' \\ \sqrt{2}\tau_{xy} \\ \sqrt{2}\tau_{yz} \\ \sqrt{2}\tau_{xz} \end{bmatrix} \qquad \text{(A.2)}$$

$$\underline{\alpha_d} = \begin{bmatrix} \alpha_x - 1 \\ \alpha_y - 1 \\ \alpha_z - 1 \\ \sqrt{2}\alpha_{xy} \\ \sqrt{2}\alpha_{yz} \\ \sqrt{2}\alpha_{xz} \end{bmatrix} \qquad \text{(A.3)}$$

Due to assumed plane strain constraints ($\tau_{xy} = \tau_{yz} = 0$) and cross-anisotropy ($\alpha_x = \alpha_y$, $\alpha_{xy} = \alpha_{yz} = \alpha_{xz} = 0$) the vectors can be written as:

$$\underline{\sigma'_d} = \begin{bmatrix} \sigma'_x - p' \\ \sigma'_y - p' \\ \sigma'_z - p' \\ 0 \\ 0 \\ \sqrt{2}\tau_{xz} \end{bmatrix} \qquad \text{(A.4)}$$

$$\underline{\alpha_d} = \begin{bmatrix} \alpha_x - 1 \\ \alpha_x - 1 \\ \alpha_z - 1 \\ 0 \\ 0 \\ 0 \end{bmatrix} \qquad \text{(A.5)}$$

It is more convenient to express the components of the fabric tensor as functions of the scalar anisotropy parameter α_{rot}. The components have the property:

$$\frac{1}{3}(\alpha_x + \alpha_y + \alpha_z) = 1 \tag{A.6}$$

The scalar anisotropy parameter is given as:

$$\alpha_{rot}{}^2 = \frac{3}{2}\underline{\alpha_d}^T \underline{\alpha_d} \tag{A.7}$$

The previous equations lead to the expression:

$$\underline{\alpha_d} = \begin{bmatrix} -\alpha_{rot}/3 \\ -\alpha_{rot}/3 \\ 2\alpha_{rot}/3 \\ 0 \\ 0 \\ 0 \end{bmatrix} \tag{A.8}$$

The deviatoric stress vector is expressed in terms of Cartesian stresses. These can in turn be expressed using principal stresses, principal stress rotation θ and the intermediate principal stress term b:

$$\sigma'_x = \frac{\sigma'_1 + \sigma'_3}{2} - \frac{\sigma'_1 - \sigma'_3}{2} \cdot \cos(2 \cdot \theta) \tag{A.9}$$

$$\sigma'_z = \frac{\sigma'_1 + \sigma'_3}{2} + \frac{\sigma'_1 - \sigma'_3}{2} \cdot \cos(2 \cdot \theta) \tag{A.10}$$

$$\sigma'_y = \sigma'_3 + b \cdot (\sigma'_1 - \sigma'_3) \tag{A.11}$$

$$\tau_{xz} = \frac{\sigma'_1 - \sigma'_3}{2} \cdot \sin(2 \cdot \theta) \tag{A.12}$$

$$p' = \frac{\sigma'_1 + \sigma'_2 + \sigma'_3}{3} = \frac{\sigma'_1 + \sigma'_3 + b(\sigma'_1 - \sigma'_3) + \sigma'_3}{3} \tag{A.13}$$

$$\Rightarrow \sigma_3 = \frac{b+1}{b-2}\sigma'_1 - \frac{3}{b-2}p' \tag{A.14}$$

The aim is to express the yield surface as a function of *p'*, *b* and θ.

By substituting the previous equations into the deviatoric vector we get:

$$\underline{\sigma'_d} = \begin{bmatrix} \sigma'_x - p' \\ \sigma'_y - p' \\ \sigma'_z - p' \\ 0 \\ 0 \\ \sqrt{2}\tau_{xz} \end{bmatrix} = \begin{bmatrix} \frac{\sigma'_1+\sigma'_3}{2} - \frac{\sigma'_1-\sigma'_3}{2}\cdot\cos(2\cdot\theta) - p' \\ \sigma'_3 + b\cdot(\sigma'_1-\sigma'_3) - p' \\ \frac{\sigma'_1+\sigma'_3}{2} + \frac{\sigma'_1-\sigma'_3}{2}\cdot\cos(2\cdot\theta) - p' \\ 0 \\ 0 \\ \sqrt{2}\frac{\sigma'_1-\sigma'_3}{2}\cdot\sin(2\cdot\theta) \end{bmatrix} \tag{A.15}$$

$$\underline{\sigma'_d}(p', b, \theta, \sigma'_1) = \begin{bmatrix} \frac{\sigma'_1 + \frac{b+1}{b-2}\sigma'_1 - \frac{3}{b-2}p'}{2} - \frac{\sigma'_1 - \frac{b+1}{b-2}\sigma'_1 + \frac{3}{b-2}p'}{2}\cdot\cos(2\cdot\theta) - p' \\ \frac{b+1}{b-2}\sigma'_1 - \frac{3}{b-2}p' + b\cdot(\sigma'_1 - \frac{b+1}{b-2}\sigma'_1 + \frac{3}{b-2}p') - p' \\ \frac{\sigma'_1 + \frac{b+1}{b-2}\sigma'_1 - \frac{3}{b-2}p'}{2} + \frac{\sigma'_1 - \frac{b+1}{b-2}\sigma'_1 + \frac{3}{b-2}p'}{2}\cdot\cos(2\cdot\theta) - p' \\ 0 \\ 0 \\ \sqrt{2}\frac{\sigma'_1 - \frac{b+1}{b-2}\sigma_1 + \frac{3}{b-2}p'}{2}\cdot\sin(2\cdot\theta) \end{bmatrix}$$

(A.16)

The vectors in the yield function can be combined, resulting in (intermediate steps omitted):

$$\underline{\sigma'_d} - p'\cdot\underline{\alpha_d} = \begin{bmatrix} \dfrac{(6-9\cdot\cos^2(\theta)-2\alpha_{rot}-3b+\alpha_{rot}\cdot b)\cdot p'+(-6+9\cdot\cos^2(\theta)+3b)\cdot\sigma'_1}{3b-6} \\ -\dfrac{(1+2\alpha_{rot}/3-2b-\alpha_{rot}\cdot b)\cdot p'-(1-2b)\cdot\sigma'_1}{b-2} \\ \dfrac{(6-9\cdot\cos^2(\theta)+4\alpha_{rot}-3b-2\alpha_{rot}\cdot b)\cdot p'+(-6+9\cdot\cos^2(\theta)+3b)\cdot\sigma'_1}{3b-6} \\ 0 \\ 0 \\ \dfrac{3\sqrt{2}\cdot\sin(2\theta)\cdot(p'-\sigma'_1)}{2b-4} \end{bmatrix}$$

(A.17)

Using the previous expression the S-CLAY1 yield function (Eq. A.1) can be solved for σ'_1 (intermediate steps omitted):

$$\sigma'_{1S} = \frac{2/3\cdot\alpha_{rot}-\alpha\cdot\sin^2\theta+\alpha_{rot}\cdot b\cdot(b/6-2/3+(\sin^2\theta)/2)+B}{B}\cdot p' \pm \frac{(b-2)\sqrt{p'}\sqrt{4B\cdot M^2\cdot p'+(b^2+6b\cdot\sin^2\theta-4b+9\cdot\sin^4\theta-12\cdot\sin^2\theta+4)\cdot\alpha_{rot}{}^2\cdot p'+4B(M^2+\alpha_{rot}{}^2)\cdot p'_m}}{6B}$$

(A.18)

where

$$B = b^2 - b + 1 \qquad \text{(A.19)}$$

The parameters M and α_{rot} can at this point be considered known soil parameters and used as constants.

To remove the unknown σ'_1 from the final equation of p'_f, the Drucker-Prager failure condition is used. Assuming no cohesion and triaxial compression, the Drucker-Prager criterion can be expressed as:

$$f_{DP} = \sqrt{J_2} - \frac{2\sqrt{\sin\varphi'}}{\sqrt{3}(3+\sin\varphi')} \cdot 3p' = \sqrt{J_2} - C_4 \cdot 3p' \tag{A.20}$$

where

$$J_2 = -(\sigma'_1 - p')(\sigma'_2 - p') - (\sigma'_1 - p')(\sigma'_3 - p') - (\sigma'_2 - p')(\sigma'_3 - p') \tag{A.21}$$

Using the relationships between the principal stresses, J_2 can be rewritten as

$$J_2(p', b, \theta, \sigma'_1) = \left[\frac{(b-1)(b+1)^2}{(b-2)^2} - \frac{2b+2}{b-2} - b\right]\sigma'^2_1 + \left[2p' + 2bp' + \frac{6p' - (b+1)\cdot(2p' - 2p'(b-1))}{b-2} - 6p'\frac{(b-1)(b+1)}{(b-2)^2}\right]\sigma'_1 + \left[9\frac{(b-1)}{(b-2)^2} - 6\frac{2-b}{b-2} - 3\right]p'^2 \tag{A.22}$$

The Drucker-Prager criterion can then be solved for σ'_1, eventually resulting in:

$$\sigma'_{1DP}(p', b) = \frac{B - \sqrt{3}(\pm 2 + b)\cdot C_1 \cdot \sqrt{B}}{B} \tag{A.23}$$

where

$$C_1 = \frac{2\sin\varphi'}{\sqrt{3}(3-\sin\varphi')} \tag{A.24}$$

At failure, the S-CLAY1 and Drucker-Prager yield rules coincide (i.e. the stress state at failure lies both on the S-CLAY1 surface and the Drucker-Prager cone). By assuming:

$$\sigma'_{1DP} = \sigma'_{1S} \tag{A.25}$$

p'_f as a function of b and θ can be solved:

$$p'_f(b, \theta) = \frac{B(M^2 - \alpha_{rot}{}^2)}{M^2 + M^2 b^2 - b(M^2 - C_2) + 27C_1{}^2 \cdot B - 2C_2 + 3C_2 \cdot \sin^2\theta} p'_m \tag{A.26}$$

where

$$C_2 = 3\sqrt{3}C_1\sqrt{B}\cdot\alpha_{rot} \tag{A.27}$$

The previous form only describes the intersection of the initial yield surface and the Drucker-Prager cone i.e. there is no hardening. Volumetric hardening (i.e. change of p'_m) needs to be accounted for.

At failure it can be written after Equation A.26 that:

$$p'_f(b,\theta) = \frac{B(M^2 - \alpha_{rot}{}^2)}{M^2 + M^2 b^2 - b(M^2 - C_2) + 27C_1{}^2 \cdot B - 2C_2 + 3C_2 \cdot \sin^2\theta} p'_{mf} \tag{A.28}$$

Now p'_{mf} needs to be solved.

The volumetric hardening law in S-CLAY1 is given as

$$dp'_m = \frac{\nu \cdot p'_m \, d\varepsilon_v^p}{\lambda - \kappa} \tag{A.29}$$

$$d\varepsilon_v^e = \frac{\kappa}{\nu} \cdot \frac{dp'}{p'} \tag{A.30}$$

For undrained conditions the following applies:

$$d\varepsilon_v^p = -d\varepsilon_v^e \tag{A.30}$$

This results in:

$$dp'_m = \frac{\nu \cdot p'_m \cdot (-d\varepsilon_v^e)}{\lambda - \kappa} = -\frac{\nu \cdot p'_m}{\lambda - \kappa} \cdot \frac{\kappa}{\nu} \cdot \frac{dp'}{p'} = \frac{\kappa \cdot dp' \cdot p'_m}{p'(\kappa - \lambda)} \tag{A.31}$$

To simplify the expression it can be written that:

$$A = \frac{\kappa}{\kappa - \lambda} \tag{A.32}$$

The volumetric hardening law the can be expressed as the differential equation:

$$dp'_m = A\frac{dp'}{p'} \cdot p'_m \tag{A.33}$$

$$\frac{dp'_m}{p'_m} = A\frac{dp'}{p'} \tag{A.34}$$

The expression is then integrated from the initial state "*0*" to failure "*f*":

$$\int_{p'_{m0}}^{p'_{mf}} \frac{dp'_m}{p'_m} = A \int_{p'_0}^{p'_f} \frac{dp'}{p'} \tag{A.35}$$

$$\ln p'_{mf} - \ln p'_{m0} = A(\ln p'_f - \ln p'_0) \tag{A.36}$$

The unknowns here are p'_f and p'_{mf}, (the initial state variables p'_0 and p'_{m0} are known). Solving for p'_{mf} we get:

$$p'_{mf} = \frac{{p'_f}^A \cdot p'_{m0}}{{p'_0}^A} \tag{A.37}$$

Previously it was written that:

$$p'_f(b,\theta) = \frac{B(M^2 - {\alpha_{rot}}^2)}{M^2 + M^2 b^2 - b(M^2 - C_2) + 27{C_1}^2 \cdot B - 2C_2 + 3C_2 \cdot \sin^2\theta} p'_{mf} \tag{A.28bis}$$

It can be further expressed that

$$p'_f = C_6 \cdot p'_{mf} = C_6 \cdot \frac{{p'_f}^A \cdot p'_{m0}}{{p'_0}^A} \tag{A.38}$$

where

$$C_6 = \frac{B(M^2 - {\alpha_{rot}}^2)}{M^2 + M^2 b^2 - b(M^2 - C_2) + 27{C_1}^2 \cdot B - 2C_2 + 3C_2 \cdot \sin^2\theta} \tag{A.39}$$

By further arranging the expression, we can write the easily solvable form for p'_f:

$$p'_f = C_6 \cdot \frac{p'_{m0}}{{p'_0}^A} {p'_f}^A = E \cdot {p'_f}^A \tag{A.40}$$

where (after some simplifying):

$$E = \frac{M^2 - {\alpha_{rot}}^2}{2M^2 + \frac{M \cdot \alpha_{rot}}{\sqrt{B}} \cdot (3\sin^2\theta + b - 2)} \cdot \frac{p'_{m0}}{{p'_0}^A} \tag{A.41}$$

Solving Eq. A.40 for p'_f we get:

$$p'_f = e^{\ln(1/E)/(A-1)} \tag{A.41}$$

where:

$$A = \frac{\kappa}{\kappa - \lambda} \tag{A.32bis}$$

(For equations for the other parameters in the equations, see Section 5.6)

Finally, s_u can be calculated as:

$$s_u = \frac{q_f}{2} = \frac{p'_f \cdot M}{2} \qquad \text{(A.42)}$$

Tampereen teknillinen yliopisto
PL 527
33101 Tampere

Tampere University of Technology
P.O.B. 527
FI-33101 Tampere, Finland

ISBN 978-952-15-3603-8
ISSN 1459-2045